JOURNAL OF GEOPHYSICAL RESEARCH

The continuation of

RESTRIAL MAGNETISM AND ATMOSPHERIC ELECTRICITY
(1896-1948)

An International Quarterly

LUME 61 December, 1956 NUMBER 4

CONTENTS

(Contents concluded on outside back cover)

Part one of two parts, December, 1956

Published at

THE WILLIAM BYRD PRESS, INC.

P. O. Box 2-W, SHERWOOD AVE. AND DURHAM ST.

RICHMOND 5, VIRGINIA

Address all correspondence to

JOURNAL OF GEOPHYSICAL RESEARCH

5241 BROAD BRANCH ROAD, NORTHWEST

WASHINGTON 15, D.C., U.S.A.

SIX DOLLARS A YEAR SINGLE NUMBERS, TWO DOLLARS

JOURNAL OF GEOPHYSICAL RESEARCH

The continuation of

Terrestrial Magnetism and Atmospheric Electricity

(1896-1948)

An International Quarterly

Founded 1896 by L. A. BAUER *Continued 1928-1948 by* J. A. FLEMING

Fields of Interest

Terrestrial Magnetism
Atmospheric Electricity
The Ionosphere
Solar and Terrestrial Relationships
Aurora, Night Sky, and Zodiacal Light
The Ozone Layer
Meteorology of Highest Atmospheric Levels
The Constitution and Physical States of the Upper Atmosphere
Special Investigations of the Earth's Crust and Interior, including experimental seismic waves, physics of the deep ocean and ocean bottom, physics in geology
And similar topics

This Journal serves the interests of investigators concerned with terrestrial magnetism and electricity, the upper atmosphere, the earth's crust and interior by presenting papers of new analysis and interpretation or new experimental or observational approach, and contributions to international collaboration. It is not in a position to print, primarily for archive purposes, extensive tables of data from observatories or surveys, the significance of which has not been analyzed.

Forward *manuscripts* to one of the Associate Editors, or to the editorial office of the Journal at 5241 Broad Branch Road, Northwest, Washington 15, D.C., U S A It is preferred that manuscripts be submitted in English, but communications in French, German, Italian, or Spanish are also acceptable. A brief abstract, preferably in English, must accompany each manuscript. A *publication charge* of $8 per page will be billed by the Editor to the institution which sponsors the work of any author; private individuals are not assessed page charges. Manuscripts from outside the United States are invited, and should not be withheld or delayed because of currency restrictions or other special difficulties relating to page charges Costs of publication are roughly twice the total income from page charges and subscriptions, and are met by subsidies from the Carnegie Institution of Washington and international and private sources.

Back issues and *reprints* are handled by the Editorial Office, 5241 Broad Branch Road, N.W., Washington 15, D.C., U.S.A.

Subscriptions are handled by the Editorial Office, 5241 Broad Branch Road, N.W., Washington 15, D.C., U.S.A.

Second-class mail privileges authorized at Richmond, Virginia

[Plate I]

John Adam Fleming (1877–1956)

Journal of

GEOPHYSICAL RESEARCH

The continuation of

Terrestrial Magnetism and Atmospheric Electricity

VOLUME 61 DECEMBER, 1956 No. 4

JOHN ADAM FLEMING, 1877-1956

BY W. E. SCOTT

Department of Terrestrial Magnetism,
Carnegie Institution of Washington,
Washington 15, D. C.

(Received September 27, 1956)

On July 29, 1956, quite suddenly as a result of a heart attack, the remarkably active and fruitful career of Dr. John Adam Fleming, the retired director of the Department of Terrestrial Magnetism of the Carnegie Institution of Washington, came to an end at San Mateo, California.

The Journal of Geophysical Research, the continuation of "Terrestrial Magnetism and Atmospheric Electricity," esteems it a privilege to honor the memory of Dr. Fleming, its former able editor from 1928-1948 and subsequently its honorary editor.

As director of the Department of Terrestrial Magnetism from 1935 to 1946, Dr. Fleming's success in supplementing and completing the world magnetic survey and in effecting international cooperation in that survey and at international gatherings was due to his first-hand knowledge of the fundamentals of terrestrial-magnetic investigations. He exercised great directive influence over all of these, at a time when it was still necessary to fill in gaps of our knowledge and accumulate magnetic and electric data in order that theoretical conclusions could be reached applicable to the whole earth.

He was a well-known figure at the meetings of the American Geophysical Union, National Academy of Sciences, and Philosophical Society in Washington, D. C., and at the triennial international assemblies of the Association of Terrestrial Magnetism and Electricity, International Union of Geodesy and Geophysics, in all of which he held high offices.

His life spanned a period of great changes and two world wars, but despite these modifying circumstances his biography is a pleasant and inspiring one. He left many friends who rejoiced in his success and who mourn his passing.

John Adam Fleming was born on January 28, 1877, at Cincinnati, Ohio, the son of Americus V. and Catherine B. Fleming. He graduated from the University of Cincinnati as a civil engineer in 1899. Years later, in 1933, the same University conferred upon him the degree of Doctor of Science. Joining his brother following graduation, his career commenced as a building contractor, but only briefly. He met Dr. Louis A. Bauer and became associated with him in the newly created Division of Terrestrial Magnetism at the U. S. Coast and Geodetic Survey in Washington, D. C., from 1899 to 1903.

In 1904, the new Department of Terrestrial Magnetism of the Carnegie Institution of Washington was established, and Dr. Bauer was entrusted with its direction. At that time, as compared with the Coast and Geodetic Survey, the Carnegie Institution was a private organization, and according to its statutes even an international one, which not only undertook and supported American scientific enterprises but also those of other countries or of private individuals. Briefly, the plan of work outlined for the Department of Terrestrial Magnetism embraced the following chief problems of investigation: (*a*) a magnetic survey of ocean areas and unexplored regions; (*b*) international observations of the variations; and (*c*) observations in ocean depths and atmospheric regions.

Under Dr. Bauer, Fleming became Chief Assistant. The association of these two men was fortunate, indeed, as subsequent events and successes of the Department of Terrestrial Magnetism were to prove. On a field trip, from February 21 to June 28, 1907, Fleming determined the three magnetic elements at 3 stations in British Honduras, 2 stations in Honduras, 12 stations in Guatemala, 5 stations in Panama, 8 stations in Costa Rica, and 1 station in the Canal Zone; 31 stations in all. In those early days, Fleming reduced observations, improved instrumental equipment, and designed magnetic observatories.

As the program of the Department of Terrestrial Magnetism expanded, Fleming was successively honored by appointments to the following positions, which he administered with skill and effectiveness: Chief of the Observatory Division in 1916; Chief of the Magnetic Survey Division in 1919; Assistant Director for Observational and Administrative Work in 1922; Acting Director in Charge of Operations in 1924; Acting Director of the Department in 1930; and Director in 1935 until his retirement in 1946.

The first goals of the Department of Terrestrial Magnetism were magnetic surveys of the oceans, erection of various new magnetic observatories in the hitherto neglected regions of the earth, particularly in the southern hemisphere and the tropics, and land expeditions to all parts of the world. The work of ocean magnetic survey was initiated in August 1905 by the chartered sailing ship *Galilee*, which on three cruises covered over 60,000 nautical miles, completing a general magnetic survey of the greater part of the Pacific Ocean. The specially-constructed non-magnetic survey ship *Carnegie* was put in service in 1909 and made seven cruises to all oceans, totaling 343,000 miles. On the final cruise of the *Carnegie* in 1928-29, in addition to the usual magnetic and atmospheric-electric programs, scientific oceanographic investigations, depth-determinations by echo-methods, and short-wave radio communication studies were undertaken. In the years 1905 to 1944, some 6,580 magnetic stations were occupied, and assistance was given to

over 200 expeditions. A major purpose of the observing program was the securing of secular-variation data through reoccupation of magnetic stations established previously. For over a score of years, the Department operated, principally under Dr. Fleming's direction, two magnetic observatories at Watheroo (Western Australia) and Huancayo (Peru). Dr. Fleming also played a leading international role in developing and maintaining the magnetic standards of the world. In later years, two primary standards of great accuracy (constant determined by the mutual inductance between a primary coil and a rotating secondary coil) were constructed for the use of the Cheltenham and new Fredericksburg magnetic observatories of the U. S. Coast and Geodetic Survey.

Life's prime must have been especially gratifying to Dr. Fleming. New vistas in science were opening around the time of completion of magnetic surveys. In the early and mid-twenty's, the advantage of combination of facilities for observation, experiment, and investigation became apparent. Experiments on magnetization by rotation were undertaken by Dr. S. J. Barnett. Several recent investigations had conclusively shown that the earth's magnetic field has an appreciable effect on the electric waves used in wireless transmission, and that there is a distinct relationship between terrestrial magnetic disturbances and certain radio phenomena. For many years prior, it was thought there existed in the region above us an electrically conducting layer, and this was experimentally verified by Messrs. Tuve and Breit of the Department of Terrestrial Magnetism in collaboration with the Naval Research Laboratory by obtaining oscillographic records of echoes of radio waves. Experimental work in atomic physics was also commenced about this same time by Drs. Gregory Breit and M. A. Tuve, first by developing the Tesla coil as a source of high potential, followed in subsequent years by two Van de Graaff electrostatic generators and cyclotron, with the aim of providing a means for investigating the innermost structure of matter—the atomic nucleus—and studies involving both chemistry and biology. A program of cosmic-ray recordings was initiated in 1936, later to prove of great importance. When a new type of atomic transmutation in the heaviest element uranium was discovered by chemical methods in January 1939, the Department of Terrestrial Magnetism using its new high-voltage equipment was one of the first laboratories to confirm (with Profs. Fermi and Bohr in attendance) the discovery of the fission-process by direct observation of the high-energy particles, leading to the possibility of chain reaction and atomic power.

During World War II, Dr. Fleming was in charge of all work at the Department of Terrestrial Magnetism under war contracts of the Institution concerned with ordnance devices, including proximity fuze, radio-wave and communications improvement, magnetic compasses and odographs, and uranium and ionospheric studies. Also during the war, the Department undertook the task of preparing new isomagnetic and isoporic charts. In this way, the results of voluminous surveys on land and sea, made over many years by the Department and other agencies, were used in improving the description of the earth's main field and its secular change.

Dr. Fleming published as author over 130 articles. The "Researches of the Department of Terrestrial Magnetism" (some 12 volumes), the journal of "Terres-

trial Magnetism and Atmospheric Electricity" during 1928-1948, and the early offset editions of the Transactions of the American Geophysical Union serve as notable monuments to him. Mention should be made of the 794-page book, "Terrestrial Magnetism and Electricity" (volume 8 of the "Physics of the Earth" series, sponsored by the National Research Council), which was prepared under his editorship in 1939, as also the earlier book edited by him on "Scientific Results of the Ziegler Polar Expedition of 1903-1905" (published under the auspices of the National Geographical Society, 1907).

After his retirement as Director of the Department of Terrestrial Magnetism in 1946, Dr. Fleming acted as adviser in international scientific relations to the Carnegie Institution of Washington.

Among the numerous medals received by Dr. Fleming were the William Bowie medal of the American Geophysical Union in 1941, and the Charles Chree medal of the Physical Society of London in 1945. He was a member of the National Academy of Sciences and many other professional organizations.

He is survived by his daughter, Mrs. H. E. Atkinson of San Mateo, California, and a brother Oliver Fleming of Nashville, Tennessee.

MEASUREMENTS AT SEA OF THE VERTICAL GRADIENT OF THE MAIN GEOMAGNETIC FIELD DURING THE *GALATHEA* EXPEDITION

BY J. ESPERSEN* AND P. ANDREASEN**

Geophysical Research Institution, University of Copenhagen, Denmark

AND

J. EGEDAL AND J. OLSEN

Danish Meteorological Institute, Copenhagen, Denmark

(Received June 25, 1956)

ABSTRACT

During the Danish *Galathea* expedition, 1950-52, investigations were made of the vertical gradient of the geomagnetic field, in an attempt to test the probability of the new "fundamental" theory for the main geomagnetic field proposed by P. M. S. Blackett in 1947.

Three relative, self-recording magnetometers—one needle instrument measuring the Z-component, one needle and one rotating-coil instrument measuring the H-component—are described. All instruments may be lowered to extreme depths in the sea in non-magnetic containers.

In the Pacific Ocean, a series of trial measurements were carried out, and at least one of the H magnetometers proved to be of the desired accuracy of 10γ during a single relative measurement. All trial stations were situated in places with locally disturbed geomagnetic field, which makes the gradient results unreliable, and a breakdown of the technical equipment of the surveying vessel prevented measurements at stations better suited to magnetic work. However, summed up, the trial results indicate a case against the fundamental theory—in accordance with gradient measurements ashore in mines and collieries.

INTRODUCTION

From October 1950 until June 1952, the frigate *Galathea* of the Royal Danish Navy accomplished a circumnavigation of the globe, serving during its cruise as an expedition vessel for comprehensive deep-sea explorations.

The main purpose of the expedition was marine biological and hydrographical investigations in the very deepest parts of the oceans, and for this purpose the vessel was fitted with a more efficient and extensive equipment than any previous deep-sea expedition. The most important special outfit was a 12,000-meter steel wire with a tensile strength of 7 tons, and a powerful high-speed trawl-winch for

*Now with the Department of Mineralogy and Geology, University of Copenhagen.
**Now with Telefon Fabrik Automatic A/S, Copenhagen.

drawing the wire. Besides the ship was equipped with a special deep-sea echo-sounder and radar, Loran, and other modern navigational aids.

The presence of this special equipment made the *Galathea* particularly adapted for other scientific investigations demanding lowering of heavy instruments or other gears to extreme depths in the oceans. In the autumn of 1949, N. Arley, head of the Geophysical Research Institution at the University of Copenhagen, indicated that among such problems which could be taken into account under these favorable circumstances was the possibility of making measurements of the vertical gradient of the main magnetic field of the earth by lowering magnetometers into the sea.

Great interest was taken in such investigations since P. M. S. Blackett (1947, 1948) advanced his "bulk" theory for the main magnetic fields of celestial bodies, claiming such fields to be a fundamental property of rotating masses. During the discussion following the proposal, it was suggested by E. C. Bullard that for the earth a decision of the probability of the bulk theory against any "core" theory—claiming the sources of the geomagnetic field to be placed in the core of the earth—might be made through measurements of the variation of the main geomagnetic field with the depth below the surface of the earth. While the horizonta field component H in the field of a core dipole will increase downwards by 0.05 per cent of the surface value per 1,000 meters, it was proved by S. K. Runcorn (1948) and S. Chapman (1948) that H after the bulk theory will decrease by 0.1 per cent per 1,000 meters (a separate formula is advanced, claiming a decrease of only 0.003 per cent per 1,000 meters at sea, giving local significance to the lower mass flux of sea water in proportion to crustal rocks). The vertical field component Z is in both cases expected to increase downwards by 0.05 per cent of the surface value per 1,000 meters. Under these circumstances, it would just be possible with existing field instruments to carry out measurements which in a decisive way may distinguish between the two opposite interpretations of the main geomagnetic field.

The strong claim of accuracy still makes measurements ashore in mines and collieries a very delicate business. The most significant measurements of this kind were made by Runcorn, Benson, Moore, and Griffiths (1951) in five collieries in Lancashire and Yorkshire. A remarkably extensive field survey was undertaken and immense care exercised in making proper corrections for local anomalies arising from the rocks of the igneous basement of the region (partly known in depth and relief from collieries and bore-holes), as well as from quite local disturbances in the mine galleries. In this survey, Runcorn, *et al.*, on the average, found the H field to increase downwards even more rapidly than expected after a core dipole theory, the difference being ascribed to a local anomaly of great extent affecting the three collieries of largest increase in H.

To avoid the great difficulties encountered in magnetic work in mines, an attempt to carry out similar measurements at sea naturally suggests itself. First of all, the attainable depths are much greater at sea, and the stations of measurement may be chosen in places where the important H component is particularly large, the oceans offering many deep basins near the magnetic equator.

As to the quite local disturbances, the advantage of working in a non-magnetic and homogeneous medium as ocean water is obvious. Local anomalies of greater

extent, arising from awkward distribution of more or less magnetic rocks in the sea bottom, claim careful consideration, a demand which may be difficult to fulfil as long as very little is actually known about the composition of the bottom rocks of the oceans. But even in this case, measurements at sea may be preferred to land measurements, because it is comparatively easy with instruments lowered from a vessel to make measurements in different depths at the same station, for example, for every 500 or 1,000 meters below the surface, thus making it possible to distinguish the depth at which the magnetic effect of the bottom rocks is asserted. With a suitably developed technique, even horizontal surveys of the local anomalies from the sea bottom may be made, when the surveying vessel is sailing with the instruments in any fixed depth.

Opposing these favorable conditions for sea measurements are some equally obvious disadvantages—in the first place, the difficulties of construction of adequate instruments for the purpose.

The very short time available for preparation of the magnetic work prevented a more detailed analysis of suitable instrument types for the expedition. However, it proved possible to build three magnetometers, mainly designed on principles known from previous Danish instruments of the la Cour types. Two of these instruments, working on quite different methods, were designed to measure the important H component and the other to measure Z.

As all the instruments mentioned were constructed for use in atmospheric air, they had to be protected against the water during lowering in the sea by non-magnetic containers. Containers which could be lowered even to the very greatest depths of the oceans were aimed at from the beginning. Consequently, the containers had to be able to withstand a hydrostatic pressure of 1,000 atmospheres, so great wall thicknesses had to be used, which in turn resulted in very heavy units.

Of the restricted allowance for working time during the expedition, a considerable part had to be spent on tests of containers and instruments. Further, the problem of checking, at least to a certain degree, the movements of the containers at the end of the long wire, proved to be rather complicated.

During the cruise of the *Galathea* in African and Indian waters in 1950-51, most of these problems were solved. Early in 1952, the expedition vessel crossed the Pacific, and there we were able to carry out more elaborate trial measurements. These measurements proved that at least one of the H magnetometers was able to operate, even at great depths, with the accuracy aimed at, that is, 10γ in a single relative measurement. However, a most unfortunate breakdown of the trawl-winch and a reduction of the cruise due to lack of means to meet rising costs prevented the exploitation of the experiences procured so far in final decisive measurements (Arley, Andreasen, Espersen, and Olsen, 1953).

INSTRUMENTS

Containers—The containers intended to protect the magnetometers against the water are cast in a bronze alloy, completely devoid of any iron, produced by Messrs. Paul Bergsøe and Son, Copenhagen, especially for our purpose (Lunn, 1953). Of this alloy, Messrs. Burmeister and Wain, Copenhagen, constructed two containers in the form of hollow spheres, the shape meeting best the requirement for resistance against hydrostatic pressure. In Figure 1 are shown the two con-

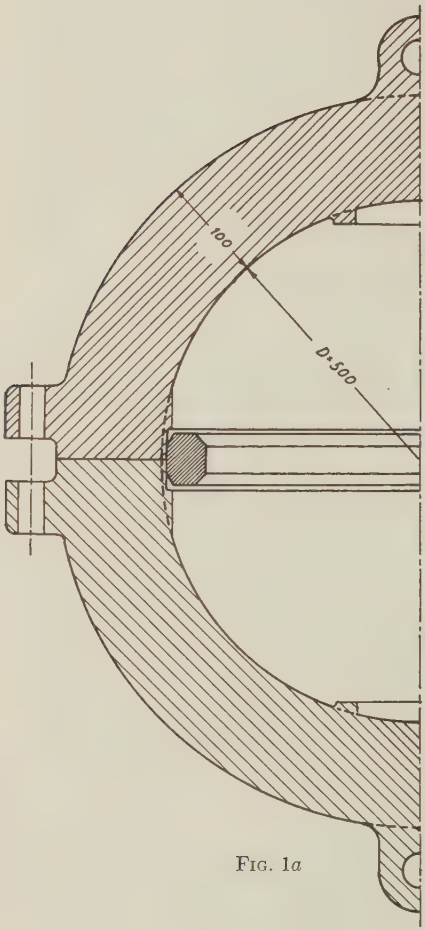

FIG. 1*a*

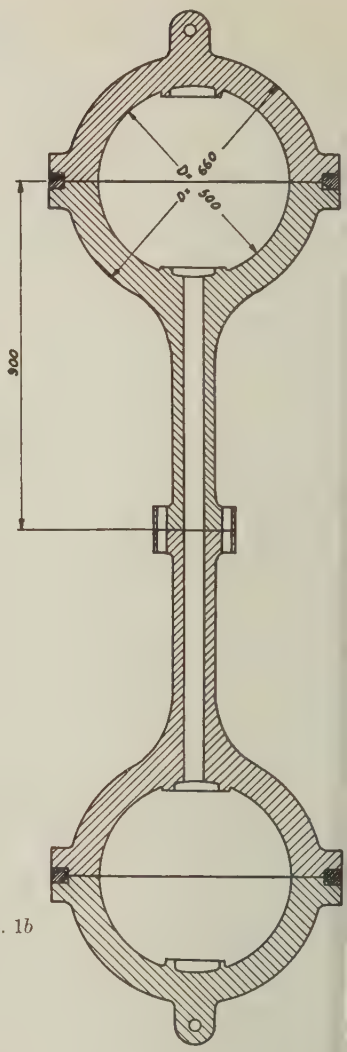

FIG. 1*b*

FIG. 1—The containers: (*a*) the single sphere; (*b*) the double sphere

tainers, one being a single sphere, internal diameter 50 cm, wall thickness 10 cm weight 1,100 kg, while the other is a double sphere made up of two identical singl spheres, internal diameter 50 cm, wall thickness 8 cm, and a connecting tube 10 cm long, internal diameter 5 cm, wall thickness 3 cm. The total weight of th double sphere is 1,700 kg, and the total height 270 cm. For technical details, test at sea during lowerings to 10,000 meters and 6,900 meters for the single and doubl sphere, respectively, and results of measurements of elastic properties during suc lowerings, the reader is referred to Arley, Lunn, Nielsen, and Nørgård (1953).

Magnetometers—The three magnetometers were constructed by Messrs Andersson and Sørensen, Copenhagen. The detail design was carried out by E

Johansen, engineer, on proposals outlined by J. Olsen (RNM-Z), J. Egedal (RNM-H), and J. Egedal/G. Brun (RCM-H).

Recording needle magnetometer, Z-component, RNM-Z—Only one Z instrument was planned, as measurements of changes in the Z component could after all merely be used for control and not for gaining decisive information as to the reliability of one of the theories to be tested. Furthermore, most of the measurements were planned to be carried out in areas with a strong H field and accordingly weak Z field.

The BMZ (la Cour 1942) forms the basis of RNM-Z, which is actually a slightly rebuilt BMZ suspended in a gimbal stand and used as a variometer. By means of a simple optical arrangement, the instrument is made photographic recording; and by the insertion of a testing coil, it is made self-adjusting.

In the partly schematic sketch, Figure 2, N is a usual balance magnet, suspended in a horizontal position and able to rotate in a vertical plane about a horizontal axis perpendicular to its magnetic axis. As in the BMZ, N is a monad magnet, the magnet, mirror, and knives (resting on agates, not shown) being made of one piece of steel. The light from the single-filament lamp L passes through a prism-lens-mirror system to the slightly inclined mirror of N, and from there to the film R in the film casing Q, thus recording the movements of N. The light from a fixed mirror F and from a mirror T attached to a bimetallic lamella will also reach R, resulting in a base and temperature recording, respectively. The broken light-path from N to R increases the magnification without demanding an unjustifiable height of the instrument. Small copper blocks D around the poles of N serve to damp oscillations of the needle.

The film is pulled forward by the clockwork U, which likewise through the bar system B pulls the clamping device A. By means of this device, N may be clamped for a given time at the beginning of a measurement to protect the needle during the rough handling of the sphere when it is put out from the ship. Further, during the whole measurement, the clockwork every quarter of an hour clamps the needle for a short time. On its top, A carries a saddle-formed piece, which gently lifts N from the agates when A is raised. If the needle for one reason or another (for example, radical movements of the sphere during lowering or heaving) has shifted its position on the agates, the saddle is formed so as to lead the needle back to its normal position during the clamping.

The magnetic axis of N being horizontal, the center of gravity of N is situated exactly vertically below its axis of rotation, and the horizontal (or "neutral") position of the needle is thus obtained in a zero Z field. At any station of measurement, the geomagnetic Z component—as derived from the tables of Vestine, *et al.* (1948)—is compensated by means of the vertical permanent magnet C, thus procuring as nearly as possible a zero field at the place of N. C may be adjusted in vertical direction by the micrometer-screw K, covering in this manner a wide range of Z (a series of five reversible compensating magnets is used, covering Z fields from $\pm 8{,}000$ to $\pm 55{,}000\gamma$). To begin with, RNM-Z, of course, is a relative magnetometer, but as it is experimentally adjusted in an observatory ashore for all expected Z values and temperatures, it is able to reproduce the actual Z field within an error—as far as the uncertainty in the setting of C is concerned—of only two to three gammas.

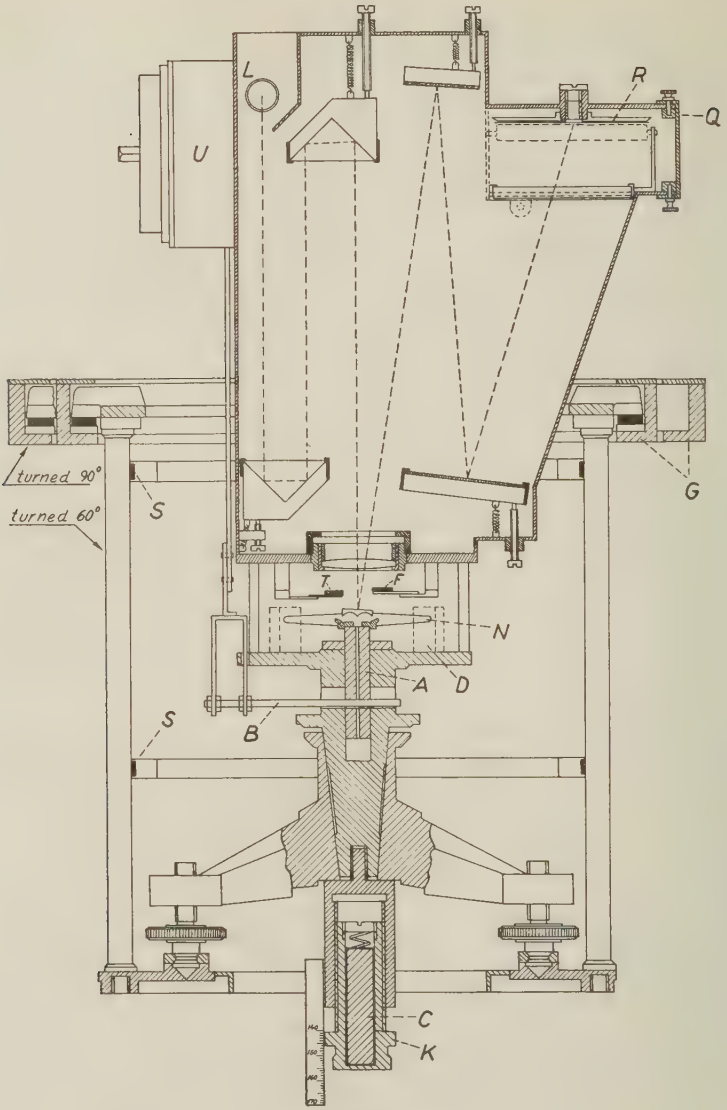

FIG. 2—RNM-Z

As in a normal variometer, the deviation of the needle N from the neutral position gives a measure of the uncompensated or residual Z field. For a given value of H, the scale-value E_t is varying, of course, with the instantaneous azimuth t (from north eastwards) of the needle (sphere) after the well-known relation

$$E_t = E_0 + H \cos t/3438 \ \gamma \text{ over minute of arc } (H \text{ in } \gamma)$$

E_0, the scale-value in the east-west position of the magnetic axis of N, is a basic instrumental constant involving the dimensions and magnetic moment of N,

which for the present instrument is chosen as 14.5 $\gamma/'$, answering to 48.0 γ/mm on the record.

It has been necessary, therefore, to introduce a testing device in the form of the double coil S (Fig. 2). Controlled by a contact arrangement in the clockwork, a known current is switched on every 2.5 minutes for 30 seconds in S. The magnitude of the resulting extra Z field acting on N being known, the topical scale-value may consequently be calculated from the corresponding deflection of N. S, as well as the lamp L, is generated from a six-volt battery of dry-cell accumulators, which it has been found keeps a suitably steady voltage for a very long time. Since a technique of measurement has been worked out where the azimuth of the sphere, although unknown, is kept fairly constant during a lowering, this method of securing the scale-value should be reasonably accurate.

From the relation given above, it is readily seen that the variation of E_t with t is inconveniently great for strong H fields. Measurements have been carried out at stations with an H of little more than 30,000γ, which gives for E_{south} only 19 γ/mm, but on the other hand for E_{north} not less than 77 γ/mm on the record.

From these figures, a measurement which by chance takes place with the needle pointing at south may be regarded as the best attainable, the sensitivity having here a maximum (minimum of scale-value). However, this has turned out not to hold good. Unavoidable oscillations of the instrument in the gimbal suspension give rise to a widening of the recording track, which has proved to be the greatest source of error in the measurements. As the widening of the track grows worse with greater sensitivity (the sensitivity, moreover, being measured by the difference between two tracks), the attainable accuracy has proved to be very nearly the same in all azimuths.

As a consequence of this, a high value of E_t must on the contrary be hoped for, as this gives the largest range of measurement. The effective recording interval of the film is only 50 mm, and with the neutral division placed in the middle of the film, this gives with a scale-value of 19 γ/mm a range of less than 500γ to each side of the field chosen for compensation. As local deviations from the figures given by Vestine, *et al.*, of this order of size are often met with, a small value of E_t is rather dangerous.

The instrument as a whole is suspended in a solid frame in the Cardan rings G (Fig. 2). In this construction, a place fairly near to the Cardan center is obtained for the important needle N. Unfortunately, this arrangement caused a rather high position of the center of gravity of the Cardan-suspended system, which makes it somewhat unstable to movements of the outer part of the gimbal stand (sphere). Two levels (not shown) indicate the vertical position of the suspended system.

The mentioned widening of the recording track caused by the rapid and irregular movements of N did not permit us to reach the desired accuracy of 10γ in a single measurement. Of course, the accuracy of a measurement may be raised by keeping the instrument in the depth concerned for a long time, the average of readings on a long record being more accurate than on a short one, but even by this means we were unable to attain a satisfactory accuracy. However, we believe that merely an improved damping of the Cardan system and the needle N will remove the present shortcomings.

Recording needle magnetometer, H-component, RNM-H (Fig. 3a, 3b, and 3c)—Like RNM-Z, this instrument is a known field-type instrument, which is adapted for use at sea and made photographic recording (Egedal, 1953).

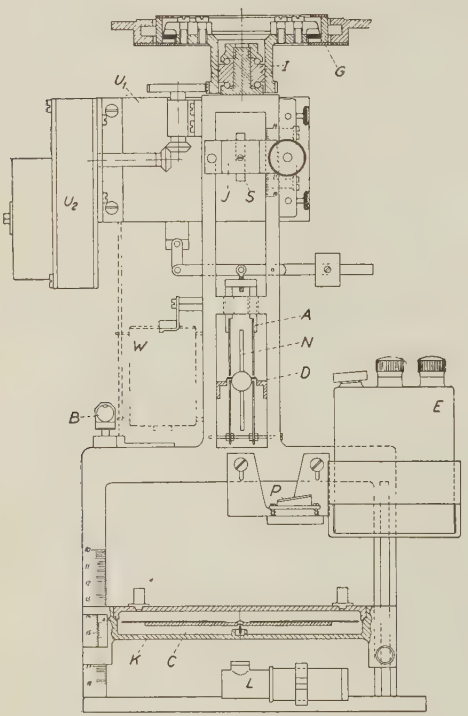

Fig 3a

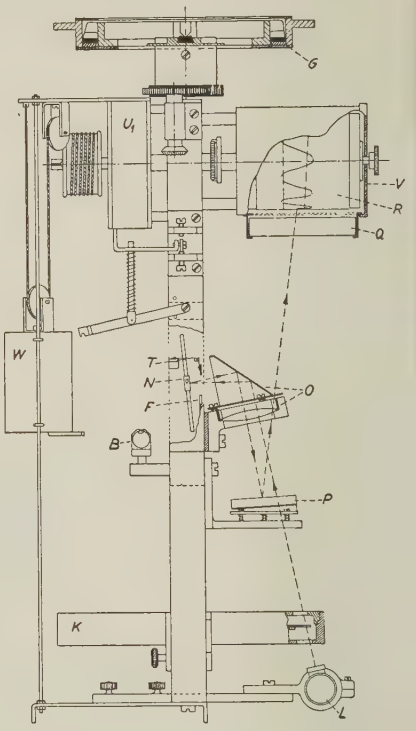

Fig. 3b

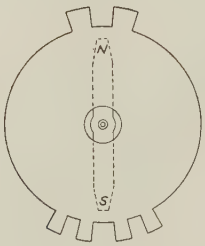

Fig. 3c

FIG. 3—RNM-H: (*a*) front view, with film casing and lens system removed; (*b*) side view, with clockwork U_2 and accumulator removed; (*c*) compass-needle C with screening disk

Here again the essential part of the instrument is a monad magnet N, although this time suspended in a vertical position, its horizontal axis of rotation being defined by the knife-edges of N resting on the agates D. The center of gravity of N is placed in the axis of rotation, which serves to diminish the influence on N of

movements of the instrument as a whole, and consequently N takes up a vertical position when the H field is zero, kept in this position by the vertical component Z, provided, of course, that the vector of the magnetic moment of the needle is pointing in the positive direction of Z.

The compensation of H at a station of measurement (as computed from the tables of Vestine, *et al.*) is made by means of the horizontal compass-needle C, which in its casing (the circular box K) may be moved in a vertical direction to yield a wide range of H fields at the place N. For the instrument in question, two compass-needles with different magnetic moments are covering H fields ranging from 10,000 to 40,000 gammas.

The optical system consists of the point-lamp L (energized by the dry-cell accumulator E), from which the light through the lens-prism system O reaches the mirror of N. Reflected from the mirror, the light passes O once more, and after a reflection in the oblique mirror P goes to the photographic recording paper R in the casing V, passing the cylindrical lens Q. A fixed mirror F and a mirror T attached to the end of a bimetallic lamella provide recordings of the base-line and temperature, respectively.

The recording paper is pulled forward by the clockwork U_1 . By means of a bar system, U_1 also draws a clamping device consisting of the vertically movable strips A, which by means of V-shaped slits are able to raise N by the knife-arms and always let it down again on the agates in a definite position. N may be clamped for a chosen time at the beginning of a measurement, and later is clamped for a short time every 15 minutes. The start-clamping is maintained by means of the weight W for U_1 .

The instrument is built on a solid brass frame, suspended in the gimbal stand G.

As the measurements in question deal with a field component onto a plane (and not, like Z, along a line), it is necessary to measure in a definite azimuth, preferably, of course, in the magnetic meridian. As the arbitrary azimuth of the sphere however cannot be controlled at will, the problem has been solved by making the instrument rotate about a vertical axis, defined by the ball-bearing I in the inner part of the gimbal stand. The clockwork U_2 pulls the apparatus with the measuring system as a whole around in the Cardan suspension, one revolution being completed in about 10 minutes (if the sphere itself is spinning, the time interval will naturally change). Now a possible small residual field H acting on N will cause a sine-formed recording track (or a straight line if $H = 0$), the extremes of the sine wave answering the passages of the magnetic meridian. The amplitude of the sine wave will be a measure of H.

The light from L on its way to O passes through holes in the bottom and lid of the box K. The compass-needle C is provided with a screen formed as a thin circular disk with projecting lamellas (Fig. 3c), which break the light-beam just before and after the needle N (more exactly, the perpendicular to the mirror of N) passes its north and south positions—once in north and twice in south, to distinguish the two passages. Consequently, these important passages appear as conveniently separated points on the photographic record. The screening disk of C at the same time serves to subdue oscillations and rocking movements of C around its supporting point.

It will be quite obvious that, besides the delicate workmanship of the important

magnets, the salient point of the instrument is the mechanical elaboration of the axes entering the design. Even if it is not quite necessary, it is from a constructional point of view an advantage if the main instrumental axis of rotation goes through the Cardan center, and, consequently, for maintenance of its vertical direction, through the center of gravity of the suspended system. Further, the point of intersection between the magnetic axis and the axis of rotation of the needle N, as well as the tip of the needle supporting C, must lie in the vertical axis of rotation of the instrument as a whole. Finally, the axis of rotation of N has to be exactly horizontal. During the use of the instrument, it proved in the long run difficult to comply with these rigorous demands, especially since testing devices for the position of the axes (such as the levels B) cannot be used at sea. However, the errors caused by failures of this kind were at all times minor compared to the inaccuracy due to movements of the instrument in the Cardan suspension.

In the magnetic meridian, which is the only azimuth to be considered, the condition of equilibrium for N, making the small deflection p from the vertical under the influence of the residual horizontal field H, is the following:

$$H = Ztgp \simeq Zp \ (p \text{ being but a small angle})$$

and the scale-value becomes

$$E = dH/dp = Z\,\gamma \text{ per radian } (Z \text{ in gammas})$$

or

$$E = Z/3438\,\gamma \text{ over minute of arc } (Z \text{ in gammas})$$

Thus, the scale-value is controlled solely by the value of Z. By the introduction of the vertical permanent magnet S (Fig. 3a) in the vertically adjustable holder J, the Z field acting on N, and thereby the scale-value, may be given any wanted value. The record space of the photographic paper is 55 mm.

As with RNM-Z, the main source of error in measurements at sea has proved to be the inevitable movements of the instrument in the Cardan suspension during an immersion, these causing irregular movements of the needle N resulting in an inopportune widening of the recording track. An improved damping of the moving systems may raise the quality of the record. However, as RNM-H is fairly well balanced in the gimbal stand, the movements of N are not really fatal. Since most of the irregular motions of N have proved to be generated from small rotational oscillations of the compass-needle C about its vertical axis (generated in turn from similar oscillations of the sphere in the wire), this is valid, at least in the significant meridian positions where such oscillations have very little influence on N. [If H_c is the compensating field exercised by C at the place N, and if C makes the small (varying) angle v with the meridian, the field affecting N in the meridian positions is $H_c \cos v$, being practically like H_c . In the east and west positions of N, on the other hand, the component of H_c affecting N is $H_c \sin v$, which varies rapidly with v.]

After the development of a suitable measuring technique, successful relative measurements with an accuracy of 10 to 15 gammas for a single revolution of the instrument were made to a depth of 3,000 meters.

Like the Z instrument, RNM-H is planned merely as a relative instrument, but it is experimentally adjusted in known fields and temperatures in an observatory ashore.

Recording coil magnetometer, H component, RCM-H—The great importance attached to measurements of the H component justified the attempt to construct another relative H magnetometer, a spinning-coil type being selected, as it appeared rather promising for sea use.

Whereas RNM-Z or RNM-H may be housed in the single sphere, RCM-H requires a double sphere to remove the necessary (and partly magnetic) auxiliary gears to an appropriate distance from the measuring coil proper.

In Figure 4*a* is shown the measuring arrangement in the lower half of the double sphere. Its essential part is the coil N, which has 10,000 windings with an average diameter of 10 cm. The vertical axis of rotation, being a diameter of N, is defined by the brass cups B running on the agate cones A, lubricated with graphite grease. The alternating current induced in the coil when spinning is picked up through the slip-rings P and the plain-strip phosphor-bronze brushes Q. The vertical position of the axis of rotation may be controlled by the level L.

Like in RNM-H, the geomagnetic H field (as computed from the tables of Vestine, *et al.*) is compensated for by means of a horizontal permanent magnet C in the form of a compass-needle, capable of being adjusted in vertical direction in the casing K. However, in this instrument, the magnet C is automatically temperature-compensated by means of permalloy strips.

The measuring system as a whole is mounted solidly in a brass frame, which is again suspended in the gimbal stand G. In its lower end, the frame is provided with damping wings D intended to reduce oscillations in the gimbal suspension. The wings D are immersed in a vessel with viscid oil standing in the bottom of the sphere.

The arrangement of the attendant gears in the upper sphere is shown roughly in Figure 4*b*. By means of a brass-tube shaft through the tube connecting the spheres, a motor drives the coil at a speed of about 1,200 r.p.m. The transmission between the shaft and the coil is accomplished by means of two flexible joints over a ball-bearing (Fig. 4*a*). The motor is generated from a 10-volt accumulator battery.

The a. c. from the coil is sent through a cable to an electronic amplifier in the upper sphere, where it is amplified and rectified at the same time. The output direct current operates an ordinary recording ammeter.

With the aid of a contact clock, the apparatus may be switched on at a chosen time, and later on switched off again. Thus, it is possible to postpone the start of a measurement while the sphere is put out from the ship.

The measuring arrangement of the instrument having been described, its working principle may be explained easily. As the a.c. voltage induced in the coil is proportional to the area of windings and the frequency of rotation of the coil, and to the residual horizontal field H at the place N, this is valid too for the reading of the ammeter. To avoid the inconvenient dependence on the frequency, the constancy of which cannot be maintained with the accuracy desired, the amplification is by way of a feed-back arrangement, made exactly inversely proportional to the frequency of the a.c. in the range 15 to 25 cycles per second. As the area of windings is an instrumental constant, the readings of the ammeter consequently become directly proportional to H, and only H.

The following figures will illustrate the constants of the instrument. A residual

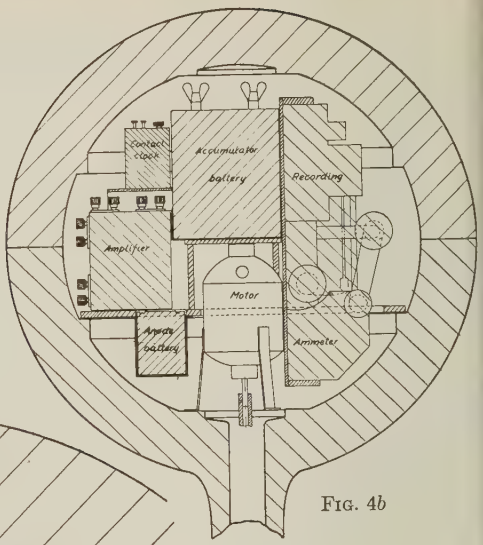

FIG. 4b

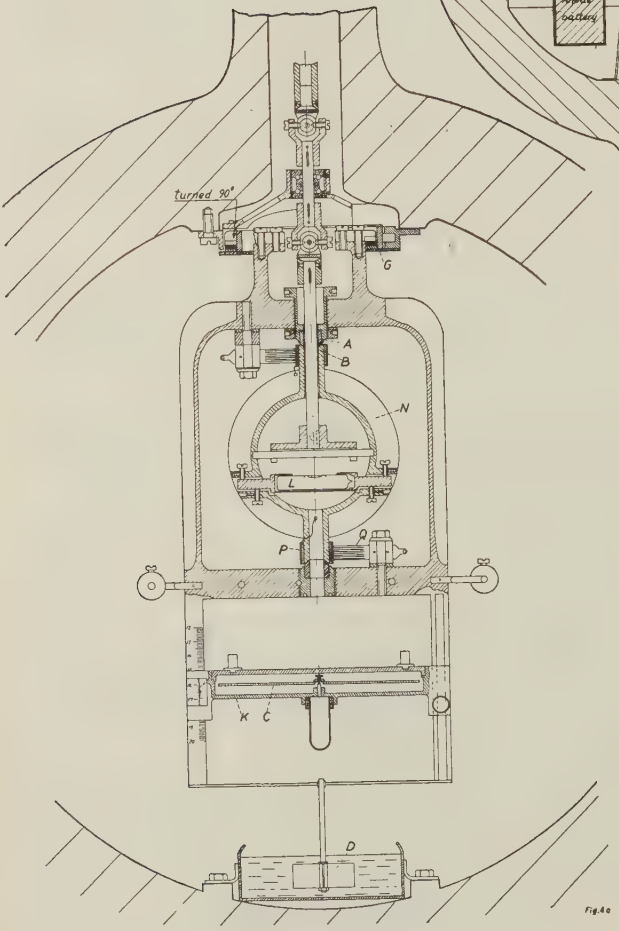

FIG. 4—RCM-H: (*a*) lower sphere; (*b*) upper sphere

H of 500γ gives rise to an a.c. voltage of about 5 mv, which is amplified to abou 1.5 v of d.c., and which over the resistance of 3,000 ohms in the ammeter give a d.c. of 0.5 ma. As the ammeter has a total range of 0–1 ma, corresponding to

record space of 100 mm, this gives a scale-value of around 10 γ/mm and a range of registration of 1,000γ.

The coil cannot, of course, distinguish between over- and under-compensation, and therefore the expected surface field is compensated only to a residual H of 500γ, corresponding to the middle position of the record. If local anomalies of more than 500γ in H are suspected, the amplification may be reduced 3, 5, or 10 times by application of attenuators, raising the range of registration by the same factors, but of course with a corresponding loss of sensitivity.

This instrument also is experimentally adjusted at an observatory in known H fields.

Inaccuracies due to parasitic voltages arising from different reasons in the slip-rings and brushes of the coil, and to failing constancy in the amplification, difficulties which are well known from similar measuring arrangements, may all be controlled to a sufficient degree.

The main source of error in RCM-H, however, is expected to be rotational oscillations of the compass-needle C, which are inevitably generated by similar movements of the sphere. As soon as C deviates from the meridian, the vector difference between the geomagnetic H field and the field of C at the place N will increase considerably above the meridian (minimum) value. For a geomagnetic H field of 30,000γ and a residual field (in the meridian) of 500γ, the change of the resulting H runs into 16γ for a deviation of C from the meridian of only 15′—a quantity easily met with in laboratory experiments where "sea conditions" are imitated. For a deviation of 30′ and 60′, the errors are 65 and 225 gammas, respectively.

As a matter of fact, it has not been possible to test these objections to the instrument at sea. Purely practical troubles, that is, the difficulties in handling the unwieldy double sphere on board a rolling vessel, have allowed only two trial measurements with RCM-H during the cruise, and both times the record was spoiled because of mechanical breakdowns in the ammeter. So practically no evidence of the measuring ability of the instrument at sea was obtained.

TECHNIQUE OF MEASUREMENTS AT SEA

In the account of the properties of the instruments, it is emphasized how far it has been possible to adapt their measuring ability to the working conditions prevailing in the spheres when they are lowered from a ship following the gentle swell of the ocean. However, a happy issue of a measurement also involves an appropriate measuring technique, suitable to meet the special difficulties encountered in measurements at sea. In the following, a few of the more significant problems encountered will be outlined.

As the measurements in question had to be carried out in a normal iron vessel, the surface measurements could not take place on the ship itself, but had to be made in a depth of 500 meters—the smallest depth at which magnetic disturbances from the ship may be considered insignificant. Disturbances from the supporting steel wire were avoided by the insertion of 15 meters of copper wire between the main wire and the sphere.

Possible changes in the geomagnetic field due to daily variation cannot be ascertained during a measurement, unless the station is by chance situated very

near a magnetic observatory, which naturally is very unlikely. However, the effect to be measured is rather great compared with normal daily variation, but if it develops later that a measurement has taken place on a magnetically very-disturbed day, this measurement may have to be cancelled. But on the *Galathea*, most of the magnetic work was practiced during the night when the variation is least.

A more serious source of error is the variation of the field due to horizontal movements of the vessel over the bottom during a measurement. Even if the vessel does not use its propellers, wind and ocean current will shift the position of the ship, and a planetary correction for field change is accordingly necessary. In the open ocean, it is normally not possible to make use of the modern radio-navigation methods. Nautical methods are accurate to 0.5-1 nautical mile, which is sufficient in most cases, but they are useless in cloudy weather. On the *Galathea*, this problem was avoided by making surface measurements (in a depth of 500 meters) before as well as after lowering of the instruments to greater depths. As the ocean currents, which will in the main control the drift of the ship, are very steady in speed and direction, the ship will be moving principally in the same direction during the entire measurement. By using linear interpolation regarding time between the two surface measurements, a suitably accurate planetary correction is obtained. This method also has the advantage that a possible drift in the base-values of the instruments is corrected for at the same time, provided the drift is linear in time.

The difficulties in the very management of the ponderous double sphere on board the rolling vessel have already been mentioned. Even the handling of the single sphere, however, proved to be rather troublesome, and in the first part of the cruise many breakdowns in the instruments were caused by heavy thumps of the sphere against the ship when it was put out or taken in. After the introduction of special fenders and other assisting gears, these shortcomings were mainly overcome, but "sphere weather" still comprised only perfectly calm weather conditions.

Very early, it proved necessary to master, at least to a certain degree, the movements of the spheres when hanging in the water on the end of the wire. Most of our troubles originated from a swift rotation of the spheres due to the untwisting of the wire when it was running out and suddenly was loaded with the heavy sphere. Originally the copper wire was provided with a small four-armed damping wing and connected to the main wire by means of a swivel link, but this damping device appeared to be absolutely worthless.

In order to investigate thoroughly this important problem, a special instrument was invented to record the movements of the sphere during a lowering. The applicability of different damping systems was tested (Andreasen and Espersen, 1957), and as a result of the measurements a one-bladed damping wing—or rather a damping rudder—in combination with a more effective swivel was decided on.

In its final elaboration, the rudder consisted of a 2-meter long and 50-cm high aluminum wing with modified stream-line appearance (see Fig. 6). Just above the rudder, a special light-running ball-bearing swivel is inserted between the copper wire and the main steel wire. When the surveying vessel is then given but a slight speed, the damping wing acts as a rudder, stabilizing the copper wire with the sphere in a fixed azimuth, while the swivel takes the untwisting of the steel wire

FIG. 5—Double sphere and single sphere (front, left) on the deck of the *Galathea*

running out. Later measurements demonstrated definitely that the remaining rotational movement is due only to small oscillations of the sphere in the 15 meters of copper wire below the rudder. Unfortunately, at the time, technical reasons prevented the placing of the rudder on the sphere itself, which is no doubt the final solution of the problem of controlling rotation of the spheres.

It has proved necessary to use a very large rudder, as the speed in the horizontal movement of the sphere in the water, particularly at great depths, will always be very slow, even for a considerable speed kept on the propellers of the ship, that is, "nominal" speed. This is due to the enormous dragging effect of the long wire suspended vertically in the water. This effect also prevented us from choosing the azimuth of measurement at will, which might otherwise be thought possible after the introduction of the rudder. The reason is partly because the slow speed of the ship relative to the surface waters normally will not reach the steering speed of the vessel, and partly because the speed and course of vessel sphere over the bottom can only rarely be calculated, as they are influenced by, besides the nominal speed and course of the ship, also by wind and current (comprising only the upper

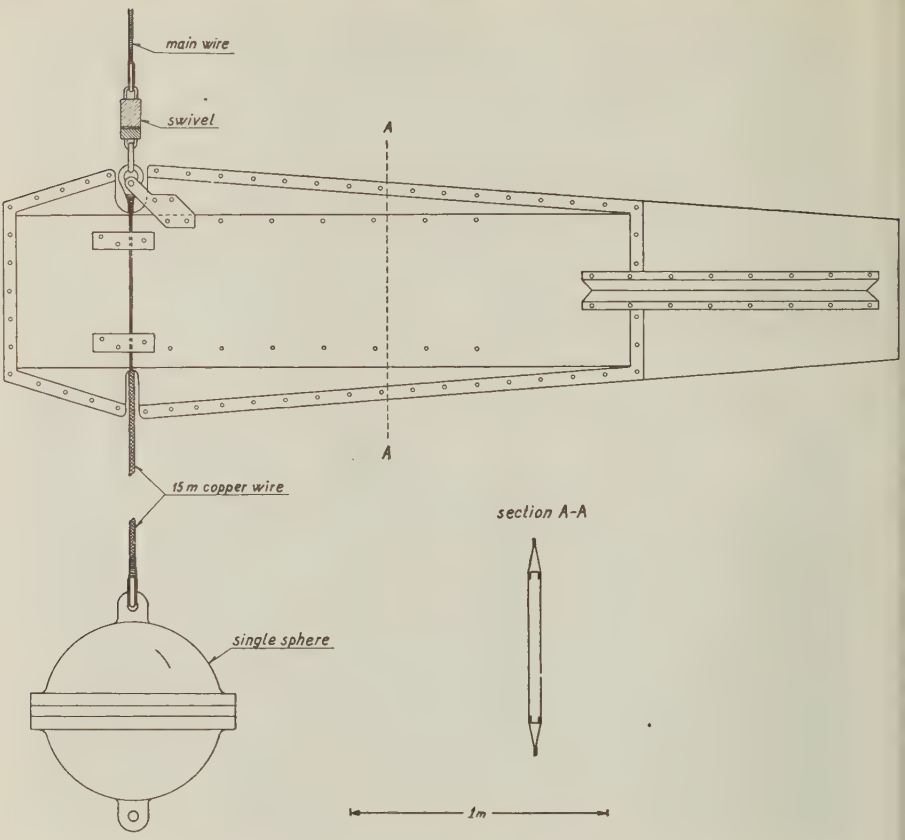

FIG. 6—Measuring arrangement with damping rudder and swivel

200 to 300 meters of water) acting on the vessel and upper end of wire, and the combined effect of these agents cannot be determined beforehand with sufficient certainty.

The records of the movements of the spheres also demonstrated that the spheres in any depth make pitching (vertical) movements of the same size and period as the ship itself. Furthermore, other different types of pendulous movements were found to exist—presumably oscillations of the sphere around its point of suspension and around its center of gravity. Nothing could be done under the circumstances to reduce these movements, but a series of laboratory investigations in which sea-conditions were imitated as nearly as possible indicated that moderate movements of this type would not be fatal.

MEASUREMENTS IN THE PACIFIC OCEAN

In advance, the Pacific was looked on as the principal working place for the magnetic investigations of the expedition. In the central part of the ocean, extensive basins are found with an extraordinary plain bottom and an average depth of 5,000 to 6,000 meters. The plains are undoubtedly due to the smooth outflow of

highly mobile lavas of ultrabasic composition, the floor of the Pacific being generally accepted as pure Sima without any cover of Sial (east of the andesite line). Even if the nature of the rocks suggests a high magnetic susceptibility, the bottom may be supposed to have a very uniform composition and to be quite homogeneous over the great areas in question. Local anomalies, therefore, should be very unlikely to exist, and the level surface of the bottom excludes dangerous topographic effects. A station with a strong H field in one of these basins should be an ideal place for measurement of the vertical gradient of H, the expected increase in H after the core theory running into almost 100γ for a depth difference of 5,000 meters.

Certainly a single aeromagnetic (total intensity) traverse over broad ocean areas—from Adak, Aleutian Islands, to Kwajalein, Marshall Islands—has been reported (Alldredge and Keller, 1949), which reveals several relatively large anomalies over deep areas, presumably arising from unexpected susceptibility contrasts in the ocean bottom, but the anomalies may be caused by uncharted topographic relief escaping the hydrographic charts due to the scarcity of depth data. However, there are extended sections of the traverse of more than 150 km with quite uniform field.

During the months of February and March 1952, the *Galathea* crossed the Pacific from New Zealand to the United States. Utilizing earlier results, the magnetic equipment had been rebuilt and improved, and at stations in the deep Kermadec-Tonga trench a series of final trial measurements were carried out with the aim of gaining experience concerning the best working conditions during a lowering for all instruments, especially as regards the choice of speed of the surveying vessel for the best exploitation of the new damping rudder.

The narrow trench which extends most of the way from New Zealand to the Samoan Islands (2,000 km)—see Figure 7—actually forms the boundary between the complex Melanesian region to the west and the uniform Pacific basin to the east. The trench was an important working place for biological investigations, but was, of course, unsuited for ultimate magnetic work, which was planned to be carried out later in the central Pacific.

Before the trial measurements were finished, however, a most unfortunate breakdown of the big trawl-winch impeded further measurements. The magnetic work could not be resumed until the month of May, when the expedition vessel had reached the Gulf of Panama. A few lowerings were made there at a station, where again disturbances in the geomagnetic field from the bottom rocks spoiled the relative field values. However, we succeeded in proving that measurements with RNM-H could be made with the accuracy aimed at, which means that this instrument under the best attainable working conditions in the sphere will be able to render decisive measurements at undisturbed stations. The measurements in the Gulf of Panama were, however, the last which time allowed to be carried out on this expedition.

The results obtained at the trial stations will be given below for each station.

Kermadec trench, South—The name of this station is a little overstated, as the place was actually only just outside the Bay of Auckland on the continental shelf edge, midway between Auckland and the southern part of the trench. The mean depth at the place was 2,500 meters.

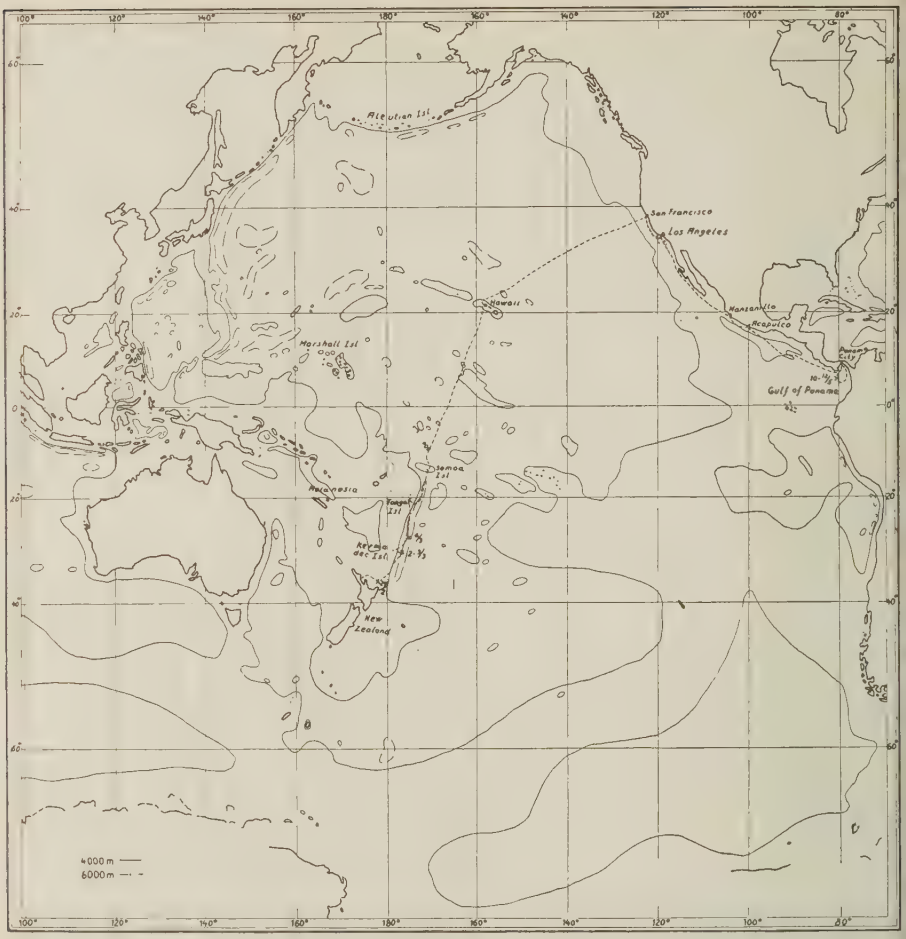

FIG. 7—Pacific Ocean: route with stations of measurements

The measurements only comprised brief lowerings to shallow depths for initial technical control of all instruments. However, weather conditions did not allow work with the double sphere and RCM-H, and a measurement with RNM-Z failed in so far as most of the record fell outside the film in consequence of a difference of at least 600γ between the actual Z field and the compensating field computed from the Vestine tables, combined with an accidentally low scale-value of the instrument in the azimuth taken up—and retained steadily—during the measurement.

With RNM-H, a successful record was obtained during a lowering of four hours to 500, 1,000, and 500 meters. In Table 1 are given the H values obtained for the middle of each clamping-interval, and the estimated experimental error ΔH involving the uncertainty in the reading of the record. The low accuracy of the results is caused by the very high scale-value chosen for this preliminary test. Further, the Table gives depth of sphere and bottom, and nominal course and

TABLE 1—*Kermadec trench, South; 36° 00′ S, 178° 00′ E; February 29, 1952*
Expected H: 26,300γ Instrument: RNM-H
Expected Z: −48,200γ Scale-value: 100 γ/mm

Local time		Depth of sphere	Bottom depth	Nominal		H	ΔH
				Course	Speed		
h	*m*	*meters*	*meters*	°	*knots*	γ	γ
18	10	500	1,970	90	2	27,130	±50
18	30	500	1,850	90	2–1	27,210	50
18	43	500	1,780	90	1	27,230	30
18	58	500	1,710	90	1	27,290	150
19	47	1,000	1,550	90	1	27,490	30
20	04	1,000	1,430	90	1	27,470	30
20	22	1,000	1,330	90–0	2	27,380	100
20	55	500	1,600	0	2	27,130	200
21	13	500	1,780	0	2	26,990	100
21	30	500	1,930	0	2	26,930	100

speed of the vessel. The figures of the Table are represented graphically in Figure 8.

During the lowering, the ship happened to navigate over an uncharted seamount. The nominal speed of the vessel was lowered, therefore, from 2 knots initially to only 1 knot. The nominal course, 90° (= east), was the course taken up by the vessel itself in the prevailing current (which was later estimated to be rather strong—around 1 knot—and so dominated the movement of vessel/wire/sphere). However, as the depth still diminished alarmingly, the speed was once more set to 2 knots to give steering speed, and the course was changed to 0° (= north), after which the depth soon began to increase again rapidly.

As will be seen, a difference of about 200γ appears between the averages of the H values in the two 500-meter measurements, and further the H value at 1,000 meters is almost 350γ higher than the mean of H at 500 meters. Apparently the H field also varies considerably during the periods of recording in a fixed depth. This remarkable change of H with depth and time must, of course, be due to the horizontal transport over and the changing distance to the irregular bottom (several smaller precipices could be identified in the echogram; the figures given for bottom depths are always average depth inside the angle covered by the echo-sounder).

The small relative change in H looked for, of course, is lost in the local disturbances. During the two stays in a depth of 500 meters, the instrument had been from 1,000 to 1,500 meters above the bottom, and yet variations of the H field of the order of size of 100γ occurred for a horizontal displacement estimated around one nautical mile. The importance of the influence of magnetic anomalies originating from the structure and petrological composition of the ocean bottom is thus strongly emphasized.

As regards the working conditions for the instrument during the lowering, the

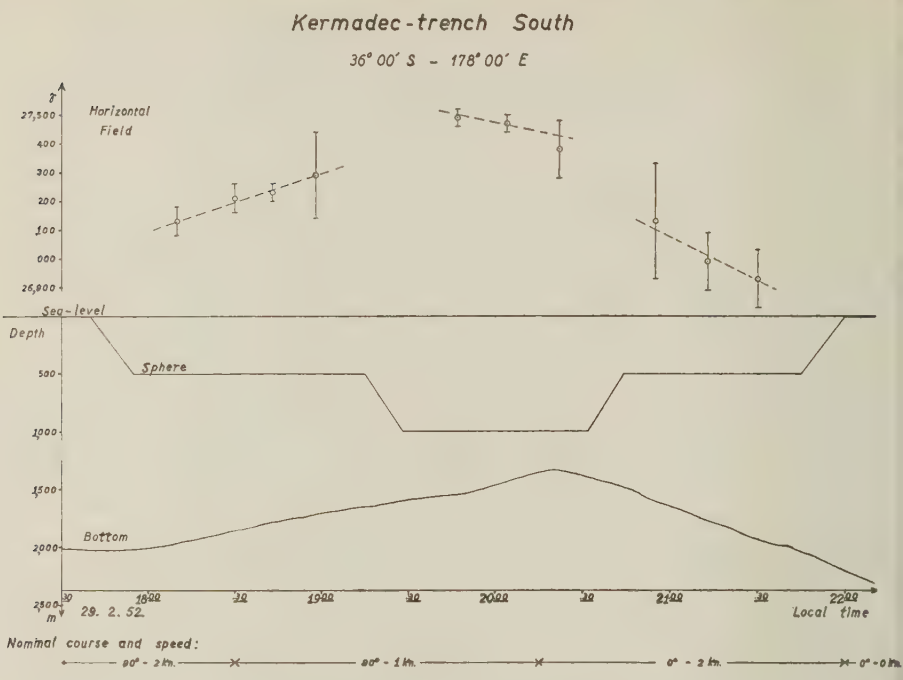

FIG. 8

record proved that even the slowest speed kept gave a very steady steering of the sphere, there being only exceedingly small rotational oscillations of the instrument. But, on the other hand, there were severe pendulations undoubtedly generated from vibrations of the wire, probably due ultimately to the screw-race of the vessel.

Kermadec trench, Middle —The first opportunity of making measurements at greater depths was offered in the central part of the Kermadec trench. In this place, the trench has only a width of 2 to 5 km, and in cross-section it is characterized by an extremely precipitous western acclivity, rising from a maximum depth of 10,000 meters to above sea-level in the Kermadec Islands at a distance of 120 km. The slope steepens with the depth. The offshore flank is less high and less steep, passing in its upper part gently into the ocean bottom to the east in a depth of 5,000 to 6,000 meters. A detailed account of the topography of the Tonga trench—which is also representative of the Kermadec trench—is given in the report of the Capricorn expedition (Raitt, Fischer, and Mason, 1955). This report, moreover, discusses possible basement structures as deduced from seismic refraction data and two magnetic surface profiles recorded with a towed total-intensity magnetometer. A most interesting detail of the magnetic profiles is the surprisingly smooth field revealed over the deepest part of the trench proper.

At a station placed over the middle of the narrow trench, a measurement was carried out with RNM-H to a depth of 5,000 meters with a stop of 45 minutes in 500 meters, 45 minutes in 2,000 meters, 30 minutes in 3,500 meters, three hours in 5,000 meters (partly due to a breakdown in the trawl-winch), and again 45 minutes

in 500 meters. To avoid pendulations of the sphere due to screw-race, no speed of the vessel was kept during the entire measurement. The results of the first measurement indicated that the ocean current by itself might be able to give a sufficiently firm steering of the sphere.

With an estimated current of half a knot, however, this hope proved to be valid only for relatively small depths. The steering was excellent in a depth of 500 meters, but rapidly grew less firm when more wire was put out, braking the speed of the vessel and sphere. The record could still be read in the depth of 3,500 meters, but in 5,000 meters the sphere was able to make great rotational movements which spoiled the record, and vessel/sphere consequently must have had practically no horizontal velocity. The pendulations, on the other hand, were diminished considerably.

For those sections of the recording for which readings could be made, the results are given in Table 2, and represented graphically in Figure 9. By linear interpolation as regards time, the H values in the depths of 2,000 and 3,500 meters appear to be 15γ and 50γ less than in 500 meters. This somewhat startling result, however, first of all has to be confronted with the uncertainties of the values which greatly surpass the differences found. Furthermore, the difference of 90γ between the two 500-meter measurements—which cannot be explained by drift in an undisturbed geomagnetic field (supposed drift from nautical observations: 3 to 4 miles west)—immediately suggests the existence of strong magnetic disturbances, which might also be expected considering the singular structure of the ocean bottom (this conception is not necessarily at variance with the Capricorn total-intensity results in the Tonga trench). If the surface field difference of 90γ is interpreted as being due to a disturbing effect from the enormous western precipice—toward which the vessel moved—the value of H at greater depth would be even more influenced by the anomaly, as the instrument in this case is much closer to the source of the disturbances.

TABLE 2—*Kermadec trench, Middle; 30° 23′ S, 176° 39′ W; March 2-3, 1952*

Expected H: 29,100γ Instrument: RNM-H
Expected Z: −41,400γ Scale-value: 80γ/mm

Local time		Depth of sphere	Bottom depth	Nominal		H	ΔH
				Course	Speed		
h	*m*	*meters*	*meters*	°	*knots*	γ	γ
19	20	500	9,580	250	0	29,420	±40
19	34	500	9,580	250	0	29,410	20
20	24	2,000	9,580	250	0	29,390	40
20	43	2,000	9,580	250	0	29,380	60
21	31	3,500	9,580	250	0	29,340	80
02	43	500	9,580	250	0	29,330	40
03	01	500	9,580	250	0	29,320	40

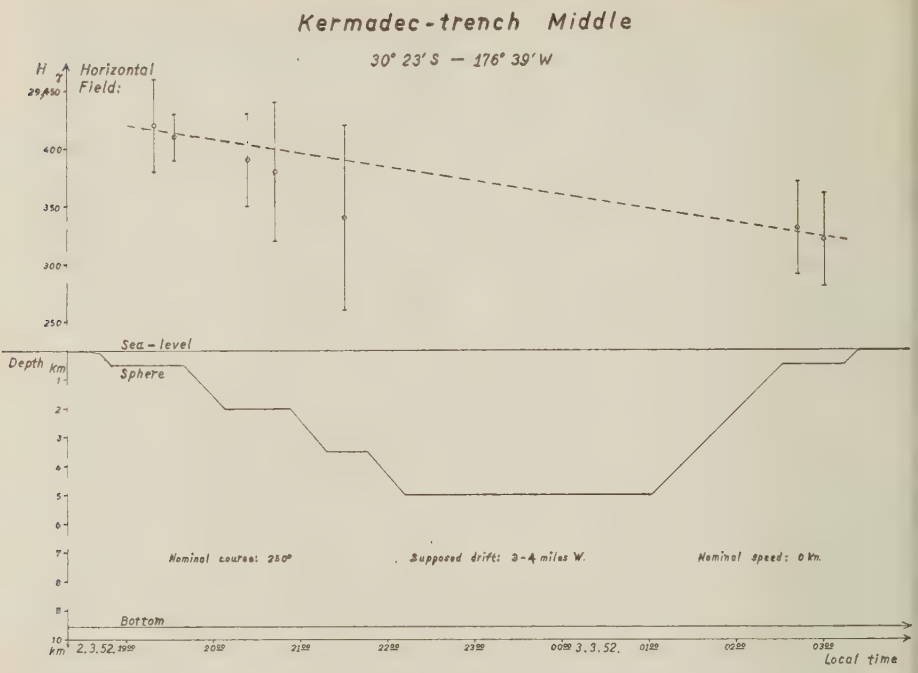

FIG. 9

Kermadec trench, North—Two lowerings were carried out in the northern part of the trench, which displayed here the same characteristic cross-section as in the central part. According to the last experience, the station of measurement was chosen a good distance east of the deepest part of the trench, the bottom depth varying here between 8,650 and 8,800 meters.

A measurement with RNM-H mainly failed, as the clockwork U_2 suffered a breakdown when the sphere was put out from the ship, after which it worked only at intervals. The fragmentary record furnished only two readings, one in a depth of 500 meters and one in 5,000 meters. Both give an H field of 29,950γ, but both cases are encumbered with an uncertainty of $\pm 100\gamma$.

Also the succeeding measurement with RNM-Z suffered from a technical mishap, affecting the current of the testing coil, with the result that the scale-value could not be computed with the expected certainty. In Table 3 are given the Z values for the depths of 500 meters, 5,000 meters, and again 500 meters, derived from readings of parts of the record where the coil current had apparently been constant for some time (the record obtained during a stay in 2,500 meters could not be read at all). The experimental error ΔZ is rather high owing to the mishap, but as the scale-value happened to be very great its uncertainty is at least limited in one respect because it cannot possibly overstep the maximum value for the H field.

From the graphical representation in Figure 10, it appears that a numerical increase downwards in Z is evident. The expected theoretical increase of 85γ also lies within the limit given by the uncertainties in the measurement.

TABLE 3—*Kermadec trench, North; 28° 15′ S, 176° 05′ W; March 6, 1952*
Expected *H:* 29,900γ Instrument: RNM-Z
Expected *Z:* −39,000γ

Local time	Depth of sphere	Bottom depth	Nominal		*Z*	Δ*Z*
			Course	Speed		
h *m*	*meters*	*meters*	°	*knots*	γ	γ
01 18	500	8,720	85	0	−38,250	+40 to −80
05 09	5,000	8,780	150	4	−38,470	+40 to −80
07 10	500	8,760	180	0	−38,340	+40 to −80

Local disturbances in this case appear to have been small, which was to be expected too, since the sphere had the entire time been at least 3,700 meters above a rather level bottom, and especially since the drift of the ship during the lowering was estimated afterwards to be only two to three nautical miles in a southward direction, that is, lengthwise the trench. The numerical increase in *Z* of 90γ between the two surface measurements is not definitely verified with the uncertainties involved. As it happened, a slight increase was to be expected, since the *Z* field increases southward by 18γ per nautical mile.

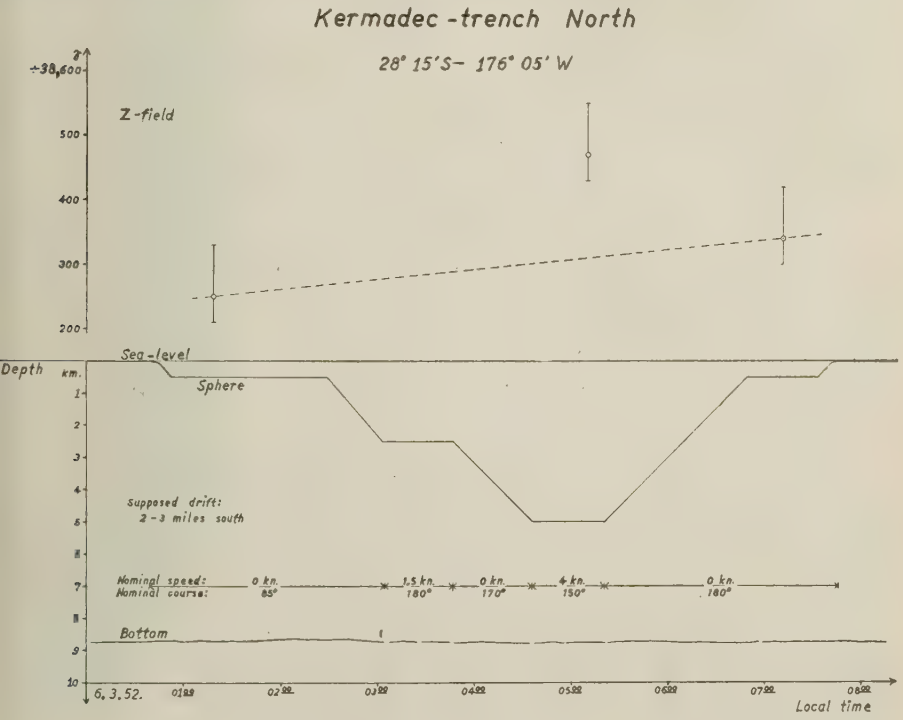

FIG. 10

The nominal speeds kept during the Z measurement (see Table 3) were determined by experiments during the H measurements as those giving, under the circumstances, the best attainable compromise between rotational oscillations and pendulations of the sphere.

Gulf of Panama, 5° 37′ *N*, 79° 37′ *W*—The position given for this station answers the center of a small narrow basin, 5 miles long (E-W) and two to three miles broad (N-S), with a maximum depth of 4,800 meters, situated in an area in the Gulf of Panama, where the normal bottom depth is otherwise only 3,000 meters. At this station, the last magnetic investigations had to be carried out, but the strong and irregular currents of the Gulf made the work over the small depression with its steep walls very troublesome, and the rugged bottom caused disturbances in the geomagnetic field which made all gradient measurements most unreliable.

During the Kermadec measurements, it had proved difficult to reach a satisfactory compromise between oscillations and pendulations of the single sphere. In accordance with this experience, the damping rudder was extended to a total length of 3 meters. To test working conditions with the new rudder, different nominal speeds were tried during the first lowering to the various depths.

The measurements commenced with RNM-H, which was lowered to depths of 500, 3,900, 2,600, and 500 meters. The stop in 3,900 meters was interrupted and the sphere raised, as the echo-sounder failed for a while (it was too dangerous to work without exact knowledge of the depth at this station). The sounder set repaired, the sphere was once more lowered to 3,900 meters.

At the beginning of the measurement, the ship was lying over the western part of the basin. The strong current (about two knots?) kept the vessel on a nominal course of 70° to 90°, and nautical observations indicated that the total drift during the lowering had been not less than 6 to 8 miles east-northeastward. The depth decreased during the lowering from 4,740 meters to 4,200 meters.

A successful record was obtained, and the results for all clamping-intervals are given in Table 4, together with the uncertainties involved in the readings. On the assumption that the H field during the stops in different depths remained at a constant value—which appears probable after the values of the individual readings—average values H_{av} with corresponding smaller uncertainties ΔH_{av} were computed for each depth (the long stop in 3,900 meters, however, was divided into three periods according to different nominal speeds). These average fields are represented graphically in Figure 11 for comparison with sphere and bottom depths.

The two 500-meter values seem to indicate a slight increase in H during the measurement—a planetary decrease of about 15γ was to be expected with the drift stated. The conspicuous downward increase in H of about 150γ encountered during the second (B) stop in 3,900 meters greatly surpasses the 50γ expected after the core theory—all uncertainties considered. But the increase found during the first stop (A) in this depth is certainly much less—if any at all—and this unquestionably serves to demonstrate that the observed field differences must be attributed mainly to influences from the bottom. As the distance of the instrument from the rugged ocean floor diminished from 700 meters during the first stop to only 300 meters towards the end of the second stop, the remarkable field changes in this depth

TABLE 4—*Gulf of Panama; 05° 37′ N, 79° 37′ W; May 11, 1952*
Expected H: 31,300γ Instrument: RNM-H
Expected Z: 20,700γ Scale-value: 100γ/mm

Local time		Depth of sphere	Bottom depth	Nominal		H	ΔH	H_{av}	ΔH_{av}
				Course	Speed				
h	*m*	*meters*	*meters*	°	*knots*	γ	γ	γ	γ
23	52	500	4,740	90	0	31,660	±30		
00	09	500	4,740	90	0	31,660	50	31,660	±20
00	26	500	4,740	90	0	31,660	50		
00	43	500	4,720	90	0	31,630	70		
01	55	3,900(*A*)	?	?	6 knots on	31,680	100	31,700	40
02	12	3,900(*A*)	?	?	bb screw*	31,710	50		
03	00	3,900(*B*)	4,500	70	0	31,810	70		
03	12	3,900(*B*)	4,500	70	0	31,810	70	31,800	40
03	30	3,900(*B*)	4,500	70	0	31,770	100		
03	47	3,900(*B*)	4,520	70	1	31,830	70		
04	17	3,900(*B*)	4,460	70	1	31,840	100	31,840	40
04	29	3,900(*B*)	4,380	70	1	31,840	70		
04	50	3,900(*B*)	4,280	70	3	31,840	50		
05	04	3,900(*B*)	4,240	70	3	31,820	40	31,840	25
05	19	3,900(*B*)	4,240	70	3	31,860	50		
06	06	2,600	4,220	60	0	31,760	80		
06	21	2,600	4,220	60	0	31,710	80	31,730	40
06	36	2,600	4,200	60	0	31,740	80		
07	09	2,600	4,200	60	1	31,720	80		
08	10	500	4,300	80	0	31,690	50		
08	27	500	4,320	80	0	31,680	40	31,690	20
08	45	500	4,320	80	0	31,700	30		

*Due to loss of echo, a maneuver was tried, but it was soon given up and the sphere raised.

are presumably in the first place caused by a topographical magnetic effect. During the stop in 2,600 meters, where the instrument had been 1,600 meters above a more level bottom, the apparent downward increase in H of 50γ just cannot be verified with the relatively high uncertainty involved in the measurement, but at least it may be said that the H field does not decrease.

The record immediately demonstrates that in a depth of 3,900 meters the most accurate readings are obtained with high nominal speed of the vessel—as is readily seen from the figures given for ΔH in Table 4. In 500 meters, the strong current alone gives sufficiently firm steering of the sphere. It is very questionable whether still higher nominal speeds may render even better results. Unfortunately, time did not allow further investigations of this important problem. During the last

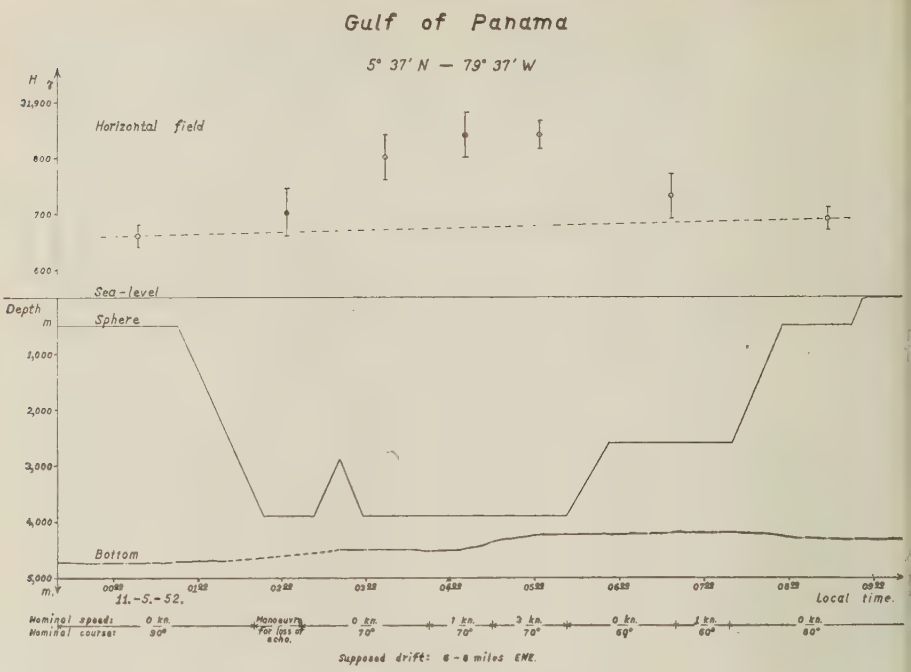

FIG. 11

two lowerings, the nominal speeds yielding the best record in this preliminary measurement had to be chosen.

After the H measurement, the expedition vessel navigated back to the starting position over the western part of the basin, and a short Z measurement was made with RNM-Z. The instrument was kept for an hour and a half in a depth of 500 meters and then for half an hour in depths of 3,500, 2,000, and 500 meters. In spite of the rather short time elapsed during the lowering, the drift of the vessel was afterwards estimated to be as much as 8 to 10 miles toward the northeast. As usual, the ship was allowed to follow its own course under influence of current, wind, sea, and nominal speed on the screws. The nominal course taken up was 70°, but when the sphere was lowered to greater depths the ship obviously tried to stabilize on a little more northerly course, 40° to 60°, under the altered drifting conditions. The bottom depth decreased during the lowering from 4,410 meters at the beginning to 4,060 meters at the end.

The scale-value happened to be very high during the whole measurement (firm steering), which, in fact, was very fortunate, as the Z field computed from the Vestine tables for compensation turned out to be 1,000γ higher than what was actually found.

The improved measuring conditions with the longer damping rudder did not manifest themselves for this instrument, presumably because RNM-Z is more sensitive to pendulations and pitching. The uncertainty in the readings, therefore, is still very high, as will be seen in Table 5, which gives Z readings for individual clamping-intervals.

TABLE 5—*Gulf of Panama; 05° 37′ N, 79° 37′ W; May 11, 1952*
Expected *H:* 31,300γ Instrument: RNM-Z
Expected *Z:* 20,700γ

Local time		Depth of sphere	Bottom depth	Nominal		Z	ΔZ	Z_{av}	ΔZ_{av}
				Course	Speed				
h	*m*	*meters*	*meters*	°	*knots*	γ	γ	γ	γ
15	32	500	4,400	70	0	19,530	±100		
15	44	500	4,390	70	0	19,530	70		
16	00	500	4,380	70	0	19,540	70	19,570	±30
16	18	500	4,350	70	0	19,560	70		
16	34	500	4,320	70	0	19,580	100		
17	05	500	4,240	70	0	19,650	70		
18	14	3,500	4,180	40	3	20,050	150	20,050	150
19	09	2,000	4,120	60	1	19,860	70	19,850	50
19	25	2,000	4,100	60	1	19,850	70		
20	15	500	4,040	70	0	19,910	30	19,900	25
20	29	500	4,040	70	0	19,890	40		

During the first long stop in 500 meters, an apparent increase of the field with time is seen. As the increase, however, appears to be almost linear—the linearity including, in fact, the Z values of the second 500-meter stop—the computation of an average field for the stop as a whole, referred to an "average time," may be permitted. The same is valid for other depths. The Z values obtained in this way (see Table 5) are represented graphically in Figure 12.

During the half-hour stop in 3,500 meters, the vessel apparently did not reach stabilization on the new course taken up, and, as a consequence, the uncertainty of the reading was unfortunately very large. It is obvious, though, that a considerable field increase of at least 150γ was found from 500 meters down to 3,500 meters. So the Z field, too, is evidently influenced by strong local disturbances from the bottom rocks, since the theoretical increase is only 30γ. The result of the measurement in the depth of 2,000 meters appears to be more reasonable; at least, the expected increase of 15γ lies well within the uncertainty of the observed value.

Perhaps the most conspicuous feature in Figure 12 is the large—and apparently roughly linear—field increase of 300γ between the two surface measurements. About half of the increase is explained by the planetary correction for drift, since the undisturbed Z field rises by 15γ per mile to the northeast. The remaining part of the increase must be attributed to local anomalies—both the great discrepancy with the Vestine Z field and the extraordinarily large vertical gradient appearing in the measurement serve to establish the existence of such anomalies, which may easily give rise to a horizontal gradient of the Z field of the size in question.

For the last measurement at the station, RNM-H was used again, but this time it was possible to apply an essentially lower scale-value than normally used, as the H field of the station was known from the previous H measurement.

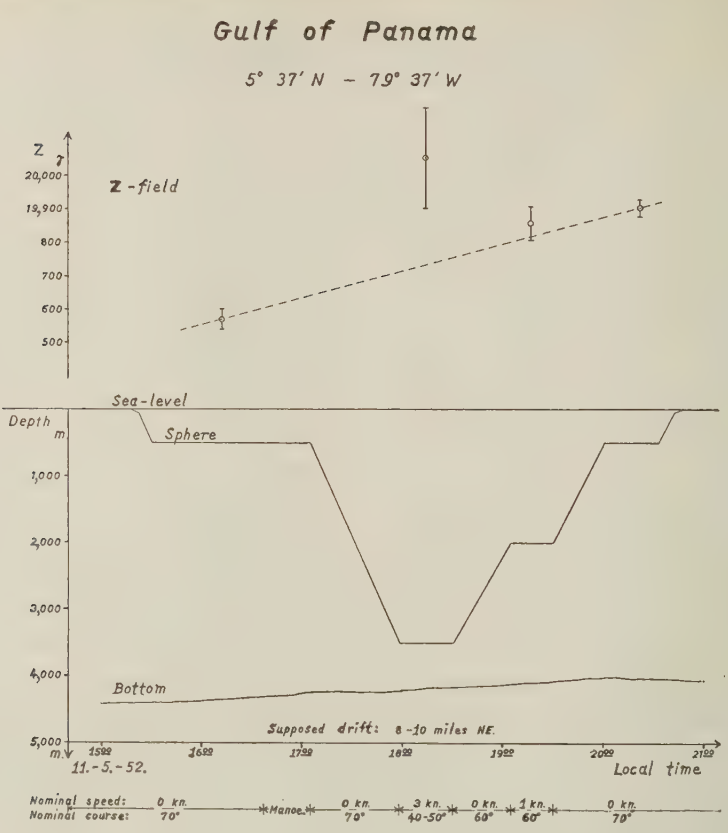

FIG. 12

During the latter part of the Z lowering, cloudiness prevented nautical observations and the capricious currents troubled the navigation to such an extent that it proved impossible to find again the original starting point or even the basin proper. Finally, lack of time forced us to put out the sphere at a place where the depth was only 3,600 meters. Later observations suggested that the ship at this point of time was over the northeastern slope of the basin and during the measurement moved entirely out of it. From earlier experiences at the place, the drift was estimated to be 4 to 6 miles east-northeastward during the part of lowering for which recording was available. The bottom depth decreased during the measurement to only 3,000 meters. The echo-sounder revealed a very rugged bottom, with numerous precipices, the heights sometimes exceeding 200 meters.

While the sphere was being put out from the ship, a sea knocked off a fender and the sphere thumped against the stern. As an effect of this mishap, the apparatus jammed in its gimbal suspension and did not work during the first stop in 500 meters. Shaking during the lowering to greater depth, however, luckily liberated the instrument again, and during the following one-hour stops in depths of 3,000, 1,800, and 500 meters successful records were obtained. The records profited greatly by another little mishap, which caused the damping rudder to break away

from its normal position and slide down along the 15 meters of copper wire, stopping only 3 meters above the sphere. In this position, it brought about a still better steering than was obtained during the first H measurement. This accident contributed to the great accuracy of the H values obtained in the reading of the record, the results of which are given in Table 6 and Figure 13.

TABLE 6—*Gulf of Panama; 05° 37′ N, 79° 37′ W; May 12, 1952*
Expected H: 31,300γ Instrument: RNM-H
Expected Z: 20,700γ Scale-value: 25 γ/mm

Local time	Depth of sphere	Bottom depth	Nominal		H	ΔH
			Course	Speed		
h m	*meters*	*meters*	°	*knots*	γ	γ
05 02	3,000	3,440	80	2.5	31,750	±15
05 17	3,000	3,410	80	3.5	31,715	15
05 35	3,000	3,070	80	3.5	31,695	15
05 50	2,800*	3,010	80	3.5	31,660	15
06 20	1,800	2,990	80	2	31,640	15
06 35	1,800	2,970	80	2	31,625	15
06 53	1,800	3,160	80	2	31,625	20
07 07	1,800	3,170	80	2	31,600	10
07 53	500	3,000	80	0	31,525	15
08 08	500	3,040	80	0	31,515	10
08 22	500	3,050	80	0	31,520	5

*According to the log of the trawl-winch, heaving had started at this point of time, but as the record showed no sign of extraordinary movement the clock-correction used in the log is probably wrong.

Perhaps the most important result of the measurement is that it definitely proves—thanks to the high accuracy of the individual readings—the existence of quite local disturbances from the bottom. As the steering—and consequently the speed—of the sphere must have been very nearly the same in all depths, it may be inferred that the horizontal displacement of the sphere during one hour's stay in any depth was the same—presumably a little more than one nautical mile. While the sphere was hanging in a depth of 3,000 meters (at the beginning of the stay more than 400 meters above the bottom, but in the end only a few meters), this displacement gave rise to a field change of not less than 100γ. In a depth of 1,800 meters, that is, 1,180 to 1,400 meters above the bottom, the field change was only around 40γ, and finally in a depth of 500 meters, or 2,450 to 2,680 meters above the bottom, there was no change at all, or at least it was very small.

No matter whether the disturbances met with are due to topographical effects or to local changes in composition of the bottom rocks, the measurement thus confirms previous results at the Panama station (and Kermadec trench, South). It gives an idea of the disturbances which may "at least" be encountered over the bottom structure in question, and renders an important hint as to the distance

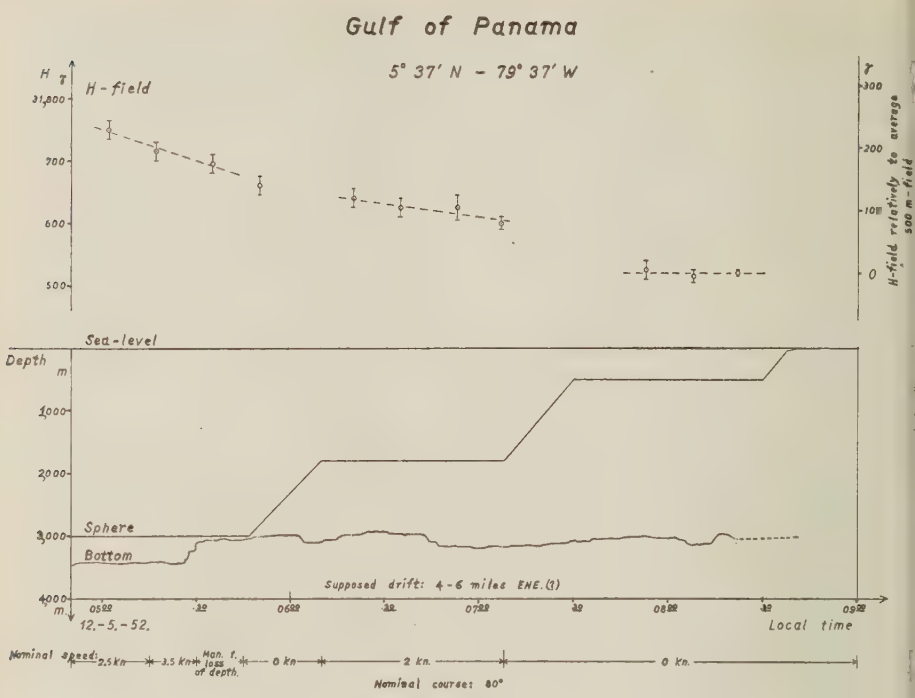

FIG. 13

which must in such cases be kept from the bottom to be out of reach of local anomalies.

It will be noticed that the values obtained for the H field are certainly larger for greater depths, but the size and rate of the field changes found prove immediately that the variation of the main geomagnetic H field is lost again in the disturbances.

CONCLUSION

The magnetic investigations on the *Galathea* naturally had to conform to the general plan of the expedition, the primary objective of which was biological work. Further, many "outside" conditions, such as weather, bottom depth, actual geomagnetic field strengths and expected daily variation, etc., had to be taken into consideration. Under these circumstances, a total "expedition time" of 300 hours was spent on magnetic work during the cruise. In the course of this time, it proved possible to test containers and instruments and to determine the best attainable measuring technique.

As appears from the results of the last H measurement in the Gulf of Panama, we succeeded with the instrument RNM-H in making measurements down to a depth of 3,000 meters with an accuracy of 15γ on a single rotation of the instrument. Over stations with undisturbed H field, where average values may be taken for more individual measurements through a suitably long stop in each depth, there should be nothing to prevent the achievement of H measurements with the desired

accuracy of 10γ, or even less. Further, there is every reason to presume that this will be valid, too, even for greater depths than the 3,000 meters reached at the Panama station.

However, the unhappy mishap to the trawl-winch in the Kermadec trench prevented the utilization of previous experiences in the central Pacific. This was highly deplorable, as much greater importance might have been attached to the Panama H measurements had they been conducted at a station better suited for magnetic work.

Even if local anomalies appear to have influenced more or less all measurements in the Pacific, it is rather suggestive that most of them indicate a distinct increase in H and Z with increasing depth, with not a single decrease proved.

The investigations in the Pacific have shown the existence of great local anomalies over a mountainous ocean bottom. The magnitude of the disturbances encountered may be roughly estimated to be in accordance with those found in aeromagnetic flights over structures rich in basic rocks.

Of the instruments, RNM-H fully justified our expectations, and it is supposed that relatively small innovations may improve further its measuring ability. Moreover, to a certain degree, the same is true for RNM-Z. We have the impression, therefore, that needle magnetometers may still perform useful work in sea measurements, even if smaller and less complicated instruments (demanding smaller and lighter containers) than the *Galathea* types must be aimed at in future design. As regards the rotating-coil instrument RCM-H, only very few experiences were obtained owing to the troubles with the unwieldy double sphere, but it appears it would be difficult to meet the demand of a reduction in size and weight with this instrument.

Even if the theory for the main geomagnetic field proposed by P. M. S. Blackett has lost some of its original interest during the last years—not least due to the work of Prof. Blackett himself (Blackett, 1952)—magnetic measurements at sea still have a strong claim to attention as long as the geomagnetic field of the oceans is only superficially explored, and we do hope on some future occasion to be able to utilize the experiences gained in magnetic work at sea during the *Galathea* expedition.

ACKNOWLEDGMENTS

We are greatly indebted to Dr. Niels Arley, until 1953 head of the Geophysical Research Institution, University of Copenhagen, who suggested these investigations, made the expedition arrangements, and conducted the whole campaign with unfailing energy and encouragement.

The work was made possible thanks to a grant of 125,000 Danish crowns from the Carlsberg Foundation, and later another grant of 25,000 Danish crowns from the Danish Expedition Foundation. We wish to express our sincere gratitude for this generous aid.

Invaluable help was received from several Danish establishments. Especially we should like to mention the following: Messrs. Paul Bergsøe and Son, who produced and cast the alloy for the containers and presented us with the single sphere as a gift; Messrs. Burmeister and Wain, who constructed the single sphere free of charge and

the double sphere and damping rudder for an extremely favorable price; and A/S Nordiske Kabel-og Trådfabrikker, who presented us with the copper wire.

Previous to the important measurements in the Pacific Ocean, all instruments had a final repair and adjustment at the Physical Laboratory of the Australia National University, Canberra. Our thanks are due to the kind hospitality of Prof. Oliphant, chief of the laboratory, and to his staff for the kind interest taken in our work.

For valuable suggestions and help in design, construction, and testing of the instruments, we are grateful to G. Brun, chief engineer, Radio Research Laboratory, Technical University of Denmark; to K. J. Brostrøm, Institute for Theoretical Physics, University of Copenhagen; to H. Boie Hansen, chief mechanic, Physical Laboratoy, University of Copenhagen; and to A. Lundbak, Danish Meteorological Institute.

Finally, we acknowledge with pleasure the collaborating spirit among fellow-scientists, officers, and crew of the expedition vessel.

References

Alldredge, L. R., and F. Keller (1949); Preliminary report on magnetic anomalies between Adak, Alaska, and Kwajalein, Marshall Islands, Trans. Amer. Geophys. Union, **30**, 494–500.

Andreasen, P., and J. Espersen (1957); Investigations during the *Galathea* expedition of the movements of heavy containers lowered on a steel wire (to be published in Deep-sea Research).

Arley, N., B. Lunn, M. Nielsen, and C. Nørgård (1953); Magnetic measurements in deep-sea investigations. Construction of non-magnetic containers, Nature, **171**, 383–384.

Arley, N., P. Andreasen, J. Espersen, and J. Olsen (1953); Magnetic investigations on the *Galathea* expedition, Nature, **171**, 384–385.

Blackett, P. M. S. (1947); The magnetic field of massive rotating bodies, Nature, **159**, 658–666.

Blackett, P. M. S. (1948); The magnetic field of massive rotating bodies, Phil. Mag., **40**, 125–150 (Solway report, 1948).

Blackett, P. M. S. (1952); A negative experiment relating to magnetism and the earth's rotation, Phil. Trans. R. Soc., A, **245**, 309–370.

Chapman, S. (1948); The supposed fundamental geomagnetic field, Ann. Géophys., **4**, 109–123.

Egedal, J. (1953); On the magnetic *H*-balance for the *Galathea* deep-sea expedition, Geofisica pura e appl., **25**, 26–28.

la Cour, D. (1942); The magnetometric zero balance—the BMZ, Det Danske Meteorologiske Institut, Comm. Magn., **19**, 1–57.

Lunn, B. (1953); The development of a high-strength non-magnetic alloy, Bull. Inst. Metals, **1**, 209.

Raitt, R. W., R. L. Fischer, and R. G. Mason (1955); Tonga trench, Geol. Soc. Amer. Spec. Paper, **62**, 237–254.

Runcorn, S. K. (1948); The radial variation of the earth's magnetic field, Proc. Phys. Soc., **61**, 373–382.

Runcorn, S. K., A. C. Benson, A. F. Moore, and D. H. Griffiths (1951); Measurements of the variation with depth of the main geomagnetic field, Phil. Trans. R. Soc., A, **244**, 113–151.

Vestine, E. H., L. Laporte, I. Lange, C. Cooper, and W. C. Hendrix (1948); Description of the earth's main magnetic field and its secular change, 1905–1945, Washington, D. C., Carnegie Inst. Pub. No. 578.

ON THE GEOMAGNETIC STORM EFFECT

By E. N. Parker

Enrico Fermi Institute for Nuclear Studies, The University of Chicago, Chicago 37, Illinois

(Received June 14, 1956)

ABSTRACT

The high electrical conductivity of the region surrounding Earth, inferred from the observations of atmospheric whistlers and the zodiacal light, requires abandoning the customary models for producing a geomagnetic storm field with impressed current system. It becomes necessary to adopt a purely hydromagnetic approach wherein one focuses his attention only on the magnetic lines of force of the geomagnetic field and their displacement with the conducting gas surrounding Earth. From the hydromagnetic point of view, a decrease of the horizontal component is brought about by lifting the lines of force in the region above the observer. It is suggested that heating in the upper atmosphere may produce the necessary lifting; this model, along with another, is developed quantitatively to show that lifting the lines of force a distance of only 5 km will produce a decrease in the horizontal component of 0.2 per cent at the equator.

1. INTRODUCTION

A magnetic storm is most readily observed in the horizontal component of the geomagnetic field and consists of an abrupt and short-lived increase, the *initial phase* of the storm, followed by a more prolonged decrease, the *main phase*, which may last several days (Chapman and Bartels, 1940). Most any sort of crowding in of the geomagnetic field by interplanetary matter will explain the initial phase, but a complete explanation of the main phase of the storm is not yet available. The best existing mechanism for the decrease is probably the well-known ring-current model of Chapman and Ferraro; they suggest that the passage of high-velocity clouds of material past Earth sets up a ring current about our planet with such a sense that its magnetic field opposes, and therefore partially cancels, the horizontal component of the geomagnetic field.

Now any such model as the ring current tacitly assumes that space outside the terrestrial atmosphere is a sufficiently good vacuum to have essentially zero electrical conductivity. But Storey (1954) has found from observations of atmospheric whistlers that the electron density five or ten thousand kilometers above the surface of Earth is of the order of $500/\text{cm}^3$, in agreement with the interplanetary electron density inferred by Behr and Siedentopf (1953), so that the electrical conductivity is 1.0 mks or more (Schlüter, 1950).

That this modest conductivity will profoundly alter the ring-current model may be seen from the following considerations. Suppose that when $t = t_0$, a ring

current, such as proposed by Chapman and Ferraro, comes into being a distance l above the surface of Earth. Due to the electrical conductivity σ of the tenuous ionized gas in the space around Earth, the magnetic field of the current will not immediately penetrate to the surface of Earth. In fact, a time of the order of $\frac{1}{4}l^2\mu\sigma$ will elapse before the effect of the current is observed on the planet. As a lower limit on l, we take 5,000 km. Then the lower limit of the lapse time $\frac{1}{4}l^2\mu\sigma$ turns out to be 87 days, which is much too long to explain either the observed delay of only one day after violent solar activity or the observed onset time of the main phase of half a day or less.

Therefore, it would seem that Storey's observations require some revision of the existing theories. It is the purpose of this paper to suggest how we should revise our approach to the geomagnetic problem and to demonstrate at least one possible solution.

II. HYDROMAGNETIC FORMULATION

1. *General relations*

The magnetic field $\mathbf{B}$ in a conducting fluid medium with velocity $\mathbf{v}$ is given by the well-known hydromagnetic equation

$$\frac{\partial \mathbf{B}}{\partial t} = \nabla \times (\mathbf{v} \times \mathbf{B}) + \frac{1}{\mu\sigma} \nabla^2 \mathbf{B} \quad \ldots\ldots\ldots\ldots\ldots\ldots (1)$$

in mks units. If one wishes the current density $\mathbf{j}$ associated with $\mathbf{B}$, it is readily computed from the relation

$$\mathbf{j} = \frac{1}{\mu} \nabla \times \mathbf{B} \quad \ldots\ldots\ldots\ldots\ldots\ldots\ldots\ldots (2)$$

However, with high electrical conductivity σ, the basic field quantity is $\mathbf{B}$, given by (1), and not $\mathbf{j}$ (Cowling, 1934); $\mathbf{B}$ cannot be computed from the impressed current system alone, since a given current will induce other currents of equal importance. Thus, a magnetic storm becomes a search for a suitable fluid motion $\mathbf{v}$, to insert in (1), rather than for a suitable impressed current system.

The main phase of a magnetic storm has a life of a few days, which is very much less than the characteristic diffusion time $\frac{1}{4}l^2\mu\sigma$. Hence, at least for the onset of the main phase, the diffusion term in (1) may be neglected to good approximation, yielding

$$\frac{\partial \mathbf{B}}{\partial t} = \nabla \times (\mathbf{v} \times \mathbf{B}) \quad \ldots\ldots\ldots\ldots\ldots\ldots\ldots (3)$$

This is the same equation as the Helmholtz vorticity equation

$$\frac{\partial \boldsymbol{\omega}}{\partial t} = \nabla \times (\mathbf{v} \times \boldsymbol{\omega}) \quad \ldots\ldots\ldots\ldots\ldots\ldots\ldots (4)$$

for an inviscid fluid; Cauchy's integral of the Helmholtz equation is also the solution of (3) (Lundquist, 1952; Brand, 1947).

Cowling (1934) has shown that the magnetic lines of force given by (3) move

xactly with the fluid, just as do the vortex lines in (4). It follows that the magnetic nes of force have a permanent connectivity and are to be found threading the ame elements of fluid at all times. Thus, *we will discuss the main phase of a magnetic torm in terms of displacement of the lines of force of the geomagnetic field, and, hence, n terms of the displacement of the conducting gas in which the lines are imbedded.*

Magnetic storm

It will greatly simplify our discussion if we introduce the idealization that rom the surface of the Earth up to some definite uniform height h the atmosphere s non-conducting, $\sigma = 0$, and that above h the gas is highly ionized and may be egarded a perfect conductor, $\sigma = \infty$. The height h we shall call the *top of the tmosphere*, having in mind the dense lower non-ionized regions as the basic planeary atmosphere. The effective height at which σ may be regarded as infinite epends upon the characteristic period τ of the hydromagnetic processes in which re are interested; h will have such a value that the hydromagnetic decay time $l^2\mu\sigma$ is somewhat larger than τ, and will probably fall somewhere in the ionosphere.

From (1), it is clear that below h there is no interaction between **B** and the uid motion **v**; above h, **B** varies according to (3), the lines of force moving exactly ith the gas. Hence, the fluid motion responsible for the observed storm variation f **B** must occur above the top of the atmosphere h.

To decrease the horizontal component of **B** at the surface of Earth, it is necessary nd sufficient to raise the lines of force above the top of the atmosphere to make nore room for the lines of force below. Thus, if there is an upward displacement f the conducting fluid above the top of the atmosphere and an increase in h, the nagnetic field below the top of the atmosphere will expand upward into the dditional room provided, thereby increasing the spacing of the lines of force and ecreasing the horizontal component. The remainder of this paper is devoted to he formal solution of (3) for two simple cases to demonstrate quantitatively how he mechanism works.

Stresses involved in lifting the lines of force to produce the observed field ariations seem rather modest: A change, ΔB, of 0.2 per cent in a field B, which s of the order of 0.4 gauss, requires a stress variation of $B\Delta B/\mu = 2.6 \times 10^{-8}$ m wt/cm^2.

III. CAUSES OF DISPLACEMENT

If we conclude that the decrease of the horizontal component of the geomagnetic eld can occur only as a result of the upward displacement of the top of the atmosphere and the gases above, then the next step is to suggest what physical processes ight produce such a displacement. From the theoretical point of view, the most bvious suggestion is that perhaps somewhere in the ionosphere below the "top f the atmosphere" an abnormal amount of heating may suddenly occur as a esult of solar corpuscular emission, causing expansion of the gas and lifting the verlying embedded lines of force. In connection with this purely *a priori* theoetical suggestion, it is interesting to note that some years ago Kirby, *et al.* (1937), uggested, purely on the basis of their observations of the change in the electron

density and virtual height of the F-layers during a magnetic storm, that the ionosphere was violently heated during the onset of the main phase of a magnetic storm; they also suggested that the heating and expansion might in some way be responsible for the decrease of the horizontal component of the geomagnetic field. Therefore, it would seem that the heating hypothesis has some basis aside from simplicity and may be seriously considered as the source of the main phase of a magnetic storm.

However, though the heating seems the more likely candidate, we shall later on develop the following second mechanism, involving the gravitational capture of interplanetary hydrogen, in order to demonstrate what other processes might be possible.

Let us assume that the terrestrial gravitational field captures a certain amount of interplanetary hydrogen. We suppose that the hydrogen is highly conducting and free of internal magnetic fields. We represent the kinetic temperature by T, the gas pressure by p, the total cloud volume by V, the mass of an individual atom by m, and the number of atoms per unit volume by n.

The weight of the gas in the terrestrial gravitation field will pull the hydrogen down into the geomagnetic field; the lines of force will be pushed aside by the passage of the cloud and will not penetrate into the hydrogen because of the high electrical conductivity. For equilibrium, it can be shown that p or nkT must be equal to the magnetic pressure $B^2/2\mu$ of the magnetic field into which the gas is thrust, so that

$$p = nkT = \frac{B^2}{2\mu} \qquad (5)$$

and the field will exert a force

$$\mathbf{F} = -\frac{VB}{\mu} \nabla B \qquad (6)$$

on the cloud (Parker, 1956).

The equipotential surfaces for the force $\mathbf{F}$ are the surfaces of constant B; for the dipole geomagnetic field, the surfaces are given by

$$r^6 = \wedge^2(3 \cos^2 \theta + 1) \qquad (7)$$

in spherical coordinates (r, θ, ϕ). $\wedge$ is a constant on any given equipotential surface. The surfaces are lowest, that is, nearest the center of Earth, above the equator, $\theta = \pi/2$. Therefore, it is obvious that, in combination with the gravitational force on the hydrogen, the hydrogen will tend toward the equatorial plane.

The weight W of the hydrogen is

$$W = g_E\left(\frac{b}{r}\right)^2 nmV \qquad (8)$$

where g_E is the acceleration of gravity at the surface of Earth, $r = b$. If W is to be in equilibrium with the magnetic force (6), then, as already stated, $\theta = \pi/2$,

nd combining (6) and (8) we have

$$-\frac{VB}{\mu}\frac{\partial B}{\partial r} = g_E\left(\frac{b}{r}\right)^2 nmV \quad \ldots\ldots\ldots\ldots\ldots\ldots\ldots\ldots (9)$$

Using (5) to eliminate n, we obtain the gas temperature

$$T = \frac{mg_E}{2k}\left(\frac{b}{r}\right)^2\left(-\frac{1}{B}\frac{\partial B}{\partial r}\right)^{-1} \quad \ldots\ldots\ldots\ldots\ldots\ldots\ldots\ldots (10)$$

n the equatorial plane of a dipole, $(\partial/\partial r)\ lnB = -3/r$, so that

$$T = \frac{mg_E b^2}{6kr} \quad \ldots\ldots\ldots\ldots\ldots\ldots\ldots\ldots\ldots\ldots (11)$$

In order that the hydrogen sink as far as r, the temperature must not exceed he value given in (11); in order that the hydrogen sink as far as the top of the tmosphere, $r = 6400$ km, the temperature must not exceed 1280°K. Hence, rom (5), the density n must be at least as large as 2.0×10^{10} hydrogen atoms/cm^3. ' would be larger for objects with more intense gravitational fields.

Some doubt is cast on the mechanism by the required low temperature in ombination with the required high conductivity; thus, again, let us emphasize hat the process is to be regarded as an illustrative example of the general type of ydromagnetic processes that can occur rather than a definite proposal as to the rigin of geomagnetic storms.

It can be shown (Parker, 1956) that a highly conducting gas cloud encysted n a large-scale magnetic field is unstable and will either flatten or split into smaller nd smaller fragments until the dimension l is so small that the time of diffusion $l^2\mu\sigma$ into the magnetic field is as small as we please. Thus, no matter how large ay be the electrical conductivity, σ, the cloud gas will rapidly diffuse into the eomagnetic field, once the cloud comes to rest, because of the sequence of splitting hich occurs.

We mean to suggest, then, that capture of interplanetary hydrogen gas may ave the result of introducing gas *into* the geomagnetic field at the top of the tmosphere, which we put at $r = c$. As more and more conducting hydrogen is aptured and introduced into the field, we will have a layer of conducting gas of ncreasing thickness accumulating on top of the atmosphere. The hydrogen appears t $r = c$ and cannot expand downward into the very much denser air; thus, with ach new addition of hydrogen at $r = c$, the gas is displaced upward and, as will e shown in section V, would produce a decrease in the horizontal component of he geomagnetic field below the top of the atmosphere.

It can be shown that the characteristic time for the splitting of a gas cloud is f the order of $L(\mu\rho)^{\frac{1}{2}}/B$, where L is the longest dimension of the cloud, and ρ is he gas density. At the top of the atmosphere, where $B \cong 0.3$ gauss and $\cong 2 \times 10^{10}$/cm^3, a hydrogen cloud 1,000 km in length will have a splitting time f the order of 215 sec, or about 3.5 minutes. Thus, there should be ample time or splitting, after falling under gravity for an hour or so, to produce a decrease n the horizontal component with a characteristic time of onset of several hours.

IV. ATMOSPHERIC HEATING

Let us idealize the Earth to the simple form shown in Figure 1. At the center of Earth, we have the metallic core of radius $r = a$, which is highly conducting. Above the core, there is the mantle and crust, extending out to a distance $r = b$ from the center of Earth, which we take to be non-conducting. Above the surface of Earth at $r = b$, we have the atmosphere, extending to $r = c = b + h$, which is also a non-conductor. As mentioned above, we choose c in such a way that

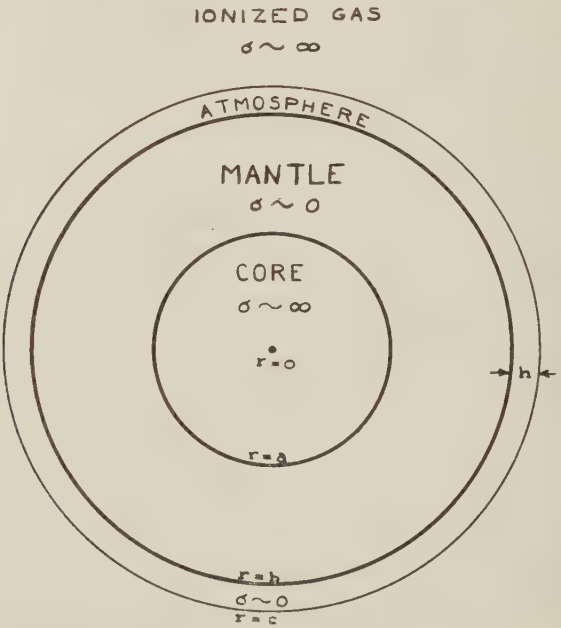

FIG. 1—Idealized model of Earth used in calculations. The electrical conductivity σ is taken to be effectively infinite for $r < a$ and $r > c$, and to be zero in the region $a < r < c$.

above $r = c$ the gas may be regarded as highly conducting to the extent that (3) is applicable. Thus, $r = c$ is at least as high as the ionosphere. In view of the observations of Storey and of Behr and Siedentopf, we assume that high electrical conductivity extends from $r = c$ to infinity.

Suppose now that some process were to heat the upper portion of the non-conducting atmosphere between $r = b$ and $r = c$, causing the atmosphere to expand and the outer radius to increase from c to $c + \delta c$. According to the physical arguments given above, this should have the effect of decreasing the horizontal component of the geomagnetic field observed below $r = c$. To demonstrate in the simplest way the decrease of the horizontal component, we suppose that the expansion is purely radial and that initially the geomagnetic field was a perfect dipole, given by the scalar potential

$$\psi = \frac{B_0 a^3}{r^2} \cos\theta \quad \ldots\ldots\ldots\ldots\ldots\ldots\ldots\ldots \quad (12)$$

for $r > a$.

As a consequence of the high electrical conductivity of the core, the radial component, B_r , of the geomagnetic field does not change at $r = a$ during the expansion; as a consequence of the high electrical conductivity for $r > c$, it follows that the flux crossing the top of the atmosphere per unit solid angle is unchanged by the expansion, so that B_r decreases from the initial value $2B_0\ (a/c)^3 \cos\theta$ at $r = c$ to the final value $2B_0\ (a/c)^3 \cos\theta \times (c/(c + \delta c))^2$ at $r = c + \delta c$.

Following the expansion, the geomagnetic field is still describable in terms of a scalar potential in the region $a < r < c + \delta c$, the most general form of which is

$$\psi' = B_0\left(\frac{a^3}{r^2} A_1 + rA_2\right) \cos\theta \qquad (13)$$

where A_1 and A_2 are constants to be determined from the above boundary conditions: In order that B_r remain unchanged on $r = a$, we must have

$$2B_0 \cos\theta = B_0(2A_1 - A_2) \cos\theta \qquad (14)$$

In order that B_r decrease by the factor $(1 - 2\delta c/c)$ at the top of the non-conducting atmosphere, we must have

$$2B_0\left(\frac{a}{c}\right)^3 \cos\theta\left(1 - 2\frac{\delta c}{c}\right) = B_0\left[2A_1\left(\frac{a}{c}\right)^3\left(1 - 3\frac{\delta c}{c}\right) - A_2\right] \cos\theta + O^2\left(\frac{\delta c}{c}\right) \qquad (15)$$

For convenience, we let $\epsilon = \delta c/c$. Then, simultaneous solution of (14) and (15) yields

$$A_1 = 1 - \frac{(a/c)^3\epsilon}{1 - (a/c)^3} + O^2(\epsilon)$$

$$A_2 = -\frac{2(a/c)^3\epsilon}{1 - (a/c)^3} + O^2(\epsilon)$$

Accordingly, the horizontal component B_θ is

$$\left.\begin{aligned} B_\theta &= -\frac{1}{r}\frac{\partial\psi'}{\partial\theta} \\ &= B_0\left\{\left(\frac{a}{r}\right)^3\left[1 - \frac{(a/c)^3\epsilon}{1 - (a/c)^3}\right] - \frac{2(a/c)^3\epsilon}{1 - (a/c)^3}\right\} \\ &\quad \times \sin\theta + O^2(\epsilon) \end{aligned}\right\} \qquad (16)$$

The change in B_θ from the pre-expansion value, (12), is

$$\Delta B_\theta = -B_0 \frac{(a/c)^3\epsilon}{1 - (a/c)^3}\left[2 + \left(\frac{a}{r}\right)^3\right] \sin\theta$$

so that

$$\frac{\Delta B_\theta}{B_\theta} = -\frac{(a/c)^3\epsilon}{1 - (a/c)^3}\left[2\left(\frac{r}{a}\right)^3 + 1\right] \qquad (17)$$

Thus, $\Delta B_\theta/B_\theta$ is negative everywhere below the top of the atmosphere; the expansion produces a decrease of the horizontal component, as suggested by our physical arguments with the magnetic lines of force.

B_θ is observed at $r = b$, but since $(c - b) \ll c$ we would find essentially the same effect at $r = c$, for which

$$\frac{\Delta B_\theta}{B_\theta} = -\frac{3(a/c)^3\epsilon}{1 - (a/c)^3}\left[2\left(\frac{c}{a}\right)^3 + 1\right] \quad \ldots\ldots\ldots\ldots\ldots\ldots (18)$$

The radius a of the core is about half the radius of the planet, $a \cong \frac{1}{2}c$, so that the observed change in the horizontal component is

$$\frac{\Delta B_\theta}{B_\theta} \cong -\frac{17}{7}\epsilon \quad \ldots\ldots\ldots\ldots\ldots\ldots\ldots\ldots\ldots (19)$$

A typical magnetic storm might decrease B_θ by 0.2 per cent, requiring that $\delta c \cong 5.3$ km.

Thus, δc is rather less than the observed increase in height of the F-layers of the ionosphere during a magnetic storm, which suggests that our "top of the atmosphere," $r = c$, may be somewhat higher. An upper limit on c may be obtained from the stresses required to produce the observed deformation of the geomagnetic field. In Section II, we estimated that the stresses were of the order of 3×10^{-5} dyne per cm^2; a kinetic temperature of 2,000°K during a storm requires 10^8 particles per cm^3 to produce this stress. Existing estimates of the particle density (Bates, 1954) would seem to limit $r = c$ to a maximum height of the order of 400 km $(= h)$ above the surface of Earth.

V. CAPTURE OF INTERPLANETARY HYDROGEN

1. *Equilibrium conditions*

Let us again use the idealized form of Earth shown in Figure 1, but this time suppose that the terrestrial gravitational field captures interplanetary hydrogen which is introduced into the geomagnetic field at the top of the atmosphere $r = c$. We presume that the hydrogen will float on the top of the much denser atmosphere of air, so that to a useful degree of approximation $r = c$ may be taken as a rigid impenetrable surface.

If Ψ represents the potential of the terrestrial gravitational field, ρ the density of the hydrogen, and p the hydrostatic pressure, then for equilibrium we require that

$$0 = -\nabla p - \rho\nabla\Psi + \frac{1}{\mu}(\nabla \times \mathbf{B}) \times \mathbf{B} \quad \ldots\ldots\ldots\ldots\ldots (20)$$

in the geomagnetic field $\mathbf{B}$. We let $\mathbf{b}$ represent the change in the field produced by the introduction of the gas, so that

$$\mathbf{B} = \mathbf{B}_0 + \mathbf{b} \quad \ldots\ldots\ldots\ldots\ldots\ldots\ldots\ldots (21)$$

$\mathbf{B}_0$ is the unperturbed field given in terms of ψ in (12). Then, assuming that $\mathbf{b}$ is small compared to $\mathbf{B}_0$, we write

$$\nabla p + \rho\nabla\Psi = \frac{1}{\mu}(\nabla \times \mathbf{b}) \times \mathbf{B}_0 + 0^2(\mathbf{b}) \quad \ldots\ldots\ldots\ldots\ldots (22)$$

for equilibrium.

We assume that ρ and p are independent of azimuth ϕ, so that $\mathbf{b}$ will have no ϕ component and will be independent of ϕ. Hence $\mathbf{b}$ is an axially symmetric poloidal vector and may be expressed (Schlüter and Lüst, 1954; Chandrasekhar, 1956) in terms of the function $P(r, \theta)$ as

$$\mathbf{b} = \nabla \times [\mathbf{e}_r r \sin \theta P(r, \theta)] \quad (23)$$

where $\mathbf{e}_r$, $\mathbf{e}_\theta$, and $\mathbf{e}_\varphi$ represent unit vectors in the r, θ, and φ directions. It can be shown that

$$\nabla \times \mathbf{b} = -\mathbf{e}_\varphi r \sin \theta \Delta_5 P \quad (24)$$

where Δ_5 is the operator

$$\Delta_5 = \frac{\partial^2}{\partial r^2} + \frac{4}{r}\frac{\partial}{\partial r} + \frac{1}{r^2}\left[(1 - \mu^2)\frac{\partial^2}{\partial \mu^2} - 4\mu \frac{\partial}{\partial u}\right] \quad (25)$$

and $\mu = \cos \theta$. It follows that

$$(\nabla \times \mathbf{b}) \times \mathbf{B}_0 = \frac{B_0 a^3}{r^2} \sin \theta \Delta_5 P(\mathbf{e}_r \sin \theta - 2\mathbf{e}_\theta \cos \theta)$$

Thus, from (22), we see that $\nabla p + \rho \nabla \Psi$ must have the form

$$\nabla p + \rho \nabla \Psi = -f(r, \theta)(\mathbf{e}_r \sin \theta - 2\mathbf{e}_\theta \cos \theta) \quad (26)$$

The equilibrium condition reduces to

$$\Delta_5 P(r, \theta) = -\frac{\mu}{B_0 a^3} \frac{f(r, \theta) r^2}{\sin \theta} \quad (27)$$

Since $f(r, \theta)$ is a measure of the hydrostatic forces exerted on the magnetic field by the hydrogen, it follows that $f(r, \theta)$ will be small at the poles and large above the equator, in accordance with our observation in Section III that the captured gas will tend toward the equatorial plane. Thus, it is not unreasonable to suppose that $f(r, \theta)$ varies roughly as $\sin \theta$ and

$$f(r, \theta) \cong h(r) \sin \theta \quad (28)$$

Thus,

$$\Delta_5 P(r, \theta) = -\frac{\mu}{B_0 a^3} r^2 h(r) \quad (29)$$

We let

$$P(r, \theta) = P_1(r) + P_2(r, \theta) \quad (30)$$

where

$$\Delta_5 P_2(r, \theta) = 0 \quad (31)$$

and $P_1(r)$ is the solution of the inhomogeneous equation

$$\frac{d^2 P_1}{dr^2} + \frac{4}{r}\frac{dP_1}{dr} = -\frac{\mu}{B_0 a^3} r^2 h(r) \quad (32)$$

It follows immediately that P_2 must be of the form

$$P_2 = \frac{C_1}{r^2} + C_2 \quad \ldots\ldots\ldots\ldots\ldots\ldots\ldots\ldots (33)$$

where C_1 and C_2 are constants; in order that $P_1(r)$ vanish at infinity, it is readily shown that

$$P_1(r) = -\frac{\mu}{B_0 a^3}\int_r^\infty \frac{dv}{v^4}\int_v^\infty du\, u^6 h(u) \quad \ldots\ldots\ldots\ldots\ldots\ldots (34)$$

b may now be computed from P_1 and P_2 with the aid of (23). The total field $\mathbf{B}_0 + \mathbf{b}$ is

$$B_r = 2\cos\theta\left\{B_0\left(\frac{a}{r}\right)^3 + \frac{C_1}{r^3} + C_2 - \frac{\mu}{B_0 a^3}\int_r^\infty \frac{dv}{v^4}\int_v^\infty du\, u^6 h(u)\right\}$$

$$B_\theta = \sin\theta\left\{B_0\left(\frac{a}{r}\right)^3 + \frac{C_1}{r^3} - 2C_2 + \frac{\mu}{B_0 a^3}\left[2\int_r^\infty \frac{dv}{v^4}\int_v^\infty du\, u^6 h(u) - \frac{1}{r^3}\int_r^\infty du\, u^6 h(u)\right]\right\}$$

Now $C_2 = 0$ in order that **B** vanish for large r, and C_1 must have such a value that B_r is continuous across the surface of the core, $r = a$. Hence $B_r = 2B_0\cos\theta$ at $r = a$, and

$$C_1 = \frac{\mu}{B_0}\int_0^\infty \frac{dv}{v^4}\int_v^\infty du\, u^6 h(u)$$

Thus,

$$B_r = 2B_0\left(\frac{a}{r}\right)^3\cos\theta\left\{1 + \frac{\mu}{B_0 a^3}\left[\int_a^\infty \frac{dv}{v^4}\int_v^\infty du\, u^6 h(u) - \left(\frac{r}{a}\right)^3\int_r^\infty \frac{dv}{v^4}\int_v^\infty du\, u^6 h(u)\right]\right\} \quad \ldots\ldots (35)$$

$$B_\theta = B_0\left(\frac{a}{r}\right)^3\sin\theta\left\{1 - \frac{\mu}{B_0 a^3}\left[\frac{1}{a^3}\int_r^\infty du\, u^6 h(u) - 2\left(\frac{r}{a}\right)^3\int_r^\infty \frac{dv}{v^4}\int_v^\infty du\, u^6 h(u) - \int_a^\infty \frac{dv}{v^4}\int_v^\infty du\, u^6 h(u)\right]\right\} \quad \ldots\ldots (36)$$

2. *Displacement of lines*

We shall now determine the vertical displacement of the lines of force above the equator for a given gas distribution $h(r)$. Consider the lines of force which pass through $r = c$, $\theta = \pi/2$ before the introduction of the hydrogen. Following the introduction, these lines of force cross the equatorial plane farther out than $r = c$, say at $r = c'$ $(c' > c)$. We know that the total flux Φ crossing the equatorial plane between $r = a$ and $r = c'$ is the same as that which initially crossed between $r = a$ and $r = c$. Thus, we know that Φ may be calculated from the initial field $\mathbf{B}_0$ and is just

$$\Phi = 2\pi\int_a^c dr\, r\left(\frac{1}{r}\frac{\partial\psi}{\partial\theta}\right)_{\theta=\pi/2}$$

$$= 2\pi B_0 a^2\left(\frac{c-a}{c}\right)$$

Subsequently,

$$\Phi = 2\pi \int_a^{c'} dr\, r(B_\theta)_{\theta=\pi/2}$$

where B_θ is given in (36). Equating these two expressions for Φ and solving for the vertical displacement $c' - c$ of the lines of force above the equator, we obtain

$$\frac{c' - c}{c'c} = \frac{\mu}{B_0 a^6}\left[\int_a^{c'} \frac{dr}{r^2}\int_r^\infty du\, u^6 h(u) - 2\int_a^{c'} dr\, r \int_r^\infty \frac{dv}{v^4}\int_v^\infty du\, u^6 h(u) - \frac{a^2(c' - a)}{c'}\int_a^\infty \frac{dv}{v^4}\int_v^\infty du\, u^6 h(u)\right.$$

giving c' in terms of $h(r)$.

3. *Force on field*

We must relate the force per unit volume, $h(r)$, exerted on the magnetic field to the displacement of the lines of force, $c' - c$. We assume that the hydrogen is introduced sufficiently slowly that the magnetic field and gas pressure satisfy (22) at all times during the expansion. By maintaining equilibrium, we know that the magnetic field and the hydrogen gas are displaced together, upward from $r = c$, as the hydrogen is introduced at $r = c$. It follows that $h(r)$ moves with the lines of force; hence $h(r)$ remains zero above $r = c'$ and is non-zero only in the interval (c, c').

We are considering small displacements of the lines of force, so that $(c' - c) \ll c$. Thus, we write

$$c' = c(1 + \epsilon), \qquad \epsilon \ll 1$$

The total force required to bring about the displacement of the lines of force from the stable equilibrium configuration $\mathbf{B}_\theta$ increases linearly with the displacement $c' - c$. Thus, we write that the total force is

$$\int_c^{c'} dr\, h(r) \propto c' - c$$

from which it follows that $h(r)$ is constant over (c, c'). We write

$$h(r) = \begin{cases} 0 & \text{for } r < c, \quad r > c' \\ H & \text{for } c < r < c' \end{cases}$$

where H is a constant which we have yet to determine.

Using (38) and (39), it is readily shown that

$$\int_r^\infty du\, u^6 h(u) = \begin{cases} 0 & \text{for } r > c' \\ \frac{H}{7}(c'^7 - r^7) & \text{for } c < r < c' \\ Hc^7\epsilon & \text{for } r < c \end{cases}$$

$$\int_r^\infty \frac{dv}{v^4} \int_v^\infty du\, u^6 h(u) = \begin{cases} 0 & \text{for } r > c' \\ \frac{H}{7}\left(\frac{c'^7}{3r^3} - \frac{7c'^4}{12} + \frac{1}{4}r^4\right) & \text{for } c < r < c' \\ \frac{Hc^7\epsilon}{3}\left(\frac{1}{r^3} - \frac{1}{c^3}\right) & \text{for } r < c \end{cases}$$

$$\int_a^{c'} \frac{dr}{r^2} \int_v^\infty du\, u^6 h(u) = \frac{Hc^6(c-a)}{a}\epsilon$$

$$\int_a^{c'} dr\, r \int_r^\infty \frac{dv}{v^4} \int_v^\infty du\, u^6 h(u) = \frac{Hc^4(c-a)^2(2c+a)}{6a}\epsilon$$

neglecting terms $0(\epsilon^2)$.

With these values, (37) reduces to

$$\frac{\epsilon}{c} = \frac{1}{3}\epsilon H\left(\frac{\mu}{B_0^2}\right)\frac{c^3(c^3-a^3)}{a^6} + 0(\epsilon^2) \quad \ldots\ldots(40)$$

which requires that

$$H = 3\left(\frac{B_0^2}{\mu}\right)\frac{a^6}{c^4(c^3-a^3)} + 0(\epsilon) \quad \ldots\ldots(41)$$

The horizontal component at $r = c$, $\theta = \pi/2$ is computed from (36) to be

$$B_\theta = B_0\left(\frac{a}{c}\right)^3\left\{1 - H\epsilon\left(\frac{\mu}{B_0^2}\right)\frac{c^4(2c^3+a^3)}{3a^6}\right\} = B_0\left(\frac{a}{c}\right)^3\left(1 - \epsilon\frac{2c^3+a^3}{c^3-a^3}\right) \quad \ldots\ldots(42)$$

Since ϵ is a positive quantity, we see that B_θ decreases from the initial value B_0a^3/c^3. Denoting the magnitude of the decrease by ΔB_θ, we have

$$\frac{\Delta B_\theta}{B_\theta} = \epsilon\frac{2c^3+a^3}{c^3-a^3} + 0(\epsilon^2) \quad \ldots\ldots(43)$$

For Earth $a \cong 0.5\ c$, (41) and (43) reduce to

$$H = \frac{3}{56}\frac{B_0^2}{c\mu} \quad \ldots\ldots(44)$$

$$\frac{\Delta B_\theta}{B_\theta} = -\frac{17}{7}\epsilon \quad \ldots\ldots(45)$$

(45) is just the result obtained in the previous section, (19). For a magnetic storm in which B_θ decreases by 0.2 per cent, we have $\epsilon = 0.82 \times 10^{-3}$. Since $c = 6.4 \times 10^3$ km, it follows that the upward displacement is 5.3 km. The horizontal component at the surface of Earth at the equator is of the order of 0.3 gauss. Hence $B_0 = 2.4$ gauss and (44) gives $H = 0.38 \times 10^{-10}$ dyne/cm^3. The gravitational term, $\rho \nabla \Psi$, in (22) is negligible and the gas pressure p_0 at $r = c$ is $(c' - c)\ H$, to the order we are considering. Thus, the necessary pressure is $p_0 = 2.0 \times 10^{-5}$ dyne/cm^2 = 2.0×10^{-8} gm wt/cm^2, in close agreement with our first estimate.

VI. CONCLUDING REMARKS

We have attempted to illustrate the approach to the problem of the geomagnetic storm which seems to be required by Storey's observations of high electron density, and therefore high electrical conductivity, in the space surrounding Earth. In place of current systems, we have discussed the displacement of magnetic lines of force; the main phase of a geomagnetic storm seems to imply a lifting of the lines of force. The terrestrial atmosphere is the most obvious foundation from which to do the necessary lifting, and for this reason the two models developed quantitatively have been based on an upward displacement of the lines of force brought about by forces at the top of the atmosphere, say within about 400 km of the surface of Earth. Such low altitudes for the production of a magnetic storm explain automatically the large irregular variation of ΔB_θ over the surface of Earth.

The simpler of the two models for the geomagnetic storm effect is based on the assumption that the upper atmosphere is heated (presumably by solar corpuscular emission) and expands upward, lifting the lines of force to produce a decrease of the horizontal intensity below. The heating seems to have independent conformation in the direct observation of the variation of density and altitude of the F-layers, and was suggested by Kirby, *et al.* (1937), as a possible cause of geomagnetic storms.

References

Bates, D. R. (1954); The Earth as a Planet, edited by G. P. Kuiper, University of Chicago Press, Chicago, p. 597.
Behr, A., and H. Siedentopf (1953); Zs. Astroph., **32**, 19.
Brand, L. (1947); Vector and Tensor Analysis, John Wiley and Sons, Inc., New York.
Chandrasekhar, S. (1956); Proc. Nat. Acad. Sci., **42**, 1.
Chapman, S., and J. Bartels (1940); Geomagnetism, Oxford, Clarendon Press, Vol. II.
Cowling, T. G. (1934); Mon. Not. R. Astr. Soc., **94**, 39.
Kirby, S. S., N. Smith, T. R. Gilliland, and S. E. Reymer (1937); Phys. Rev., **51**, 992.
Kirby, S. S., N. Smith, and T. R. Gilliland (1937); Phys. Rev., **54**, 234.
Lundquist, S. (1952); Ark. Fys., **5**, 297.
Parker, E. (1956).
Schlüter, A. (1950); Zs. Naturf., **5a**, 72.
Schlüter, A., and R. Lüst (1954); Zs. Astroph., **34**, 265.
Storey, L. R. O. (1954); Phil. Trans. R. Soc., A, **246**, 113.

TIME VARIATIONS OF COSMIC-RAY INTENSITY

By Robert R. Brown*

Department of Physics, University of New Mexico, Albuquerque, New Mexico

(Received May 14, 1956)

ABSTRACT

The time variations of cosmic-ray intensity associated with a large solar flare and a period of strong solar activity are reported. A possible interpretation of these semi-regular time variations in terms of matter emanating from the sun is considered.

INTRODUCTION

The study of cosmic radiation over the past 20 years has shown that, while the intensity of the cosmic-ray beam is relatively time-independent and isotropic, sudden and semi-regular time variations do occur [see 1 and 2 of "References" at end of paper]. The isotropy and time independence suggest a galactic origin of the radiation [3]. However, the larger time variations have been found to be correlated with solar activity and thus indicate local influence on the cosmic-ray beam. Examples of this are given by the sudden variations which follow shortly after some large solar flares and semi-regular variations with periods suggesting solar origin.

The sudden increases in intensity which follow within an hour after some large solar flares are rapid in onset, large in amplitude, and of short duration. Until recently, only four or five such events [4 to 10] had been observed in the last 15 years. While these increases are world-wide, the observed variations depend strongly on the type of detector and its altitude, geomagnetic latitude, and longitude [11]. It has been recognized that these extraordinary events represent the acceleration of charged particles in the vicinity of the sun to energies of the order of 10 Bev. The distribution of the impact points of these flare particles on arriving at the earth [11] indicates that the trajectories followed in going from the sun to the earth are essentially straight lines, except for the deflections produced in the vicinity of the earth by its magnetic field.

The sudden intensity decreases which sometimes follow these large flare events usually occur with a time delay of from 24 to 48 hours and are associated with geomagnetic disturbances. The intensity decreases are also world-wide, but slower in onset and longer in duration than the flare increases. While flare increases have been observed mainly at intermediate geomagnetic latitudes, the sudden decreases have been observed at all latitudes, including the geomagnetic equator.

The semi-regular variations with periods comparable to that of solar rotation are characterized by small and variable amplitudes. While the origins of the semi-regular variations and the sudden decreases are not clear, recently [12] it

*Now at the National Science Foundation, Washington 25, D. C.

has been suggested that both arise from the modulation of the isotropic cosmic-ray beam by turbulent magnetized clouds emanating from the sun.

With the outbreak of strong solar activity in the current solar cycle, a new flare increase has been observed. This flare event is interesting in that it occurred during a sequence of semi-regular intensity decreases and was accompanied by a number of terrestrial disturbances. It is the purpose of this paper to consider this extraordinary increase in cosmic-ray intensity and the disturbed period surrounding it.

APPARATUS

A local neutron production detector similar to that described by Simpson [13] was used in studying the time variations of the low energy nucleonic component of cosmic radiation. It consists of four enriched $B^{10}F_3$ neutron counters, 5 cm in diameter and 61 cm in active length, each counter being located at the center of a 15 cm × 15 cm × 80 cm paraffin block. The paraffin blocks are separated by 5 cm of *Pb*, then covered top and bottom by a 5 cm layer of *Pb*, and surrounded by more paraffin, until the entire structure occupies a volume of dimensions 134 cm × 136 cm × 84 cm.

The counter pulses are amplified by a linear amplifier and then scaled by a factor of 16. A camera photographs the scaler register, a clock, and an aneroid barometer every 15 minutes. The detector is located at an altitude of 1,575 *m* and geographic latitude 35.5° north and longitude 106.4° west (approximately 45° north geomagnetic latitude). The barometric coefficient of the apparatus has been determined to be -9.68 ± 0.22 %/cm Hg, and when intensity data are corrected to a pressure of 63.3 cm Hg, an average counting rate of approximately 310 counts/minute is obtained.

The over-all efficiency and operation of the apparatus was checked at frequent intervals by inserting a 2 mc Ra-Be neutron source into the structure. For the period of operation considered in this paper, the efficiency of the apparatus was constant to within ± 0.2 per cent.

TIME VARIATIONS

A. Solar-Flare Event

A large cosmic-ray intensity increase was observed on February 23, 1956, following a solar flare [14] of importance 3+ beginning at 0334 UT at 85° west heliographic longitude and 25° north heliographic latitude. The visible flare activity reached a maximum at 0342 UT and ended at 0414 UT. A radio-noise outburst and sudden short-wave fadeout were observed [15] in association with this event.

In the period preceding the cosmic-ray increase, 0203 to 0303 UT, the counting rate of the local neutron production detector was 289 ± 2 counts/minute. In the interval 0303 to 0318 UT, the intensity dropped to 258 ± 4 counts/minute, and then rose to 330 ± 4 counts/minute in the interval 0318 to 0333 UT and 404 ± 5 counts/minute in the interval 0333 to 0348 UT. The main increase began at approximately 0348, increasing by 1240 per cent in the interval 0348 to 0403 UT and then

slowly returning to within a few per cent of the pre-flare value after about seven hours. The intensity variations cited above are shown in Figure 1.

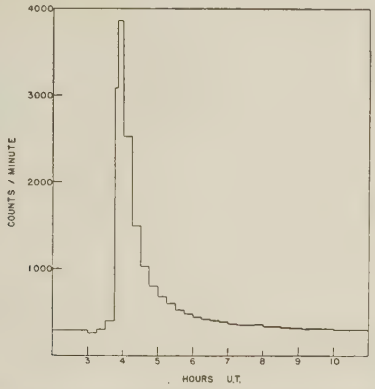

FIG. 1—Intensity of nucleonic component during the flare increase on February 23, 1956, as observed with local neutron production detector

B. Semi-Regular Variations

The extraordinary increase in intensity occurred in the middle of an intensity decrease associated with enhanced solar activity. The decrease was part of a semi-regular variation which first emerged from a period of more or less small intensity fluctuations in January, returned and grew in amplitude in February, and then reappeared but slowly decreased in amplitude in March. In particular, the intensity started to decrease in January on about the 12th, reached a minimum of about 4 per cent below normal on the 21st, and was almost normal again on the 28th. In February, the intensity started to decrease on about the 11th, reached a minimum of about 8 per cent below normal on the 20th, and returned to normal on the 29th. In March, a small decrease started on the 3rd and was followed by an abrupt decrease on the 11th, after which the intensity slowly and erratically returned toward normal. The 24-hour intensity averages for these months are shown in Figure 2.

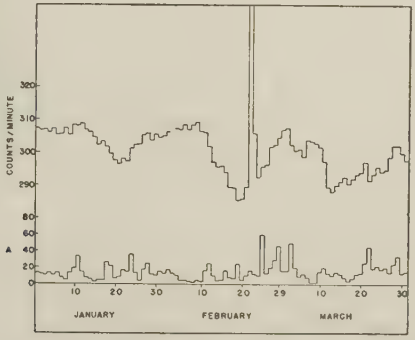

FIG. 2—Daily averages of intensity for the three-month period, January to March, 1956

C. Solar Acitivity

The period from January 1, 1956, to March 31, 1956, was one containing the greatest outburst of solar activity in the current solar cycle; in particular, two regions of rather pronounced activity [16] developed—High Altitude Observatory regions 55-Kp and 56Cp. HAO region 55-Kp began its 10th solar rotation in January showing pronounced activity, appeared at east limb on January 12, went through central meridian passage on about the 20th, and around the west limb on about the 27th. In February, pronounced activity was again displayed during the 11th rotation; the region appeared at east limb on the 9th, went through central meridian passage on the 17th, and around west limb on the 24th. The activity in this region declined markedly in March, and for the 12th rotation the region appeared at east limb on the 8th, went through central meridian passage on the 16th, and around west limb on the 23rd. In this period, HAO 55-Kp extended over a considerable range of heliographic longitude; approximately 30° in January, joining with region 56-Cp in February to form an active region approximately 60° wide, and then separating from 56-Cp in March.

HAO region 56-Cp developed first in January, showing only weak activity. The region appeared at east limb on the 15th, went through central meridian passage on the 22nd, and around west limb on the 29th. In February, the region displayed moderate activity; it appeared at east limb on the 13th, went through central meridian passage on the 20th, and around west limb on the 27th. In March, the region showed pronounced activity; it appeared at east limb on the 9th, went through central meridian passage on the 16th, and around west limb on the 23rd.

Flare activity was evident in HAO 55-Kp in January, reached a maximum in February with the large flare of February 23, and then declined in March. HAO 56-Cp showed only slight flare activity in February and some increase in March. The flares of importance 2 or greater which occurred in these regions during this three-month period are given in Table 1. Numerous flares of importance 1 and subflares were also reported in these regions.

Geomagnetic activity was evident in this three-month period, a number of geomagnetic storms being observed. The dates of occurrence and duration of the storms are given in Table 2.

DISCUSSION

In regard to the flare event, a number of interesting features present themselves. First, it would appear from the intensity variations at Albuquerque, New Mexico, in the hour *before* optical flare activity was observed that solar processes capable of influencing the cosmic-ray beam near the earth were in operation. This is suggested by the fact that the intensity decreased significantly approximately 15 minutes before the flare started and then increased at a slow rate until the main burst arrived at approximately 0348 UT.

Next, from the close time association of the flare activity and the cosmic-ray burst, and the fact that European observers [17], near the 0400 local-time impact zone, observed the largest intensity increase, it would seem to follow from the calculations of Firor [11] that this event represents another instance in which particles were accelerated near the sun. Also, neutral particles in appreciable

TABLE 1—*Solar flares*

Date	Time (UT) Start	Time (UT) End	Importance	Region
1956	*h m*	*h m*		
Jan. 14	10 07	10 30	2	55-Kp
19	22 44	22 54	2	55-Kp
23	12 45	13 07	2	55-Kp
23	16 20	17 05	2	55-Kp
Feb. 10	21 10	21 40	3	55-Kp
13	14 38	15 58	2	55-Kp
16	18 05	19 25	2+	55-Kp
17	10 30	11 38	2−	55-Kp
17	11 25	.. ..	2	55-Kp
23	03 34	04 14	3+	55-Kp
Mar. 13	14 53	15 23	2	56-Cp
15	16 30	17 20	2	56-Cp

TABLE 2—*Geomagnetic storms*

Start (UT)	End (UT)
Jan. 10, ...	Jan. 10, ...
17, 2343	17, ...
23, ...	23, ...
27, 0858	27, ...
Feb. 11, 1847	Feb. 12, 12XX
19, 0222	12, 22XX
21, 2005	22, 17XX
25, 0309	25, 22XX
29, 00XX	Mar. 1, 01XX
Mar. 3, 00XX	4, 09XX
10, 21XX	11, 09XX
22, 00XX	23, 06XX
28, 21XX	28, ...

numbers would seem to be ruled out on the basis of radiation reaching the dark hemisphere of the earth and the fact that observers [18] near 1200 local time observed a much smaller increase than those near the 0400 impact zone.

Next, since the visible flare activity ended at 0414 UT, the decaying tail of the intensity curve, which lasted for several hours, probably represents flare radiation returned to the earth from other regions in the solar system. This argument is strengthened, as Simpson [19] has pointed out, by the lack of intensity increase near the 0900 local-time impact zone, which would be expected if the sun continued to emit particles as the observer passed through this zone.

Further, the flare radiation appears to be predominantly of low energy, of the

order of a few Bev. This is suggested by the marked latitude and longitude variations; for example, 24 fold increase at Chicago [19] against 4 to 5 fold increase at Albuquerque, after correction to sea-level.

Also, the longer persistence of the flare radiation suggests this interpretation: 26 per cent above normal at Chicago [19] at 1400 UT against one per cent above normal at Albuquerque at 1100 UT, in spite of the altitude difference. It is interesting to note, however, that Simpson [20] and Forbush [21] report intensity increases at the geomagnetic equator, indicating that the flare radiation has a spectrum extending to energies of the order of 20 Bev.

In regard to the semi-regular decreases during the three-month period, it would seem that they are related to the outbreak of solar activity which occurred. While the exact mechanism is not clear, it is to be noted that a close time association exists, at least for the months of January and February, between the growth and disk passage of the active regions, 55-Kp and 56-Cp, and the cosmic-ray intensity. In particular, as the sunspots in the regions developed in area and appeared at east limb, the intensity began to decrease, reached a minimum at approximately the same time as the central meridian passage and maximum development of the sunspots, and then increased again as the sunspots declined in area and moved toward west limb. The sunspot data [22] for these regions are given in Table 3, where date-area-count are given for these regions when first seen, at maximum, and when last seen.

Table 3—*Sunspot data*

Date	Region	Date-Area*-Count		
		First seen	Maximum	Last seen
January	55-Kp	13–270–1 14–480–2	18–1320–13 20–1930–18	25–390–1 26–1400–2
	56-Cp	. . . . .	. . . . .	. . . . .
February	55-Kp	10–340–1	18–650–6 14–2410–28 21–1730–15	24–870–2
	56-Cp	14–150–1	20–1280–35	26–580–3
March	55-Kp	10–50–x	14–130–2	14–130–2
	56-Cp	11–1120–4	14–1490–22	22–680–6

*Area expressed in millionths of area of the solar hemisphere, with measurements corrected for foreshortening.

With the exception of the 3+ flare on February 23, no direct correlations are evident between flares and cosmic-ray intensity in the three-month period. However, there remains the possibility that the decrease in intensity starting on February 11 and the geomagnetic storm on the 11th are related to the flare of importance 3 observed on February 10.

The over-all correlation of cosmic-ray intensity and geomagnetic activity is rather poor. This can be seen from Figure 2, where the mean Cheltenham magnetic A-index [16] is shown for the three-month period. In addition, while a number of geomagnetic storms occurred in the period, it is difficult to find direct correlations of cosmic-ray intensity with the storms. This is due mainly to the disturbed character of the entire period: brief variations, of the order of one per cent in amplitude, were frequently superimposed on the general variation, as shown by the daily averages in Figure 2.

CONCLUSIONS

While the flare increase of February 23 serves as an example of solar injection of particles into the cosmic-ray beam, the semi-regular decreases observed in the three-month period show that the solar influence does not only involve the acceleration of particles. More specifically, the observations indicate that a solar mechanism may bring about a *downward* modulation of the cosmic-ray beam near the earth. These observations may find their explanation in the recent suggestion by Morrison [12], involving the modulation of the cosmic-ray beam by magnetized clouds emanating from active regions on the sun. However, it should be pointed out that the suggestion of Morrison, based as it is, in part, on the observations of Simpson, Babcock, and Babcock [23], considers the 27-day recurrences as intensity *increases* resulting from particles leaking into regions swept clear of more magnetic clouds by well-ordered clouds emanating from unipolar regions on the sun and traveling along the lines of force starting in these regions. It would seem that there is no objection to considering the slow decreases observed here in a manner similar to the sudden magnetic storm decreases (Forbush events) which involve the emission of fresh clouds following solar flares. In the present instance, however, the clouds would originate in the regions of strong solar activity and not with large flares.

ACKNOWLEDGMENT

The author is indebted to the High Altitude Observatory and the National Bureau of Standards for the Weekly Preliminary Report of Solar Activity and to the Research Corporation for a Cottrell grant.

References

[1] J. G. Wilson (Ed.), Progress in Cosmic Ray Physics, North-Holland Publishing Co., Amsterdam (1952); chap. VII.
[2] L. Biermann, Origin and Propagation of Cosmic Rays, Annual Review of Nuclear Science, Vol. 2 (1953).
[3] P. Morrison, S. Olbert, and B. Rossi, Phys. Rev., **94**, 440 (1954).
[4] I. Lange and S. E. Forbush, Terr. Mag., **47**, 331 (1942).
[5] A. Ehmert, Z. Naturf., **3a**, 264 (1948).
[6] J. Lord, A. Elston, and M. Schein, Phys. Rev., **79**, 540 (1950).
[7] D. C. Rose, Phys. Rev., **78**, 181 (1950).
[8] S. E. Forbush, T. B. Stinchcomb, and M. Schein, Phys. Rev., **79**, 501 (1950).
[9] J. W. Graham and S. E. Forbush, Phys. Rev., **98**, 1348 (1955).
[10] N. Adams, Phil. Mag., **41**, 503 (1950).
[11] J. Firor, Phys. Rev., **94**, 1017 (1954).

[12] P. Morrison, Phys. Rev., **101**, 1397 (1956).
[13] J. A. Simpson, W. Fonger, and S. B. Treiman, Phys. Rev., **90**, 934 (1953).
[14] T. Hatanaka, Tokyo Astronomical Observatory (private communication).
[15] S. F. Smerd, Radiophysics Laboratory, Commonwealth Scientific and Industrial Research Organization (private communication).
[16] Preliminary Report of Solar Activity, High Altitude Observatory and National Bureau of Standards, Boulder, Colorado.
[17] H. Elliot (private communication).
[18] Y. Sekido, C. Ishii, and Y. Miyazaki, Working Association of Primary Cosmic-Ray Research, Japan (private communication).
[19] J. A. Simpson, Phys. Rev. (in press).
[20] J. A. Simpson, Phys. Rev. (in press).
[21] S. E. Forbush, J. Geophys. Res., **61**, 155 (1956).
[22] Central Radio Propagation Laboratory, National Bureau of Standards, Solar-Geophysical Data, Ser. F, Pt. B.
[23] J. A. Simpson, H. W. Babcock, and H. D. Babcock, Phys. Res., **98**, 1402 (1955).

LOW FREQUENCY ELECTROMAGNETIC RADIATION 10-900 CYCLES PER SECOND

By Jules Aarons

Propagation Laboratory, Air Force Cambridge Research Center, L. G. Hanscom Field, Bedford, Massachusetts

(Received June 25, 1956)

ABSTRACT

During the period of July 10 to September 15, 1955, detection of electromagnetic signals in the frequency range 10 to 900 cycles per second was undertaken. Loops and a vertical antenna were used in a site remote from man-made interference. The spectrum was analyzed with a narrow bandwidth (2 to 6 cycles per second) amplifier. Indicated diurnal patterns show a maximum around local midnight. The peak in the band lies in the region 40 to 200 cycles per second. During one period of several hours, a large increase in narrow band energy was seen near 33 cycles per second. The possibilities of this being radiation at the gyrofrequency of the sodium ion is discussed.

I. 10-900 CPS EXPERIMENT

A. Introduction

Two approaches are possible in the field of the detection of audio-frequency components of atmospherics. One technique consists of direction finding on individual atmospherics and comparing components of the signal as regards diurnal variations, absorption as a function of distance, and other parameters. This has been investigated by Chapman and Matthews [see 1 of "References" at end of paper] and Bowe [2].

A second method is to take the sum total of energy arriving at a given point and to note its characteristics. This latter method was chosen for this study, since a direction-finding network was not available to pin-point the atmospheric source position. The diurnal pattern as a function of frequency was of interest. The gyrofrequency experiment also necessitated an integration study.

A sweep-frequency continuously-operated equipment was used. Background level changes could be recorded, as well as analysis made of local thunderstorms. This would aid in one of the aims of the study, that is, to bridge the gap between rapid fluctuations of the earth's magnetic field and atmospheric noise. A narrow band unit would also look into the problem of emission or absorption of energy at the gyrofrequency of ions in the upper atmosphere.

B. Site and Measurement Period

Previous work done by the author [3, 4] indicated the necessity for making audio-frequency measurements at a remote site. Power-lines at 60 cps produce energy at all harmonics, as well as being responsible for transients at all frequencies.

Therefore, a field site was chosen near Mescalero, New Mexico. The site, a meadow, was seven miles from the nearest power-line, a low power unit to a farmhouse. The measurement period covered was July 10 to September 5, 1955. Many local thunderstorms were seen during the period, and days without thunderstorm activity in the region were also available for analysis.

Earlier measurements with the same equipment in a location near Boston, Massachusetts, had been taken in the summer of 1952. The relatively high level of 60-cycle interference led to the gathering of only a small amount of usable data. The results of this short study are in agreement with the data reported in this paper.

C. Instrumentation

(1) *Detection technique*—The pick-ups for the experiment consisted of a 10,000-turn loop, electrostatically shielded, approximately one meter in diameter, and a 24-foot vertical antenna.

A timing system was set up so that during any one hour the following sequence took place:

a. A complete sweep would be taken with either the loop or the vertical antenna.
b. A four-minute period of set noise was measured.
c. The remainder of the hour was used for the output of the second antenna.

Both detectors were set over 40 feet from the van used to house the electronic equipment.

(2) *Electronics*—Figure 1 is the block diagram of the battery-operated system.

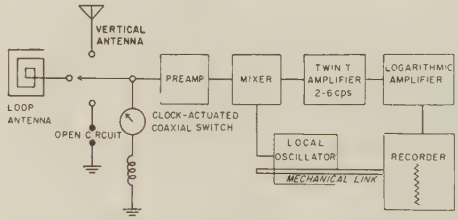

BLOCK DIAGRAM OF
LOW FREQUENCY ANALYZER SYSTEM
FIG. 1

The analyzer timed-scanned the audio-frequency spectrum in 2-, 4-, or 6-cycle sections (according to the bandwidth setting for the day) and recorded the intensity. The local oscillator output (1,990 to 1,100 cycles per second) was added to the input signal to obtain an intermediate frequency of 2,000 cycles per second. Due to feed-through problems (because of the proximity of the local oscillator and the IF), frequencies lower than 10 cycles per second could not be used.

A logarithmic frequency sweep was chosen so that the low frequencies would have sufficient time to record with a time constant of one second for the system. The time for a complete sweep was approximately 15 minutes.

The output of the mixer system was fed to a Twin T filter and then to a logarithmic amplifier. The motor which drove the oscillator also provided the recorder drive.

Bandwidth, gain characteristics, and frequency were checked each day, since a change in battery voltages might change equipment characteristics. Each daily record contains its individual gain *vs* frequency calibration.

With the vertical antenna, a signal of 0.1 microvolt per meter per cycle per second could be detected above the noise. For the loop, the minimum detectable change in magnetic field (fB) was $4 \times 10^{-3}\gamma$.

D. The Data

(1) *Diurnal pattern*—Figure 2 is the pattern of several 15-minute sweeps, taken on August 31, 1955, and September 1, 1955. The records are calibrated in $\mu v/m/cps$. The noon record (Fig. 2*a*) shows the high signal level between 40 to 90

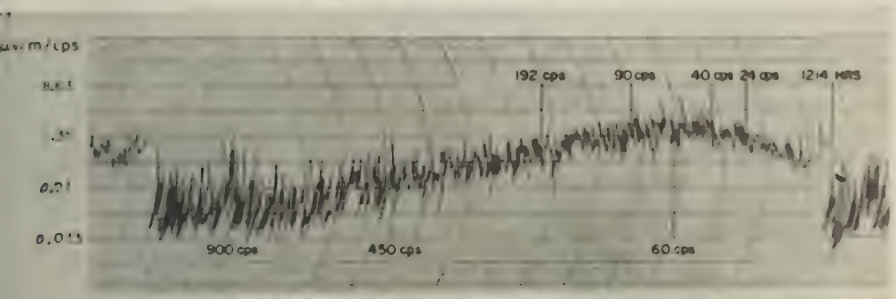

a) SWEEP RECORDED ON A VERTICAL ANTENNA, 1214, AUGUST 31, 1955.
A 14 MINUTE, 20 SECOND TIME PERIOD IS SHOWN.

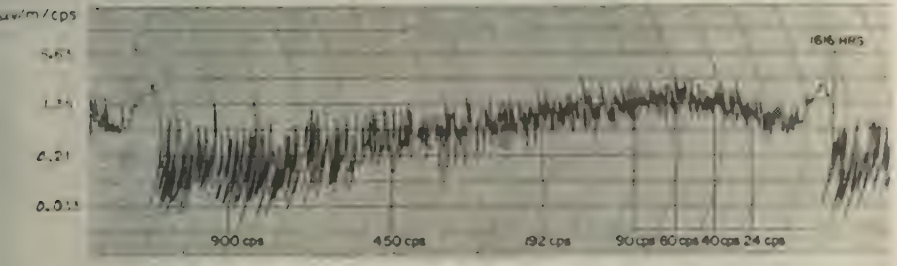

b) SWEEP RECORDED ON A VERTICAL ANTENNA, 1616, AUGUST 31, 1955.
A 14 MINUTE, 20 SECOND TIME PERIOD IS SHOWN.

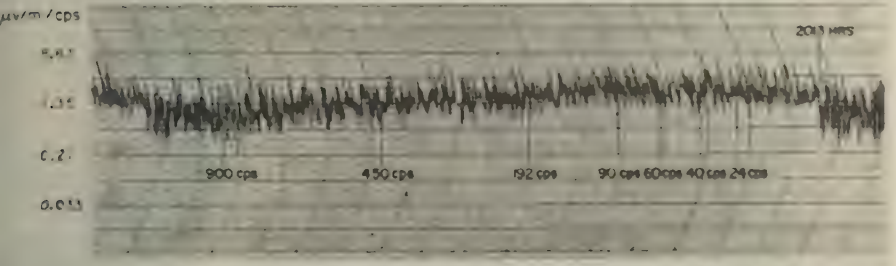

c) SWEEP RECORDED ON A VERTICAL ANTENNA, 2013, AUGUST 31, 1955.
A 14 MINUTE, 20 SECOND TIME PERIOD IS SHOWN.

FIG. 2

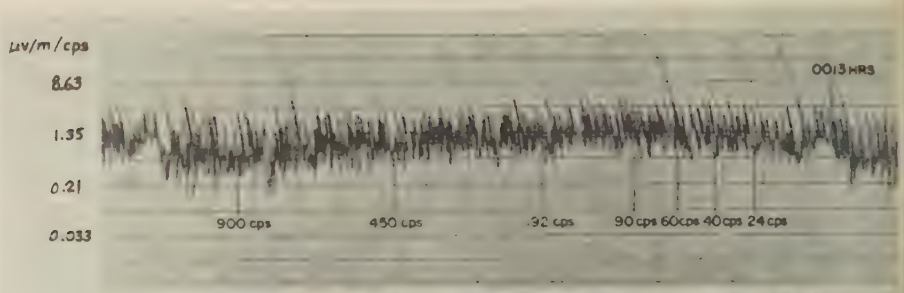

d) SWEEP RECORDED ON A VERTICAL ANTENNA, 0013, SEPTEMBER 1, 1955. A 14 MINUTE, 20 SECOND TIME PERIOD IS SHOWN.

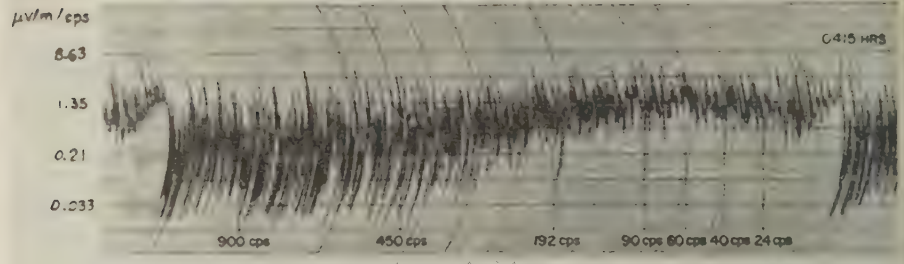

e) SWEEP RECORDED ON A VERTICAL ANTENNA, 0415, SEPTEMBER 1, 1955. A 14 MINUTE, 20 SECOND TIME PERIOD IS SHOWN.

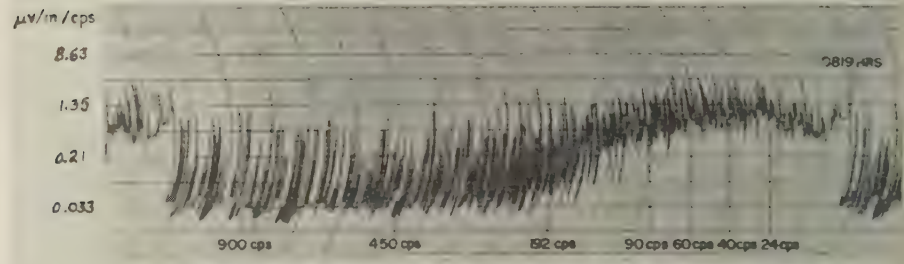

f) SWEEP RECORDED ON A VERTICAL ANTENNA, 0819, SEPTEMBER 1, 1955. A 14 MINUTE, 20 SECOND TIME PERIOD IS SHOWN.

FIG. 2

cycles per second with a breadth considerably greater than the normal bandwidth curve exhibited during a calibration of 60-cycle intensities. The high end of the frequency band shows a relatively low intensity.

Figure 2b (1616 hours) shows an increase in the high frequency energy with the 40-90 cycle portion at about the same level. This is typical of the late afternoon record. During this particular afternoon, the weather in the area was generally cloudy, with towering cumulus reported from stations within a 100-mile radius.

Early evening records show a slight increase in general level in the central portion of the band and an even greater increase in the high frequency amplitudes. The minima are not as deep as they were in the previous record, indicating a larger number of signals, as well as an increase in field strength. During the night-time

period, many atmospherics are received. Thus, the time constant of the equipment does not allow the level recorded to fall to low values and the ratio of maximum to minimum signal is small.

Around local midnight (0013) for the particular sweep recorded in Figure 2*d*, the minima are slightly lower. However, the flattest spectrum is usually received at this time.

A dramatic change is seen as dawn is approached, with fewer signals received and a lower intensity recorded for the high end of this spectrum. Individual atmospherics are more readily seen beyond 200 cycles than were evident in the previous records illustrated.

The morning record (0819 hours) shows the decrease in over-all level and the absorption of high frequency signals. Periods of several seconds are shown when no atmospherics with components in the upper frequencies were received.

Sunrise patterns (ground sunrise occurred in this area between 0500-0545 during these months) show consistently a maximum amount of attenuation in the region of the band above 450 cps, with relatively few atmospherics being received.

A hypothesis for the high flat level recording at night is that propagation conditions are excellent for receiving distant atmospherics. The high intensity in the 400 to 900 cps region during this period points to long-distance propagation.

Peak signals of high maximum to minimum ratio indicate local activity or a more selective channeling of energy to the receiver. It is difficult to account for the vast differences in upper frequency changes as due to world-wide thunderstorm activity alone. The variations given in the few studies made [5, 6] would not account for the day-night ratios as indicated in the data. It seems more reasonable that the variability of ionospheric absorption accounts for the diurnal pattern in the high end of this portion of the audio spectrum. Figure 3 summarizes the day's data. It is a spectrum analysis of this information with one complete sweep plotted for each hour.

(2) *Data at* 96 *cycles per second*—In order to demonstrate more clearly the dynamic range of the amplitudes and to compare more simply the two antennas, the analyzer was stopped from August 8 to 10, 1955, at 96 cycles per second. This particular frequency was chosen because it is apparently the maximum in the signal level distribution.

The weather in the area was generally cloudy, with towering cumulus reported from stations within a 100-mile radius.

Figure 4 illustrates the diurnal pattern for the two types of antennas. The sunrise dip is similar to that on other records of atmospherics at 50 kc taken at Scituate, Massachusetts. The sunset rise is not as sharp. The minimum signal level was received at 0915, with a peak reception at local midnight. A secondary maximum is seen in the afternoon.

The ratio of maximum to minimum signal was 40:1 for the vertical antenna and 12:1 for the loop antenna. It seems reasonable to believe that the DC component of the static field of discharges affected the vertical antenna input circuit, while the loop, which was electrostatically shielded, was not as affected by this component of the discharge pulse.

However, the variations in the 40 to 200 cycles level may well be due to world-

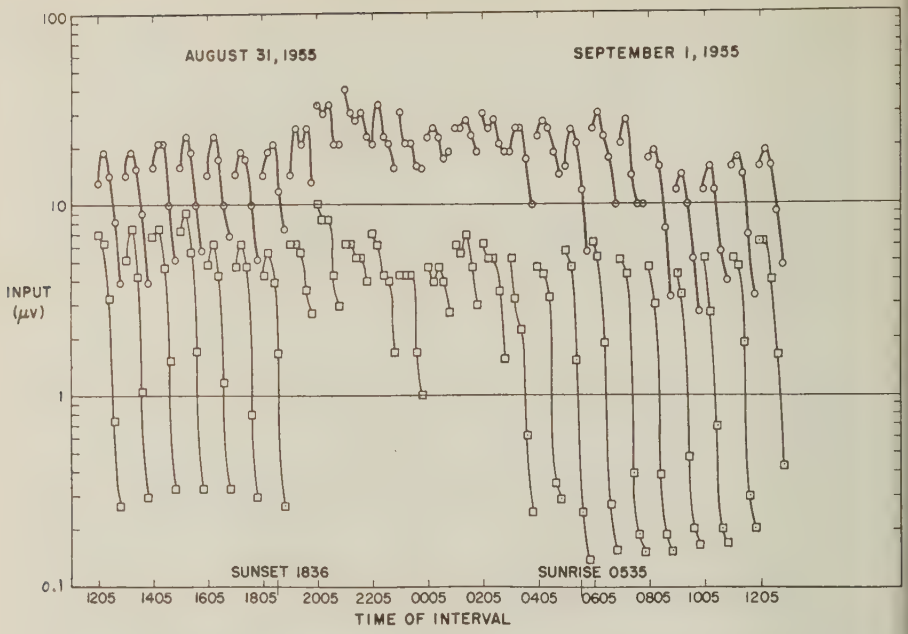

FIG. 3

(*Note:* In Fig. 3, the circles represent maximum values of a sweep with the vertical antenna, while the boxes are minimum signals for the same sweep.)

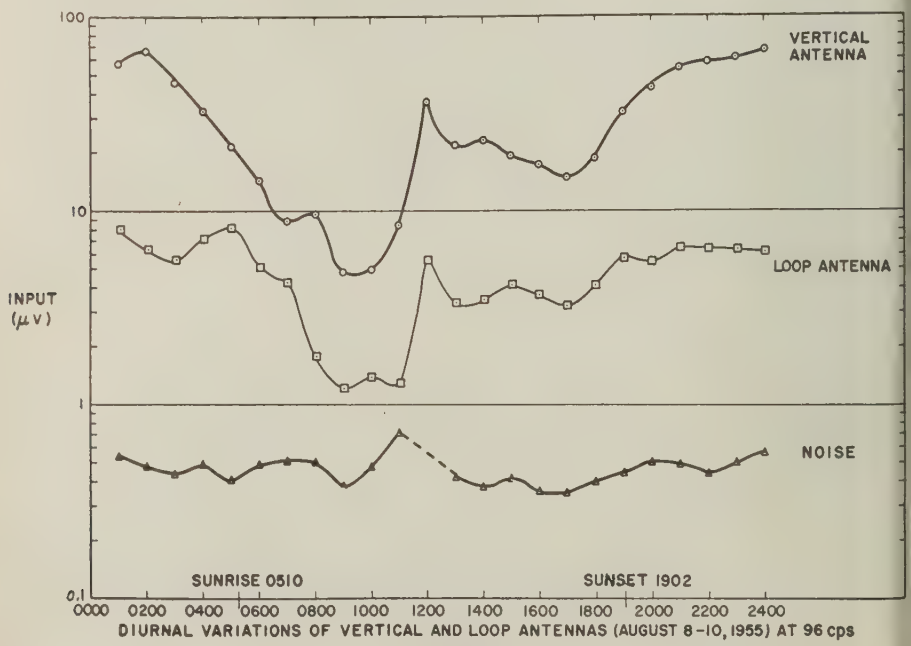

FIG. 4

ride thunderstorm activity, as indicated by Holzer and Deal [7]. This portion of he spectrum shows little variation and a constant high level, indicating good propagation conditions over daylight and night paths.

(3) *Storm period*—Figure 5 is an illustration of a typical thunderstorm period,

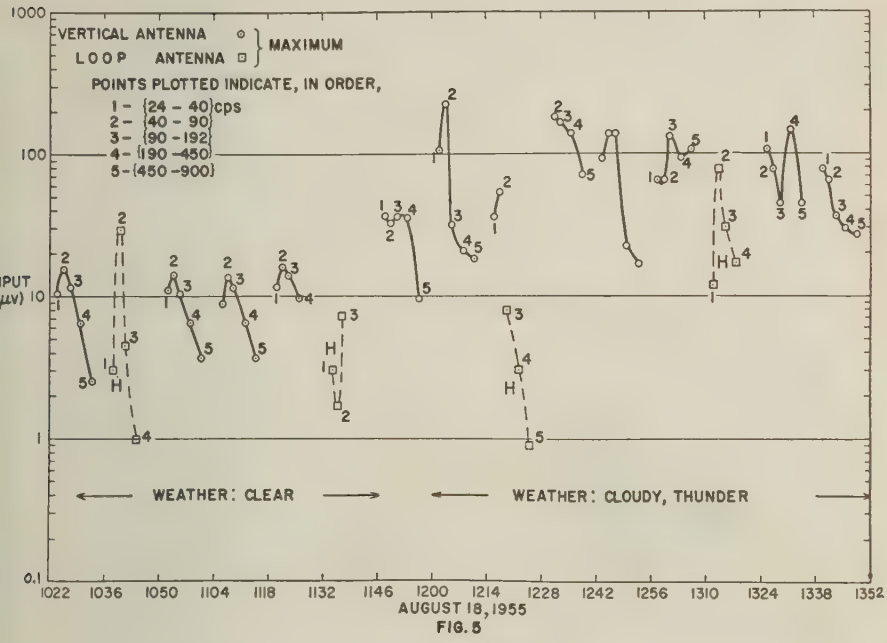

FIG. 5

howing the spectrum of atmospherics from towering cumulus and cumulo-nimbus ypes of clouds present.

The normal spectrum is shown in the period 1022 to 1125, August 18, while ightning was recorded during the time 1200 to 1352. These recordings show the ime bursts of discharges which skew the analyzer records when thunder was heard. This pattern, therefore, is a function of time rather than frequency.

(4) *One-half to 20 cycle per second noise*—In order to supplement the data which tarted at 10 cps, a relatively wide band system ($\frac{1}{2}$ to 20 cps) was used to directly ecord the variations from a loop similar to that used on the higher frequency ystem. During the periods of intense local storms, an increase in level took place ith a spike-type signal recorded. However, several specific evening levels were ow compared to the daytime periods, indicating a somewhat different mechanism esponsible for the steady-state component in the $\frac{1}{2}$ to 20 cps study and the 10 o 900 cps region. It seems reasonable that with previous work in the field the oise storms of the low frequency end of the spectrum are associated with sudden ommencement of magnetic disturbances, while the energy from atmospherics redominates at the frequencies in the region above 15 to 20 cps.

It is of interest to note the results reported by Maple [8] on the correlation of nagnetic storms and low audio frequencies and the spectrum analysis performed y Wilcox and Maple [9] on audio-frequency atmospherics.

II. TWO HYPOTHESES FOR ELECTROMAGNETIC RADIATION AT AUDIO FREQUENCIES

A. The Gas Discharge Analogue

In order to explain the association of the very low frequency ($\frac{1}{2}$ to 20 cps) data with the magnetic storms, a mechanism is suggested which uses the analogue of the gas discharge tube and the aurora. It should be emphasized that it is only this portion of the spectrum for which the mechanism is postulated. The atmospherics above 15 cps are a different phenomenon, and it is their propagation which has been described up to this point.

Basic similarities exist between auroral processes and laboratory experiments concerned with gas discharge. The gas discharge experiments supply a mechanism for the generating and coupling of noise signals into a circuit. From experiments within a narrowly confined region, the gas discharge tube, both wide band noise and enhancements of energy at specific frequencies have been produced.

One of the phenomena described by experimenters is that of moving striations in changing layers of ionized gas. In the cold cathode glow discharge, both at the beginning and after a steady-state condition has been reached, patches of luminosity move between the negative glow and the anode in both directions. One of the types observed consists of a series of luminous pulses [10]. Moving striae have been found in most gases, over large pressure and current ranges.

In aurora, similar forms exist. Arcs, bands, and draperies lie in a horizontal plane. These forms are dynamic. Arc sections flash up and disappear regularly with a period of several seconds [11]. Radar reflection fading rates show the rapidly changing aspect of auroral radiations, particularly in the frequency region below several hundred cycles per second.

Several experimental workers [12, 13, 14] have found that noise levels in gas discharge tubes exceeded shot noise, in one case as much as 80 db, and that this energy was centered at audio frequencies.

It is suggested that the aurora, which is closely correlated with magnetic storms, acts as a gas discharge source. The process of coupling is similar to that in which the current within the gas discharge tube is linked with its external circuit, an impedance varying technique. The ionospheric current system is analogous to the external circuit of the discharge tubes.

The gas discharge tube, however, has several points where it does not bear comparison to the aurora. The latter has a dynamic character. Limb flare data and solar radio emission show fluctuations ranging from several seconds to minutes. These variations result in modulations of the general discharge noise and are coupled into the ionosphere, appearing as a component of scintillations and other ionospheric variations. A second variance with the analogue is that the ionosphere has a particular impedance configuration which varies as a function of time. This makes each storm different as opposed to the constant impedance presented to the gas discharge tube. The entire previous history of the ionosphere plus the flare parameters are needed to assess the effect of any one particular aurora.

These fluctuations and variations emerge as the below 15 cycle components of the variations of the earth's magnetic field. The amplitude level of these variations

is itself geomagnetic and is under solar control. The amplitude of the higher frequency signals is derived from atmospherics, but its propagation is under solar control.

B. An Hypothesis for the Dawn Chorus

The dawn chorus is a series of bursts occurring around dawn on days when auroral activity was high. The frequency components of the pulses and steady hiss range from 1.5 to 4 kc [15].

Given the data on the propagation of atmospherics over long distances, it is difficult to see how atmospherics can be the source of this energy, unless a rather unique mode of propagation is assumed.

In analyzing the spectrum of individual spherics, Bowe [2] and Edwards [16] found heavy attenuation in the region around 3.5 kc. Edwards points out this distinct trough, noting that its wavelength is somewhat greater than the earth-ionosphere separation. If the tendencies shown in the data within this paper continue to 5 kc, the heaviest absorption will occur in the early morning hours. The frequencies will be above 200 cps to approximately 4 kc. While individual atmospherics are of course received, the dawn chorus comes in as distinctive high level signals over the background noise.

It seems difficult then to attribute the dawn chorus to propagation of atmospherics. A suggested hypothesis is that the auroral discharge (which continues at dawn according to radio reflection studies [17], but disappears during the remainder of the morning and the early afternoon) couples audio-frequency energy into the ionospheric current system. It is these induction components which are seen clearly as the dawn chorus "hiss" signals above the relatively quiet atmospherics level. The dawn chorus would therefore appear to be rapid variations of the earth's magnetic field.

III. THE GYROFREQUENCIES OF IONS IN THE UPPER ATMOSPHERE

A. The Data

On August 14, 1955, the spectrum analyzer was set up to record for the major portion of the hour with the loop oriented in the east-west direction. For a period of 12 minutes each hour, the input was shifted to a second coil with its plane north-south. For four minutes, vertical intensities were recorded.

An enhancement was noted starting at 1400 local time on the coil oriented in the EW plane. During one sweep, a low level was recorded in the NS coil. The early sweep with an enhancement equivalent to 47.5 microvolts is recorded in Figure 6*a*. This level continued for an hour and 15 minutes. The type of signal displayed was more of a coherent tone than an impulse noise signal increase. A lower level but distinct enhancement at this frequency was received throughout the day.

Figure 6*a* is a recording of one of the sweeps which show the large signal level of the 33-cycle signal. This type of signal continued for several sweeps.

Later in the day, an enhancement was seen, as shown in Figures 6*b* and 6*c*, but the level had decreased considerably.

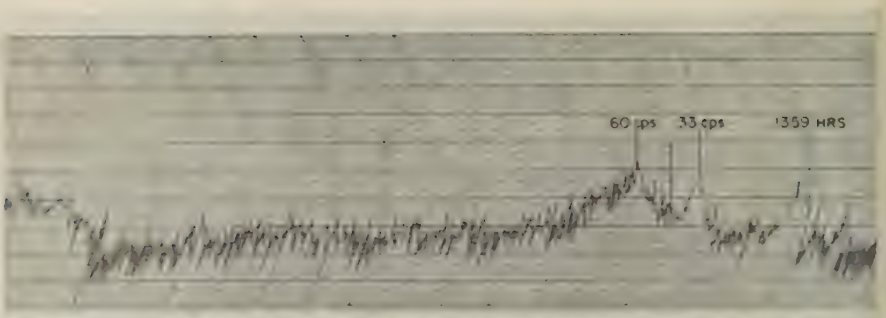

a) SWEEP RECORDED ON A LOOP ANTENNA, ORIENTED E-W, 1359, AUGUST 14, 1955, SHOWING 33 cps PEAKING EFFECT. A 14 MINUTE TIME PERIOD IS SHOWN.

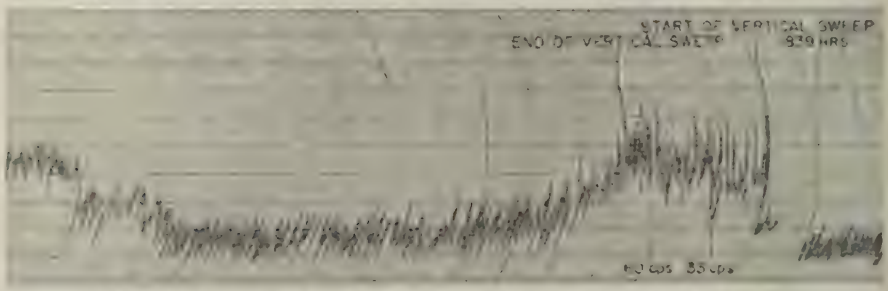

b) SWEEP RECORDED ON A VERTICAL ANTENNA, 1839, AUGUST 14, 1955, SHOWING 33 cps PEAKING EFFECT. A 14 MINUTE TIME PERIOD IS SHOWN.

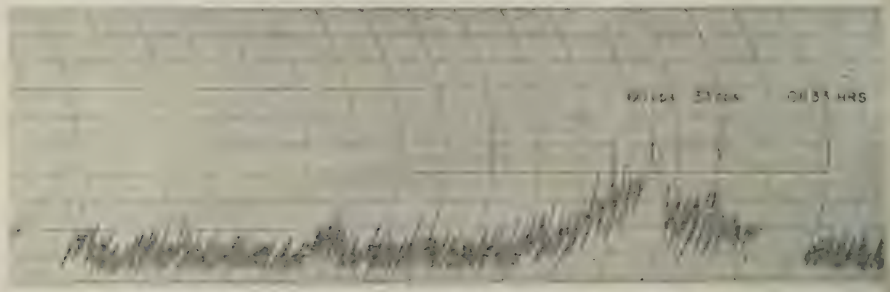

c) SWEEP RECORDED ON A LOOP ANTENNA, ORIENTED E-W, 0633, AUGUST 16, 1955, SHOWING 33 cps PEAKING EFFECT. A 14 MINUTE TIME PERIOD IS SHOWN.

FIG. 6

The signal level recorded for this enhanced component was 12 μv above the background noise level. At 33 cps, this corresponds to a change of 5.5×10^{-7} γ or $16.5 \times 10^{2} \mu$v/m/cps.

Figure 7*a* is a graph of the intensity of the signal received along with a comparison of the signal at 60 cycles. The two do not correlate, indicating their independence. Beyond the time encompassed by this Figure, the 60-cycle signal stayed at about the same level as recorded above, while the 33-cycle signal fell to amplitudes rising only slightly above background.

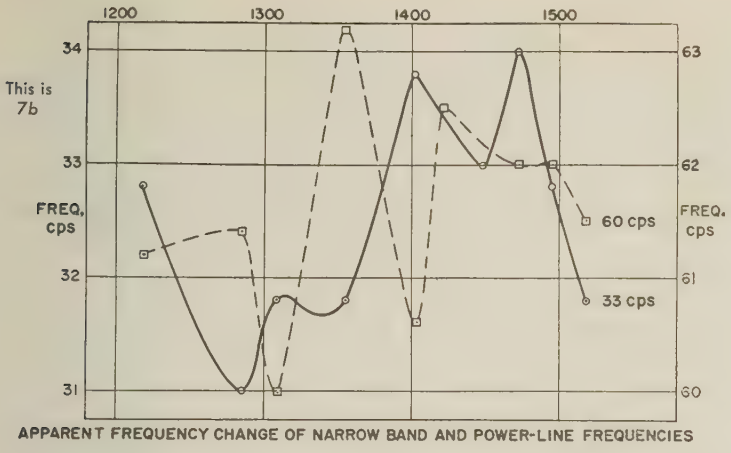

APPARENT FREQUENCY CHANGE OF NARROW BAND AND POWER-LINE FREQUENCIES

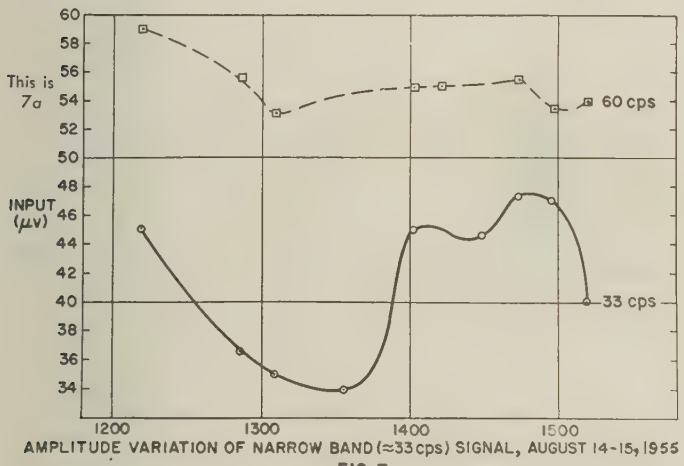

AMPLITUDE VARIATION OF NARROW BAND (≈33 cps) SIGNAL, AUGUST 14-15, 1955

FIG. 7

The frequency of the signal has also been noted in Figure 7*b*. The 60-cycle signal deviations from the calibration points are seen. The recording techniques used were such that an accuracy of ±1.5 cycles was achieved. The frequency variations during the main portion of the enhancement were probably apparent rather than real.

The evidence is that during this period an enhancement was noted at 33 cycles per second with an accuracy of calibration of plus or minus 1.5 cycles per second. The nature of the signal seen was a coherent one rather than a noise increase.

B. The Gyromagnetic Frequencies

The revolution of ions and electrons in the earth's atmosphere expresses the equilibrium between the centrifugal force on the particle (mv^2, r) and the deflecting force of the earth's magnetic field (Hev).

We are interested for purposes of this study in the gyrofrequency of ions

known to exist in the ionosphere or possibly existing in the solar corpuscular stream.

Table 1 lists the gyrofrequency of these ions, using for reference a magnetic

Table 1

Ion	Mass number	Frequency
		(cycles per second)
(Electron)	1/1837	1,400,000
Nitrogen + (N)	14	55
Nitrogen ++	..	110
$Nitrogen_2$ + (N_2)	28	27.5
Oxygen + (O)	16	48
Oxygen ++	..	96
$Oxygen_2$ +	32	24
OH +	17	45
Sodium + (Na)	23	33.5
Nitric oxide (NO)	30	25.5
Hydrogen + (H)	1	765
Hydrogen ++	..	1,530
Helium + (He)	4	192
Helium ++	..	384
Calcium + (Ca)	40	19

field intensity of 0.5 gauss. These fall, for the most part, within the audio-frequency spectrum, and radiation or enhancement at these frequencies was one object of this study.

Table 2 is a grouping of the frequencies of the sodium ion, using the value of

Table 2—*Gyrofrequency of sodium ion at Mescalero, New Mexico, 1955*

Altitude	Frequency
km	*cycles per second*
0	36
60	35
100	34.3
200	32.6
300	30.9

H for the Mescalero site and the diminution of the H value as a function of altitude.

If the radiation comes from the sodium ion, it seems likely that this would take place at the top of the D layer or within the E layer. Previous data on the Perseids shower have shown [18] that meteors have excited sodium. The ionization potential of sodium is small, 5.12 volts. Recent rocket experiments [19] have dramatically demonstrated the ease with which sodium is ionized in the upper atmosphere.

C. The Radius of Oscillation

The radius of oscillation is directly proportional to the mass and velocity of the particle and inversely proportional to the charge and magnetic field. Calculations have been made for the radius of the gyration in Table 3.

TABLE 3—*Radius of Gyration of H and O_2*

	100 km	*200 km*	*300 km*
H	37 cm	52 cm	110 cm
O_2	210 cm	305 cm	620 cm

The thermal velocity has been calculated from the formula $v = \sqrt{8kt/\pi m}$. The values used are taken from the Rocket Panel data [20]. A temperature of 2,000°K has been assumed for 300 km.

The importance of the radius of gyration lies in determining the method for calculating the bandwidth. If an ion oscillates many times before colliding with other particles, it is regarded as radiating at a rate given by an ion moving continuously in a circular orbit. However, if the ion collides with other particles before completing several rotations, then the collisional frequency determines the bandwidth. In the ionosphere, this results in wide band (megacycle) signals. It should be stressed that, in the hypothesis advanced for the emission of radiation at the gyrofrequencies of the ion, the collisions do not contribute to the emission bandwidth but rather to the absorption. The gyrating portion of the orbit determines the signal characteristics.

In the case of the 100-km layer, the mean free path is about 10 cm. The radius range is from 37 to 210 cm.

At 300 km (the *F*2 layer), the mean free path is 150 meters, with the ion radii ranging from 1.1 to 6.2 meters. A large number of oscillations are completed before collision.

The bandwidth of radiation emitted by the ion is extremely narrow, even when thermal broadening is taken into account [21]. It amounts to 10^{-22} cps for the hydrogen proton before broadening and 10^{-8} cps at 200 km after broadening. The increase in bandwidth is a factor of 95.6 for O_2 compared to the proton. Another increase of 2.2 is seen for the change of height from 200 to 300 km.

It is to be expected using this approach that the line will be narrow. The mean free path in the layer determines the time spent in radiations by the ion at each layer. Collisions produce an absorption of energy and a broadening of the line.

The mechanism advanced, therefore, is an external force giving energy to the ion, which then starts its oscillation in the lines of force of the earth's field. The narrow band emission takes place up until the particle collides with another particle. Absorption and broadening occur at this point.

The mechanism postulated must take place in an ionospheric layer where a portion of a gyration can be produced. The frequency itself is determined by the magnetic field at that point. Table 3 has indicated the decrement of H by the factor $1/d^3$.

D. Absorption or Emission

The problem of absorption or emission of energy at the gyrofrequency depends on the system proposed. If the energy causing a sudden increase of the ion spiraling is kinetic energy, such as meteors, emission would be expected. The meteor particles give up their energy to the ions, which in turn convert kinetic into electromagnetic energy. The ionization transfer from lightning discharge into the ionosphere in a manner such as suggested by Isted* [22] is a second possible mechanism, although not as probable as the first.

If, however, energy were coupled into the ionosphere from the aurora (with a mechanism similar to that of the gas discharge tube coupling signals into its output circuit), absorption would take place. The ions would use some of the wide band auroral noise for their motion and subsequent collisions. In this case, the gyro motion will drain energy from the background noise level. Although there is evidence of this type of energy present, it would be difficult to detect this absorption. From the equipment standpoint, the emission of a narrow band continuous-wave signal will produce a large deflection. Its absence or absorption within a band of noise signal will only reduce the level an infinitesimal part.

E. Other Possibilities

A possibility exists for this enhancement being man made. No unusual solar conditions were seen and the magnetic index was low. The Perseids meteor shower was in progress during this period, but no direct evidence is available as to the two events being correlated.

It seems unlikely that the increase is due to 60-cycle harmonics or "subharmonics." If so, the frequency and amplitudes of the 33-cps and the 60-cps data would be better correlated.

The appearance and disappearance of the signals, the run through of several complete sweeps, and the quality of the data before and after the event show that the signal was not due to equipment problems. The smaller amount of energy present during the rest of the day also rules out passing vehicles, etc.

However, further verification is necessary before the data are accepted as conclusive proof that ions in the upper atmosphere radiate at their gyromagnetic frequency.

IV. SUMMARY

The diurnal pattern of the low audio-frequency atmospherics reaches a maximum around local midnight, with a secondary maximum in the afternoon. The spectrum, however, shows varied amounts of attenuation as a function of local time. There is a large absorption of signals above 450 cps in the period before and after dawn, with a low signal level in this portion of the frequency spectrum during the day.

Night-time levels are high at all frequencies, indicating long-distance transmission of many individual atmospherics.

*Isted had proposed that a current from charged cumulus-nimbus clouds leaks through the upper atmosphere into the E region. Ionization by cosmic radiation in the region between the clouds and the E layer is the transport mechanism.

With the data in this study combined with other data, a hypothesis for the dawn chorus is evolved. This postulates a band rejection filter which acts on atmospherics. This is characteristic of the ionosphere before and after dawn. Magnetic fluctuations from the auroral discharge are coupled into the ionosphere. The apparent output is narrow band audio energy, which other experimenters have shown is characteristic of the dawn chorus.

Radiation at the gyrofrequency of the sodium ion has been detected. The hypothesis for the transmission of radiation is that a mechanism such as meteor particle impact has given energy to the sodium ions. The kinetic energy is converted into electromagnetic energy and heat (through collisions).

I would like to thank Dr. Philip Newman and Dr. Marcus O'Day for their assistance in carrying out the project. I would also like to thank Prof. E. Vassy for his encouragement of the development of the ideas in the research. Mr. William Barron assisted greatly by analyzing the data presented.

References

[1] F. W. Chapman and W. D. Matthews, Nature, **172**, 495 (1953).
[2] P. W. Bowe, Phil. Mag., **44**, 833 (1953).
[3] J. Aarons, Proc. Amer. Acad. Arts Sci., **79**, 4 (1951).
[4] J. Aarons and M. Henissart, Nature, **172**, 682 (1953).
[5] F. J. W. Whipple and F. J. Scrase, London, Met. Office, Geophys. Mem., No. 68 (1936).
[6] C. E. P. Brooks, London, Met. Office, Geophys. Mem., No. 3, p. 145 (1925).
[7] R. E. Holzer and O. E. Deal, Nature, **177**, 536 (1956).
[8] E. Maple, Spring meeting, American Geophysical Union, Washington, D. C.
[9] J. B. Wilcox and E. Maple, Naval Ordnance Laboratory, NOL Rep. No. 4009, White Oak, Maryland.
[10] N. D. Sayers and K. G. Emeléus, Proc. Phys. Soc., A, **65**, 219 (1952).
[11] L. Harang, The Aurorae, Chapman and Hall, Ltd., London (1951).
[12] J. D. Cobine and C. J. Gallagher, J. Frank. Inst., **243**, 41 (1947).
[13] W. Funk and R. Seeliger, Zs. Physik, **113**, 203 (1939).
[14] I. Langmuir and L. Tonks, Phys. Rev., **33**, 195 (1929).
[15] J. Watts, National Bureau of Standards (private communication).
[16] A. G. Edwards, J. Brit. Inst. Radio Eng., **16**, 31 (1956).
[17] B. W. Currie, P. A. Forsyth, and F. E. Vawter, J. Geophys. Res., **58**, 179 (1953).
[18] F. E. Roach, Astrop. J., **110**, 314 (1949).
[19] H. Edwards, J. F. Bettinger, and E. R. Manring, The Airglow and Aurora, Pergamon Press, Ltd., London (in press).
[20] The Rocket Panel, Phys. Rev., **88**, 1027 (1952).
[21] J. F. Denisse, Ann. Astroph., **10**, 1 (1947).
[22] G. A. Isted, Marconi Review, **17**, 37 (1954).

A CALCULATION OF THE SODIUM DAYGLOW INTENSITY*

By T. M. Donahue

The University of Pittsburgh, Pittsburgh, Pennsylvania

(Received July 16, 1956)

ABSTRACT

A calculation of the resonance scattering from a sodium layer between 70 and 100 km for all daylight angles of solar depression is presented. Observations at zenith distance zero and in a plane perpendicular to the sun are considered. The calculation is based on a previous computation of the density of sodium excited by the sun. The effect of absorption in the sodium layer is taken into account. The intensity rises by a factor of about 5 from sunset to noon for a layer 2×10^{11} cm^{-2} thick and by about 27 for a layer only 2×10^{9} cm^{-2} thick.

1—THE SODIUM DAYGLOW

Unless the neutral sodium atom population below 100 km should decrease to an extremely low level during the daytime, the D lines should be a prominent feature of the dayglow. To instruments at low altitudes, these emission lines should lie deep in the Fraunhofer lines and in the atmospheric sodium absorption lines as well. But it should be possible to overcome the difficulties with scattered background light and to measure the intensity of the sodium dayglow lines themselves. These should presumably consist almost entirely of solar photons which have suffered resonance scattering. It is the purpose of this note to predict the intensity of the D_2 line throughout the day for three assumptions concerning the thickness of the sodium layer. The prediction is based on a calculation of the density of sodium atoms excited by direct sunlight, by sunlight reflected from the earth's surface, but not by the imprisoned radiation. Extremely important also for thicker layers, as far as the emitted flux is concerned, is the resonance absorption in the layer itself of the photons scattered.

2—THE COLUMN OF EXCITED ATOMS

In a calculation previously published, the density of excited sodium atoms in a layer located between 70 and 100 km above the earth's surface for all angles of solar depression from $-\pi/2$ to the end of twilight was obtained [see 1 of "References" at end of paper]. The method was based heavily on an accounting for the effect of previous absorption in the layer on the locally incident flux. Reflection from the earth's surface but not reradiation were included. The resulting distribution may be integrated in any selected direction to give a first approximation to the scattered intensity in the daytime as well as in twilight.

*This work was supported in part by the National Science Foundation.

Two special cases afford an easy computation. One is for observation towar the zenith; the other is for observation in a plane perpendicular to the sun's ray In the latter case, it is assumed that the observations are carried out 30 km abo the surface of the earth. The sodium atoms are assumed, as before, to lie betwe 6.47×10^3 km and 6.50×10^3 km and to vary as $N_0 \exp[-(r - r_0)/H]$, whe

$$N_0 = 2.19 \times 10^8 \text{ cm}^{-3} \text{ for a layer } 2.31 \times 10^9 \text{ cm}^{-2} \text{ thick,}$$

$$N_0 = 2.19 \times 10^9 \text{ cm}^{-3} \text{ for a layer } 2.31 \times 10^{10} \text{ cm}^{-2} \text{ thick,}$$

$$N_0 = 2.19 \times 10^{10} \text{ cm}^{-3} \text{ for a layer } 2.31 \times 10^{11} \text{ cm}^{-2} \text{ thick.}$$

H^{-1} was taken as 1.27×10^{-6} cm^{-1}. The resulting thicknesses of excited ato are plotted back to solar depression $-\pi/2$ in Figure 1. (In this system of coord

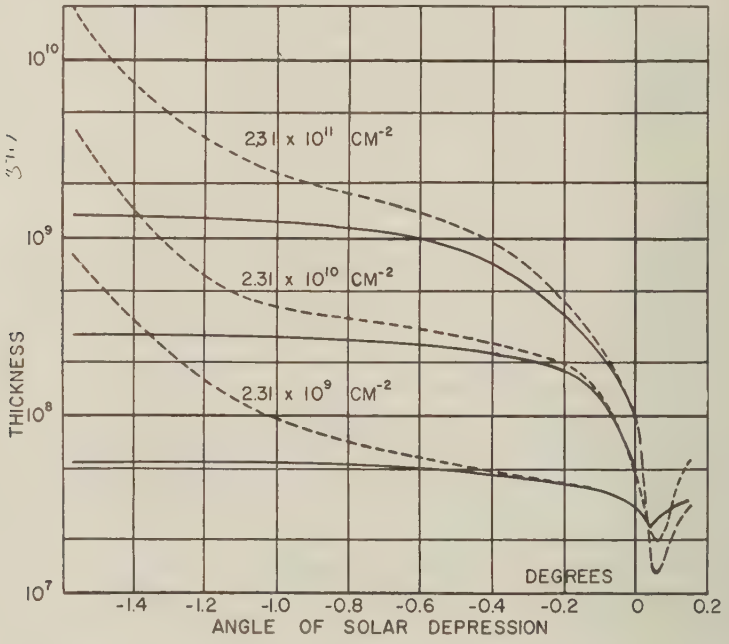

FIG. 1 -Thickness of a column of excited sodium (intensity before absorption) as a function the angle of solar depression. Solid curves are for observation toward the zenith. Dashed curv are for observation in a plane perpendicular to the sun's rays. Ordinate is the rate of excitati per cm^2 per unit incident solar intensity in unit frequency.

nates, zero solar depression occurs at sunset.) In these curves, several notab features, such as the minima after sunset and the great depression in excitati during late twilight caused by absorption in the thicker layers, have already be noted [1]. It will be seen that the effect of absorption carries back even into t daylight, so that the curves are not separated by decades by any means. In t case of observation perpendicular to the sun, a great increase in intensity wi increasing zenith angle is of course apparent.

3—CORRECTION FOR RESONANCE ABSORPTION

There is one important correction which must be made to these curves and possibly another. It has been shown that the resonance absorption of some of the photons emitted reduces the intensity at a given zenith angle appreciably [2]. This is especially true for the thicker layers. In fact, subject to the assumption that the density of excited atoms everywhere along a given line of sight bears a fixed ratio to the over-all density of sodium, the flux of photons along that line toward an observer was shown to be proportional to

$$1.26\ [1-\ \exp\ (-0.716\ \sigma_0 L)]\ +\ 0.99\ [1-\ \exp\ (-0.101\ \sigma_0 L)] \quad \ldots\ldots\ldots (1)$$

L is the thickness of sodium atoms in the direction of observation. In the present case, it depends only on θ_0 the angle of solar depression when the observations were made. Use of this result provided an attenuation factor to be applied to the curves of Figure 1 for every value of θ_0 . This factor actually was the ratio of (1) to $\sigma_0 L$ in that direction.

In Figure 2, it will be noticed that attentuation in the layer itself would

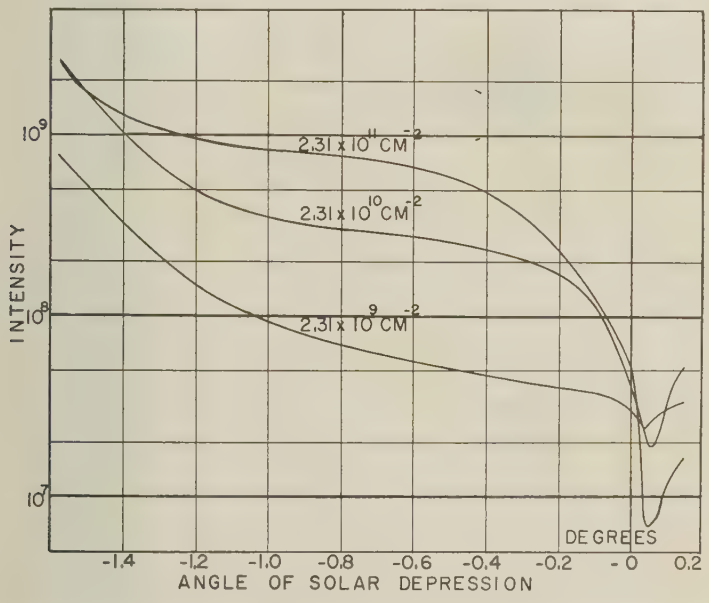

FIG. 2—Intensity of dayglow sodium D_2 radiation as function of angle of solar depression. This is for the plane perpendicular to the sun's rays after absorption in the layer itself. Ordinate should be divided by 4π to give the number of photons emerging from the layer per sec per cm^2 per steradian for unit incident solar intensity per unit frequency.

reduce enormously the escaping flux for a layer 2.31×10^{11} cm^{-2} thick. At $\theta_0 = -\pi/2$ for observation perpendicular to the sun direction, the intensity from this layer is no greater than that from a layer containing 0.1 times as many atoms per square centimeter column.

For observations toward the zenith, the curves of Figure 1 should be multiplied by 0.535, 0.935, and 1.00 for descending thickness. The correction there is the same for all θ_0 .

4—OTHER CORRECTIONS

One other correction will usually be sizable if the background is great. This is a consequence of the fact that even the light scattered below the layer as background will have been attenuated in the *D*-line region by one passage through the sodium layer. This effect is also important for the interpretation of measurement of the twilight flash, and a method for handling such a correction has been given in another paper [3]. The details of this correction depend so much on the type of instrument used and the altitude of observation that they will not be given here. They should be applied separately in each particular case if they are important. In general, their effect is further to introduce a reduction in intensity compared to the surrounding continuum. This correction also discriminates against the thicker layers.

References

[1] T. M. Donahue, R. Resnick, and V. R. Stull, Phys. Rev. (in press).
[2] T. M. Donahue and A. Foderaro, J. Geophys. Res., **60, 75** (1955).
[3] T. M. Donahue, J. Atmos. Terr. Phys. (in press).

A METHOD OF INTERPOLATING MAGNETIC DATA UNDER CONDITIONS OF MUTUAL CONSISTENCY*

By Alfred J. Zmuda

Applied Physics Laboratory, Johns Hopkins University, Silver Spring, Maryland

AND

John F. McClay

Air Force Cambridge Research Center, Geophysics Research Directorate, Bedford, Massachusetts

(Received July 9, 1956)

ABSTRACT

Because of the discreteness of the data obtained in magnetic surveys, it is necessary to interpolate between measured points before charts can be drawn. Rigorous relations connecting surface variations of different elements are herein introduced into the interpolation formulas, so that the resulting charts are mutually consistent. Related elements are continued by a power series in which the unknown coefficients are computed under the conditions for consistency.

INTRODUCTION

In magnetic surveys, measurements are usually made at discrete points or on discrete lines, and before charts, either isomagnetic or isoporic, can be drawn it is necessary to continue the magnetic element into regions where no data were taken. In the continuation, to make charts that are mutually consistent, the cartographer can apply theoretical relationships that connect surface variations of the various elements. Often the theoretical relations are applied after the continuation of the related elements has been independently effected. It is the purpose here to incorporate the conditions for consistency into the equations governing the surface variations. As the law of continuation, a power series is used in which the coefficients are computed under the conditions of mutual consistency.

BRIEF REVIEW OF THEORETICAL RELATIONS

In the region outside magnetic matter, the geomagnetic elements are expandable in a power series. With spherical polar coordinates, this expansion about a point with coordinates θ_0 and λ_0, on a surface of fixed radius, may be written as

$$\left.\begin{aligned} f(\theta, \lambda) = f(\theta_0, \lambda_0) + c_1(\theta - \theta_0) + c_2(\lambda - \lambda_0) \\ + c_3(\theta - \theta_0)^2 + c_4(\theta - \theta_0)(\lambda - \lambda_0) + c_5(\lambda - \lambda_0)^2 + \cdots \end{aligned}\right\} \quad \ldots\ldots(1)$$

*This work was supported in part by the Department of the Navy, Bureau of Ordnance, under contract NOrd 7386.

where f is a geomagnetic element with a value $f(\theta_0 , \lambda_0)$ at $\theta = \theta_0$ and $\lambda = \lambda_0$; θ and λ represent the colatitude and east longitude in circular measure, respectively; and the c's are coefficients which are determined in the analysis.

If charts of different elements are to be mutually consistent, the series of the various elements from which data for the charts may be computed must satisfy certain rigorous conditions of electromagnetic theory. For example, from the r-component of curl $\vec{F} = 0$, where $\vec{F}$ is the magnetic intensity, surface variations of the northern component X and eastern component Y are related by

$$\frac{\partial X}{\partial \lambda} + \frac{\partial}{\partial \theta}(Y \sin \theta) = 0 \quad \ldots\ldots(2)$$

With the substitutions of $H \cos D$ for X and $H \sin D$ for Y, where D is the declination and H the horizontal force, equation (2) can be transformed into

$$\left.\begin{aligned} \sin \theta \sin D \frac{\partial H}{\partial \theta} + \cos D \frac{\partial H}{\partial \lambda} + H \cos \theta \sin D \\ + H \sin \theta \cos D \frac{\partial D}{\partial \theta} - H \sin D \frac{\partial D}{\partial \lambda} = 0 \end{aligned}\right\} \quad \ldots\ldots(3)$$

or

$$\frac{\partial H}{\partial e} + H \cot \theta \sin D - H \frac{\partial D}{\partial n} = 0 \quad \ldots\ldots(4)$$

where in (4), $\partial/\partial e$ and $\partial/\partial n$ denote differentiation along the directions of magnetic east and north, respectively.

Equations (2), (3), and (4) were first discussed by Chapman [see 1 of "References" at end of paper], and then later by Vestine [2] and Davids and Bernstein [3]. Additional relationships for mutual consistency among different elements were obtained by Zmuda [4] by differentiation of

$$F = [X^2 + Y^2 + Z^2]^{1/2} \quad \ldots\ldots(5)$$

where Z is the downward component of F.

These additional relations are given by

$$F \frac{\partial F}{\partial \theta} = X \frac{\partial X}{\partial \theta} + Y \frac{\partial Y}{\partial \theta} + Z \frac{\partial Z}{\partial \theta} \quad \ldots\ldots(6)$$

and

$$F \frac{\partial F}{\partial \lambda} = X \frac{\partial X}{\partial \lambda} + Y \frac{\partial Y}{\partial \lambda} + Z \frac{\partial Z}{\partial \lambda} \quad \ldots\ldots(7)$$

Substituting a time derivative of an element for the element itself in equations (1) through (7) gives relations for use with isoporic charts.

Note that surface gradients in two directions are used for each element in (3), but gradients in a single direction are connected in the remaining equations. Therefore, in tests for mutual consistency with H and D charts, for example, equation (3) is a complete relationship while (4) is not.

METHOD OF INCORPORATION

Assuming X, Y, Z, and F are the observed elements, one may write the relevant power series as

$$X(\theta, \lambda) = X(\theta_0, \lambda_0) + a_1\alpha + a_2\beta + a_3\alpha^2 + a_4\alpha\beta + a_5\beta^2 + \cdots \quad (8)$$

$$Y(\theta, \lambda) = Y(\theta_0, \lambda_0) + b_1\alpha + b_2\beta + b_3\alpha^2 + b_4\alpha\beta + b_5\beta^2 + \cdots \quad (9)$$

$$Z(\theta, \lambda) = Z(\theta_0, \lambda_0) + c_1\alpha + c_2\beta + \cdots \quad (10)$$

$$F(\theta, \lambda) = F(\theta_0, \lambda_0) + d_1\alpha + d_2\beta + \cdots \quad (11)$$

where $\alpha = \theta - \theta_0$; $\beta = \lambda - \lambda_0$; and θ_0 and λ_0 are the surface coordinates of the point about which the series expansion is made.

Coefficients in the power series of an element may be determined from the measured data on that element alone and used in computations for unmeasured points. However, a chart of an element drawn from data computed in this manner is not mutually consistent with charts of other elements, since the connecting relations in (2) to (7) were not considered.

With X and Y data as examples, a condition for consistency is introduced into the power series by applying the mathematical operations of (2) to (8) and (9). The resulting relation between parts of the X and Y series, using terms up to the third order, is

$$a_2 + a_4\alpha + 2a_5\beta + Y\cos\theta + \sin\theta[b_1 + 2b_3\alpha + b_4\beta] = 0 \quad (12)$$

As previously noted, equation (2), and therefore (12) also, is an incomplete criterion for consistency, since it does not give any information regarding the θ-variation of X and the λ-variation of Y. However, if charts compatible only with (2) are desired, then from the measured data one can evaluate from (12) coefficients for insertion into (8) and (9), where the remaining unknowns may then be determined. The complete series may be applied to compute values of the elements at unmeasured points.

If it is of interest to compute data on X, Y, Z, and F that are mutually consistent, then the mathematical operations in (6) and (7) are applied to the respective series. The resultant expressions, again using terms up to the third order, are

$$\left.\begin{aligned} F[d_1 + 2d_3\alpha + d_4\beta] = {} & X[a_1 + 2a_3\alpha + a_4\beta] \\ & + Y[b_1 + 2b_3\alpha + b_4\beta] + Z[c_1 + 2c_3\alpha + c_4\beta] \end{aligned}\right\} \quad (13)$$

and

$$\left.\begin{aligned} F[d_2 + d_4\alpha + 2d_5\beta] = {} & X[a_2 + a_4\alpha + 2a_5\beta] \\ & + Y[b_2 + b_4\alpha + 2b_5\beta] + Z[c_2 + c_4\alpha + 2c_5\beta] \end{aligned}\right\} \quad (14)$$

Note that some coefficients in (13) and (14), such as a_4, appear in both equations. Also note that if the appropriate coefficients in the X and Y series are first computed by (12) and then used in (13) and (14), the four series which are ultimately formed will yield data that are consistent to the extent that (2), (6), and (7) are satisfied.

This case is of importance if the components are extrapolated vertically by a recently reported method of vertical continuation [5, 6]. In this method of extrapolation, derivatives in the vertical direction are computed from surface derivatives. These surface derivatives may be obtained by differentiating with respect to θ and λ the series in (8), (9), and (10).

SAMPLE CALCULATION

The coefficients in the power series for X and Y were determined under the condition of consistency in (12) for a simple field which is independently representable by a few spherical harmonics. On the surface of the earth, the components in harmonics are given in γ's ($1\gamma = 10^{-5}$ gauss) by

$$X = 30{,}570 \sin\theta + 21{,}000 \sin^3\theta \cos\theta \cos 4\lambda + 10{,}500 \sin^3\theta \cos\theta \sin 4\lambda \ldots (15)$$

$$Y = 21{,}000 \sin^3\theta \sin 4\lambda - 10{,}500 \sin^3\theta \cos 4\lambda \ldots (16)$$

The field is that of the centered dipole plus a harmonic of fourth order and degree. The coefficients in the latter harmonics are adjusted so that the surface gradient of D in the southern direction is roughly equal to that in the northeastern part of the United States, 30 minutes of D per degree of colatitude. The coefficient of the dipole field is that determined by Vestine [2].

From (15) and (16), at points spaced at 1° intervals in colatitude and longitude, values of the components were computed in an area where θ varied between 40° and 43°, and λ between 300° and 303°. These computed values are assumed to be the measured values from which the power series will be formed.

The measured values are first put into (12), which is solved by a method of least squares. The coefficients in (12) are then put into (8) and (9), and the remaining unknown coefficients are computed, again by a method of least squares. The series expansion was made around the point where $\theta_0 = 41°$ and $\lambda_0 = 301°$.

When angular differences α and β are in degrees, the resultant series are

$$X = 19{,}408 + 340\alpha - 320\beta - 5\alpha^2 - \alpha\beta - \beta^2 \ldots (17)$$

$$Y = 6{,}574 + 370\alpha - 50\beta + 2\alpha^2 + 4\alpha\beta - 5\beta^2 \ldots (18)$$

While a detailed discussion of the procedure and inherent errors of the calculation will not be presented here, a few general items may be of interest.

Since there are 16 measured points for each component, there are 16 residual equations which are used to form the normal equations. To determine the coefficients in (12), the normal equations (which here constitute a set of six simultaneous linear equations) were solved by a method of elimination discussed by Milne [7]. It developed that the determinant of the unknown coefficients in the normal equations was extremely small, about 1.9×10^{-9}, so that it was necessary to carry approximately 12 significant figures throughout the calculation before good results could be achieved. The use of this large number of significant figures in the calculation is not to be interpreted as an indication of the number of significant figures required in the original data. It is, however, pertinent to a complete error analysis which would include errors in the measured data; this type of analysis was not made.

The errors in the coefficients in the power series, computed by the least-squares ıethod, may be obtained from a comparison (see Table 1) with the theoretical ıes. Because of the uniqueness theorem of the power series, the theoretically

TABLE 1—*Comparison between exact and approximate values of coefficients in the power series*

Coefficient	Values*	
	Exact	Approximate
a_1	373	340
a_2	−346	−320
a_3	−3	−5
a_4	−16	−1
a_5	2	−1
b_1	396	370
b_2	−60	−50
b_3	5	2
b_4	−4	4
b_5	−16	−5

*The dimensions of the coefficients a_1 , a_2 , b_1 , and b_2 are γ's per degree; the remaining coefficients have units per degree squared.

ıact coefficients are given by the derivatives and numerical multipliers that ecur in the Taylor series for the separate components, that is,

$$\left.\begin{aligned} = \frac{\partial X}{\partial \theta}\,; \quad a_2 = \frac{\partial X}{\partial \lambda}\,; \quad a_3 = \frac{1}{2}\frac{\partial^2 X}{\partial \theta^2}\,; \quad a_4 = \frac{\partial^2 X}{\partial \theta\, \partial \lambda}\,; \quad a_5 = \frac{1}{2}\frac{\partial^2 X}{\partial \lambda^2}\,; \\ = \frac{\partial Y}{\partial \theta}\,; \quad b_2 = \frac{\partial Y}{\partial \lambda}\,; \quad b_3 = \frac{1}{2}\frac{\partial^2 Y}{\partial \theta^2}\,; \quad b_4 = \frac{\partial^2 Y}{\partial \theta\, \partial \lambda}\,; \quad b_5 = \frac{1}{2}\frac{\partial^2 Y}{\partial \lambda^2} \end{aligned}\right\} \quad \ldots . (19)$$

All derivatives in (19) are evaluated by differentiating (15) and (16) at the oint with surface coordinates $\theta_0 = 41°$ and $\lambda_0 = 301°$.

The agreement between theoretical and calculated coefficients is good even ıough the sign of the computed coefficients a_5 and b_4 is incorrect. Because of the nallness of the magnitude of these latter two coefficients, the error in sign there roduces a negligible effect.

For points spaced at intervals of 15′ in both longitude and latitude, a comarison was made for X, Y, and D computed by harmonics and the power series of 7) and (18); D is computed from $\tan D = Y/X$. In addition were computed eviations from zero of the left-hand side of (12).

With harmonic values as the standard, the rms errors in gammas for X and Y, nd minutes of arc for D, are, respectively, 40, 30, and 2. These errors could be scribed also to the charts drawn from the data computed with the power series (17) and (18). The rms value of (12) was 10 gammas per degree.

Additional computations, preferably taking into account errors of experimental ata, are required before the advantages and disadvantages of this method of terpolation may be properly determined.

ACKNOWLEDGMENT

The authors wish to gratefully acknowledge fruitful discussions of the problem with Dr. E. H. Vestine, of the Department of Terrestrial Magnetism, Carnegie Institution of Washington.

References

[1] S. Chapman, Terr. Mag., **47**, 1–13 (1942).
[2] E. H. Vestine, L. Laporte, I. Lange, C. Cooper, and W. Hendrix, Washington, D. C., Carnegie Inst. Pub. No. 578 (1947).
[3] N. Davids and A. Bernstein, Terr. Mag., **50**, 199–214 (1945).
[4] A. J. Zmuda, J. Geophys. Res., **63**, 57–58 (1956).
[5] A. J. Zmuda and L. McClung, Trans. Amer. Geophys. Union, **36**, 939–942 (1955).
[6] A. J. Zmuda, Trans. Amer. Geophys. Union, **37**, 9–12 (1956).
[7] W. Milne, Numerical Calculus, Princeton University Press, Princeton, N. J. (1949); pp. 15–27.

TURBULENCE IN THE IONOSPHERE WITH APPLICATIONS TO METEOR-TRAILS, RADIO-STAR SCINTILLATION, AURORAL RADAR ECHOES, AND OTHER PHENOMENA*

By H. G. Booker

School of Electrical Engineering, Cornell University, Ithaca, New York

(Received July 26, 1956)

ABSTRACT

The irregularities in electron-density responsible for incoherent scattering of radio waves in the ionosphere are discussed on the assumption of isotropic turbulence in the neutral molecules, with allowance made for the effect of the earth's magnetic field on the associated irregularities in the density of the charges particles. The atmospheric model used is based on rocket observations, extrapolated upwards in height where necessary. Tentative formulas are deduced for the large eddies based on a non-standard application of the Richardson number. For the small eddies, the standard formulas of turbulence-theory are used.

These formulas all depend on a quantity w, which is the rate of supply of turbulence-energy to the large eddies and also the rate of removal of turbulence-energy from the small eddies, measured per unit mass of atmosphere. The value of w at the meteoric level (90 km) is found to be around 25 watts/kg by comparison between the theory and meteoric observations (both visual and radio). By the same technique, a more tentative value of 1,000 watts/kg is deduced for the level responsible for scintillation of radio stars, although a lower value is probably appropriate when scintillation is weak. These values of w in the ionosphere are high compared with Brunt's value of 5×10^{-4} watt/kg for the troposphere. It is shown, however, that these high values of w in the ionosphere are quite possible and even reasonable.

It is deduced that the time of onset of irregular fading of meteoric echoes in the VHF band is more likely to be due to roughness of the trail caused by the small eddies than to gross distortion of the trail caused by the large eddies. It follows that, after about a second, VHF radar echoes from a meteor-trail must be calculated using a theory based on incoherent scattering, thereby questioning the theory of Kaiser and Closs [37] as an explanation of long-duration meteor-echoes. It is also shown that radio-star scintillation cannot be explained in terms of turbulence at a level of 400 km, but that

*This research was supported by the U. S. Signal Corps under Contract No. DA36-039-sc-5748 and by the National Science Foundation.

reasonable results can be obtained if the level is reduced to 200-300 km.

Among other applications considered is the possibility of radio communication *via* incoherent scattering in the *F* region of the atmosphere. The conditions under which such communication should be sought are described in section 11.

1. *Introduction*

It is the object of this paper to examine certain features of the theory of atmospheric turbulence in relation to phenomena involving irregular scattering of radio waves in the ionosphere. There are many such phenomena, and in no case is there a generally accepted quantitative explanation at the present time. In some cases there is no agreement even on qualitative cause. These phenomena are listed below,

(*i*) Even for a quiet ionosphere, the simplest radio echo at normal incidence has a fading range comparable with the mean signal, indicating that, in the formation of the echo, some kind of irregular scattering is nearly as important as classical internal reflection [see 1 of "References" at end of paper].

(*ii*) Under certain ionospheric conditions, including magnetically disturbed conditions, echoes from the *F* region of the ionosphere become extremely spread in range. The fading of the parts of the echo at different ranges is largely uncorrelated, and the fading range is comparable with the mean signal. This phenomenon of "spread *F*" has been known for more than 20 years but is still without satisfactory explanation [2].

(*iii*) Radar echoes are obtained in the HF band above the penetration-frequency of the ionosphere in such directions and at such ranges as to suggest back-scattering from irregularities of electron-density aligned along the earth's magnetic field [3]. There is also a similar phenomenon associated with the *E* region [3].

(*iv*) Noise from radio stars received in the VHF band shows twinkling similar to that produced in the troposphere with visual stars [4, 5]. Radio-star twinkling frequently shows correlation with spread *F* and is believed to be associated with irregularities in the *F* region that are elongated along the earth's magnetic field [6]. Correlation with sporadic ionization in the *E* region also occurs, however [7].

(*v*) Radar echoes from meteor-trails, after about half a second, develop irregular fading that cannot be explained in terms of a trail that remains straight [8]. Visual observations of meteor-trails likewise indicate twisting of the trail in a manner suggesting atmospheric turbulence at heights between 80 and 100 km [9]. It is usually assumed that the irregular fading of radar echoes from meteor-trails is due to the effect of turbulence on the ionized trail and that this turbulence is not produced by passage of the meteor.

(*vi*) At frequencies of the order of 2 Mc/sec, weak echoes can be obtained almost continuously at normal incidence from levels somewhat below the level of reflection for the regular *E* region [10, 11]. The echoes are

spread in range, have uncorrelated fading at different heights, and a fading range comparable with the mean signal. It is presumed that they are due to scattering by irregularities of electron-density in the D and lower E regions.

(*vii*) Above the maximum usable frequency for regular ionospheric transmission, signals can be received at distances from a few hundred kilometers up to two thousand kilometers at frequencies up to about 100 Mc/sec [12, 13]. Signals have fading that is characteristic of scattering from a large number of irregularities. The height at which the scattering occurs is about 90 km at night, and perhaps a little lower during the daytime. Somewhat similar observations have been made at ranges of the order of 2,500 km and 2,900 km, possibly due to scattering in the F region [14].

(*viii*) At times of auroral activity, radar echoes are obtained in the VHF band from regions of the sky that bear some relation to the regions of visual activity [15, 16, 17]. There is sometimes a close correspondence between the regions of visual activity and those from which radio echoes are obtained. However, radio echoes do not usually occur overhead or at short ranges, and are mainly confined to the quadrant centered on magnetic north. Fading is of the type associated with random scattering and is at least a power of ten faster than would be expected for a quiet ionosphere. There is a Doppler shift in the frequency of auroral echoes comparable in magnitude to the fading rate. The Doppler shift does not correlate with the rate of change in the slant range of echoes. The height from which echoes come is almost certainly that of the E region.

All of the above phenomena could be explained qualitatively in terms of mospheric turbulence at ionospheric levels. That such turbulence does exist up and within the E region is not in serious doubt. Whether turbulence can exist the F region, however, is debatable, although the radio data seem to suggest rbulence at this level, especially at times of magnetic disturbance. At present, wever, there is no comprehensive theory of ionospheric turbulence capable of esenting all of the above observations as different aspects of a single atmospheric enomenon. It is the object of this paper to take some steps in this direction.

Turbulence in the upper atmosphere arises in a way that theory does not at esent describe in any detail. It is assumed that large eddies of scale L_1 are proced, and that in so doing energy is used at a rate per unit mass of atmosphere at we shall denote by w. This important quantity w cannot usually be determined merically by theoretical argument, but its value can sometimes be assessed by mparison of theoretical deductions with experimental observations. Brunt [18] s estimated that the value of w in the troposphere is

$$5 \times 10^{-4} \text{ watt/kg} \quad \ldots\ldots\ldots\ldots\ldots\ldots\ldots\ldots (1)$$

At levels in the atmosphere where turbulence is important, the Reynolds mber associated with the large eddies is large, indicating that the direct effect viscosity in damping the large eddies is small. On the other hand, there is a

scale L_2 for eddies, less than L_1, for which the Reynolds number is unity, indicating that viscosity would quickly damp out eddies of scale L_2. It is supposed that the large eddies of size L_1 break up into successively smaller eddies until the size L_2 is reached, when viscosity converts the energy of turbulence into energy of thermic motion. Thus, there is a spectrum of eddy sizes from L_1 down to L_2. Energy is transferred to the large eddies at a rate w per unit mass; it is removed from the small eddies and converted into heat at practically the same rate w per unit mass [19].

The distribution of turbulent energy with eddy scale L has been studied by Kolmogoroff [20] for the range $L_1 > L > L_2$ and by Heisenberg [21] for $L < L_2$. Methods for converting the spectrum of turbulence into a function giving the dependence on radio wavelength λ of the cross-sectional scattering area per unit volume of atmosphere have been studied by Booker and Gordon [22], Megaw [23], Villars and Weisskopf [24, 25], Gallet [26], Batchelor [27], Silverman [28], and Booker [29]. The precise form of the scattering function will not be required in this paper. The following points should, however, be noted:

(*i*) For forward-scattering, involving angles of deviation less than $\lambda/(2\pi L_1)$, the phenomenon is controlled primarily by the large irregularities (those whose scale is of the order of L_1).

(*ii*) For back-scattering, the phenomenon is controlled either (*a*) by the small irregularities (those whose scale is the order of L_2), or (*b*) by the eddies whose scale is of the order of $\lambda/4\pi$, whichever is the larger.

In discussing turbulence in the ionosphere, we shall assume that the turbulence in the neutral molecules is isotropic. While this may not be true, it is considered a useful approximation at the present stage in the development of the subject. The possible effect of non-isotropic turbulence in the neutral molecules is, however, mentioned in discussion. On the other hand, we shall not, in general, assume isotropy in the irregularities of ions and electrons. Owing to the influence of the earth's magnetic field, the irregularities in the charged particles are constricted perpendicular to the field. This constriction is calculated in section 5 on the basis of certain somewhat oversimplified assumptions.

In section 2 of the paper, formulas are developed appropriate to the large eddies in the upper atmosphere. These formulas are based on a use of the Richardson number, whose properties are discussed in books on dynamical meteorology [18]. In section 3, formulas are given appropriate to the small eddies. These formulas are taken from Batchelor [19].

A number of the quantities involved in the formulas for the large and small eddies can be calculated as a function of height in the ionosphere from the atmospheric data presented by the Rocket Panel [30]. The rocket data as interpreted by Weekes [31] have been used up to a height of 160 km. Above this height, some extrapolation is necessary, though results may be considered fairly reliable up to a height of, say, 300 km. Above 120 km, it has been assumed that temperature increases with height at a rate of 5°K per kilometer up to any height used. Complete dissociation of oxygen has been assumed above 120 km, and dissociation of nitrogen has been neglected. Above 120 km, complete mixing of molecular nitrogen and

tomic oxygen has been assumed up to any level under discussion. The reason for his is that it is a basic hypothesis of this paper that turbulence exists in the atmosphere up to any level under discussion. The atmospheric model just described will e briefly designated "the rocket atmosphere."

After introducing the data from the rocket atmosphere into the formulas of ctions 2 and 3 for the large and small eddies, we are still left with the important nknown parameter w. This is the turbulence-power per unit mass. It is the rate which turbulence-energy is supplied to the large eddies and removed from the nall eddies, measured per unit mass or atmosphere. In the troposphere, the order magnitude of w is known roughly to have the value (1) from the work of Brunt 8]. At the meteoric level, which will be taken as 90 km, a value will be deduced r w by fitting the formulas of sections 2 and 3 to visual observations of meteor-ails made by Liller and Whipple [9], and to radio observations of meteor-trails ade by Greenhow [8, 34]. This comparison between turbulence-theory and eteoric observations is made in section 4.

In section 5, a similar procedure is followed at the level where scintillation of dio stars occurs, making use particularly of the observations of Spencer [6]. It ill, however, be necessary to abandon the estimate of Hewish [5] that the level which scintillation of radio stars occurs is 400 km. Not only is it difficult to xplain the existence of turbulence at 400 km, but even in the presence of turbulence this level it would be difficult to explain why the irregularities of electron-ensity have the size and shape observed. A lower height is therefore deduced for ie level of star scintillation, which is at first estimated as 170 km but is sub-quently modified in section 9 to a value between 200 and 300 km.

An important feature of the application of the formulas of sections 2 and 3 to rbulence at the meteoric and star-scintillation levels is the high values of turb-ence-power deduced for ionospheric heights. At the meteoric level, the estimate turbulence-power is 25 watts/kg, and at the star-scintillation level it is 1,000 atts/kg. These values are to be compared with Brunt's value (1) for the tropos-here. In section 6, an investigation is undertaken in order to see whether these markably high values of turbulence-power deduced for the ionosphere are nreasonable. Both a lower and an upper bound are deduced for the turbulence-ower at any level. From the lower bound, it is found that turbulence in the nosphere is only possible if the turbulence-power per unit mass is considerably eater than in the troposphere. It transpires, in fact, that the values of turbulence-ower required to explain observations at both the meteoric and the star-scintilla-on levels lie comfortably within the permitted range of values.

With only three values for the turbulence-power per unit mass (one in the oposphere, one at the meteoric level, and one at the star-scintillation level), it difficult to draw a curve of w *versus* height. Nevertheless, such a curve is ten-tively drawn in section 6, and the variations with height of the other turbulence-rameters are deduced from it. In converting these parameters into values for e scale of electronic irregularities measured along and perpendicular to the rth's magnetic field, some consideration has to be given to the minimum possible lues of these scales, and this is done in section 7. The remaining sections consider plications of the theory to auroral echoes (section 8), to radar echoes from

irregularities in the F region at frequencies above the penetration-frequency (section 9), to scattering phenomena at the 90-km level (section 10), to the possibility of F-region scatter-communication (section 11), and finally to spread F and other reflection phenomena (section 12).

2. *The Large Eddies*

In applying the theory of turbulence to the upper atmosphere, difficulty has been experienced due to the lack of suitable formulas to described the properties of the large eddies. Some formulas appropriate to the large eddies will be derived in this section using the Richardson number. The Richardson number depends on temperature T, on the rate of increase of T with height z, on the adiabatic lapse rate of temperature Γ, on the acceleration g due to gravity, and on the rate of change with height z of the horizontal velocity v of the atmosphere. The expression for the Richardson number is [18]

$$\frac{\frac{g}{T}\left(\frac{dT}{dz}+\Gamma\right)}{\left(\frac{dv}{dz}\right)^2} \qquad (2)$$

According to the simplest derivation of the Richardson number, turbulence in the atmosphere increases if the Richardson number is less than unity and decreases if the Richardson number is greater than unity.

Application of the Richardson number is not without its difficulties. It is not clear that unity is necessarily quite the proper critical value of the Richardson number for separating the domain of increasing turbulence from that of decreasing turbulence. In the ionosphere, however, where orders of magnitude are still uncertain, this is not an important point at the present time, and we shall use unity as the critical value. Another point of difficulty in using the Richardson number concerns the interpretation of the denominator in (2). This denominator might be interpreted as either (*i*) the square of the mean value of the shear, or (*ii*) the mean value of the square of the shear. The observations of Liller and Whipple [9] (see Fig. 3) at the meteoric level seem to indicate that (*i*) is less than (*ii*), sometimes by more than a power of ten. Since increasing and decreasing shears are equally associated with turbulence, we shall assume that the denominator of the Richardson number is to be interpreted as the mean value of the square of the shear.

There is little doubt that turbulence in the ionosphere sometimes increases and sometimes decreases. We shall confine ourselves to discussion of a steady state in which turbulence is neither increasing nor decreasing. In these circumstances, we assume that the Richardson number is unity, and derive from (2) the equation

$$\left(\frac{dv}{dz}\right)^2 = \frac{g}{T}\left(\frac{dT}{dz}+\Gamma\right) \qquad (3)$$

The right-hand side of this equation may be plotted as a function of height in the ionosphere from the rocket atmosphere. We thereby deduce, as a function of

eight, an order of magnitude for the mean square shear involved in a steady ate of turbulence.

We do not interpret the square root of (3) as giving the mean wind shear. stead we interpret $|dv/dz|$ as follows. The dimensions of $|dv/dz|$ are those of gular velocity, and the angular velocity concerned is the angular velocity of a rtical line drawn in the fluid. We interpret this angular velocity as the angular locity of the large eddies, and its reciprocal as the time-constant t_1 of the large dies. The formula that we shall use, therefore, for the time-constant of the the large eddies is

$$t_1 = \left\{\frac{g}{T}\left(\frac{dT}{dz} + \Gamma\right)\right\}^{-1/2} \quad \ldots\ldots\ldots\ldots\ldots\ldots\ldots\ldots (4)$$

n the basis of the rocket atmosphere described in section 1, the quantity t_1 is otted as a function of height in Figure 1. Values of the time-constant of the

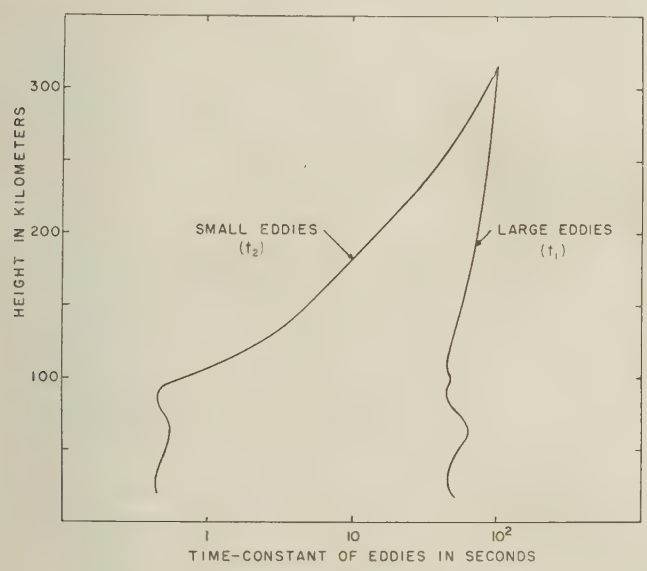

FIG. 1—The time-constants for large and small eddies

rge eddies range between 40 and 100 seconds.

The time-constant t_1 of the large eddies, besides being the time taken by a large ldy to rotate one radian, is also interpreted as the lifetime of a large eddy. It is this point that we introduce the turbulence-power w per unit mass. Energy is pplied to the large eddies at a rate w for an average time t_1. Hence the turbulence-ergy per unit mass associated with the large eddies is $w\,t_1$ per unit mass. But if v_1 the turbulence-velocity associated with the large eddies, this turbulence-energy of the order of v_1^2 per unit mass. Hence,

$$v_1^2 = wt_1 \quad \ldots\ldots\ldots\ldots\ldots\ldots\ldots\ldots\ldots\ldots (5)$$

or

$$v_1 = (wt_1)^{1/2} \quad (6)$$

This equation gives the turbulence-velocity of the large eddies in terms of the parameter w and the time-constant (4) of the large eddies.

The scale of L_1 of the large eddies is given by

$$L_1 = v_1 t_1 \quad (7)$$

This equation may be interpreted as a relation between radius L_1, linear velocity v_1, and angular velocity $1/t_1$. Alternatively, it may be interpreted as giving the distance L_1 that an eddy moves during its lifetime t_1. By substituting for v_1 from (6) into (7), we obtain

$$L_1 = (wt_1^3)^{1/2} \quad (8)$$

This equation gives the scale of the large eddies in terms of the parameter w and the time-constant (4) of the large eddies.

Since we have determined t_1 as a function of height from equation (4) and the rocket atmosphere, we are prevented from determining v_1 and L_1 as a function of height from (6) and (8) only by our ignorance of the turbulence-power w per unit mass as a function of height.

3. *The Small Eddies*

The formulas for the small eddies depend on the same parameter w involved in the large eddies and also upon the kinematic viscosity of the atmosphere. The kinematic viscosity may be taken to be identical with the coefficient of molecular diffusion D, for which there is a simple formula in the kinetic theory of gases [32]. This formula, used in conjunction with the rocket atmosphere, gives D as a function of height. In Figure 2 is shown the coefficient of molecular diffusion D as a function of height deduced in this way. The value of D has been checked experimentally at the meteoric level by Greenhow [33] from the decay time of short-duration meteor-echoes.

In terms of D and w, the formulas for the turbulence-velocity and scale of the small eddies are

$$v_2 = (wD)^{1/4} \quad (9)$$

$$L_2 = \left(\frac{D^3}{w}\right)^{1/4} \quad (10)$$

These formulas may be found in Batchelor [19] and are based on simple dimensional considerations. It is easily verified that the Reynolds number for the small eddies, namely, $v_2 L_2/D$, is unity. Formulas such as (5) and (7) apply to eddies of all sizes and therefore, in particular, to the small eddies. Hence,

$$v_2^2 = wt_2 \quad (11)$$

$$L_2 = v_2 t_2 \quad (12)$$

substituting from (9) and (10) into either (11) or (12), we obtain

$$t_2 = \left(\frac{D}{w}\right)^{1/2} \quad \ldots\ldots\ldots\ldots\ldots\ldots\ldots\ldots\ldots\ldots (13)$$

Equations (9), (10), and (13) would give the turbulence-velocity, scale, and me-constant of the small eddies as a function of height if we know the variation th height of the turbulence-power w per unit mass.

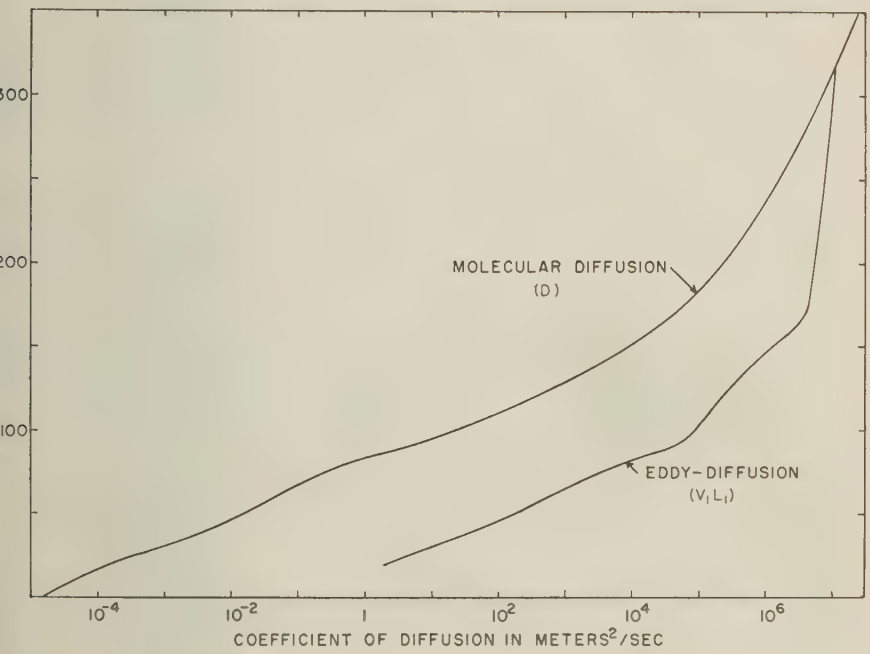

FIG. 2—The coefficients of molecular and eddy viscosity

Meteor-Trails

In discussing meteor-trails, we shall take 90 km as a convenient standard ight at which to make calculations. From the rocket atmosphere, we have at km

$$T = 212°\text{K} \quad \ldots\ldots\ldots\ldots\ldots\ldots\ldots\ldots\ldots\ldots (14)$$

$$\frac{dT}{dz} = 1.1°\text{K/km} \quad \ldots\ldots\ldots\ldots\ldots\ldots\ldots\ldots\ldots\ldots (15)$$

$$\Gamma = 9.5°\text{K/km} \quad \ldots\ldots\ldots\ldots\ldots\ldots\ldots\ldots\ldots\ldots (16)$$

$$\frac{dT}{dz} + \Gamma = 10.6°\text{K/km} \quad \ldots\ldots\ldots\ldots\ldots\ldots\ldots\ldots\ldots\ldots (17)$$

From (3), we deduce that the root-mean-square shear is

$$20(\text{m/sec})/\text{km} \quad (18)$$

While this might at first sight seem a high value, it is nevertheless of the order of magnitude observed by Liller and Whipple [9]. Figure 3 illustrates one of Liller and Whipple's curves for meteoric trail velocity *versus* height, and the large cross drawn on the diagram corresponds to shears of ± 20 (m/sec)/km.

By taking the reciprocal of (18), we deduce that the time-constant of the large eddies at 90 km is of the order of

$$t_1 = 50 \text{ seconds} \quad (19)$$

Let us turn now to formula (6) for the turbulence-velocity v_1 of the large eddies. There are three sources of experimental information concerning the turbulence-velocity of the large eddies:

(*i*) The photographic observations of Liller and Whipple [9], which clearly reveal the motions due to the large eddies.

(*ii*) The radar measurements of "wind," particularly those of Greenhow [34]. Wind as measured by Greenhow includes the turbulence-velocity, which shows up as variability in the wind.

(*iii*) Measurements of the fading rate of long-duration meteor-echoes [35]. These fading rates are proportional to the radio frequency used, showing that the phenomenon can be explained as Doppler broadening of the transmitted frequency due to turbulent motion.

All three methods lead to turbulence-velocities of the order of 30 to 40 meters/sec. We therefore adopt for the turbulence-velocity of the large eddies the value

$$v_1 = 35 \text{ meters/second} \quad (20)$$

We now substitute the value (19) for t_1 and the value (20) for v_1 into formula (6) and deduce that the turbulence-power per unit mass at 90 km is of the order of

$$w = 25 \text{ watt /kg} \quad (21)$$

This value seems remarkably high in comparison with the value (1) for the troposphere. By multiplying w by the atmospheric density, we deduce that the turbulence-power per unit volume in the troposphere is about 5×10^{-4} watt/meter^3, while that at 90 km is about 10^{-4} watt/meter^3. Thus, turbulence-energy is being supplied to the atmosphere at the meteoric level at a rate per unit volume not much less than that prevailing in the troposphere in spite of the drastic difference in atmospheric density. The high value (21) deduced for the turbulence-power per unit mass at 90 km will be subjected to further study in section 6. It may be stated immediately, however, that the value (21) for w implies a turbulence-energy wt_1 per unit mass which is only a fraction 3×10^{-4} of the thermic energy per unit mass at 90 km.

With the value (21) for w and the value (19) for t_1, we can now substitute into (8) and deduce for the scale of the large eddies at the 90-km level,

$$L_1 = 1.6 \text{ km} \quad (22$$

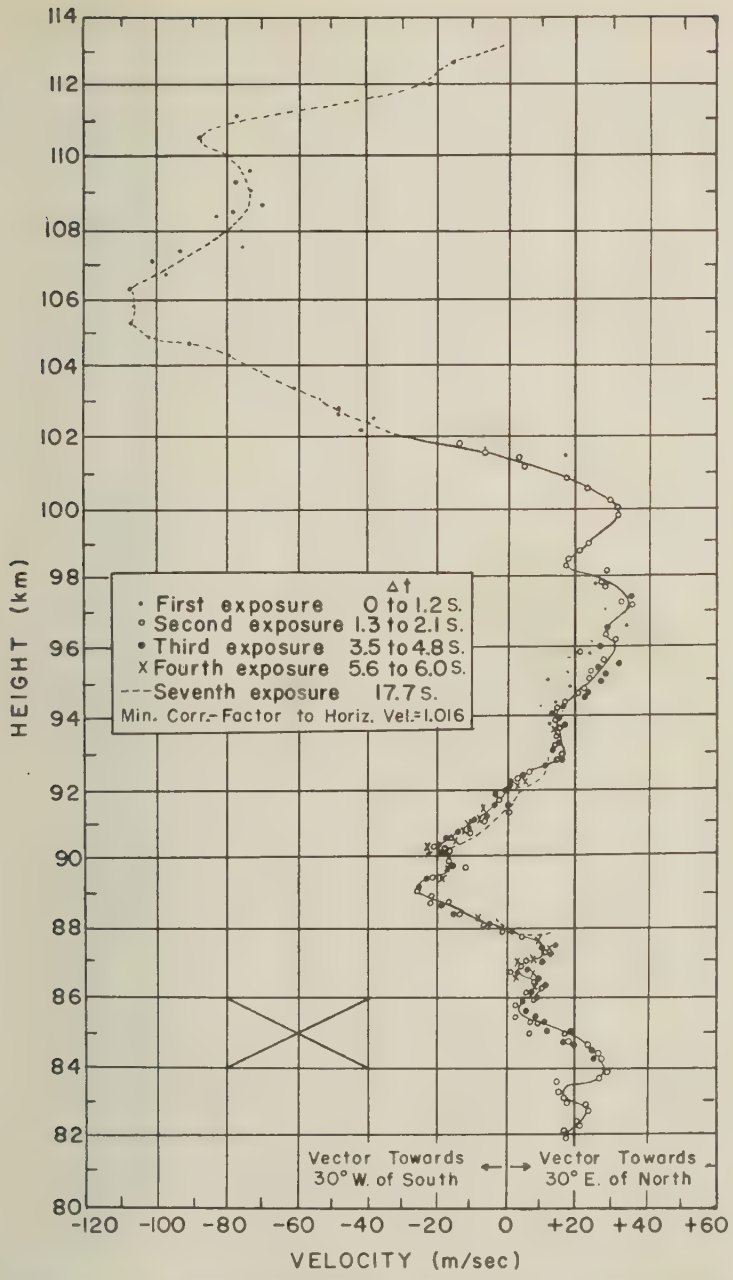

G. 3—Observations by Liller and Whipple [9] of the velocity of a meteoric trail as a function of height

This value is in tolerable agreement with the observations of Liller and Whipple [9].

Having now put numerical values on the principal quantities associated with the large eddies at 90 km, let us now turn our attention to the small eddies. For this purpose, we need a value for the coefficient of molecular diffusion at 90 km. We shall use the value

$$D = 4 \text{ meters}^2/\text{second} \quad (23)$$

which may be derived either from the rocket atmosphere or from the decay time of short-duration meteor-echoes [33].

Substituting the value (21) for w and the value (23) for D into equations (9), (10), and (13), we deduce for the turbulence-velocity of the small eddies

$$v_2 = 3 \text{ meters/second} \quad (24)$$

for the scale of the small eddies

$$L_2 = 1.3 \text{ meters} \quad (25)$$

and for the time-constant of the small eddies

$$t_2 = 0.4 \text{ second} \quad (26)$$

The turbulence-velocity v_2 of the small eddies cannot be conveniently observed in practice by any method at present available, since its effect is overshadowed by the turbulence-velocity (20) of the large eddies, which is ten times bigger.

The value (25) for the scale of the small eddies is susceptible to experimental verification. The value of L_2 vitally affects the frequency-dependence in the strength of long-duration meteor-echoes. The value of L_2 also vitally affects the frequency-dependence of long-distance VHF scatter-communication. The value of L_2 required to explain these phenomenon is, in fact, quite close to the value (25). This matter is taken up in greater detail in a companion paper by Booker and Cohen [36].

In discussing radar reflection from long-duration meteor-trails, some importance attaches to the wavelength

$$4\pi L_2 = 16 \text{ meters} \quad (27)$$

using the numerical value (25) for L_2 . For a wavelength λ longer than (27), incoherent back-scattering is controlled by irregularities whose scale is of the order of $\lambda/(4\pi)$. But for wavelengths shorter than (27), incoherent back-scattering is controlled by the small eddies, whose scale is given by (25). Since most radar observations of meteor-trails are made in the VHF band, it follows that the strength of incoherent back-scattering from meteor-trails is controlled almost entirely by the small eddies.

We now come to discussion of the value (26) for the time-constant of the small eddies. This value for t_2 appears to cut across much of the current thinking concerning radar reflections from long-duration meteor-trails. What (26) shows is that the trail is mixed on the scale L_2 of the small eddies after a time of the order of 0.4 second from formation of the trail. Since the value (27) for $4\pi L_2$ exceeds

ne wavelengths normally used for radar investigation of meteor-trails, it follows nat, after about 0.4 second, the trail is rough instead of smooth. Thus, when the me since the formation of the trail exceeds the time-constant of the small eddies, ne echo from the trail should be calculated by an incoherent scattering theory nd not by a smooth reflection theory. This rules out the theory of Kaiser and loss [37] as a theory of long-duration echoes from meteor-trails. The theory of aiser and Closs is a correct modification of the theory of Lovell and Clegg [38] allow for overdense ionization, but it applies only before the eddies have rendered ne trail rough, that is, for a few tenths of a second. There is a possibility that me extension of this time arises from the modification in local wavelength as the ave enters the trail. But there seems no likelihood of the theory of Kaiser and loss being applicable in the VHF band at times large compared with a second fter formation of the trail. An alternative theory of long-duration meteor-echoes ased on incoherent scattering is presented in the companion paper by Booker nd Cohen [36].

Although it is true that incoherent back-scattering from a meteor-trail at mes greater than (26) and at wavelengths less than (27) involves scattering by regularities associated with the small eddies, it should not be assumed that larger ddies play no part in the phenomena. Let us first consider fading phenomena. only the turbulence-velocity v_2 of the small eddies were involved, the fading equency would be $2v_2/\lambda$ and would have a Rayleigh distribution of amplitude fter time t_2 . However, because the small eddies partake of the much larger rbulence-velocity v_1 of the large eddies, the fading frequency of long-duration eteor-echoes is actually controlled by the large eddies and is

$$\frac{2v_1}{\lambda} \qquad (28)$$

fter time t_2 , this fading should also develop a Rayleigh distribution of amplitude hen a sufficient number of irregularities associated with the large eddies have ecome involved in forming the echo. The fading of a long-duration meteor-echo ould therefore have a frequency of the order of (28), should develop in amplitude uring a time t_2 given by (26), and should ultimately develop a Rayleigh distri-ution of amplitude.

Greenhow [8] has demonstrated experimentally that long-duration meteor-choes ultimately develop a Rayleigh distribution of amplitude. Moreover, he as ascertained experimentally the time taken by an echo to develop deep fading. lis results are reproduced in Figure 4 for a wavelength of 4 meters and a wave-ngth of 8 meters. It is seen that the time taken to develop deep fading varies etween 0.1 and 1.6 seconds, with a median value of 0.4 second. In other words, reenhow has demonstrated experimentally that the time taken by a radar echo om a meteor-trail to develop deep fading is approximately equal to the expected alue at 90 km for the time-constant of the small eddies. It is concluded, therefore, nat the time measured in this experiment of Greenhow is the time-constant of the mall eddies.

That the time of development of deep fading in long-duration meteor-echoes ay be controlled primarily by the time-constant of the small eddies is a concept

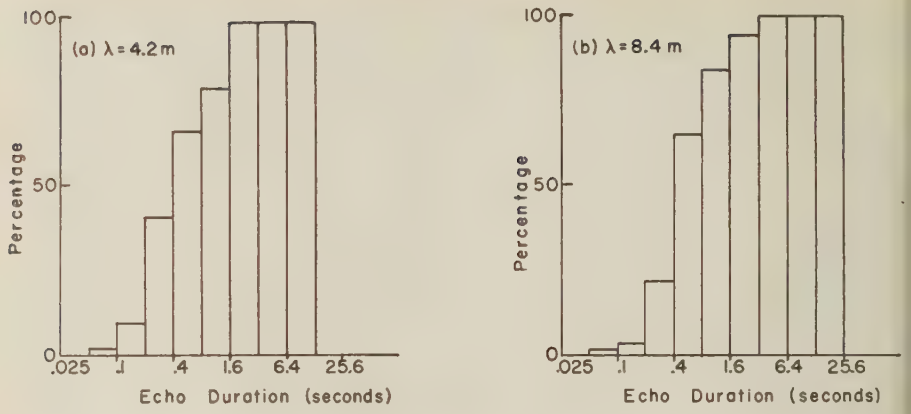

FIG. 4—Observations by Greenhow [8] of the time taken for meteoric echoes to develop deep fading

that does not seem to have been considered anywhere in the literature on radio-meteoric echoes. The conventional viewpoint is that the development of deep fading is due to distortion of the trail produced by the large eddies, and that deep fading sets in when multiple perpendiculars from the radar onto the distorted trail are possible. Let us calculate this effect on the assumption of a linear profile of mean wind. Consider an initial trail for which the perpendicular from the radar falls within the length of the trail, and let the length of the perpendicular be r. Consider the effect on the trail of the large eddies only, and suppose that these render the trail sinuous with a wavelength $2\pi L_1$ and with an amplitude $v_1 t$ at time t after formation of the trail. The maximum deviations in slope of the trail at time t are therefore of the order

$$\frac{v_1 t}{L_1} = \frac{t}{t_1} \qquad (29)$$

from (7). Now, when two perpendiculars onto the trail develop, their feet will have a separation of the order of either about $\frac{1}{4}\ 2\pi L_1$ or about $\frac{3}{4}\ 2\pi L_1$. The angle between the two perpendiculars may therefore be taken to be roughly

$$\frac{\pi L_1}{r} \qquad (30)$$

Multiple perpendiculars will not develop until the deviation (29) in slope has reached the angle (30). Equating (29) and (30), we see that the time taken to develop multiple perpendiculars is of the order

$$t = \pi \frac{L_1 t_1}{r} \qquad (31)$$

The question at issue is whether the time t_2 taken by the small eddies to render the trail rough is less or greater than (31). The condition that the development of deep fading should be controlled by the large eddies is

$$t < t_2$$

$$r > \pi L_1 \frac{t_1}{t_2} \quad \ldots\ldots\ldots\ldots\ldots\ldots\ldots\ldots\ldots\ldots (32)$$

$$= 600 \text{ km}$$

sing the values of L_1 , t_1 , and t_2 given by (22), (19), and (26). Thus, for a linear rofile of mean wind, it is possible for the time taken to develop deep fading to be ontrolled by the large eddies, but only for meteors at extremely long range. Of ourse, it is also possible to devise non-linear profiles of mean wind that would ther increase or decrease the time taken by the large eddies to make multiple erpendiculars possible. For a linear profile of mean wind, however, and for a easonable mean meteoric range of 150 km, the small eddies render the trail rough or a VHF radar in about a quarter of the time that the large eddies take to make ultiple perpendiculars possible. Of course, after the small eddies have made the ail rough, perpendiculars from the radar onto the trail are no longer of interest.

It is concluded therefore that, while it is possible in some cases for the time of evelopment of deep fading to be controlled by the large eddies, this time will sually be controlled by the small eddies and will be equal to their time-constant . Since this time-constant is of the order of 0.4 second at 90 km, it is not surprising iat, in averaging results for some hundreds of meteor-trails, Greenhow obtained ie results reproduced in Figure 4.

Effects due to eddies other than the small ones are involved not only in the ading frequency (28) of long-duration meteor-echoes but also in the mean echo rength. Although the back-scattering concerned is from the irregularities associated with the small eddies, nevertheless the diffusion of the trail, and therefore ie relevant scattering volume, is controlled after time t_2 by eddy motion and ultiiately by the large eddies. To understand this, it is necessary to consider eddyiffusion. The usual expression for the coefficient of eddy-diffusion is the product f the turbulence-velocity v_1 and the scale L_1 of the large eddies. At 90 km, therefore, ie coefficient of eddy-diffusion has, from (20) and (22), the value

$$v_1 L_1 = 6 \times 10^4 \text{ meters}^2/\text{second} \quad \ldots\ldots\ldots\ldots\ldots\ldots (33)$$

he ratio of the coefficient of eddy-diffusion to that for molecular diffusion (which atio is the Reynolds number of the large eddies) is therefore about ten thousand. n experimental value for the coefficient of eddy-diffusion at the meteoric level as been estimated by Dobrovol'skii [39] from observations of the rate of spread f those occasional visual meteors which, for some reason, can be seen for periods f many minutes. Dobrovol'skii estimates from the observations of various Russian orkers that the coefficient of eddy-diffusion is large compared with the coefficient f molecular diffusion. The value derived, however, is about a power of ten less ian (33), probably because the height involved is less than 90 km.

Since there is such a drastic difference between the values of the coefficients f molecular and eddy diffusion, it is necessary to be clear about the significance f each coefficient, about when each should be applied, and about how, for a ieteor-trail, a transition takes place from the one to the other. Diffusion of a ieteor-trail should be calculated as follows:

(*i*) At a time t after formation of the trail less than the time-constant t_2 of the small eddies, the appropriate coefficient of diffusion is the coefficient of molecular diffusion D.

(*ii*) At a time t greater than the time-constant t_1 of the large eddies, the appropriate coefficient of diffusion is the coefficient of eddy-diffusion $v_1 L_1$.

(*iii*) As the time t after formation of the trail increases from t_2 to t_1 , there is a continuous increase in the appropriate coefficient of diffusion from the value D to the value $v_1 L_1$.

This state of affairs is illustrated in Figure 5 using the numerical values for t_1 , t_2 , D, and $v_1 L_1$ previously derived.

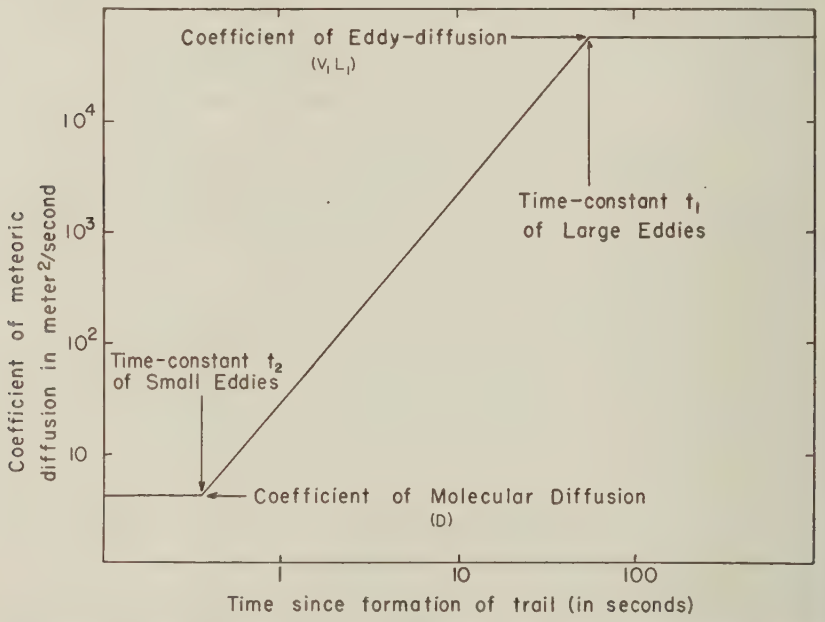

Fig. 5—Variation of the coefficient of meteoric diffusion with time measured from formation of the trail

The reasons that the coefficient of meteoric diffusion behaves in the above way are the following. For $t \ll t_2$, rotation even of the smallest eddies is small compared with one radian. In this interval of time the trail, besides suffering molecular diffusion, becomes distorted, but not drastically. For $t < t_2$, the distortion of the trail is still sufficiently simple so that its geometry can be imagined. Now consider the situation for $t \gg t_1$. By this time, the rotation of all eddies, including the largest, has become large compared with one radian, and the trail is hopelessly tangled. In principle, we could still take the trouble to describe this complicated geometry, and think of the tangled trail as subject merely to molecular diffusion. In practice, however, this is inconvenient and, indeed, virtually impossible. For $t > t_1$, we make no attempt to describe the detailed contortions of the trail and

ntent ourselves by merely stating the rate of expansion of a cylinder enveloping
ie tangled trail. It is the rate of expansion of this enveloping cylinder that is
escribed by the coefficient of eddy-diffusion $v_1 L_1$. Now consider the situation at
time t intermediate between the time-constant t_2 of the small eddies and the
me-constant t_1 of the large eddies. For the smaller eddies, whose time-constants
e less than t, distortion of the trail is drastic and it is convenient to use the concept
eddy-diffusion. For the larger eddies, however, whose time-constants exceed t,
stortion of the trail is still moderate and capable of being imagined. At a time t
etween t_1 and t_2 , therefore, it is convenient to think of an enveloping cylinder
iat is expanding at the rate corresponding to eddies of time-constant t; this
panding cylinder is being distorted, however, by the eddies whose time-constants
ceed t. The appropriate coefficient of diffusion required at time t is therefore
lculated as follows. The turbulence-velocity v and scale L of eddies of time-
nstant t are given by (cf. equations 6 and 8)

$$v = (wt)^{1/2} \quad \ldots\ldots (34)$$

$$L = (wt^3)^{1/2} \quad \ldots\ldots (35)$$

ence, the coefficient of eddy-diffusion applicable to a meteor-trail at time t is

$$vL = wt^2 \quad \ldots\ldots (36)$$

his obviously increases to the usual coefficient of eddy-diffusion $v_1 L_1$ as t increases
t_1 , and from equations (9) and (10) it may be seen that it reduces to the co-
ficient of molecular diffusion D as t reduces to t_2 . It follows that the coefficient
meteoric diffusion is given approximately by

$$\left.\begin{array}{rl} D, & 0 < t < t_2 \\ wt^2, & t_2 < t < t_1 \\ v_1 L_1 , & t > t_1 \end{array}\right\} \quad \ldots\ldots (37)$$

is this behavior that is plotted in Figure 5, using the values of the parameters
iat we have deduced for the 90-km level.

The upshot of this section is that the formulas of sections 2 and 3 appear to
ccount satisfactorily for the known phenomena of turbulence associated with
eteor-trails, and that the value for the turbulence-power per unit mass is of the
rder of 25 watts/kg at a height of 90 km.

Scintillation of Radio Stars

Let us turn now to the more difficult problem of scintillation of radio stars.
uch scintillation can occur in both the E region and the F region. It is the F-region
henomenon that has been studied more intensively, however, and it is to this
iat we shall confine our attention.

Maxwell [40] has already made an attempt to explain scintillation of radio
ars in terms of turbulence in the F region, after offering criticisms of certain alter-
ative suggestions. It is our objective to reconsider the approach of Maxwell with
rtain important changes. Since the scintillation phenomenon is one of forward-
attering, it depends on the irregularities associated with the large eddies. While

Maxwell had available the formulas for small eddies given in section 3 of this paper, he did not have available the formulas for large eddies given in section 2. Thus, he did not have available formulas for eddies of the size directly involved in the scintillation phenomenon. Furthermore, at the time of Maxwell's work, it had not been demonstrated that the electronic irregularities responsible for scintillation are constricted perpendicular to the earth's magnetic field, so that he omitted the major allowance that has to be made for this important phenomenon. Thus, while our objective in this section is broadly the same as that of Maxwell, the development will follow different lines in certain major respects.

Owing to the influence of the earth's magnetic field, care is necessary in the F region to distinguish between the eddies in the neutral molecules and the irregularities of ion-density and electron-density to which they give rise. Even in the E region this effect is of some importance for the electrons. Let ν be the collisional frequency of collisions between charged particles and neutral molecules and ω_M be the radian gyromagnetic frequency for the charged particles in the presence of the earth's magnetic field. Values of ν and ω_M are different for the ions from what they are for the electrons. Appropriate numerical values can be derived from the rocket atmosphere interpreted in the manner described in section 1. If the neutral molecules move parallel to the earth's magnetic field with a certain velocity, then (after a collision interval) both the ions and electrons will move parallel to the earth's magnetic field with the same velocity. The same is not, in general, true in a direction perpendicular to the earth's magnetic field, however. Motion of the charged particles is not, in general, in the same direction as that of the neutral molecules, and the velocity of the charged particles is reduced [32] in the ratio*

$$\frac{\nu}{(\omega_M^2 + \nu^2)^{1/2}} \qquad (38)$$

This expression is plotted in Figure 6 as a function of height for both the ions and the electrons, on the basis of the rocket atmosphere. Now consider isotropic turbulence in the neutral molecules. This involves equal turbulence-velocities along and perpendicular to the earth's magnetic field. It follows that the ratio of the drift velocity for the charged particles perpendicular to the field to that parallel to the field is (38). We shall assume that this velocity ratio for the charged particles is also the ratio of the scale of the irregularities in the density of the charged particles measured perpendicular to the field to that measured parallel to the field. On this basis, the scale of irregularities in the density of the ions or electrons measured parallel to the earth's magnetic field is the same as the scale of the corresponding eddies in the neutral molecules, and the scale of the irregularities measured perpendicular to the earth's magnetic field is obtained by multiplying the scale measured parallel to the field by the appropriate ratio read from Figure 6.

An important correction is required in the above statement arising from the tendency of irregularities in ion-density to create irregularities in electron-density of the same size and shape as a result of electrostatic forces [43]. In fact, eddies of

*Spencer [6] uses an expression which is the square of (38) due to neglect of one component in the motion of the charged particles.

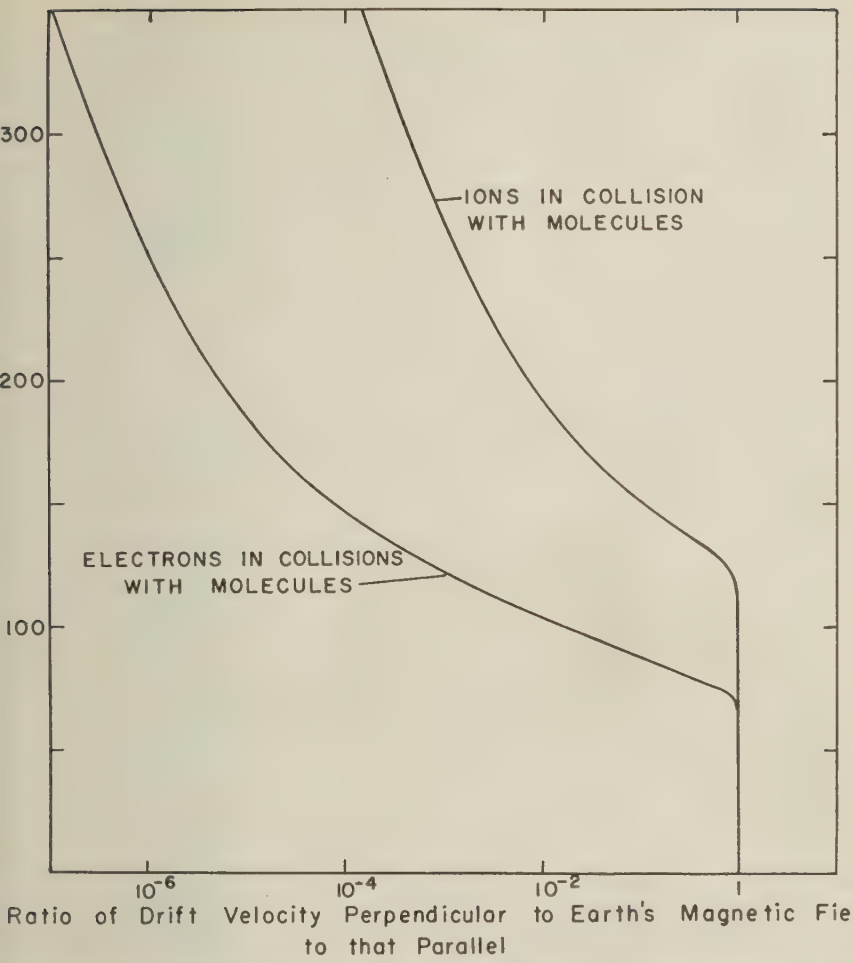

g. 6—The reduction ratio for the velocity of charged particles in motion perpendicular to the earth's magnetic field

ale L in the neutral molecules are likely to create irregularities in electron-density two mechanisms, namely:

(*i*) Collisions between electrons and neutral molecules, and

(*ii*) Collisions between ions and neutral molecules, with allowance made for electrostatic forces between ions and electrons.

both mechanisms, the scale of electronic irregularities measured along the rth's magnetic field is L. In case (*i*), the scale of electronic irregularities transverse the earth's magnetic field is T_e, where the ratio T_e/L is given by the electronic rve in Figure 6. In case (*ii*), the scale of electronic irregularities transverse to e earth's magnetic field is T_i, where the ratio T_i/L is given to only a rough proximation by the ionic curve in Figure 6. For an isolated irregularity, the

tendency of electrons to follow the ions would reduce the ratio T_i/L to unity. Since, however, we are dealing with a continuum of irregularities of small intensity, this effect is greatly reduced but not completely destroyed. The appropriate value of T_i/L is, therefore, almost certainly less than that given by the ionic curve in Figure 6, but we shall tentatively assume that it is not drastically less. The relative importance of the above two mechanisms for creation of electronic irregularities is not known theoretically. However, reasons will be given, based on observations, for thinking that both mechanisms are important in the ionosphere.

It may also be mentioned that it is in connection with the interpretation of the ratios shown in Figure 6 that the assumption of isotropic turbulence in the neutral molecules is particularly important. These ratios would have to be modified by the ratio of the turbulence-velocity of the neutral molecules perpendicular to the earth's magnetic field to that parallel to the earth's magnetic field. There is more than one respect, therefore, in which the ratios shown in Figure 6 must be applied with caution. Nevertheless, we shall use the ratios shown in Figure 6 without modification to indicate the shape of electronic irregularities controlled by collision between electrons and neutral molecules (electronic curve) and by electrostatic coupling with the ions (ionic curve).

Scintillation of radio stars, being a phenomenon of forward-scattering, depends on the largest irregularities of electron-density present. These irregularities will arise from the large eddies, of scale L_1 , in the neutral molecules, operating *via* mechanism (*ii*) to form electronic irregularities of scale L_1 measured along the earth's magnetic field and scale T_{i1} measured transverse to the earth's magnetic field, the ratio T_{i1}/L_1 being somewhat less than that given by the ionic curve in Figure 6. The measurements of Spencer [6] show that $2\pi T_{i1}$ is of the order of 3 km. We shall, therefore, take it as an observed fact that, at the level where scintillation of radio star occurs, we have

$$T_{i1} = 0.5 \text{ km} \quad \ldots\ldots (39)$$

Spencer has also attempted to measure the ratio of T_{i1} to L_1 , but the results are somewhat vague. Ratios of the order 1:10 are explicitly mentioned, but ratios as big as 1:100 are not explicitly mentioned. For the purpose of discussion, we shall assume that the value of the ratio at the scintillation level is

$$\frac{T_{i1}}{L_1} = \frac{1}{30} \quad \ldots\ldots (40)$$

The value of this ratio is important to the discussion, so that it is unfortunate that its value is not better determined. Combining (40) with (39), we see that Spencer's results indicate a scale of turbulence at the scintillation level of

$$L_1 = 15 \text{ km} \quad \ldots\ldots (41)$$

It should be realized that, of the three quantities (39), (40), and (41), only (39) may be considered a firm value.

It has been estimated by Hewish [5] that the height at which the scintillation of radio stars occurs is about 400 km. This was never a highly accurate measurement of height, however, and its reliability is further reduced now that it is known that the electronic irregularities concerned are constricted round the lines of the

arth's magnetic field. We shall assume that the Hewish argument merely indicates iat the scintillation level must be somewhere in the F region.

There seems little doubt that 400 km is an impossibly great height at which o explain the scintillation phenomenon by means of turbulence. In the first place, iere is difficulty in having turbulence at 400 km. In the second place, even if irbulence could exist at 400 km, it would not lead to electronic irregularities of ie size and shape required to explain the scintillation observations. The ratio 38) for the transverse scale to the longitudinal scale is so small at 400 km that ie largest conceivable transverse scale would be much less than the observed alue (39). If, therefore, the scintillation phenomenon is to be explained in terms f atmospheric turbulence, it will clearly have to be at a level below 400 km.

Let us tentatively accept the statement (40) and use it in conjunction with the nic curve in Figure 6. We then read off 170 km as the scintillation height. Although iis estimate is probably too low, let us use it as a basis of further discussion. It llows from this and from (41) that the scale of the large eddies at 170 km is 15 m. From the rocket atmosphere, we also derive for 170 km

$$T = 518°\mathrm{K} \quad (42)$$

$$\frac{dT}{dz} = 5°\mathrm{K/km} \quad (43)$$

$$\Gamma = 8.5°\mathrm{K/km} \quad (44)$$

$$\frac{dT}{dz} + \Gamma = 13.5°\mathrm{K/km} \quad (45)$$

rom (4), we therefore obtain for the time-constant of the large eddies

$$t_1 = 60 \text{ seconds} \quad (46)$$

ow substituting from (41) and (46) into (8), we obtain for the turbulence-power er unit mass at the scintillation level

$$w = 1{,}000 \text{ watts/kg} \quad (47)$$

his value is even higher than that found at the meteoric level. The value (47) r w implies a Reynolds number for the large eddies of about a hundred, while eeping the turbulence-energy to somewhat less than one per cent of the thermic iergy. High though the estimated value (47) for the turbulence-power per unit ass at the scintillation level may seem to be at first sight, it does not violate the bvious criterion that the turbulence-energy should be small compared with the iermic energy.

From the value (47) for w and the formulas of sections 2 and 3, we may deduce ie following numerical values for the scintillation level, none of which seem apable of verification at the present time:

$$v_1 = 250 \text{ meters/second} \quad (48)$$

$$v_2 = 80 \text{ meters/second} \quad (49)$$

$$t_2 = 7 \text{ seconds} \quad (50)$$

$$L_2 = 0.5 \text{ kilometer} \quad (51)$$

The fading rate involved in scintillation cannot be checked with the above value of v_1 because the fading rate is controlled by the rate of horizontal drift of irregularities, due presumably to the influence of an electric field.

We conclude that it is feasible to explain the phenomenon of scintillation of radio stars in terms of turbulence in the F region. The height, however, must be less than 400 km, although it no doubt exceeds somewhat the value of 170 km used above. To explain star scintillation by means of turbulence, the rate of supply of turbulence-energy to the large eddies, and its rate of conversion into thermic energy by the small eddies, must have the high value of about a thousand watts per kilogram.*

6. *Discussion of the Magnitude of the Turbulence-Power*

At present, we only have three approximate values for the turbulence-power w per unit mass, namely:

(*i*) 5×10^{-4} watt/kg in the troposphere
(*ii*) 25 watts/kg at the meteoric level, and
(*iii*) 1,000 watts/kg at the scintillation level.

Moreover, the last of these values refers to conditions of strong scattering in the F region, and a value for w of perhaps 100 watts/kg might be more appropriate to a quiet ionosphere. While it is impossible to construct a reliable curve of w as a function of height from this information, there are, nevertheless, some useful statements that can be made.

At each level in the rocket atmosphere, it is possible to specify a range of values within which w must lie, and to plot the upper and lower bounds as a function of height. This is done in Figure 7, where the stippled area denotes the portion of the diagram within which w cannot lie. The curve specifying the left-hand edge of the permitted area expresses the condition that the Reynolds number for the large eddies is unity. Since the Reynolds number for the small eddies is always unity, the equation of this curve is given by

$$L_1 = L_2 \quad \ldots\ldots (52)$$

Using the formulas (8) and (10) for L_1 and L_2, equation (52) reduces to

$$w = \frac{D}{t_1^2} \quad \ldots\ldots (53)$$

Hence, a lower bound for the value of the turbulence-power per unit mass at any height is

$$\frac{D}{t_1^2} \quad \ldots\ldots (54)$$

For the rocket atmosphere, we have already calculated D as a function of height (see Fig. 2) and also t_1 as a function of height [see eq. (4) and Fig. 1]. We can,

*It is understood that the fraction (40) is now estimated at about 1/5 by workers at Cambridge University. This would lead to a value of w much closer to the meteoric value (21), but at a height (140 km) that it is more difficult to modity to an F-region level.

herefore, calculate (54) as a function of height, and it is this curve that gives the eft-hand boundary of the permitted area in Figure 7.

Since the energy of turbulence is associated mainly with the large eddies, the urbulence-energy per unit mass is approximately wt_1 . This must obviously be

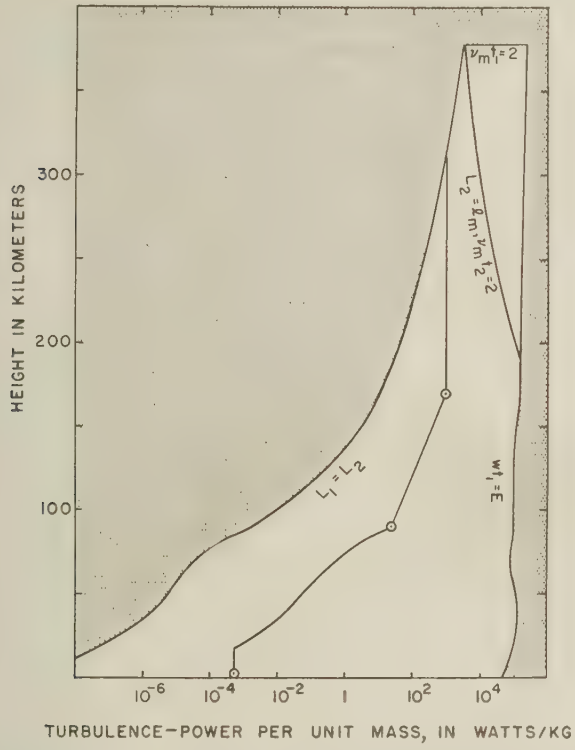

Fig. 7—Restrictions on the value of the turbulence-power per unit mass

ess than the thermic energy E per unit mass. Hence an upper bound for the value f w at any level is

$$\frac{E}{t_1} \qquad (55)$$

nd the value of this can be calculated for the rocket atmosphere at any height. The right-hand boundary of the permitted area in Figure 7 is a plot of (55) as a unction of height for the rocket atmosphere.

The top of the permitted area in Figure 7 is set by the fact that a molecule nust make collisions within a time equal to the time-constant t_1 of a large eddy.

We deduce from Figure 7 the important fact that it is impossible to have urbulence in the ionosphere unless the turbulence-power per unit mass is much igher than Brunt's value, 5×10^{-4} watt/kg, for the troposphere. We further notice that the value 25 watts/kg we have deduced for the meteoric level lies in

the middle of the permitted range at 90 km. The value of 1,000 watts/kg for the scintillation level is also satisfactory, provided that this level is significantly below 400 km.

The permitted area in Figure 7 is cut into two parts by a curve marked $L_2 = l_m$. This curve expresses the condition that the scale L_2 of the small eddies given by (10) is equal to the molecular mean free path l_m. Below this curve, the cut-off in the spectrum of turbulence at the small eddy end is controlled by viscosity in the usual way and occurs at the scale L_2. Above this curve, the cut-off in the spectrum of turbulence is given by the molecular mean free path l_m, as contemplated by Dungey and Willson [41]. It is seen that, over the majority of the permitted area, and over practically all of the area in which we are likely to be interested, the cut-off in the spectrum of turbulence is likely to be determined by viscosity in the usual way. This means that we are unlikely to encounter any revolutionary modification in the principles that form the basis of the Kolmogoroff-Heisenberg theory of turbulence.

For purposes of illustration, a curve of turbulence-power per unit mass *versus* height has been drawn in Figure 7 through the three points corresponding to the troposphere, the meteoric level, and the scintillation level. The departure from a linear segment in the interval of height from 18 to 90 km arises from an arbitrary (and unimportant) assumption that the turbulence-energy per unit volume does not vary with height in this range. Using this curve of w *versus* height, we may calculate for the rocket atmosphere the variation with height of the various parameters associated with the large and small eddies. On this tentative basis, the time-constant t_2 of the small eddies has been added to Figure 1, and the coefficient of eddy-diffusion has been added to Figure 2. The ratio of the two coefficients of diffusion gives the Reynolds number of the large eddies. On the same basis, the turbulence-velocities for the large and small eddies are plotted as functions of height in Figure 8, and the scales of the large and small eddies are plotted as functions of height in Figure 9.

It may be noted that the scale of the large eddies indicated in Figure 9 becomes comparable with the scale-height of the atmosphere at F-region levels. This is not thought to be objectionable. If the size of eddies is not small compared with the scale-height of the atmosphere, this merely underlines the importance of allowing for adiabatic expansion and contraction in picturing the eddy motion. Furthermore, if under quiet ionospheric conditions the turbulence-power per unit mass at 200 km were only 100 watts/kg, it follows from Figure 7 that there would be little turbulence above 200 km and that the scale of the large eddies would be less than the scale-height of the atmosphere at all relevant levels.

7. *Discussion of the Scales of Electronic Irregularities*

It has been pointed out by Dungey and Willson [41] that eddy scales less than the molecular mean free path are impossible. Some care, however, is necessary in making corresponding statements about electronic irregularities. For electronic irregularities, the scale along the earth's magnetic field cannot be less than the electronic mean free path l_e, and it has to be remembered that

$$l_e = 4\sqrt{2}\, l_m \qquad (56)$$

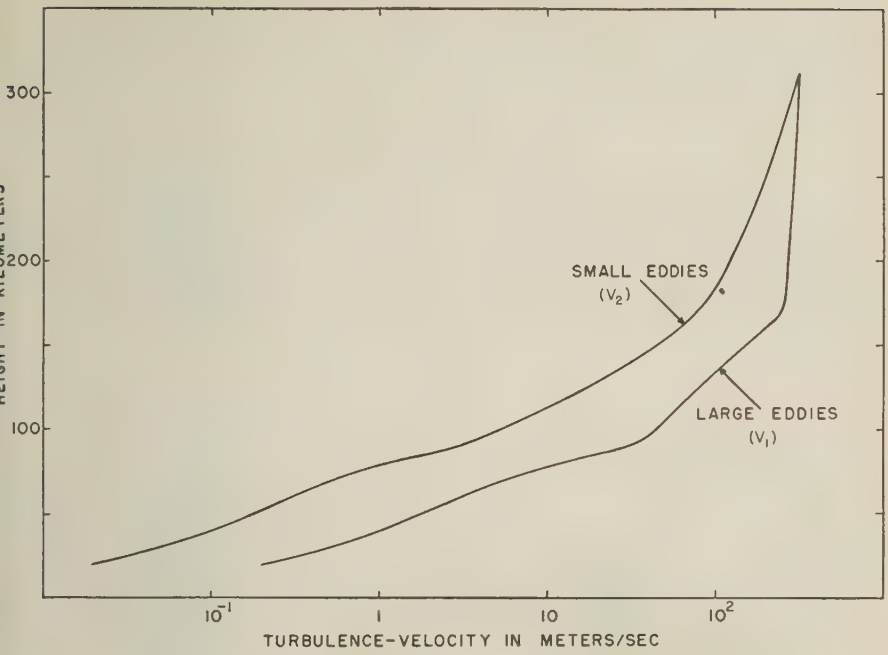

FIG. 8—The turbulence-velocities for the large and small eddies

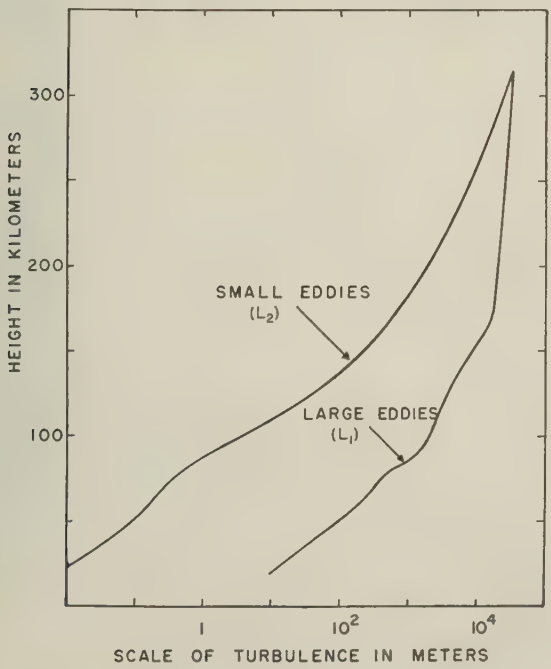

FIG. 9—The scales of the large and small eddies

where l_m is the molecular mean free path. In a direction perpendicular to the earth's magnetic field, however, the minimum permissible scale for electronic irregularities is, from (38),

$$\frac{\nu}{(\omega_M^2 + \nu^2)^{1/2}} l_e \quad \ldots\ldots\ldots\ldots\ldots\ldots\ldots\ldots\ldots\ldots (57)$$

where ν is the electronic collisional frequency and ω_M is the electronic radian gyrofrequency. When $\nu \gg \omega_M$ (heights below about 70 km), (57) simply reduces to the electronic mean free path l_e , and there is no constriction of electronic irregularities perpendicular to the earth's magnetic field. However, when $\nu \ll \omega_M$ (heights above 90 km), (57) becomes

$$\frac{\nu l_e}{\omega_M} \quad \ldots\ldots\ldots\ldots\ldots\ldots\ldots\ldots\ldots\ldots\ldots\ldots (58)$$

Now the numerator of (58) is the thermic velocity of the electrons, and the denominator is the angular velocity with which electrons spiral round the earth's magnetic field. Hence (58) is the gyroradius of electrons in the earth's magnetic field, which is of the order of a centimeter or two. Thus, above 90 km, the minimum possible scale of electronic irregularities measured transverse to the earth's magnetic field is given by the electronic gyroradius, although the minimum possible scale measured along the earth's magnetic field is given by the electronic mean free path.

For the ions, there are similar considerations that are important because of the control that ionic irregularities are likely to have on electronic irregularities. For the ions, the minimum possible scale of irregularities measured along the earth's magnetic field is the molecular mean free path

$$l_m \quad \ldots\ldots\ldots\ldots\ldots\ldots\ldots\ldots\ldots\ldots\ldots\ldots (59)$$

and the minimum possible scale measured transverse to the earth's magnetic field is

$$\frac{\nu}{(\omega_M^2 + \nu^2)^{1/2}} l_m \quad \ldots\ldots\ldots\ldots\ldots\ldots\ldots\ldots\ldots\ldots (60)$$

where ν must now be interpreted as the molecular collisional frequency and ω_M as the ionic radian gyrofrequency. The various minimum possible scales are plotted in Figure 10 as functions of height, using the above formulas in conjunction with the rocket atmosphere.

For ionic irregularities, and consequently also for electronic irregularities controlled by ionic irregularities, the large and small scales measured along the earth's magnetic field are simply the scales of the large and small eddies in the neutral molecules, and may consequently be read from Figure 9. For electronic irregularities controlled directly by collisions with the neutral molecules, the same is true, except that some account has to be taken of the minimum possible scale along the earth's magnetic field plotted in Figure 10. The appropriate curve from Figure 10 intersects the curves in Figure 9, thereby removing electronic irregularities at the greater heights. Above about 160 km, an electron can pass right through a small eddy without making a collision, and above about 260 km it can

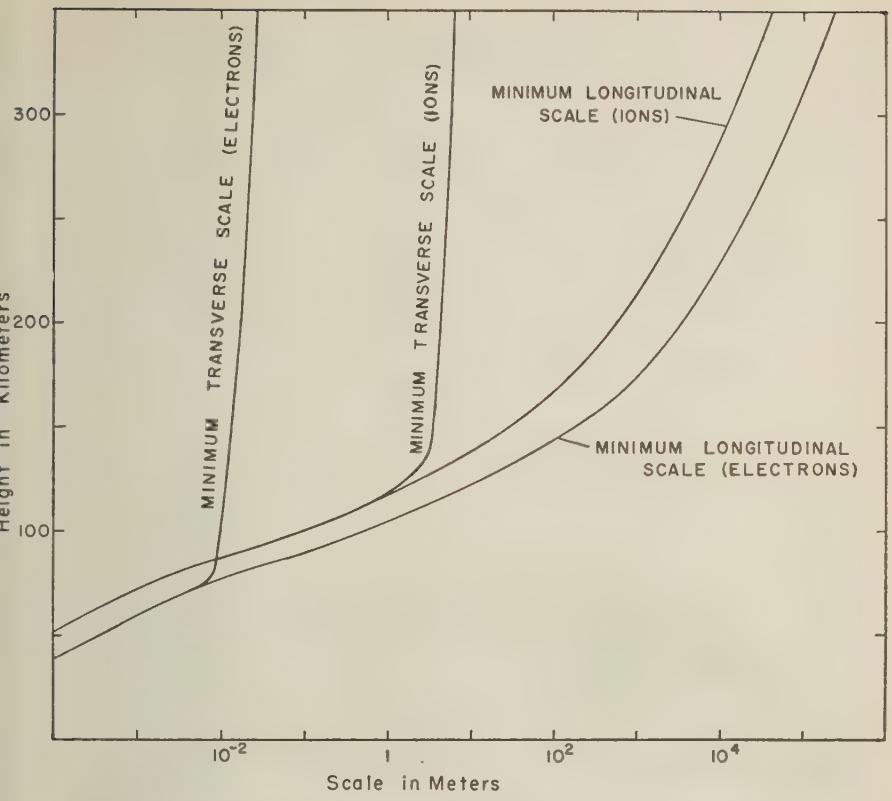

FIG. 10—The minimum scales for irregularities in the density of charged particles

do this even for a large eddy. This does not happen for electronic irregularities controlled by ionic irregularities because of the lower mean free path for ions.

Let us now turn our attention to the scale of electronic irregularities measured transverse to the earth's magnetic field. These are obtained by applying to the scales shown in Figure 9, the fractions plotted in Figure 6, and paying attention to the appropriate minimum possible scales shown in Figure 10. We thereby obtain the diagram of Figure 11. It is seen that, for electronic irregularities controlled by collision between electrons and neutral molecules, the curves giving the scale of irregularities are decapitated by the curve giving the minimum possible scale of irregularities in the same way as for scales along the earth's magnetic field and for the same reason. For electronic irregularities controlled by ionic irregularities, no such limitation is involved.

It will be noticed that, while we have considered the controlling effect of ionic irregularities on electronic irregularities *via* electrostatic forces, we have not considered any such control *via* collisions between ions and electrons, even though these collisions are the ones of greatest frequency in the F region. It is not difficult to show that any electronic irregularities occurring in the F region as a result of

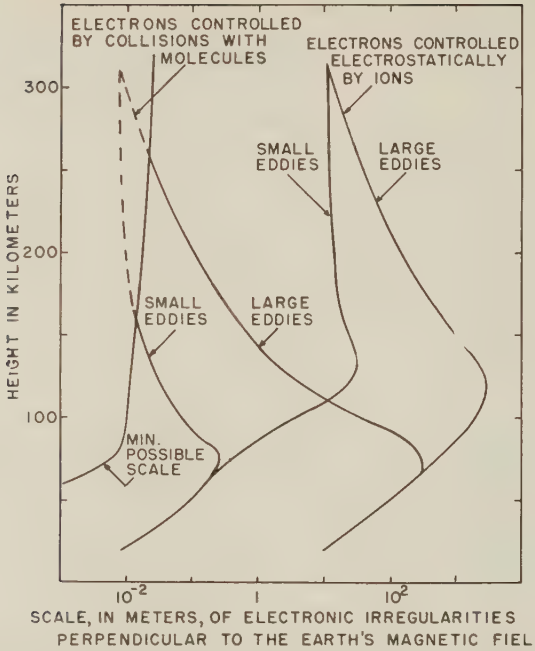

FIG. 11—The scales of irregularities of charged particles measured perpendicular to the earth's magnetic field

collisions between ions and electrons would have scales so small that they would be blurred by the spiraling of electrons round the earth's magnetic field.

8. *Auroral Echoes*

Let us now consider the significance of the curves in Figures 9 and 11, turning our attention first to the phenomenon of auroral echoes [15]. It is well known that ionospheric echoes are obtained by radars operating in the VHF band during auroral activity, and that these echoes occur predominantly at long range in the northern quadrant, even when the auroral activity is distributed over practically the whole sky. It has been shown by Booker [29] that this aspect sensitivity is to be explained in terms of irregularities of electron-density that are elongated along the earth's magnetic field and have a scale along the field of the order of 7 meters. The scale transverse to the field is small compared with this, and controls the shortest wavelength down to which auroral echoes can be observed. Let us assume that these irregularities arise from turbulence in the E region. On this view, the only functions of the auroral activity would be

(*i*) To provide increased electron-density and increased gradients of electron-density, thereby increasing the intensity of the electronic irregularties, and

(*ii*) To provide, in association with phenomena of terrestrial magnetism, an unusually large electric field that would cause drift of the electronic irregularities at such a speed as to explain the fading and Doppler phenomena observed with auroral echoes [17].

If auroral echoes are due to electronic irregularities caused by turbulence, these irregularities would have to be the smallest irregularities present at the level concerned. The 7 meters derived by Booker would therefore have to be the scale measured along the earth's magnetic field of the smallest electronic irregularities, and this is the same as the scale of the small eddies in the neutral molecules. We accordingly deduce that, at the level where auroral echoes occur, we have

$$L_2 = 7 \text{ meters} \quad \ldots\ldots\ldots\ldots\ldots\ldots\ldots\ldots\ldots\ldots (61)$$

approximately. From Figure 9, we deduce therefore that auroral echoes must occur at a height of about 100 to 110 km. This is in remarkably good agreement with the other features of auroral echoes.

Let us now read from Figure 11 the transverse scale for the smallest electronic irregularities at the level where (61) applies. We deduce

$$T_{2e} = 6 \text{ cm} \quad \ldots\ldots\ldots\ldots\ldots\ldots\ldots\ldots\ldots\ldots (62)$$

from which it should follow that the wavelength below which auroral echoes diminish in importance is

$$4\pi T_{2e} = 70 \text{ cm} \quad \ldots\ldots\ldots\ldots\ldots\ldots\ldots\ldots\ldots\ldots (63)$$

This fits in with the experimental observation that auroral echoes are obtained in the VHF band but not in the UHF band, though it should be noted that sufficiently careful experiments may not yet have been made in the UHF band. We conclude that the turbulence-explanation of auroral echoes is highly likely.

It will be observed that we would not have been able to explain the phenomenon of aspect sensitivity of auroral echoes in terms of turbulence if we had not taken account of the electronic irregularities produced directly from eddies by collision between electrons and neutral molecules without the ions being involved. However, it is equally true that we would have been unable to explain the phenomena of star scintillation in terms of turbulence if we had not taken account of electronic irregularities controlled electrostatically by ionic irregularities. It is for these reasons that we believe in the importance of both of these mechanisms for converting eddies in the neutral molecules into irregularities of electron-density.

. Radar Echoes from Irregularities in the F Region at Frequencies Above the Penetration-Frequency

Aspect sensitive echoes from *E*-region levels having properties somewhat like auroral echoes, but not associated with auroral activity, have been observed by workers at Stanford University [3] in the HF band and presumably have the same explanation. Similar echoes have also been obtained by these observers in the HF band from *F*-region levels, and again the explanation is presumably the same. From geometrical considerations, it has been deduced that these *F*-region echoes originate at heights between about 200 and 300 km. It seems quite likely that this phenomenon, the phenomenon of spread *F*, and the phenomenon of star scintillation all arise from the effects of turbulence in the *F* region at levels between 200 and 300 km. But whereas scintillation of radio stars is produced by the largest electronic irregularities present, the aspect sensitive *F*-region echoes should be

produced by the irregularities whose scale transverse to the earth's magnetic field is as near as possible to $\lambda/(4\pi)$. There is no doubt that the scale of irregularities in the F region along the earth's magnetic field is large compared with any HF wavelength, and the primary cause of the aspect sensitivity of the F-region echoes reported from Stanford University is obvious. The variation with frequency of the strength of these echoes is not known, however, with any certainty. From Figure 11, we would expect scales measured transverse to the earth's magnetic field at 200 km to range from 200 meters down to 10 meters and from 10 cm down to 2 cm. At 300 km, we would expect scales of the order of 10 meters. Whether these scales can explain the observations is unclear at the present time. Neither is it clear whether the two spectra of irregularities transverse to the earth's magnetic field shown in Figure 11 at F-region heights can be regarded as uncoupled.

It should be noted that there is a real likelihood of electronic irregularities in the lower part of the F region with scales measured along the earth's magnetic field of the order of 20 km and measured transverse to the earth's magnetic field of the order of a few centimeters. In principle, such irregularities should give echoes for radars in the UHF band if directed so that their beams are normal to the earth's magnetic field in the lower part of the F region. It seems unlikely that such echoes could be strong enough to be observable even with high-power equipment. It would be interesting, however, to take any opportunity that may occur to look for such echoes, especially at times of strong star scintillation and strong spread F.

10. *Scattering Phenomena at the 90-Km Level*

Another application of the results summarized in Figures 9 and 11 is to the phenomenon of long-distance scatter-communication in the VHF band [12]. This phenomenon as observed by Bailey, Bateman, and Kirby [13], over distances of the order of 1,000 to 2,000 km can be fairly completely explained in terms of scales read from Figures 9 and 11 for the 90-km level. This subject will be taken up in the companion paper by Booker and Cohen [36]. The only point that will be made here is that, in accordance with Figure 6, electronic irregularities controlled directly by collision with neutral molecules should show some constriction perpendicular to the earth's magnetic field at the 90-km level. It may be, therefore, that the beams used in this type of communication should be turned somewhat off the great-circle path in a direction away from the equator, especially at the highest frequencies involved. Likewise, for individual long-duration meteor-echoes, there may be an aspect sensitivity phenomenon qualitatively similar to that for auroral echoes, but appreciably less striking in magnitude because of the lower height involved.

There seems little doubt that the 90-km echoes of Gardner and Pawsey [10] and the similar echoes of Dieminger [11] at frequencies around 2 Mc/sec are due to radar reflections from the same irregularities that cause VHF scatter-communication. Using the scales derived for the 90-km level in section 4 in conjunction with the Kolmogoroff-Heisenberg spectrum of turbulence, it is possible to derive some equations describing the 2-Mc/sec phenomenon. It would be nice to check the spectrum of turbulence by comparing the 2-Mc/sec observations with the VHF observations. This is, unfortunately, rendered difficult because we are unable

to allow with sufficient accuracy for the effect of absorption on the 2-Mc/sec observations.

11. *The Possibility of F-region Scatter-Communication*

Ever since the discovery of long-distance communication in the VHF band using incoherent scattering in the lower part of the ionosphere, there has been discussion of the possibility of a similar phenomenon using scattering by electronic irregularities in the *F* region. It was at first argued that eddies in the *F* region were bound to be larger than in the *E* region and that this would increase the wavelength down to which communication *via* scattering in the *F* region would be possible. It is now clear that this argument was fallacious. It is quite true, as shown in Figure 9, that eddies in the neutral molecules are likely to be bigger in the *F* region than in the *E* region. This further implies that the scale of electronic irregularities measured along the earth's magnetic field is likely to be larger in the *F* region than in the *E* region. But Figure 11 shows that the scales of irregularities measured transverse to the earth's magnetic field are smaller in the *F* region than in the *E* region. This is because the effect of the earth's magnetic field in constricting the scale of electronic irregularities measured transverse to the field increases with height above the *E* region faster than does the scale of the eddies in the neutral molecules. The result is that the smallest scales of electronic irregularities occurring anywhere in the ionosphere are likely to occur in the *F* region, but only in the direction transverse to the earth's magnetic field. So far as scale is concerned, therefore, there is no reason why there should not be a phenomenon of scatter-communication employing irregularities in the *F* region, and extending down to an even shorter wavelength than is involved in scatter-communication *via* the lower ionosphere. It is essential, however, that due allowance be made for the fact that electronic irregularities in the *F* region are very elongated along the earth's magnetic field.

Our lack of knowledge of the spectrum of electronic irregularities measured transverse to the earth's magnetic field in the *F* region makes it impossible to predict the frequency-dependence of *F*-region scatter-communication at the present time. It is, however, possible to list three conditions that should be satisfied in experiments designed to investigate the phenomenon and that arise from the fact that the irregularities are very elongated along the earth's magnetic field. These are:

(*i*) Successful *F*-region scatter-communication is more likely for an east-west path than for a north-south path.

(*ii*) The east-west path should not be in too high a latitude, otherwise the "echo-point" will be in the *E* region instead of the *F* region; see Chapman [42]. For an experiment in the United States, this means that a path should be chosen near the Mexican border rather than near the Canadian border.

(*iii*) Both the transmitting and receiving beams must be swung from the great-circle path away from the equator through a substantial angle. Thus, for communication between Miami, Florida, and San Diego, California, the beams should be pointed, not at the *F* region over Texas, but at the *F* region over Iowa.

Experiments should presumably be initiated in the 20 to 30 Mc/sec band and extended upward in frequency as far as possible. Experiments that may involve scattering in the F region have recently been described by Abel and Phillips [14]. In these experiments, however, none of the above conditions were well-satisfied. It seems desirable, therefore, that these experiments be repeated, bearing in mind the three conditions listed.

12. *Spread F and Other Reflection Phenomena*

It seems fairly clear that the cause of spread F must be scattering by the electronic irregularities in the F region of the type that we have been discussing. Consider the following oversimplified picture of the phenomenon. Suppose that an HF wave that is reflected from the F region has to cross and recross the stratum of atmosphere responsible for star scintillation. Suppose furthermore that, in the stratum containing the irregularities, mean refraction is negligible, while at the level of reflection irregularities are unimportant. In the scintillation stratum, the HF wave is subjected to predominantly forward-scattering by the largest electronic irregularities. The size of these irregularities as given by Figures 9 and 11 show that angles of scattering for a wave in the HF band will be small. Consequently, the reflected wave will not involve large deviations from the vertical. Now it is known that, even in the VHF band, star scintillation sometimes involves fluctuation indexes of the order of unity, indicating that multiple scattering must be involved. Since forward-scattering increases proportionally to the square of wavelength, this would be true *a fortiori* in the HF band. It is easy to see, therefore, that the scintillation stratum could frequently involve multiple scattering at a frequency below the penetration-frequency. This leads to a qualitative explanation of spread F that does not involve large departures from the vertical in the direction of arrival of the downcoming wave.

The above picture is obviously oversimplified; it is unlikely that the scattering stratum can be dissociated from the reflecting stratum in the way supposed. As soon as one attempts to integrate the two, however, one is up against a serious theoretical difficulty. There is no theory available at present that is capable of describing the effect of turbulence upon the phenomenon of total internal reflection in an ionized medium. It is for this reason that difficulty is being experienced in relating the theory of turbulence quantitatively to observations of irregularities using waves reflected from the ionosphere, whereas comparative success is being achieved for the various ionospheric scattering phenomena observed in the VHF band.

References

[1] R. W. McNicol, J. Inst. Elec. Eng., **96**, Pt. 3, 517 (1949).
[2] J. H. Meek, Terr. Mag., 54, **339** (1949).
[3] A. M. Peterson, O. G. Villard, Jr., R. L. Leadabrand, and P. B. Gallagher, J. Geophys. Res., **60**, 497 (1955).
[4] M. Ryle and A. Hewish, Mon. Not. R. Astr. Soc., **110**, 381 (1950).
[5] A. Hewish, Proc. R. Soc., A, **209**, 81 (1951); Proc. R. Soc., A, **214**, 494 (1952).
[6] M. Spencer, Proc. Phys. Soc., B, **68**, 493 (1955).
[7] J. P. Wild and J. A. Roberts, J. Atmos. Terr. Phys., **8**, 55 (1956).
[8] J. S. Greenhow, Proc. Phys. Soc., B, **65**, 169 (1952).

[9] W. Liller and F. J. W. Whipple, Rocket Exploration of the Upper Atmosphere, Pergamon Press, Ltd., London (1954); p. 112.
[10] F. F. Gardner and J. L. Pawsey, J. Atmos. Terr. Phys., **3**, 321 (1953).
[11] W. Dieminger, Physics of the Ionosphere, Physical Society of London (1954); p. 53.
[12] D. K. Bailey, R. Bateman, L. V. Berkner, H. G. Booker, G. F. Montgomery, E. M. Purcell, W. W. Salisbury, and J. B. Wiesner, Phys. Rev., **86**, 141 (1952).
[13] D. K. Bailey, R. Bateman, and R. C. Kirby, Proc. Inst. Radio Eng., **43**, 1181 (1955).
[14] W. G. Abel and M. L. Phillips, paper presented at URSI meeting, Washington, D. C., May 1956.
[15] H. G. Booker, C. W. Gartlein, and B. Nichols, J. Geophys. Res., **60**, 1 (1955).
[16] R. Dyce, J. Geophys. Res., **60**, 317 (1955).
[17] R. Bowles, J. Geophys. Res., **59**, 553 (1954).
[18] D. Brunt, Physical and Dynamical Meteorology, Cambridge, University Press (1941); chap. 12.
[19] G. K. Batchelor, The Theory of Homogeneous Turbulence, Cambridge, University Press (1953); chap. 6.
[20] A. N. Kolmogoroff, C. R. Acad. Sci. U.R.S.S., **30**, 301; **32**, 16 (1941).
[21] W. Heisenberg, Zs. Physik, **124**, 628 (1948).
[22] H. G. Booker and W. E. Gordon, Proc. Inst. Radio Eng., **38**, 401 (1950).
[23] E. C. S. Megaw, Nature, **166**, 1100 (1950).
[24] F. Villars and V. F. Weisskopf, Phys. Rev., **94**, 232 (1954).
[25] F. Villars and V. F. Weisskopf, Proc. Inst. Radio Eng., **43**, 1232 (1955).
[26] R. M. Gallet, Proc. Inst. Radio Eng., **43**, 1240 (1955).
[27] G. K. Batchelor, Cornell University, School of Electrical Engineering, Res. Rep. EE 262 (1955); to be published.
[28] R. A. Silverman, paper presented at URSI meeting, Washington, D. C., May 1956; to be published.
[29] H. G. Booker, J. Atmos. Terr. Phys. (in press).
[30] The Rocket Panel, Phys. Rev., **88**, 1027 (1952).
[31] K. Weekes, Q. J. R. Met. Soc., **80**, 2 (1954).
[32] S. Chapman and T. G. Cowling, The Mathematical Theory of Non-Uniform Gases, Cambridge, University Press (1939).
[33] J. S. Greenhow and E. L. Neufield, J. Atmos. Terr. Phys., **6**, 133 (1955).
[34] J. S. Greenhow, Phil. Mag., **45**, 471 (1954).
[35] J. S. Greenhow, Phil. Mag., **41**, 682 (1950).
[36] H. G. Booker and R. Cohen, paper presented at URSI meeting, Washington, D. C., May 1956; J. Geophys. Res, **61**, 707 (1956).
[37] T. R. Kaiser and R. L. Closs, Phil. Mag., **43**, 1 (1952).
[38] A. C. B. Lovell and J. A. Clegg, Proc. Phys. Soc., **60**, 491 (1948).
[39] Dobrovol'skii, Bull. Stalinabad Astr. Obs., No. 1, 15 (1952); Rand Corporation translation T-39.
[40] A. Maxwell, Phil. Mag., **45**, 1247 (1954).
[41] J. W. Dungey and A. J. Willson, J. Geophys. Rev., **60**, 521 (1955).
[42] S. Chapman, J. Atmos. Terr. Phys., **3**, 1 (1952).
[43] J. W. Dungey, J. Atmos. Terr. Phys., **8**, 39 (1956).

A THEORY OF LONG-DURATION METEOR-ECHOES BASED ON ATMOSPHERIC TURBULENCE WITH EXPERIMENTAL CONFIRMATION*

By H. G. Booker and Robert Cohen†

School of Electrical Engineering, Cornell University, Ithaca, New York

(Received July 26, 1956)

ABSTRACT

A theory of long-duration meteor-echoes is developed, based on the assumption that a meteor-trail is rendered rough by the action of the small eddies in the atmosphere. This theory leads to the conclusion that, if loss of electrons from the trail by recombination and/or attachment is neglected, the field-strength of a long-duration meteor-echo in its decay-phase should be inversely proportional to the cube of time subsequent to formation of the trail. It is shown that this law is verified experimentally in the early part of the decay but that at later times the decay becomes more rapid. This can be explained in terms of the loss of electrons from the trail, provided that the loss is due to attachment to atmospheric molecules and the attachment time has an average value of the order of seven seconds.

It is shown that the spectrum of incoherent scattering associated with turbulent mixing in a gradient of electron-density may be derived experimentally by measuring the frequency-dependence of long-duration meteor-echoes during their decay-phase. This measurement is carried out, and the results are related to the CRPL experiments concerning the frequency-dependence of long-distance VHF scatter-transmission (see Fig. 12).

It is deduced that the contribution of meteoric ionization to the background-signal of scatter-transmission arises mainly from the incoherent scattering associated with mixing of this ionization by atmospheric turbulence. According to our analysis, McKinley's data concerning the contribution of meteor-trails to scatter-transmission lead to the same conclusion.

1. *Introduction*

Trails left by meteors during their passage through the upper atmosphere provide one of the most effective means available for studying atmospheric turbulence in the lower ionosphere. During their passage through the atmosphere, meteors shed particles that result in a trail that is both luminous and ionized. While there is some disturbance in the motion and temperature of the atmosphere

*This research was supported by the U. S. Signal Corps under Contract No. DA36-039-sc-56748 and by the National Science Foundation.

†The second author is now with the Central Radio Propagation Laboratory, Boulder, Colorado.

in the immediate wake of the meteor, this quickly disappears, leaving the trail to disperse under substantially normal atmospheric conditions. Studies of atmospheric turbulence in the lower ionosphere based on observations of meteor-trails have been made by Liller and Whipple [see 1 of "References" at end of paper] using photographic methods, and by Greenhow [2] and others [3, 4] using radio methods. There is little doubt that the observations of Liller and Whipple refer to the distortion produced in the trail by large eddies present in the atmosphere. The question of the size of the eddies involved in the radio observations is, however, in dispute. It seems to have been implicitly assumed by most authors that it is the largest eddies that are involved in the irregularly fluctuating signal associated with long-duration meteor-echoes. So far as the fading rate is concerned, this is almost certainly true. However, Booker [5] has shown that the intensity of long-duration meteor-echoes is in most cases likely to be controlled by the effect on the trail of the smallest eddies in the atmosphere. Before the gross distortion of the trail by the largest eddies makes possible multiple perpendiculars onto the trail from a radar, the smallest eddies have usually rendered the trail "rough" for VHF radars. After the small eddies have made the trail rough, there is no longer any special interest attaching to perpendiculars onto the trail because an incoherent scattering theory must then be applied. It is the object of this paper to develop a rough-trail theory of long-duration meteor-echoes, and to test the theory experimentally.

In a companion paper by Booker [5], certain aspects of the theory of turbulence were applied to the ionosphere, and in particular to the levels at which meteor-trails are formed. For a height of 90 km, the following orders of magnitude were deduced for some of the important parameters involved. For the turbulence-power per unit mass of atmosphere (which is the rate at which turbulence-energy is supplied per unit mass to the large eddies and removed by viscosity from the small eddies):

$$w = 25 \text{ watts/kg} \quad (1)$$

For the time-constant of the large eddies:

$$t_1 = 50 \text{ seconds} \quad (2)$$

For the turbulence-velocity of the large eddies:

$$v_1 = 35 \text{ meters/second} \quad (3)$$

For the scale of the large eddies:

$$L_1 = 1.6 \text{ km} \quad (4)$$

For the time-constant of the small eddies:

$$t_2 = 0.4 \text{ second} \quad (5)$$

For the turbulence-velocity of the small eddies:

$$v_2 = 3 \text{ meters/second} \quad (6)$$

For the scale of the small eddies:

$$L_2 = 1.3 \text{ meters} \quad (7)$$

These results led to the conclusion that, for wavelengths less than

$$4\pi L_2 = 16 \text{ meters} \quad \ldots\ldots (8)$$

and for time in excess of (5) subsequent to the fall of the meteor, the trail must be considered rough, and the echoes from it calculated on an incoherent scattering theory. This was regarded as questioning the theory of Kaiser and Closs [6] as a theory of long-duration meteor-echoes, and requiring the development of an incoherent scattering theory to replace it. It is the object of this paper to develop such a theory on the assumption that multiple scattering may be neglected, and to compare the results with appropriate observations of long-duration meteor-echoes.

For the coefficient of molecular diffusion at 90 km, we have

$$D = 4 \text{ meter}^2/\text{second} \quad \ldots\ldots (9)$$

approximately. It has been shown by Booker [5] that this is the appropriate coefficient of diffusion for a meteor-trail only up to the time (5). After time (2), on the other hand, the rate of dispersal of the trail is controlled by the standard coefficient of eddy-diffusion:

$$v_1 L_1 = 6 \times 10^4 \text{ meter}^2/\text{second} \quad \ldots\ldots (10)$$

from (3) and (4). For $t_2 < t < t_1$, the rate of dispersal of a meteor-trail is controlled by the coefficient of eddy-diffusion for the largest eddies that have so far caused major distortion of the trail. Booker [5] has shown that in this interval the appropriate coefficient of diffusion is wt^2, where w is the turbulence-power per unit mass. The coefficient of meteoric diffusion is, therefore,

$$\left.\begin{array}{ll} D, & 0 < t < t_2 \\ wt^2, & t_2 < t < t_1 \\ v_1 L_1, & t > t_1 \end{array}\right\} \quad \ldots\ldots (11)$$

approximately. The variation of the coefficient of meteoric diffusion with time t subsequent to formation of the trail is plotted in Figure 5 of Booker [5], using the numerical values quoted above.

The extreme importance of eddy-diffusion in the rate of dispersal of a meteor-trail is obvious from Figure 5 of Booker [5]. Indeed, it might well be wondered how echoes can persist for any appreciable time after eddy-diffusion begins to control dispersal of the trail. The reason is as follows. It is quite true that the process of eddy-diffusion results in individual irregularities of electron-density rapidly decreasing in intensity. But the very process of eddy-diffusion creates additional irregularities of electron-density at a rapid rate. Moreover, the portion of the trail that contributes to the echo is no longer restricted by Fresnel zone considerations after incoherent scattering has been established. Thus, after the time (5), we have a situation in which the number of relevant irregularities of electron-density is rapidly increasing, while the importance of an individual irregularity is rapidly decreasing. We shall show that the combination of these two effects for a meteor-trail leads to an incoherent echo for which the over-all

intensity decreases only slowly with time at times sufficiently large compared with (5). It is believed that this is the true explanation of long-duration meteor-echoes.

Since the coefficient of meteoric diffusion varies with time, some consideration has to be given to solution of the equation of diffusion under these circumstances. This is done in section 2. The basis for relating turbulence to the mean gradient of electron-density is described in section 3, and in section 4 the theory of back-scattering from a rough meteor-trail is developed on the assumption that multiple scattering is unimportant. This leads to a simple formula for the decay of a long-duration meteor-echo, and this formula is tested against our own experimental observations in section 5 and those of McKinley in section 6. Previous estimates of the line-density of intense meteor-trails are vitiated by neglect of the effect of atmospheric turbulence in the theory of Kaiser and Closs [6]. While the theory presented in section 4 is not adequate to determine with precision the line-densities of intense meteor-trails, nevertheless, the orders of magnitude are not in doubt and are discussed in section 7. Having obtained satisfactory agreement between the observations and the rough-trail theory, attention is turned in section 8 to the frequency-dependence of long-duration meteor-echoes in the decay-phase. This function is the spectrum-function required to describe all aspects of radio scattering in the lower E region by irregularities in electron-density arising from the existence of atmospheric turbulence in a mean gradient of electron-density. Observational results derived in this way from meteor-echoes are combined with those of Bailey, Bateman, and Kirby [15] for long-distance VHF scatter-transmission to give an experimental spectrum for radio scattering extending over nearly a decade of frequency. The spectrum-function turns out to be roughly of the type required to fit in with the Kolmogoroff-Heisenberg theory [7, 8] of turbulence with a scale of small eddies having roughly the value (7). The bearing of these results on the explanation of long-distance scatter-transmission is discussed in section 9.

2. *The Effect of Eddy-Diffusion on the Dispersal of Meteor-Trails*

To describe the dispersal of a meteor-trail, we are required to solve the equation of diffusion under conditions when the coefficient of diffusion varies with time in accordance with (11). We assume that the trail is initially straight, and that there are Q electrons per unit length. For the time being, we neglect the effects of recombination and attachment, but we shall return to this point in section 4.

For $0 < t < t_2$, we have a constant coefficient of diffusion D. In these circumstances, a standard solution of the equation of diffusion gives, for the dependence of electron-density N on radial distance r at a time t,

$$N = \frac{Q}{\pi r_t^2} \exp\left(-\frac{r^2}{r_t^2}\right) \quad \ldots\ldots\ldots\ldots\ldots\ldots\ldots\ldots\ldots\ldots (12)$$

where

$$r_t^2 = 4Dt \quad \ldots\ldots\ldots\ldots\ldots\ldots\ldots\ldots\ldots\ldots\ldots\ldots (13)$$

This formulation assumes that the radius of the trail at $t = 0$ is zero. If we require to consider a finite initial radius r_0 of the trail and can assume that the initial distribution of N with r is Gaussian, then (13) is replace by

$$r_t^2 = 4Dt + r_0^2 \quad \ldots\ldots (14)$$

For $t_2 < t < t_1$, the appropriate coefficient of diffusion varies with time in accordance with (11), and the equation of diffusion is

$$\nabla^2 N = \frac{1}{wt^2} \frac{dN}{dt} \quad \ldots\ldots (15)$$

This may be rewritten as

$$\nabla^2 N = \frac{1}{w/3} \frac{dN}{d(t^3)} \quad \ldots\ldots (16)$$

This equation is of the same form as that for a constant coefficient of diffusion $w/3$, with time t replaced by t^3. The appropriate solution, from (14), is (12) with

$$r_t^2 = 4(w/3)(t^3 - t_2^3) + r_2^2 \quad \ldots\ldots (17)$$

where r_2 is the value of r_t at $t = t_2$.

For $t > t_1$, we return to an equation of diffusion with a constant coefficient of diffusion $v_1 L_1$. The distribution of N with r and t is therefore (12), with

$$r_t^2 = 4(v_1 L_1)(t - t_1) + r_1^2 \quad \ldots\ldots (18)$$

where r_1 is the value of r_t at $t = t_1$.

We see, therefore, that the distribution of electron-density N with radial distance r is always described by (12), and that the variation of r_t with time is given by

$$r_t^2 = \begin{cases} 4Dt & 0 < t < t_2 \quad \ldots\ldots (19) \\ \frac{4}{3}w(t^3 - t_2^3) + r_2^2 , & t_2 < t < t_1 \quad \ldots\ldots (20) \\ 4(v_1 L_1)(t - t_1) + r_1^2 , & t > t_1 \quad \ldots\ldots (21) \end{cases}$$

provided that we take the initial radius of the trail to be zero. The variation of the "radius" r_t of the trail with the time t since its formation is plotted in Figure 1, using the numerical values quoted in section 1. If eddy-diffusion had been neglected, the rectilinear behavior in Figure 1 for $t < t_2$ would have continued indefinitely. It is clear that neglect of eddy-diffusion for $t > t_2$ would lead to conclusions bearing little resemblance to reality.

The maximum electron-density over the cross-section of the trail occurs where r vanishes. It follows from (12) that the maximum electron-density N_m is given by

$$\frac{N_m}{Q} = \frac{1}{\pi r_t^2} \quad \ldots\ldots (22)$$

The ratio of the maximum electron-density over the cross-section to the line-density of the trail is, therefore, equal to the reciprocal of the cross-sectional

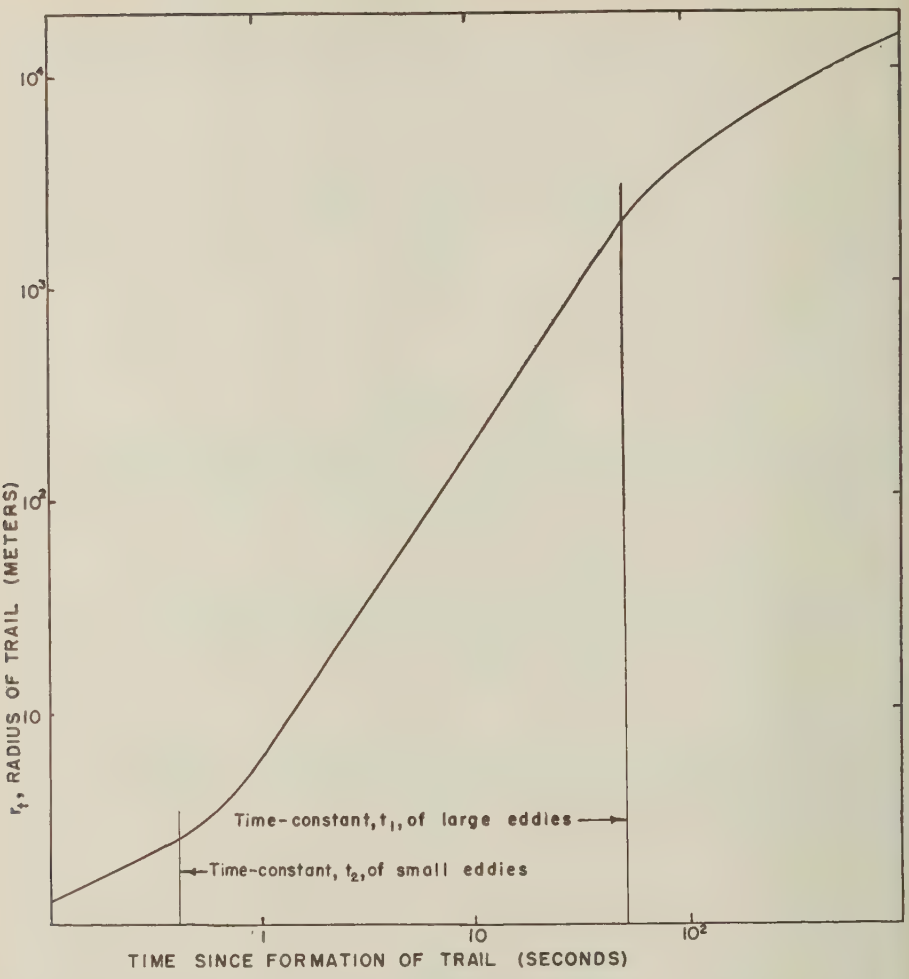

FIG. 1—The radius of a meteoric trail as a function of time subsequent to formation of the trail

"area" πr_t^2 of the trail. This is plotted in Figure 2, using the numerical values quoted in section 1. From this diagram may be calculated the time taken for a trail of given initial line-density to become underdense at a given radio frequency. For example, if at 30 Mc/sec a trail becomes underdense 10 seconds after formation, the ratio of the critical electron-density for 30 Mc/sec to the line-density of the trail must be 10^{-5}. Now the critical electron-density at 30 Mc/sec is 1.1×10^{13} electrons/meter^3. Hence the line-density of the trail must be 10^{18} electrons/meter. An enormous initial line-density is thus required to keep a trail overdense at 30 Mc/sec for as long as 10 seconds. Thus, the effect of eddy-diffusion is to make even strong trails underdense in the VHF band within a few seconds after formation.

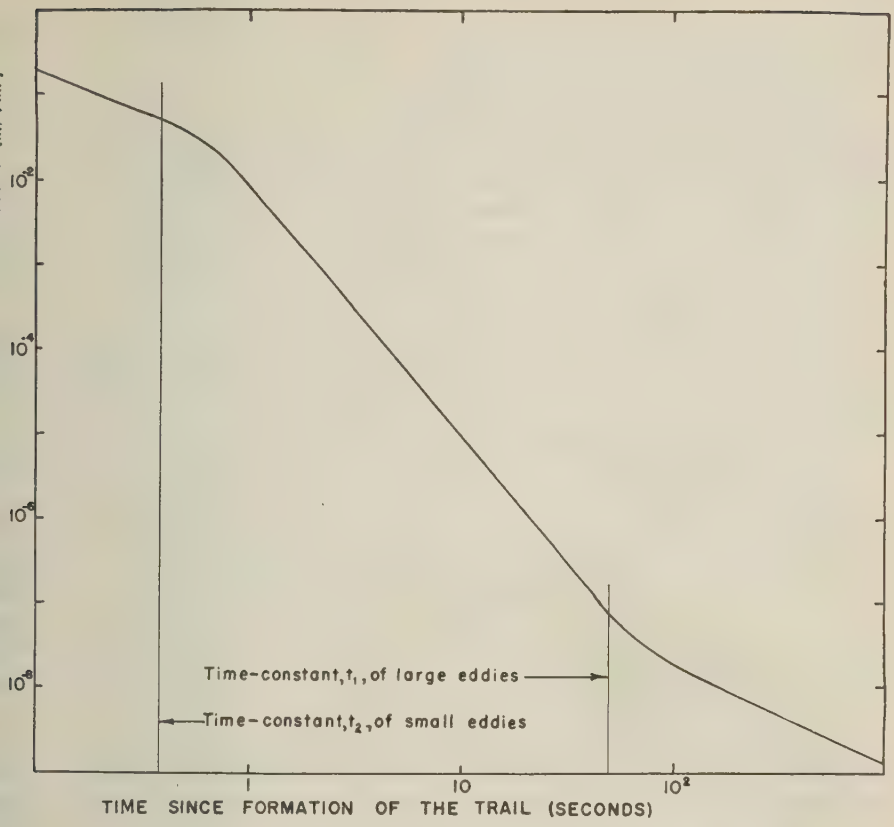

FIG. 2—The ratio of the central electron-density of a trail to the initial line-density as a function of time subsequent to formation of the trail

3. *The Relation between Turbulence and Incoherent Scattering of Radio Waves by Meteor-Trails*

Turbulence can cause irregularities of electron-density in an ionized medium in three ways:

(*i*) Through the pressure-fluctuations associated with turbulence. This mechanism would work even if there were no mean gradients of electron-density or temperature [9].

(*ii*) *Through the randomization of a mean gradient in electron-density [10].

(*iii*) *Through the randomization of a mean gradient in temperature [11].

There is little doubt that, for meteor-trails, mechanism (*ii*) is the predominant one.

Incoherent scattering of radio waves in a medium containing irregularities is described by means of a scattering cross-section σ per unit volume. The quantity σ is a function of

(*a*) The frequency f

(*b*) The angle θ through which scattering takes place

(*c*) The angle χ between the direction of scattering and the direction of the electric field of the incident wave
(*d*) The scale (4) of the large eddies
(*e*) The scale (7) of the small eddies, and
(*f*) The mean-square deviation of electron-density from mean.

When multiple scattering is neglected, the two parameters involved in (*a*) and (*b*) only occur in the combination

$$f \sin \frac{\theta}{2} \qquad (23)$$

and the variation with χ is one of proportionality to $\sin^2 \chi$. Moreover, if the irregularities of electron-density are produced by mechanism (*ii*) above, the mean-square deviation of electron-density from mean is proportional to the square of the mean gradient* of electron-density:

$$| \text{ grad } N |^2 \qquad (24)$$

We, therefore, assume that

$$\sigma = | \text{ grad } N |^2 \, S\left(f \sin \frac{\theta}{2}\right) \sin^2 \chi \qquad (25)$$

where S is a spectrum-function which also contains as parameters the scales L_1 and L_2 of the large and small eddies. It must be remembered, however, that (25) does not include the effect of multiple scattering.

In applying formula (25) to calculation of incoherent scattering by a rough meteor-trail, it will not be necessary for us to assume a special form for the spectrum-function S. We shall, in fact, develop a method whereby radio measurements of long-duration meteor-echoes may be used to determine this spectrum experimentally over an interesting range of the variable.

Application of the function (25) to a meteor-trail implies that turbulence has caused the development of a volume containing electron-irregularities and that something approaching a statistically steady state has been reached. For the irregularities associated with the small eddies, a statistically steady state is approached after time t_2 given by (5). As we consider irregularities in electron-density of progressively larger sizes, longer times must elapse before a statistically steady state is approached. For the irregularities associated with the largest eddies, a statistically steady state will only be approached after time t_1 given by (2). Now for back-scattering at wavelengths less than (8), we are primarily concerned with the electronic irregularities associated with the small eddies, so far as echo strength is concerned. Hence, we may apply a steady-state theory of incoherent back-scattering soon after the time (5), and this is adequate for a theory of the strength of long-duration meteor-echoes.

For a meteor-trail, the relevant gradient of N in (25) is the radial value dN/dr. The incoherent echoing area per unit volume of a meteor-trail at times sufficiently

*For application to ionospheric layers, these statements must be interpreted in the "potential" sense understood in meteorology, but this point is unimportant for meteor-trails.

arge compared with t_2 is, therefore,

$$\sigma_B = (\mathrm{d}N/\mathrm{d}r)^2 S(f) \quad \ldots\ldots (26)$$

provided that multiple scattering may be neglected.

Neglect of multiple scattering in calculating the echo from a meteor-trail is by no means a trivial assumption. The assumption implies that a wave incident upon the trail is, to a first approximation, undisturbed by the presence of the trail, but this is only true after the trail has become underdense. Applicability of (26) requires not only that the time subsequent to formation of the trail be greater than t_2 , but also that the trail has become underdense. A theory of back-scattering from a rough meteor-trail derived from (26) will, in short, described the echo during its decay-phase.

Kaiser and Closs [6] have contemplated the possibility that a meteor-trail giving a long-duration echo might remain overdense for most of the lifetime of the echo. These authors neglected, however, the tremendous effect of eddy-diffusion after time t_2 (see Fig. 2). In our experiments, long-duration meteor-echoes entered upon their decay-phase after only a few seconds, and during much of their lifetime they were in a phase of slow decay. The problem of explaining the existence of long-duration meteor-echoes is thus to an important extent one of accounting for the slowness of the decay. Our assumption will be that, in the decay-phase, formula (26) is applicable at wavelengths less than (8).

4. *Calculation of Incoherent Echoing from a Rough Meteor-Trail Neglecting Multiple Scattering*

The back-scattering coefficient (26) per unit volume has to be integrated through the volume of the trail. Let us first carry out this integration over a normal cross-section of the trail, thereby obtaining the echoing area for incoherent back-scattering measured per unit length of the trail. This is

$$\Sigma_B = \int_0^\infty \sigma_B \, 2\pi r \, \mathrm{d}r \quad \ldots\ldots (27)$$

$$= S(f) \int_0^\infty (\mathrm{d}N/\mathrm{d}r)^2 \, 2\pi r \, \mathrm{d}r \quad \text{from (26)}$$

$$= S(f) \frac{8Q^2}{r_i^8} \int_0^\infty r^3 \exp\left(-\frac{2r^2}{r_i^2}\right) \mathrm{d}r \quad \text{from (12)}$$

$$= S(f) \frac{Q^2}{r_i^4} \quad \ldots\ldots (28)$$

on carrying out the integration.

To obtain the complete echoing area of the rough trail, (28) has to be integrated along the length of the trail, possibly taking into account the finite pulse-length of a radar. In general, this should be done allowing not only for the variation of Q along the trail but also for the variation with height of the parameters involved in r_i and $S(f)$, particularly w and L_2 . We shall assume, however, that these quantities may be evaluated at a mean height which we shall take as 90 km. It is then merely necessary to multiply (28) by the length of the trail, or by that part of

the length which falls within the pulse of a radar. Having calculated the echoing area of the rough trail in this way, we use it in the radar equation in the usual way.

In (28), $S(f)$ is independent of time. If we neglect recombination and attachment for the moment, Q is also independent of time. Hence (28) shows that, during the decay-phase of a long-duration meteor-echo, the power received is inversely proportional to the fourth power of the radius of the trail, plotted in Figure 1. The received field-strength, therefore, is inversely proportional to the square of the radius of the trail, or, in other words, proportional to (22). Figure 2 may therefore be reinterpreted as giving, for t sufficiently greater than t_2, the received field-strength on an arbitrary scale as a function of time subsequent to formation of the trail. We may use (20) and (21) to express analytically the time-variation of the field-strength of a long-duration meteor-echo during its decay-phase. The field-strength is proportional to $1/r_t^2$ from (28), and from (20) and (21) this factor is given by

$$\frac{1}{r_t^2} = \begin{cases} \dfrac{1}{\frac{4}{3}w(t^3 - t_2^3) + r_2^2}, & t_2 < t < t_1 \quad \ldots\ldots(29) \\ \dfrac{1}{4(v_1 L_1)(t - t_1) + r_1^2}, & t > t_1 \quad \ldots\ldots(30) \end{cases}$$

A meteor-echo is not a long-duration echo unless it lasts longer than the time-constant t_2 of the smallest eddies. On the other hand, comparatively few meteor-echoes last longer than the time-constant t_1 of the largest eddies. Hence the formula that is normally required to described the variation of field-strength with time during the decay-phase of a long-duration meteor-echo is (29). Since this formula is required for values of t large compared with t_2, it may be written approximately

$$\frac{1}{r_t^2} = \frac{1}{\frac{4}{3}wt^3}, \qquad t_2 \ll t < t_1 \quad \ldots\ldots(31)$$

It follows from (28) and (31) that the time-variation in the field-strength of a long-duration meteor-echo is

$$E(t) \propto \frac{Q}{t^3}, \qquad t_2 \ll t < t_1 \quad \ldots\ldots(32)$$

If the total number Q of the electrons in the trail per unit length does not decrease, the field-strength of a long-duration meteor-echo in its decay-phase should be inversely proportional to the cube of time subsequent to formation of the trail. It should be easy to ascertain experimentally whether or not this is true.

For sufficiently long-duration meteor-echoes, it is likely that electrons are removed from the trail either by recombination or by attachment and that as a result Q in (28) and (32) decreases with time. If Q_0 is the initial line-desnity of the trail, and Q is the line-density at time t, then for recombination with a recombination-coefficient α we have

$$Q = \frac{Q_0}{1 + \dfrac{t}{t_R}}, \quad \ldots\ldots(33)$$

where t_R is the recombination-time given by

$$t_R = Q_0\alpha \quad \ldots\ldots\ldots\ldots\ldots\ldots\ldots\ldots\ldots\ldots (34)$$

The same formula would apply to electron-attachment in the case of attachment to the atoms or molecules produced by break-up of the meteor. In the case, however, of attachment to atmospheric molecules, we have

$$Q = Q_0 \exp\left(-\frac{t}{t_A}\right) \quad \ldots\ldots\ldots\ldots\ldots\ldots\ldots\ldots\ldots\ldots (35)$$

where t_A is the attachment-time. Either (33) or (35) must be substituted into (28) and (32) in order to allow for loss of electrons from the trail.

It should be noted that the time t_R given by (34) depends on the initial line-density in the trail and consequently varies considerably from meteor to meteor. The time t_A involved in (35), on the other hand, is independent of the line-density in the trail, although it does depend somewhat on altitude.

In performing experiments to check equation (32), it might be expected that the effect of electron-loss would become noticeable for echoes of sufficiently long-duration. It might then be possible to distinguish between the mechanisms described by (33) and (35), and also to measure either t_R or t_A .

Let us now suppose that experiments with long-duration meteor-echoes have been performed to check the time-dependence given in equation (28), and that the check is satisfactory. Then it further follows from (28) that the frequency-dependence of long-duration meteor-echoes during their decay-phase is a direct measure of the spectrum-function S involved in (25). To evaluate the spectrum-function applicable whenever irregularities of electron-density are caused by the action of turbulence in a mean gradient of ionization at the meteoric level, therefore, we merely have to measure the frequency-dependence of long-duration meteor-echoes during their decay-phase.

5. *Experimental Investigation of the Decay of Long-Duration Meteor-Echoes*

With a view to checking the time-dependence involved in equation (32), a program of continuous-wave observations of meteor-trails was begun. The transmitter consisted of a Wilcox 99A arranged so as to be capable of radiating continuously on frequencies of 17.31, 30.38, and 49.78 Mc/sec. The detector-outputs of the receivers were connected to a dual-channel Sanborn recorder having a time-constant of about 0.01 second. The deflection of the stylus of the recorder varied in a substantially linear manner with the voltage appearing at the terminals of the receiving antennas.

The receiving site was at the Ionosphere Laboratory, Ithaca, New York, and the transmitting site was at Blodgett Mills, New York. The distance between the two sites is 31 km, and the intervening terrain profile is as shown in Figure 3. Half-wave antennas were used for each frequency, both for transmission and reception. The dipoles at each site were erected on a common mast at 0.35λ above the ground, and were oriented along the great-circle path joining the sites. The arrangement resulted in complete suppression of the direct signal between transmitter and receiver on all three frequencies.

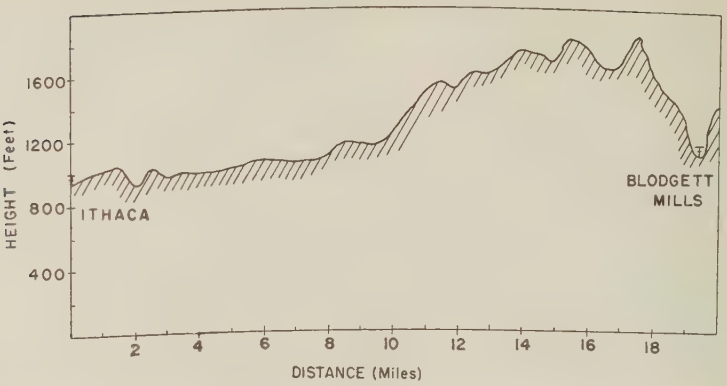

Fig. 3 —Profile of terrain between transmitting and receiving sites allowing for standard atmospheric refraction

Separation of the transmitting and receiving sites by 31 km causes departure from the condition of exact back-scattering to an extent that depends on the location of the meteor-trail. At worst, this involved a correction of 1.2 per cent in the parameter (23). It has, therefore, been assumed that the observations may be compared with theoretical formulas appropriate strictly to back-scattering.

Observations were made almost exclusively between 0000 and 0700 hours local time. Data were gathered both during known meteor-showers and when the meteors were presumably of sporadic origin only. More than 50 long-duration

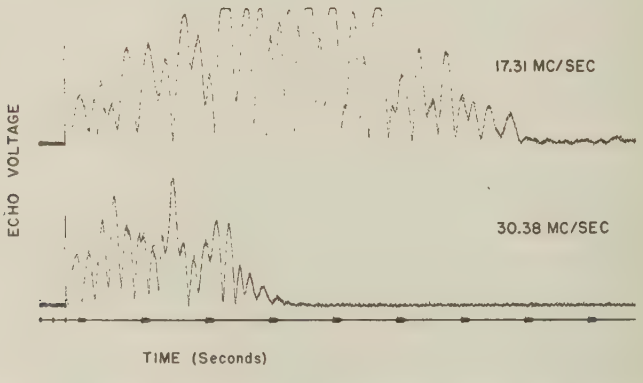

Fig. 4—Example of records of long-duration meteor-echoes observed simultaneously on 17.31 and 30.38 Mc/sec

meteor-echoes were recorded on pairs among the available frequencies. An example of a pair of observations on 17.31 and 30.38 Mc/sec is shown in Figure 4; there is a little mechanical limiting of the lower frequency echo at its extreme peaks in this case. Another example, employing 30.38 and 49.78 Mc/sec, is shown in Figure 6.

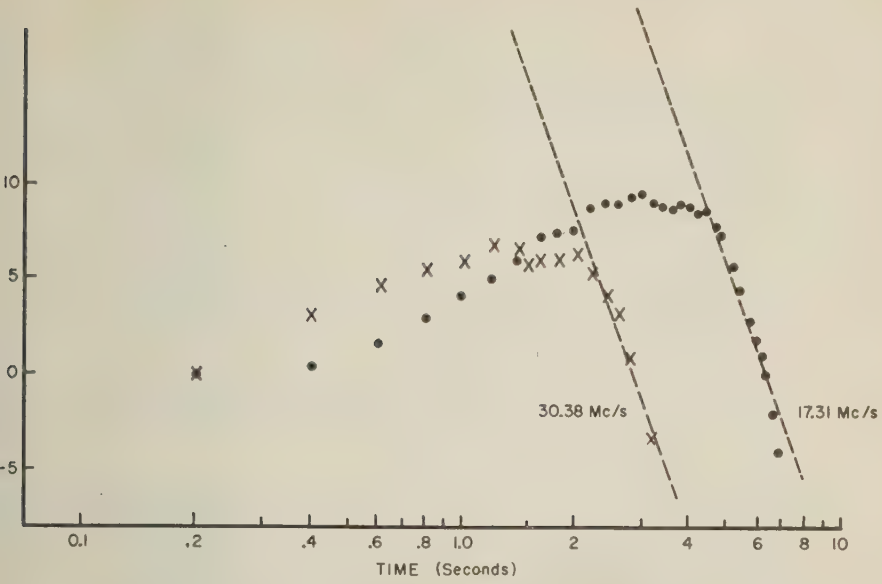

FIG. 5—Analysis of records shown in Figure 4

Meteor-echoes of the following varieties were observed:

(*i*) Echoes which rise fairly suddenly and which decay more or less exponentially to noise-level within a few tenths of a second.

(*ii*) Echoes which rise fairly suddenly, which develop irregular fading after a few tenths of a second, and which last from one to ten seconds and occasionally longer. The echoes shown in Figures 4 and 6 are examples of this type.

(*iii*) Echoes which do not have a sudden start and which always develop irregular fading. These echoes gradually rise out of the noise, attain a maximum response after a second or two, and then decay like echoes of type (*ii*).

here are also a few echoes that do not fit into the above categories and that we o not understand.

Analysis of the data is based on the following interpretation of the three categories of echoes described above:

(*i*) The first type of echo arises from specular reflection from a trail which quickly becomes underdense and to which the theories of Lovell and Clegg [12] and of Herlofson [13] may be applied.

(*ii*) Echoes other than those of the first type involve trails which remain overdense for an appreciable fraction of a second and even for several seconds. Echoes of this second type involve, for the first few tenths of a second, a phenomenon of specular reflection described by the theory of

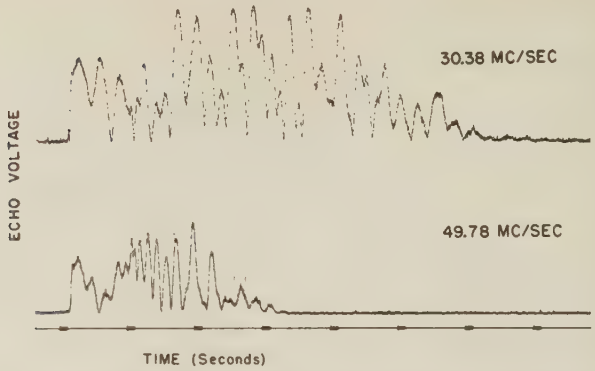

Fig. 6—Example of records of long-duration meteor-echoes observed simultaneously on 30.38 and 49.78 Mc/sec

Kaiser and Closs [6]. After a few tenths of a second, however, atmospheric turbulence mixes the trail and use must be made of an incoherent scattering theory such as that developed in section 4. When echoes of this type begin to decay, they should do so in accordance with formula (32).

(*iii*) Echoes of the third type are supposed to be identical with those of the second type, except that the "echo point" on the initial trail lies outside the section of trail that is strongly ionized. Consequently, there is no observable specular reflection, but incoherent scattering develops as the trail is mixed by atmospheric turbulence.

Echoes of the first variety are of no especial interest here, except insofar as they can help to check the relative calibration of the equipment on the three frequencies. Echoes of the third type are inconvenient for our analysis, because the time of formation of the trail, and therefore the zero time in (32), is not recorded. Our analysis, therefore, has been confined to echoes of the second type.

To compare echoes of the kind shown in Figures 4 and 6 with a relationship of the form (32), it is necessary to remove the irregular fading by a smoothing process so as to arrive at the mean amplitude. To do this, each record was divided into intervals of length τ, overlapping $\frac{1}{2}\tau$, and planimeter integration was used to find the area under the curve for each interval. The interval τ was taken to be 0.4 or 0.8 second, depending upon the fading rates involved and the length of the event being studied. A moving average was then formed from the sequence of areal values generated in this way, as follows:

(*a*) For the third interval and all successive intervals, a running mean extending over five successive values was used.

(*b*) For the second interval, a running mean over three successive values was used.

(*c*) For the first interval, no further averaging was done.

The smoothed amplitudes derived in this way from the echoes shown in Figure

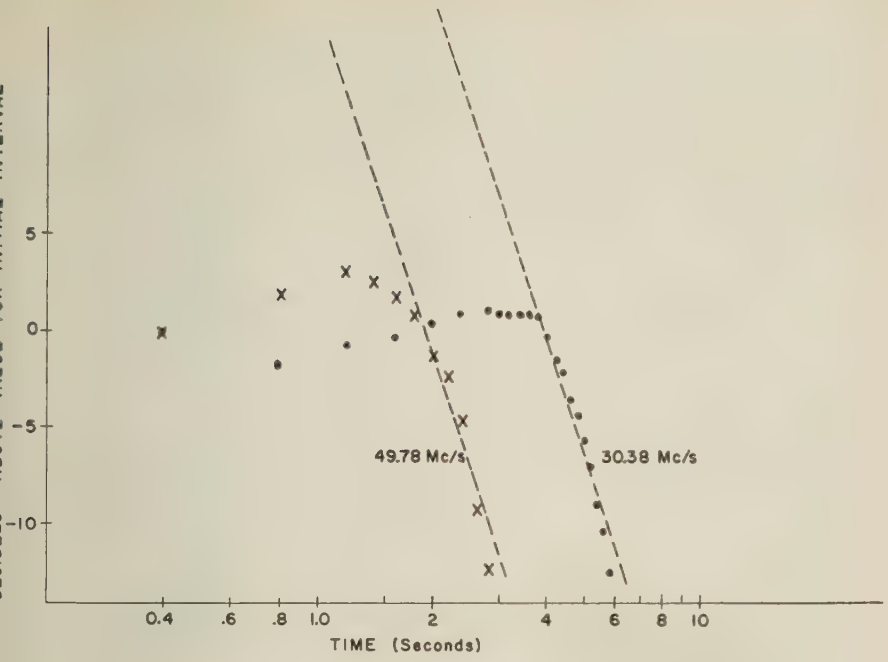

FIG. 7—Analysis of records shown in Figure 6

and 6 are plotted in Figures 5 and 7, respectively, at positions measured by the enter times of the integration-intervals.

In Figures 5 and 7, smoothed echo-voltage is shown relative to that for the irst interval, so that all curves start from zero on the decibel scale. Both signal mplitude and time are plotted on logarithmic scales, so that the t^{-3} relation nvolved in formula (32) corresponds to the slope indicated in Figures 5 and 7 by he dashed lines. If recombination, represented by (33), and attachment, repre-ented by (35), are neglected, the decay of the echoes in Figures 5 and 7 should e parallel to the dashed lines.

Of 80 curves analyzed in the manner described, about half show the degree of greement with the t^{-3} law illustrated in Figures 5 and 7. This agreement is reason-bly good, but there is an indication of some systematic departure from the simple $^{-3}$ behavior. Roughly another quarter of the curves analyzed show no significant eparture from the t^{-3} law. The remainder indicate a t^{-3} behavior, but involve epartures in the form of kinks or knees that might be associated with the super-osition of small meteor-echoes upon the event being studied.

The conclusion is drawn that, when a long-duration meteor-echo begins to ecay, it does so in accordance with the t^{-3} law, but that as time increases there is ndication that the echo falls somewhat below the value corresponding to this mple law. To demonstrate such a departure from the t^{-3} law, instrumentation ould be required with a larger dynamic range than was applied here.

6. *Comparison with McKinley's Observations of Long-Duration Meteor-Echoes*

While many investigators in the radio meteoric field have presumably had access to observations of the kind presented in the previous section, it does not seem possible to find in the literature an amplitude-time analysis of these observations such as we have carried out. It has been pointed out by Eshleman [14], however, that some data presented by McKinley [4] are relevant to the decay rate of long-duration meteor-echoes, and in particular to the question of a possible departure from the t^{-3} law indicated in Figures 5 and 7.

McKinley did not obtain, in the experiments referred to, the details of the decay of any long-duration meteor-echo. He did, however, measure the total duration of meteor-echoes simultaneously on two radar equipments whose frequencies were nearly identical and which had been measured to have a difference in sensitivity of 33 decibels. McKinley did not present results for individual meteor-echoes, but averaged the results for a number of events to obtain the experimental points reproduced in Figure 8. In this diagram is plotted the logarithm to the base ten of the ratio of the echo duration, T_h , on the high-power equipment, to the echo duration, T_l , on the low-power equipment, as a function of log T_l . Curve 2 of Figure 8 is not, however, the empirical one given in McKinley's paper, but is based on the theory presented in this paper.

It can readily be shown that, if the decay of an echo follows any power law, whether t^{-3} or not, the theoretical curve to be drawn in Figure 8 for comparison with the experimental points is a horizontal straight line. There is a clear discrepancy, therefore, between the experimental results shown in Figure 8 and any decay formula involving only a power law. For the t^{-3} law and for radars whose sensitivities differ by 33 decibels, the horizontal line to be drawn in Figure 8 intersects the vertical scale at 0.54. It will be observed that, if we disregarded temporarily the points in Figure 8 corresponding to (*a*) short-duration meteor-echoes (shorter than 0.4 second) and (*b*) the extremely long-duration meteor-echoes (longer than 5 seconds on the low-power equipment), then the average value of the ordinates for the remaining points is about 0.5. But for durations longer than 5 seconds on the low-power equipment, the ordinates are well below 0.5. If this statement is converted into a form suitable for comparison with results such as those presented in Figures 5 and 7, we obtain the following: For echoes whose durations are of the order of a few seconds, the decay in echo amplitude is given roughly by t^{-n}, where n is around 3; but for longer durations, the decay is faster. In other words, McKinley's observations prove the reality of the tendency indicated in Figures 5 and 7 for the echo intensity to fall below the t^{-3} law as t increases.

That there should be a departure from the t^{-3} law with increasing values of t follows from the theory presented in section 4, if account is taken of the loss of electrons to the trail because of recombination and/or attachment. Moreover, McKinley's observations are adequate to decide which of these mechanisms is more important and to estimate the time-constant involved.

Let us consider first the recombination formula (33). This would apply if electrons disappeared as a result of their capture or recapture by atoms or molecules of meteoric origin. When $t \ll t_R$ in (33), the effect of recombination is negligible. When $t \gg t_R$, the recombination formula merely changes the t^{-3} law to a t^{-4} law.

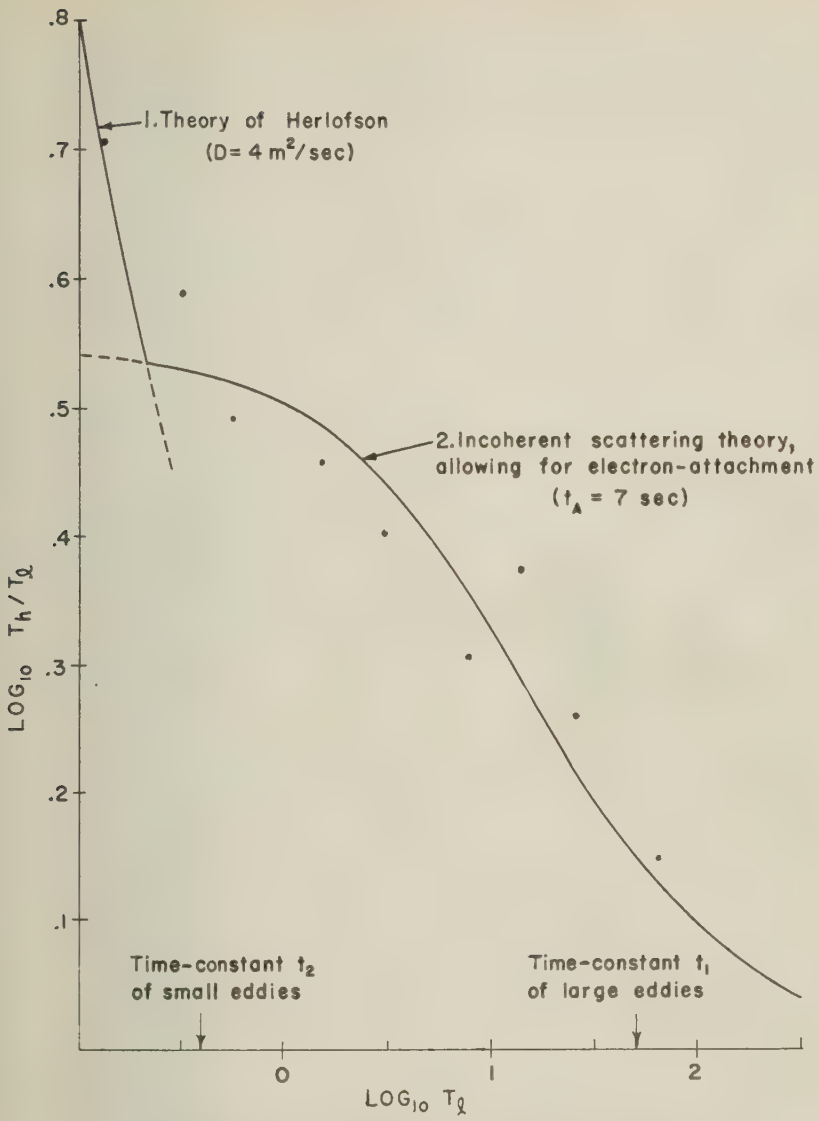

FIG. 8—A theoretical interpretation of experimental data of McKinley [12]

fter time t_1 , this would become a t^{-2} law in accordance with (30). Thus, the heoretical curve to be drawn in Figure 8 would consist of several horizontal ctions and could not be a good fit to the observational points. Moreover, allow- nce has to be made for the fact that the recombination time t_R given by (34) ould vary considerably from trail to trail. Thus, with the recombination formula 33), one would expect the experimental points in Figure 8 to occupy a roughly orizontal band with a mean of about 0.5. This is clearly not the case, and we

conclude that the observed departure from the t^{-3} law cannot be explained in terms of capture or recapture of electrons by meteoric atoms or molecules.

Let us now consider disappearance of electrons from the trail by attachment to atmospheric molecules. On this basis, the decay in the echo amplitude should, in accordance with (32) and (35), be given by

$$E(t) \propto t^{-3} \exp\left(-\frac{t}{t_A}\right) \quad \ldots\ldots(36)$$

where t_A is the time of attachment. In general, (36) should be replaced by the product of (29/30) and (35). The decay law (36) leads to a theoretical curve in Figure 8 which fits the data quite well if a suitable choice is made for the time of attachment. Curve 2 of Figure 8 is one for which

$$t_A = 7 \text{ seconds} \quad \ldots\ldots(37)$$

Curve 1 represents the short-duration echoes based on the theory of Herlofson [13]. The appropriate curve to be compared with McKinley's points is, therefore, the composite continuous curve, suitably rounded at the junction. It is clear that the agreement between this theoretical curve and the observations is good.

We conclude that the decay of long-duration meteor-echoes is satisfactorily described by the rough-trail theory developed in section 4, that electrons disappear from the trail by attachment to atmospheric molecules, and that the time of attachment has an average value of the order of seven seconds. The time of attachment may well vary from a few seconds to a few tens of seconds, depending on the meteoric altitude under consideration.

7. *Estimation of the Line-Density of Intense Meteor-Trails*

In principle, it should be possible from equation (28) to estimate the line-density Q of a meteor-trail that gives a long-duration meteor-echo. However, it is not yet possible to be sufficiently confident concerning the properties of the function $S(f)$ to make this a practicable method of determining Q at the present time. An alternative method for estimating Q roughly is the following.

Figures 4 to 7 illustrate the fact that a long-duration meteor-echo normally enters upon its t^{-3} decay an appreciable time after it develops irregular fading. Let t_c be an estimate of the time at which the t^{-3} decay commences. Then t_c is usually greater than the time t_2 at which irregular fading sets in. For $t < t_2$, the theory of Kaiser and Closs [6] applies. For $t > t_c$, the theory of section 4 applies. For $t_2 < t < t_c$, however, no satisfactory theory is at present available. It is our assumption that during this interval the central part of the trail is still overdense, so that an incident wave cannot pass through the trail undisturbed, even to a first approximation. In the interval $t_2 < t < t_c$, what is required is a theory of irregular scattering that takes into account the effect of multiple scattering. On this picture, the time t_c is roughly that at which the central part of the trail ceases to be overdense. We can therefore estimate the central electron-density of the trail at time t_c and then use Figure 2 to deduce Q.

The critical electron-density N_c at which the meteor-trail becomes underdense depends on the frequency f of the radio wave in accordance with the formula

$$N_c = 1.24 \times 10^{10} f^2 \quad \ldots\ldots(38)$$

where N_e is measured in electrons/meter[3] and f in megacycles/second. From the fact that N_e increases with frequency, we should expect that t_e would decrease with frequency. No exception to this rule has occurred in our observations. This feature of long-duration meteor-echoes may be seen in Figures 5 and 7.

Quantitatively, however, the ratio of the two values of t_e observed for a particular event on either of the pairs of frequencies involved in Figures 5 and 7 is some 30 per cent different on the average from what it should be on the simple ideas outlined in this section. This is demonstrated in Figure 9, where values of Q deduced by this method on one frequency are plotted against values deduced on another frequency for an event simultaneously observed on both frequencies. The value for the higher frequency is plotted as ordinate and that for the lower frequency as abscissa, using logarithmic scales. Ideally, the points should all lie on the line drawn. It is clear that estimates of Q are somewhat less for the higher frequency than for the lower frequency. The reason for this is not known, but it is doubtless associated with the lack of a theory incorporating multiple scattering.

Values of Q estimated by the method described are obviously rough. Not only is there difficulty in ascribing quantitative values to t_e, but estimates obtained by observing events simultaneously on two frequencies show some systematic disagreement. However, orders of magnitude of Q are not in doubt. Figure 9 shows that the meteor-trails we have studied involve line-densities ranging from about

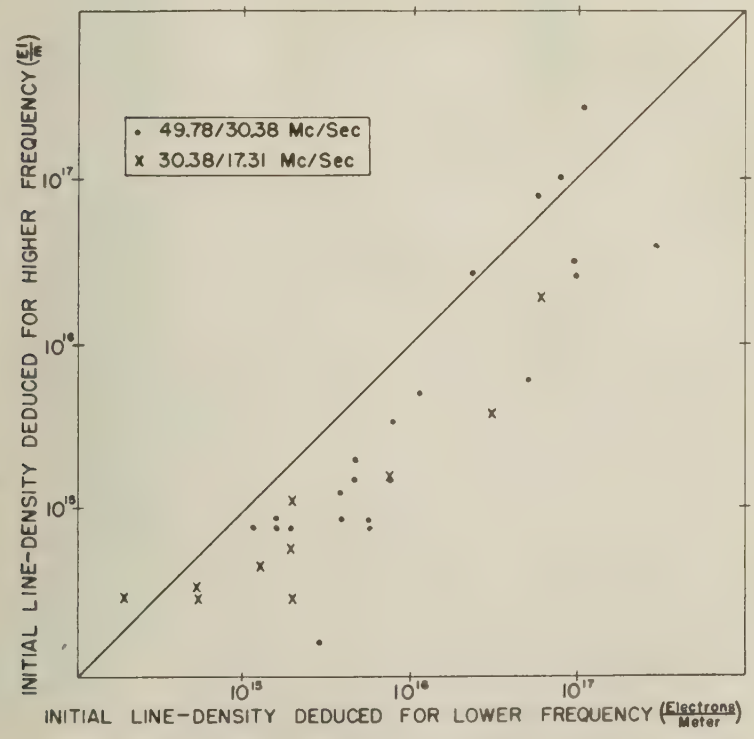

FIG. 9—Estimates of initial line-density for long-duration meteor-echoes

2×10^{14} up to 3×10^{17} electrons/meter. It should be noted that if we had used more sensitive equipment we would have obtained echoes with substantially longer lifetimes; but this would not have increased the estimates of line-density.

8. *The Spectrum of Incoherent Scattering Associated with Atmospheric Turbulence*

Since we are now satisfied that the decay of long-duration meteor-echoes is given by (28) in conjunction with (35), let us now turn our attention to the dependence on frequency. Equation (28) implies that the frequency-dependence $S(f)$ of long-duration meteor-echoes during their decay-phase is the basic spectrum-function involved in any ionospheric scattering phenomenon controlled by a formula of type (25). It is clear, therefore, that measurement of the frequency-dependence of long-duration meteor-echoes in their decay-phase is a matter of considerable importance, and should fit in with the studies that have been made [15] regarding the frequency-dependence of VHF ionospheric scatter-transmission.

It was for this purpose that all the observations that we have made of long-duration meteor-echoes have been recorded simultaneously on two frequencies, as shown in Figures 4 and 6. But to use these data to deduce the spectrum-function $S(f)$, certain difficulties have to be overcome.

It will be noticed in Figures 4 and 6 that the echo recorded on the lower frequency does not usually enter its decay-phase until the echo recorded on the higher frequency has disappeared into the noise. This situation would be improved by using equipment with a bigger dynamic range. With our equipment, this difficulty was overcome as follows: Straight lines corresponding to a t^{-3} law were fitted to the data as shown in Figures 5 and 7. The amplitude ratio on the two frequencies in the decay-phase was then read by comparing the levels of these straight lines at any arbitrary time common to both.

To derive the spectrum-function $S(f)$, it is in principle necessary to calibrate the equipment on the various frequencies in use and to verify that the calibration is maintained. It was decided to circumvent this procedure by the following device: The frequency variation of short-duration meteor-echoes has been investigated both theoretically and experimentally by Lovell and Clegg [12]. A further experimental investigation has been made by Greenhow [2]. By assuming the validity of this work, it is possible to use the relative intensities of short-duration meteor-echoes on the various frequencies as a means of relative calibration of the equipment at the several frequencies. Furthermore, it has been shown by Kaiser and Closs [6] that if, during the first few tenths of a second, specular reflection is obtained from a trail giving a long-duration meteor-echo, this specular reflection depends upon frequency in the same way as for short-duration meteor-echoes. The assumption we have made, therefore, is that the magnitude of the initial rise in records such as those reproduced in Figures 4 and 6 varies with frequency in accordance with the specular reflection theories of Lovell and Clegg [12] and of Kaiser and Closs [6]. With this assumption, one may then deduce the frequency response in the decay-phase of long-duration meteor-echoes from the dashed lines fitted to the observations shown in Figures 5 and 7, as discussed above. By operating in this way, all that is required of the equipment is that its performance should not vary during the course of an individual long-duration meteor-echo.

By analyzing our observations in the way just described, using the three frequencies available, we arrive at the results shown in Figure 10. The spectrum-function is plotted with ordinates in decibels using an arbitrary zero. Frequency is plotted as abscissa on a logarithmic scale. For each long-duration meteor-echo

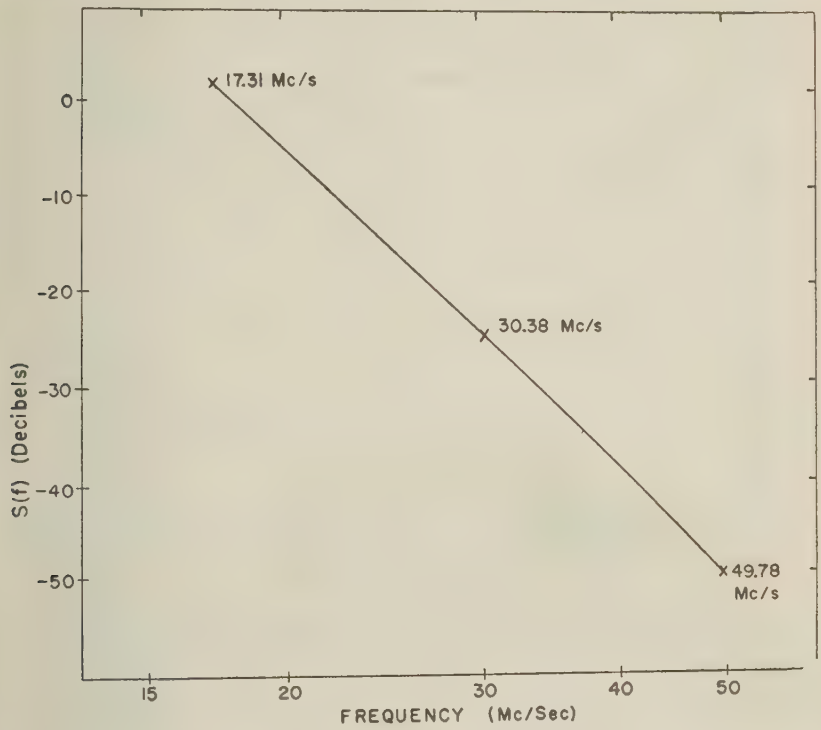

FIG. 10—The spectrum-function for incoherent scattering deduced from long-duration meteor-echoes

simultaneously recorded on 17.31 and 30.38 Mc/sec, a figure was derived for the decibel difference in the echoing area of the trail during its decay-phase. The average of these is the decibel difference plotted in Figure 10 for those frequencies. A similar procedure was followed for the frequencies 30.38 and 49.78 Mc/sec. The nearly linear variation in Figure 10 corresponds approximately to an f^{-11} variation of scattered power with frequency.

It is interesting to compare the frequency response plotted in Figure 10 with that obtained for VHF ionospheric scatter-transmission. The results of Bailey, Bateman, and Kirby [15] are reproduced in Figure 11. A straight-line variation between the points in Figure 11 corresponding to 27.775 and 49.80 Mc/sec would correspond to an $f^{-4.7}$ variation of power with frequency. A straight-line variation between the points corresponding to 49.80 and 107.8 Mc/sec would correspond to an $f^{-6.9}$ variation of power with frequency.

The two types of observations depicted in Figures 10 and 11 are brought

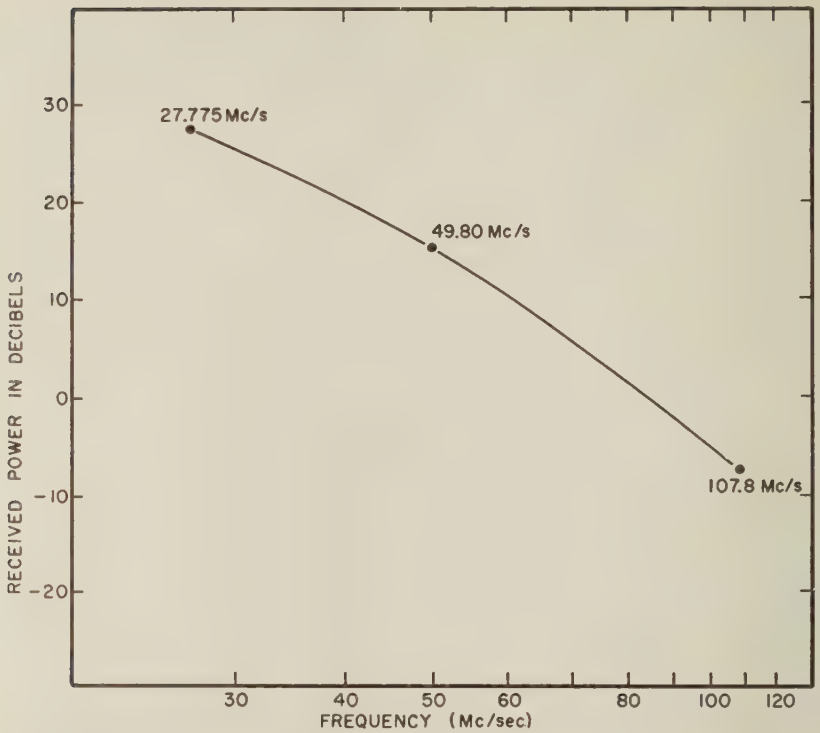

Fig. 11—The frequency variation deduced from the long-distance scatter-transmission between Cedar Rapids, Iowa, and Sterling, Virginia, for constant aperture antennas

together in a single diagram in Figure 12 with the aid of the parameter (23). It is assumed that the same basic scattering formula (25) applies in both phenomena. It is further assumed that any parameters involved in (25) have the same value in both phenomena. This applies particularly to the value of the scale L_2 of the small eddies. These assumptions are reasonable because the same ionospheric level is involved in both phenomena. Figure 12 was prepared by plotting scattered power as a function of $f \sin(\theta/2)$, in accordance with (25), allowing for the fact that $\sin(\theta/2)$ is approximately unity in the meteor observations and approximately one-fifth in the long-distance transmission measurements. The absolute levels of the two sets of points were adjusted to make them fit together, because the information available regarding absolute values was insufficient to justify a more elaborate procedure. The vertical scale in Figure 12 should, therefore, be regarded as having an arbitrary reference (although this can be placed on an absolute scale by means of Figure 19 of Bailey, Bateman, and Kirby [15]). Figure 12 may be regarded as indicating the variation in the spectrum-function S in equation (25) over almost a decade of the variable $f \sin(\theta/2)$, extending from about 5.5 to 50 Mc/sec.

From the theory of turbulence developed by Kolmogoroff [7] and Heisenberg

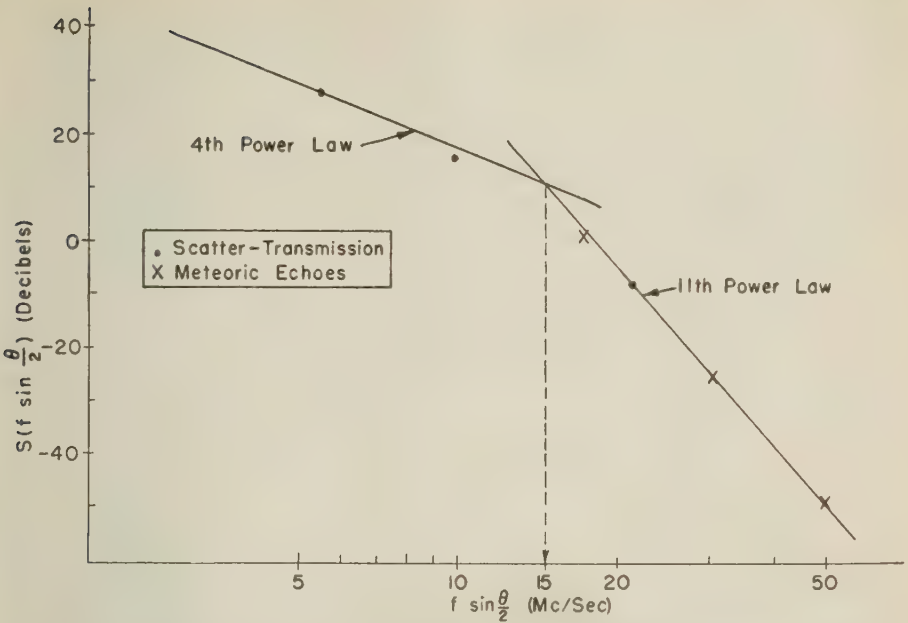

FIG. 12—The spectrum-function for incoherent scattering deduced by combining the observations derived from long-duration meteor-echoes with those derived from long-distance scatter-transmission

[8], some information is available concerning the form of the spectrum-function involved in (25) and plotted in Figure 12. The information relates to frequencies such that $f \sin(\theta/2)$, exceeds the frequency corresponding to the wavelength

$$4\pi L_1 \quad \ldots\ldots (39)$$

where L_1 is the scale of the large eddies. According to Booker [5], the value of (39) at 90 km is about 20 km. Whatever the exact value of (39) may be at the ionospheric levels under discussion, there is no doubt that the frequencies considered in Figure 12 are high compared with the frequency corresponding to the wavelength (39). In these circumstances, the Kolmogoroff-Heisenberg theory predicts a spectrum-function of the form

$$\left(f \sin \frac{\theta}{2}\right)^{-m} \quad \ldots\ldots (40)$$

at frequencies such that $f \sin(\theta/2)$ is appreciably less than the frequency corresponding to the wavelength

$$4\pi L_2 \quad \ldots\ldots (41)$$

where L_2 is the scale of the small eddies. At frequencies such that $f \sin(\theta/2)$ is appreciably larger than the frequency corresponding to the wavelength (41), the

spectrum-function should follow an inverse power law

$$\left(f \sin \frac{\theta}{2}\right)^{-n} \quad \ldots\ldots (42)$$

where n is greater than m.

The precise values of m and n in (40) and (42) are still under discussion. According to Batchelor [16] and Silverman [17]

$$m = 11/3 \quad \ldots\ldots (43)$$

but according to Villars and Weisskopf [10]

$$m = 5 \quad \ldots\ldots (44)$$

According to Batchelor [16] and Silverman [17], it would follow from Heisenberg [8] that

$$n = 9 \quad \ldots\ldots (45)$$

but according to Wheelon [18]

$$n = 13 \quad \ldots\ldots (46)$$

We regard the observations plotted in Figure 12 as describing the transition from an m^{th} power law on the low-frequency side to an n^{th} power law on the high-frequency side, with the values of m and n being of the order of magnitude required to fit the Kolomogoroff-Heisenberg theory of turbulence. On this basis, a value for the scale L_2 of the small eddies at the meteoric level may be deduced from Figure 12, using the fact that the transition between the power laws occurs near the wavelength (41). In Figure 12, a line has been drawn corresponding to $m = 4$ and one corresponding to $n = 11$, so as to fit the data in an appropriate manner. These two lines intersect at a frequency of about 15 Mc/sec, corresponding to a wavelength of 20 meters. Equating this to (41), we deduce that

$$L_2 = 1.6 \text{ meters} \quad \ldots\ldots (47)$$

approximately, and this applies to a height of the order of 90 km. This value is to be compared with the value (7) deduced for the meteoric level by Booker [5], using another argument based on different observational data.

9. *Application to VHF Scatter-Transmission*

For some years, there has been discussion of the role of meteors in long-distance VHF scatter-transmission. The results presented in this paper have a bearing on this question. Discussion of this phenomenon has often implied a choice between reflection from meteor-trails and scattering associated with atmospheric turbulence. What has been demonstrated in this paper, however, is that an important part of the phenomenon of radio returns from meteor-trails has itself to be interpreted in terms of incoherent scattering due to atmospheric turbulence. Moreover, it turns out that it is precisely the turbulence features of meteor-echoes that are most likely to be important in long-distance VHF scatter-communication. Thus, the background-signal involved in the transmission-phenomenon is likely to result

from incoherent scattering associated with atmospheric turbulence, whether or not meteors are the primary cause of ionization at this altitude.

It is desirable to state more precisely the nature of the controversy that has been in progress concerning the cause of ionospheric scatter-communication.

(*i*) The explanation of Bailey, *et al.* [19], was that the phenomenon was caused by incoherent scattering resulting from the influence of atmospheric turbulence upon ionization at the relevant level in the ionosphere. The cause of the ionization might be ultraviolet light, meteors, auroral particles, or, indeed, any ionizing agency whatsoever. The nature of the diurnal variation that they observed led them to suggest, however, a combination of a solar origin and a meteoric origin for the ionization. Subsequent observations indicated also the importance of auroral ionization [15].

(*ii*) The explanation originally suggested by Eshleman and Manning [20] was that atmospheric turbulence was not involved, and that the phenomenon could be explained entirely by specular reflection from rectilinear meteor-trails.

It should be stated that the authors who originally supported explanation (i^2) have subsequently taken the view that other factors, presumably those involved in explanation (*i*), may be important. It is, of course, true that the signal received in ionospheric scatter-transmission possesses, in addition to an irregularly fading background-signal, randomly spaced spikes with which are associated Doppler whistles. There never has been any doubt that these spikes are accounted for by explanation (*ii*). It is the view of the present authors that explanation (*ii*) is important only in connection with the spikes, and that explanation (*i*) is required to account for the background-signal.

It should be emphasized that meteoric ionization is involved both in explanation (*i*) and in explanation (*ii*). So far as meteoric ionization is concerned, the question is whether the contribution of meteor-trails to the background-signal is the specular reflection produced while the trails are essentially straight, or the incoherent scattering produced after the trails have been mixed by atmospheric turbulence. It might be supposed that specular reflection from straight meteor-trails would be particularly important in scatter-transmission, because the length of trails is large compared with the wavelength. However, although this greatly enhances the influence of appropriately located straight trails, it restricts to a compensating extent the number of trails that are important for specular reflection. For incoherent scattering from trails that have been mixed by atmospheric turbulence, there is no corresponding restriction on the number of trails to be counted. Thus, even on a qualitative basis, incoherent scattering from a large number of irregular trails that have been mixed by atmospheric turbulence is not likely to be less important than specular reflection from a smaller number of appropriately located straight trails.

Important information concerning whether the meteor contribution to the background-signal in scatter-transmission is caused by specular reflection from straight trails or by incoherent reflection from meteoric ionization that has been mixed by atmospheric turbulence is contained in the analysis of McKinley [21].

He set out to use observations concerning back-scattering from meteor-trails to calculate the contribution of meteors in long-distance scatter-transmission at 50 Mc/sec between Cedar Rapids, Iowa, and Sterling, Virginia. Now frequency f and scattering-angle θ enter into the computations through the combination (23), and sin $(\theta/2)$ for the path studied was about one-fifth. It follows that the relevant radar data for meteors should be taken on a frequency of the order of one-fifth of 50 Mc/sec, or about 10 Mc/sec. McKinley did not have data available at this frequency but presented data for the VHF band, from which a useful extrapolation to 10 Mc/sec can be made. He concluded that the meteoric contribution to ionospheric scatter-communication is of the right order of magnitude to explain the signals received. It is important, however, to notice from what type of meteor-echoes the contribution arises. Data deduced from McKinley's Table 8 are presented in the following table:

Frequency	Time during which meteor-echoes are obtained	Critical duration t_0 used by McKinley	Per cent of time accounted for by echoes of duration $> t_0$
Mc/sec	*sec/hr*	*sec*	
106	8.4	0.4	67
56	118	1.0	85
33	550	3.0	73

The table shows that most of the time during which meteoric radar echoes are obtained is accounted for by echoes whose duration is so long that they must be irregularly fading echoes associated with atmospheric turbulence. Moreover, it follows from (5) and the observations of Greenhow [2] that this table should be corrected to use a uniform value of 0.4 second in the third column at all three frequencies. This would increase somewhat the percentage in the last column at 56 Mc/sec, and substantially increase the percentage at 33 Mc/sec. After making these corrections, the data should then be extrapolated to 10 Mc/sec to obtain the radar conditions corresponding approximately to long-distance transmission at 50 Mc/sec with a scattering-angle θ for which sin $(\theta/2) = 1/5$. If one uses McKinley's data in this way, he cannot escape the conclusion that it is the contribution of the irregularly fading long-duration meteor-echoes that permitted McKinley to account for the continuous background-signal in scatter-communication by means of meteors. Thus, the conclusions that can now be drawn from McKinley's data are:

(*a*) The order of magnitude of the signal received in ionospheric scatter-transmission can be accounted for by meteoric ionization, although this may not be the only important source of ionization.

(*b*) The contribution from those meteor-echoes that indicate specular reflection is too small to permit an explanation of the background-signal by the theory of Eshleman and Manning [20].

(*c*) The contribution from those meteor-echoes that exhibit irregular fading predominates, indicating that any influence of meteoric ionization on the background-signal of scatter-transmission arises through the effect of atmospheric turbulence on the ionization.

The current status of our understanding of the cause of ionospheric scatter-transmission appears to be as follows: In middle latitudes, at night, this phenomenon arises mainly from the effect of atmospheric turbulence on ionization of meteoric origin. During the daytime, however, ionization of meteoric origin is subordinate to ionization of solar origin. In high latitudes, ionization of meteoric origin is frequently overshadowed even at night by ionization presumed to be associated with incoming charged particles. In all cases, however, it is the effect of atmospheric turbulence upon the ionization that sustains the background-signal.

References

[1] W. Liller and F. J. W. Whipple, Rocket Exploration of the Upper Atmosphere, Pergamon Press, Ltd., London (1954); p. 112.
[2] J. S. Greenhow, Proc. Phys. Soc., B, **65**, 169 (1952).
[3] L. A. Manning, O. G. Villard, Jr., and A. M. Peterson, J. Geophys. Res., **57**, 387 (1952).
[4] D. W. R. McKinley, Can. J. Phys., **31**, 758 (1953).
[5] H. G. Booker, J. Geophys. Res., **61**, 673 (1956).
[6] T. R. Kaiser and R. L. Closs, Phil. Mag., **43**, 1 (1952).
[7] A. N. Kolmogoroff, C. R. Acad. Sci. U.R.S.S., **30**, 301; **32**, 16 (1941).
[8] W. Heisenberg, Zs. Physik, **124**, 628 (1948).
[9] F. Villars and V. F. Weisskopf, Phys. Rev., **94**, 232 (1954).
[10] F. Villars and V. F. Weisskopf, Proc. Inst. Radio Eng., **45**, 1232 (1955).
[11] R. M. Gallet, Proc. Inst. Radio Eng., **43**, 1240 (1955).
[12] A. C. B. Lovell and J. A. Clegg, Proc. Phys. Soc., B, **60**, 491 (1948).
[13] N. Herlofson, Rep. Prog. Phys., **11**, 444 (1948). [Pub. by Phys. Soc.]
[14] Von R. Eshleman, discussion at URSI spring meeting, Washington, D. C., May 2, 1956.
[15] D. K. Bailey, R. Bateman, and R. C. Kirby, Proc. Inst. Radio Eng., **43**, 1181 (1955).
[16] J. C. Batchelor, Cornell University, School of Electrical Engineering, Res. Rep. EE-262 (1955).
[17] R. A. Silverman, paper presented at URSI spring meeting, Washington, D. C., May 3, 1956; to be published.
[18] A. D. Wheelon, paper presented at URSI spring meeting, Washington, D. C., May 1, 1956.
[19] D. K. Bailey, R. Bateman, L. V. Berkner, H. G. Booker, G. F. Montgomery, E. M. Purcell, W. W. Salisbury, and J. B. Weisner, Phys. Rev., **86**, 141 (1952).
[20] Von R. Eshleman and L. A. Manning, Proc. Inst. Radio Eng., **42**, 530 (1954).
[21] D. W. R. McKinley, Can. J. Phys., **32**, 450 (1954).

PALEOMAGNETISM AND MAGNETOSTRICTION

BY JOHN W. GRAHAM

Department of Terrestrial Magnetism,
Carnegie Institution of Washington,
Washington 15, D.C.

(Received November 28, 1956)

ABSTRACT

The rôle of magnetostriction in the problem of rock magnetism has heretofore been neglected. Based on some experimental observations and on reconsiderations of well-known factors affecting rocks, the conclusion is reached that magnetostriction may figure prominently in establishing the directions of magnetization observed in many cases. Therefore, the practice of interpreting meager magnetic data in terms of polar wandering and continental drift can be in error.

During the course of a visit last winter with Prof. Hales and his colleagues at the Bernard Price Institute for Geophysical Research in South Africa, the writer became concerned about the problem of grossly scattered magnetization directions noted in various surface samples of the Karroo dolerites. The usual intuitive feeling is that igneous rocks which receive their primary magnetizations at the time of their cooling should be uniformly magnetized, but actually the inconsistent magnetizations observed were strongly reminiscent of the distributions noted in some conglomerates. It was reasonable, therefore, to spend some time groping for plausible mechanisms by which scattered directions of magnetization might be explained. The result of these efforts is the realization that magnetostriction may be a factor of great importance in paleomagnetic studies.

Consider the thermal and mechanical history of a thin horizontal plate of dolerite which is cooling after having been injected molten into the inside of a thick sequence of bedded sediments. Within the melt at high temperature, hydrostatic equilibrium prevails. During the cooling and solidification process, the overburden of sediments encourages the intrusive to contract in the vertical direction, but there is no corresponding way in which it can accommodate contraction in the horizontal plane. As a consequence, cracks develop which divide the now-solidified plate into myriads of vertical columns. These columns now are supporting the overburden of sediments, and hence they are in axial compression. At the completion of cooling, we may imagine that the dolerite sill is magnetized uniformly in the direction of the earth's magnetic field, in spite of the fact that the axial compression will lower the symmetry of cubic ferromagnetic minerals and perhaps impose a preferred orientation of exsolution lamellae of ülvospinel, ilmenite, etc. With the passage of time and erosion processes, the sill is unburdened, and ultimately a sample is removed for measurement. The sample is now no longer under axial compression and is free to recover from elastic strains. Depending on

its magnetostrictive properties, the unloading may cause a new magnetic moment to be added to the original one, and the observed magnetization would then have no simple and obvious relationship to the magnetic field that was applied during the cooling. It is not yet known whether such a process accounts, for example, for the nearly vertical polarizations observed in Tasmanian dolerites [see 1 of "References" at end of paper].

To investigate the question of whether rocks might be significantly magnetostrictive, some exploratory experiments were carried out at the Department of Terrestrial Magnetism with a simple astatic magnetometer and a dural framework with which axial compression could be applied to 1″ by 1″ cylindrical samples by means of a push-rod having at its remote end a hydraulic jack. Although this equipment was adequate in that it caused no magnetometer deflections by itself, it was not refined to the point where precise measurements of directions and intensities were considered possible. Nevertheless, it was useful in showing the following:

(1) That 3,000 pounds/inch^2 axial compression is adequate to impart to many samples a new magnetic moment which is comparable to the natural moment of the sample; and
(2) The new moment added is proportional to the applied compression, and disappears when the sample is released (in short-time experiments).

The samples tested were of various basic igneous rocks and had magnetic moments greater than 10^{-5} cgs/cc. That there was considerable variation in their magnetostrictive behavior is no surprise in view of what is known about the dependence of magnetostriction constants on composition in ferrites.

Returning now to the scattered magnetizations of the dolerites, the fact noted and stressed by Gough that surface samples give scattered results and samples from depth in the same structure give consistent results has been amplified by Hales and Nairn. Weathering and lightning have generally been held responsible for this effect, but the mechanism by which the former might change the magnetic moment has never been clarified. Apart from color changes, the most conspicuous visible effect of weathering of basic igneous rocks in dry climates is in the hydration and alteration of feldspars and pyroxenes. The hydrated rock has a lower density than its parent, and because of size considerations it characteristically spalls off as sheets along curved surfaces roughly parallel to the exposed surface. Obviously, large forces have acted when a rock sheds an outer layer of tough material a few inches thick. Because of the steep stress gradient near the surface of a weathering rock, the usual sample prepared for measurement may retain stresses. These, it would seem, are adequate by magnetostriction to cause haphazard deflections of the otherwise uniform magnetization of the rock. Thermal cycling by the heat of the sun may help the rock to maintain a magnetic vector which has been deflected by magnetostriction.

It is appropriate to wonder whether the scattered magnetizations observed in some conglomerates should be explained on the basis of magnetostriction. If the conglomerate consists mainly of large fragments with little cementing matrix, it is certain that the stresses acting on any chosen piece are distinctly non-hydrostatic. Situations can be visualized where the magnetizations are quite

unstable and over a period of time come slowly into equilibrium with the earth's field while the fragments are non-uniformly stressed. If then these fragments are removed relatively quickly from their surroundings, by magnetostriction, they can acquire new directions of magnetization which are not parallel to the applied field. Following the usual interpretation, such samples would be said to have some magnetic stability, whereas actually all the fragments were, in this example, magnetized parallel to one another and the earth's field while *in situ*. Measurements made on different specimens from the same cobble would not be expected to agree with one another because of the non-uniform stresses.

Such a situation may have been encountered in some Triassic conglomerates in the eastern United States (Fig. 1). Repeat samples from the same cobble show

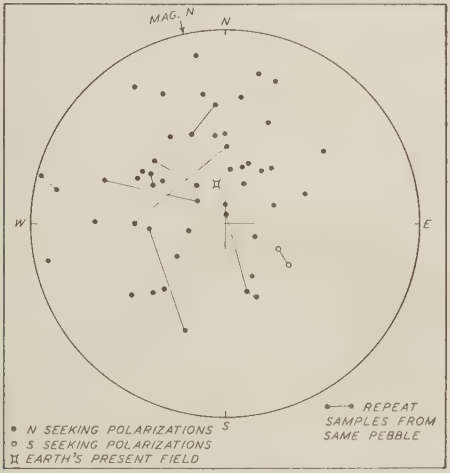

UPPER TRIASSIC CONGLOMERATES, PORTLAND AND LAKE QUONNIPAUG, CONN.; SUFFERN, N.Y.

FIG. 1

considerable differences in direction, and, furthermore, the distribution of directions does not follow the scatter pattern that would be expected if initially the magnetizations had started at random and had turned toward the earth's field at rates proportional to the sine of their angular departures from the field (magnets in tar model).

The demonstration that the magnetic moments of rocks may be significantly pressure-dependent calls for imaginative and critical consideration. The generalization may be ventured that there are no old rigid (that is, non-plastic) rocks exposed on the surface of the earth which have not been broken more or less systematically by joint planes into fairly small pieces (of the order of tens of feet or smaller). The very fact that these rocks have been broken implies that they have been subjected to large non-hydrostatic forces. The influence of these forces on the final magnetic moment we measure must be considered. At this time, we have no assurance that the long-term action of stress on the magnetic moment is completely reversible and that its final effect is nil when the stress

is released. It seems prudent to anticipate that any geologic forces which were capable of breaking rocks were likely able to produce permanent changes in their previous magnetizations.

Possibly as a case in point, we may consider the magnetizations observed in some flat-lying limestones in the eastern United States in New York State. Samples taken in a Trenton limestone conglomerate (Ordovician age) show polarizations dipping steeply toward the south in a reasonable cluster (Fig. 2). Approximately 50 miles to the east, the Onondaga limestone (Devonian) in two different settings

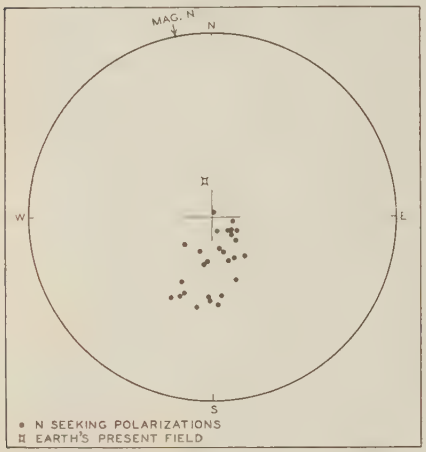

TRENTON LIMESTONE CONGLOMERATE, FLAT CREEK, SPRAKERS, N.Y., JULY 1954

Fig. 2

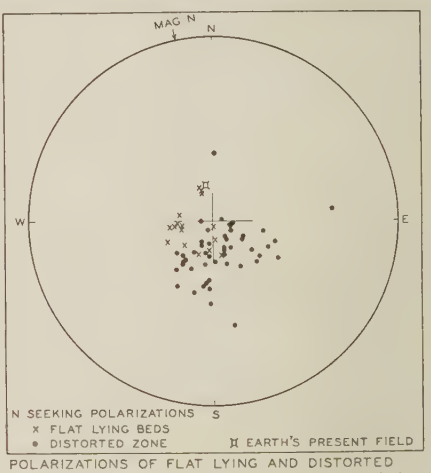

POLARIZATIONS OF FLAT LYING AND DISTORTED ONONDAGA LIMESTONE, NEW SALEM AND CLARKSVILLE N.Y., JULY 1954

Fig. 3

has the same pattern of magnetization in about the same orientation (Fig. 3). Except that all these samples are uniformly high in acid soluble carbonates, they are quite variable, particularly in color and insoluble residues. Post-depositional magnetization is indicated by the observations in the conglomerates and in the distorted zone (penecontemporaneous deformation indicated by distorted bedding containing undeformed bivalve shells and corals). That the Devonian beds have never been heated appreciably has been demonstrated on the basis of the special assortment of amino acids they contain at a concentration of only a few parts per million. The possibility that the clustering of observed directions was an artifact resulting from a systematic bias in the sampling or measuring techniques was eliminated by proper sampling procedures.

These magnetizations, according to the currently popular methods of rock magnetism, might be interpreted in one or several of the following ways:

(1) At some time since the lower Devonian, the earth's magnetic dipole axis emerged in the vicinity of the Caribbean Sea with a sufficient intensity for a long enough time that the rocks acquired, even though cool, an approximately uniform isothermal remanent magnetization which remained stable in subsequent time.

(2) The steep polarizations toward the south represent a vector sum of magnet-

izations imposed by the present earth's field and magnetizations imposed at some other time when the dipole axis emerged somewhere to the north or south of the outcrop. The various samples are sufficiently identical magnetically that in all of them the two vectors have maintained about the same ratio.

(3) This section of New York State was formerly on the opposite side of the geographic pole and has been translated along a meridian some 90°.

(4) This section of New York State has been rotated 180° on a vertical axis.

(5) Combinations of these processes have affected these rocks in unknown proportions and they are therefore not suitable for paleomagnetic purposes.

Serious specific objections can be leveled against the first four interpretations, and the value of the fifth cannot be judged at this time. In summary, the findings in these rocks are in gross conflict with currently held views (magnetostriction excepted) or common sense, or both. It seems that something must be added to our knowledge of rock magnetism.

It cannot be claimed at this time that in magnetostriction the full explanation of these puzzles has been found. It seems, however, that it may provide a better basis for understanding discrepancies and complications in meager magnetic data than the currently popular practice of interpreting magnetic evidence as support of the hypotheses of continental drift and polar wandering.

It is proposed here, for the sake of argument, that the pattern of magnetization displayed by these rocks is in some way related to the unloading and shear, and to the uniform deformation that has produced in them simple systems of vertical joints. This deformation was not sufficiently severe to produce observable folds or important faults, but was nevertheless adequate to reduce the once continuous strata into a mosaic pattern of blocks. In places, the spacing of these joints is only a matter of inches, and only rarely can one find an unbroken piece as long as 25 feet. The questions of when and how and under what conditions these joints were produced lead to many complex considerations (see, for example, reference [2]), but the very fact that the rocks are jointed indicates that they have been subjected to large stresses. The fact that in short-time laboratory experiments magnetostriction is reversible is no basis for concluding that the effect of long applied stresses will vanish when the sample is unloaded.

The writer's present feeling is that, although many of the available rock magnetism data are consistent with various (unrelated) versions of the hypotheses of continental drift and polar wandering, they by no means prove that such important processes have taken place. The data are tantalizing, but they must be greatly amplified and strengthened. We must look for wide regional consistencies in the magnetization patterns of rocks of varied types in varied settings, and we must gain accurate and ample knowledge of the processes by which rocks are magnetized.

References

[1] E. Irving, The magnetization of the Mesozoic dolerites of Tasmania, Proc. R. Soc. Tasmania, **90**, 157-168 (1956).

[2] H. J. Pincus, Statistical methods applied to the study of rock fractures, Bull. Geol. Soc. Amer., **62**, 81-130 (1951).

GEOMAGNETIC AND SOLAR DATA

INTERNATIONAL DATA ON MAGNETIC DISTURBANCES, SECOND QUARTER, 1956

Geomagnetic planetary three-hour-range indices Kp, preliminary magnetic character-figures C, average amplitudes Ap, and final selected days, April to June, 1956, are given in Table 1 on the following pages. Monthly mean values of Ci, Cp, and Ap are given in Table 2. For explanations, please refer to a previous report in this JOURNAL (Vol. 60, No. 2, June, 1955, p. 219).

The usual data on sudden commencements and solar-flare effects will appear in the next report (March 1957 issue).

TABLE 1 —*Geomagnetic planetary three-hour-range indices Kp, preliminary magnetic character-figures C, average amplitudes Ap (unit 2γ), and final selected days, April to June, 1956*

April 1956									
E	1	2	3	4	5	6	7	8	Sum
1	3 −	5 −	4o	1o	2 −	2 +	1o	2o	19 +
2	2 −	1o	2 −	4o	4o	4 −	4o	4 +	24 +
3	4 −	5 +	3o	3o	3 +	3o	2o	2 +	26 −
4	4 −	4o	3o	4 −	2 +	2o	3o	1o	23 −
5	2 +	3o	3 −	2 −	3 −	3 +	3 +	3 +	22 +
6	2 +	2 −	3o	3 −	4 +	3 −	3o	4 +	24o
7	5 +	3o	4 −	3 +	4 −	3o	2o	2 +	26 +
8	2 +	2 +	4 −	3 +	3 −	2 −	2o	1o	19o
9	1o	2 +	3o	2 +	3o	2 −	2 +	2 −	17 +
10	1o	2 −	3o	4 −	4 −	4 +	1 +	3 −	21 +
11	2o	3o	2 −	2o	3o	3 +	4o	3 −	22 −
12	3 +	2o	3 +	3 −	3 +	3o	2 −	1 +	21 −
13	2o	3o	3o	2 +	2o	1 +	1o	1o	16 −
14	0 +	2 −	3 −	2 +	2 +	2o	2 −	2 −	15 −
15	2 −	2 −	2 −	1 +	2 −	2 +	3 −	2o	15o
16	2 −	4 −	3 −	2 −	2 −	4o	3o	4 −	22o
17	5o	5 −	3o	3 −	3 +	3 −	3o	3o	27 +
18	2 +	4 −	4o	3o	3 −	2o	2 +	4 −	24 −
19	2o	4 −	4o	2o	3 −	3o	2o	1o	20 +
20	3o	2 +	2o	2 −	1 +	1 −	3 −	3 −	16 +
21	3 +	3 +	3 +	5 +	5 +	5 −	7o	7o	39 +
22	7 −	7 +	7o	7o	4 −	5 −	4 −	4o	44o
23	4o	3 +	2 +	2 +	2o	1o	1 +	2o	18 +
24	2 −	2 +	1 −	1o	2 −	1 −	1 −	2 −	10 +
25	3 +	1 +	1o	3 −	1 +	2 +	2o	2o	16o
26	2o	3 +	4 −	4o	4o	2 +	4o	8 −	31o
27	9 −	9 −	8 −	8 −	7 −	7 −	7o	6 −	59 −
28	7o	7o	4o	3 −	2o	3 +	5 +	7o	38 +
29	8 −	6 +	6o	5 +	4 −	3 +	2o	2 +	37 −
30	6o	6 +	5o	4 +	5o	5o	5 −	3 +	40 −
31									

May 1956									
	1	2	3	4	5	6	7	8	Sum
	4 −	5 −	3 +	4o	4o	3 +	2o	1o	26o
	1 −	2o	2o	1 +	1 +	0 +	1 −	1 +	10 −
	2 +	2 +	2 −	3 −	2o	2o	3 −	2 +	18o
	2o	1 +	1 +	3 +	4 −	3 −	2 +	3 −	19 +
	3 +	2o	3 +	3 +	3 −	4 +	4 −	2 +	25o
	1o	2 +	2 +	4 −	2 +	3o	1 +	2 +	18 +
	3 −	2 +	2o	2o	2o	1o	3 +	2 −	17o
	0 +	1 +	1 +	2 −	1 +	1o	1o	1 −	9 −
	1o	2 −	1o	1 −	0 +	1o	1 −	1 −	7o
	1 +	1o	1o	1 −	1 −	1o	1 −	0 +	7 −
	2 −	1 −	0 +	0 +	0 +	0o	1 −	4 −	8 −
	4 +	5 −	4 +	4 +	5o	5 +	4 +	4 +	37 −
	3 −	4o	7 −	6 −	4 −	3o	2o	3o	31 −
	2 +	2o	3 +	4 −	3o	4o	3 +	3o	25 −
	4o	4 +	4 +	5 −	5o	6 +	4 +	4 +	37 +
	5 +	7 +	8 −	7o	8 +	8 −	7o	8 −	58o
	7o	6o	6 −	5 +	5o	3 +	2 +	2o	37 −
	3 −	3o	3 +	2 +	1 +	1 +	1 +	2 −	17o
	2 −	2o	2o	4 −	1 +	2 −	2 −	3 −	17 −
	2o	2 −	4 −	6 +	6 −	4o	5o	5 −	33o
	4 +	5 −	3 +	2 −	2o	2 −	3 −	1 +	22 −
	2 +	3 −	3 +	4o	4o	2o	4 +	2 +	25o
	2 +	0 +	1o	3 +	4o	4o	4o	7 −	26 −
	6 +	6o	6 −	6 +	7o	6 +	6 −	7o	50 +
	7o	7o	7o	6o	4o	3 +	2o	4o	40 +
	5 −	2 +	3 −	1o	1 +	1 +	3o	3 +	20 −
	3 −	2 −	1 +	1 +	1 −	2 −	2o	3 +	15 −
	4 −	4 +	2 +	2 −	2 +	0 +	2 −	1 −	17o
	1 +	1 −	1 +	0 +	2o	4o	6 −	5 −	20o
	3o	3o	3o	3 −	3 −	4o	2 +	3o	24 −
	1 +	3 −	1o	1 +	0 +	2 −	1 −	2 +	11 +

June 1956									
E	1	2	3	4	5	6	7	8	Sum
1	4 −	4o	4 −	4 +	4 −	4 −	3 +	3 −	29o
2	2 +	3o	3 −	3 −	4 −	3 +	2 +	1 +	21 +
3	3o	2 −	1o	1 +	2o	2 +	2 −	3o	16o
4	2 −	2 −	1 +	2 +	3o	3 −	2 +	2 −	17 −
5	1 +	2o	3 −	1 +	2o	4 −	3 +	2o	18 +
6	1 +	2 +	2o	3 −	5o	4 −	2o	2 −	21 −
7	1 +	2o	2 +	1 +	2 −	2 +	2 +	2o	15 +
8	4 −	2o	3o	4 +	2 +	3 −	3 +	4 −	25o
9	2 +	3 −	5o	3 −	3 +	2 +	3 +	3 −	24 +
10	3o	2 +	3 −	2 +	2o	5 −	3o	4o	24o
11	4o	3 +	4 +	3 +	4o	3o	3o	3 −	28 −
12	3 +	3 −	3 −	2o	2 −	1 +	2 −	3 −	18o
13	3o	3 −	2o	2 +	3o	3o	3o	4 +	23 +
14	3 +	3 −	4 −	4 −	3 +	3o	4o	3 +	27o
15	5 −	4 +	4 +	3 +	4 −	4 −	3 +	4 +	32 −
16	3o	3o	3 +	3 −	3 +	2 +	3 +	3 −	24 −
17	1o	2 −	1 +	1o	2 +	3 +	3 −	4 −	17o
18	3o	1 +	1 +	2o	1 +	2 −	1o	2o	14 −
19	1 +	1 −	2o	1o	1 +	2o	2o	4o	14 +
20	2o	1 +	1 +	2o	2 +	2 −	2 +	3 −	16 −
21	3 +	2o	2 +	2o	1 +	2 −	3 −	3o	18 +
22	3o	2o	2 −	2o	2o	2 +	2 +	1 +	17 −
23	2 +	1 +	1o	2o	2 −	2o	5 −	6 +	21 +
24	5o	5o	3 −	3o	5o	6o	5 −	6o	37 +
25	6 +	7 −	6 +	4 −	3 +	5 −	4o	2 +	37 +
26	2 −	2 +	3 +	3 +	4 +	4 −	3 +	3 +	25 +
27	3 −	5 −	4 −	4 −	3o	4 −	3o	2o	26 +
28	2o	3 −	4o	2 +	3o	2o	3o	2o	21o
29	2 −	2o	4 −	5 −	3 −	2 +	4o	3o	24o
30	2 −	4 +	4 −	4o	4 +	5 −	4o	3o	30 −
31									

Preliminary *C*, 1956		
Apr.	May	June
0.6	1.0	1.0
1.0	0.1	0.8
1.0	0.6	0.4
0.8	0.8	0.5
0.8	0.8	0.6
0.8	0.5	0.9
1.0	0.4	0.3
0.6	0.1	0.8
0.5	0.0	0.9
0.7	0.1	0.9
0.8	0.3	1.0
0.7	1.4	0.6
0.2	1.4	0.8
0.2	0.9	0.9
0.4	1.4	1.2
0.8	2.0	0.8
1.0	1.5	0.6
0.8	0.6	0.3
0.7	0.4	0.4
0.5	1.4	0.6
1.7	0.9	0.6
1.7	0.9	0.4
0.7	1.1	0.9
0.1	1.9	1.5
0.4	1.6	1.6
1.4	0.8	0.9
2.0	0.4	1.0
1.6	0.7	0.6
1.6	0.9	0.9
1.6	0.8	1.0
	0.3	

Average amplitude *Ap*		
Apr.	May	June
14	20	22
19	5	13
20	9	8
15	11	8
14	17	10
17	10	14
20	9	7
11	4	17
9	4	17
15	4	17
13	5	20
12	38	10
8	34	15
7	16	19
7	42	27
14	156	15
22	52	10
15	9	7
13	9	8
9	39	8
59	16	10
80	18	8
10	28	21
5	95	46
8	69	52
40	14	18
172	8	19
64	11	12
58	19	17
51	15	25
	6	

TABLE 1—(Concluded)—*Final selected days, April to June, 1956*

Month	Five quiet days	Ten quiet days	Five disturbed days
1956			
April	13 14 15 24 25	8 9 12 13 14 15 20 23 24 25	21 22 27 28 30
May	2 8 9 10 11	2 7 8 9 10 11 18 19 27 31	15 16 17 24 25
June	3 7 18 19 20	3 4 7 12 17 18 19 20 21 22	1 15 24 25 30

TABLE 2—*Monthly mean values of Ci, Cp, and Ap, April to June, 1956*

Index	April 1956	May 1956	June 1956
Mean *Ci*	0.89	0.84	0.78
Mean *Cp*	0.94	0.86	0.81
Mean *Ap*	27	26	17

COMMITTEE ON CHARACTERIZATION OF MAGNETIC DISTURBANCES

J. BARTELS, *Chairman*
University
Göttingen, Germany

J. VELDKAMP
Kon. Nederlandsch Meteorologisch Instituut
De Bilt, Holland

PROVISIONAL SUNSPOT-NUMBERS FOR JULY TO SEPTEMBER, 1956

(Dependent on observations at Zurich Observatory and its station at Locarno and Arosa)

Day	July	Aug.	Sep.
1	162	140	168
2	155	148	158
3	133	146	136
4	153	149	138
5	138	152	146
6	139	149	168
7	163	151	176
8	158	140	174
9	150	152	161
10	157	165	136
11	162	146	175
12	216	148	208
13	192	150	244
14	156	140	280
15	156	143	276
16	144	143	253
17	98	131	250
18	67	173	219
19	65	192	228
20	71	217	240
21	78	224	216
22	86	237	153
23	113	213	139
24	84	232	125
25	90	154	132
26	100	178	136
27	116	196	131
28	104	198	127
29	108	200	172
30	130	214	201
31	140	182	
Means.....	128.5	171.1	182.2
No. days.....	31	31	30

Mean for quarter: 160.4 (92 days)

M. Waldmeier

Swiss Federal Observatory
Zurich, Switzerland

CHELTENHAM THREE-HOUR RANGE INDICES K FOR JULY TO SEPTEMBER, 1956

[$K9 = 500\gamma$; scale-values of variometers in γ/mm: $D = 5.4$; $H = 1.7$; $Z = 4.3$]

Gr. day	July 1956			August 1956			September 1956		
	Values K		Sum	Values K		Sum	Values K		Sum
1	2232	3333	21	4212	3222	18	3243	2133	21
2	2242	2233	20	3211	2122	14	5766	3333	36
3	2333	2221	18	1021	2112	10	6655	3222	31
4	2331	1121	14	2101	1123	11	1143	2111	14
5	2122	2223	16	2321	0011	10	3222	0102	12
6	1221	1111	10	1000	1032	7	3344	2233	24
7	1000	1022	6	1311	0012	9	3331	2222	18
8	4422	1124	20	2233	1222	17	1133	7754	31
9	4343	0112	18	2313	4344	24	2243	3234	23
10	2212	1144	17	3431	2123	19	3221	2222	16
11	3331	2234	21	5443	3453	31	2322	0122	14
12	2331	2133	18	3333	4245	27	2110	1134	13
13	4322	2335	24	1122	3112	13	4521	1222	19
14	4322	2222	19	2221	0122	12	1200	0012	6
15	2313	2232	18	1110	2032	10	2200	0013	8
16	3331	2223	19	1001	1222	9	2111	2222	13
17	1312	0013	11	3443	3222	23	1221	0111	9
18	1100	1111	6	2211	1122	12	1000	0011	3
19	3332	3345	26	1110	0002	5	1100	0012	5
20	3231	2233	19	1110	0111	6	3433	4433	27
21	2100	1132	10	1233	5344	25	5543	3332	28
22	2210	1112	10	4221	3233	20	4555	3332	30
23	2221	3246	22	3323	4344	26	3243	2112	18
24	4454	3223	27	6545	6644	40	2101	2122	11
25	3455	3233	28	3335	4444	30	4211	2122	15
26	4555	3335	33	5453	2442	29	3344	1120	18
27	5433	3333	27	3442	3223	23	1101	3222	12
28	3324	3244	25	4311	2222	17	2322	1222	16
29	2242	2432	21	1222	3232	17	1000	2132	9
30	3232	2222	18	2343	2111	17	3232	1012	14
31	1122	4322	17	1125	3343	22			

Ralph R. Bodle
Observer-in-Charge

Cheltenham Magnetic Observatory
Cheltenham, Maryland, U.S.A.

PRINCIPAL MAGNETIC STORMS

(Advance knowledge of the character of the records at some observatories as regards disturbances)

Observatory (Observer-in-Charge)	Greenwich date	Storm-time		Sudden commencement				C-figure, degree of activity[4]	Maximal activity on K-scale 0 to 9			Ranges		
		GMT of begin.	GMT of ending[1]	Type[2]	Amplitudes[3]				Gr. day	Gr. 3-hr. period	K-index	D	H	Z
					D	H	Z							
(1)	(2)	(3)	(4)	(5)	(6)	(7)	(8)	(9)	(10)	(11)	(12)	(13)	(14)	(15
	1956	*h m*	*d h*		′	γ	γ					′	γ	γ
Sitka	July 23	15 ..	28 04	.....	.....	.....	.....	s	24	4	8	89	836	599
(J. L. Bottum)	Aug. 11	00 43	12 23	s.c.	+ 2	+84	− 8	m	11	2, 3, 7	5	47	383	330
									12	3, 4, 5	5			
	Aug. 23	08 ..	26 21	.....	.....	.....	.....	s	24	5	9	165	1518	814
	Aug. 31	10 18	31 23	s.c.	− 2	+12	0	ms	31	4	7	49	433	453
	Sep. 2	01 15	3 19	s.c.	− 1	+ 6	0	s	2	2, 3, 4	9	207	2419	830
	Sep. 8	07 30	10 02	s.c.	− 1	+ 4	0	s	8	5	9	207	1182	1026
	Sep. 20	15 ..	23 00	.....	.....	.....	.....	s	22	4	8	82	989	496
Witteveen	July 13	12 00	14 02	.....	.....	.....	.....	ms	13	7	6	20	180	70
(D. van	Aug. 9	10 40	9 24	s.c.*	+ 3	+25	0	m	9	5, 6, 7	5	25	180	75
Sabben)	Aug. 11	00 43	11 24	s.c.*	− 9	+97	− 3	m	11	1,4,5,6,7	5	30	220	80
	Aug. 21	09 00	21 24	.....	.....	.....	.....	ms	21	5	6	25	160	55
	Aug. 23	11 00	26 21	.....	.....	.....	.....	ms	24	1, 6	7	55	310	285
	Sep. 2	02 31	3 15	s.c.	− 2	+68	− 1	ms	2	2, 3	7	40	295	175
	Sep. 8	10 06	8 21	s.c.*	+ 8	+12	0	s	8	5, 6	8	75	515	280
	Sep. 20	04 37	22 20	s.c.*	− 5	+24	0	ms	20	6	6	30	185	90
Cheltenham	July 23	19 00	24 10	.....	.....	.....	.....	ms	23	8	6	23	158	139
(R. R. Bodle)	Aug. 11	00 43	11 21	s.c.	+ 8	+107	....	m	11	1, 7	5	30	195	28
	Aug. 23	19 00	26 19	.....	.....	.....	.....	ms	24	1, 5, 6	6	53	237	147
	Sep. 2	01 00	3 12	.....	.....	.....	.....	ms	2	2	7	32	356	204
	Sep. 8	10 07	8 24	s.c.	− 7	+31	+ 4	ms	8	5, 6	7	61	210	83
	Sep. 22	01 00	22 12	.....	.....	.....	.....	m	22	2, 3, 4	5	18	89	60
Tucson	July 23	11 ..	24 21	.....	.....	.....	.....	ms	23	8	6	21	111	46
(R. F. White)	Aug. 10	21 ..	12 23	.....	.....	.....	.....	ms	11	1	6	20	134	44
	Aug. 23	18 ..	26 12	.....	.....	.....	.....	m	24	1, 2, 4	5	14	107	56
	Sep. 1	19 ..	3 15	.....	.....	.....	.....	ms	2	2	7	21	232	51
	Sep. 19	21 ..	22 24	.....	.....	.....	.....	m	20	5, 6	5	17	154	37
									21	1, 2	5			
									22	3, 4	5			
Honolulu	July 23	17 00	27 12	.....	.....	.....	.....	ms	24	3	6	5	100	35
(M. L. Cleven)	Aug.	None												
	Sep. 2	02 30	3 14	.....	.....	.....	.....	ms	2	2	7	5	280	50
	Sep. 8	10 09	9 03	s.c.	....	+24	+12	ms	7	5	6	7	90	40
Alibag	Apr. 2	07 21	2 23	s.c.	− 1	+ 9	−2	m	2	4, 7	5	4	122	24
(A. S. Chaubal)	Apr. 21	11 00	23 13	s.c.	− 1	+17	−13	ms	21	7	7	10	210	75
	Apr. 26	21 12	28 09	s.c.	− 1	+57	−12	ms	26	8	6	12	309	61
	Apr. 28	17 30	29 18	s.c.	0	+15	−3	ms	29	2	6	10	144	73
	Apr. 30	01 37	30 23	s.c.	− 1	+14	−7	ms	30	1	6	5	124	39
	May 11	23 41	13 19	s.c.	0	+ 8	−3	m	13	3	6	8	189	63
	May 16	04 17	17 16	s.c.	0	+28	−4	ms	16	2, 5, 6	6	6	248	76
	May 20	06 38	21 17	s.c.	− 1	+30	−11	ms	20	4	7	6	208	38
	May 23	10 09	25 16	.....	.....	.....	.....	ms	24	4	6	8	186	72
	May 24	05 48	(Sudden impulse in D, H, and Z: $D = -0.'6$; $H = +30\gamma$; and $Z = -10\gamma$)											
	June 23	18 06	25 20	s.c.	0	+10	− 2	m	24	6	5	6	99	46

[1]Approximate time of ending of storm construed as the time of cessation of reasonably marked disturbance movements in the traces; more specifically, when the *K*-index measure diminished to 2 or less for a reasonable period.

[2]s.c. = sudden commencement; s.c.* = small initial impulse followed by main impulse (the amplitude in this case is that of the *main impulse only*, neglecting the initial brief pulse); ... = gradual commencement.

[3]Signs of amplitudes of *D* and *Z* taken algebraically; *D* reckoned positive if towards the east and *Z* reckoned positive if vertically downwards.

[4]Storm described by three degrees of activity: *m* for moderate (when *K*-index as great as 5); *ms* for moderately severe (when *K* = 6 or 7); *s* for severe (when *K* = 8 or 9).

PRINCIPAL MAGNETIC STORMS—Continued

Observatory (Observer-in-Charge)	Greenwich date	Storm-time GMT of begin.	Storm-time GMT of ending[1]	Sudden commencement Type[2]	Amplitudes[3] D	H	Z	C-figure, degree of activity[4]	Maximal activity on K-scale 0 to 9 Gr. day	Gr. 3-hr. period	K-index	Ranges D	H	Z
(1)	(2)	(3)	(4)	(5)	(6)	(7)	(8)	(9)	(10)	(11)	(12)	(13)	(14)	(15
	1956	*h m*	*d h*		′	γ	γ					′	γ	γ
Instituto Geofísico de Huancayo (A. A. Giesecke, Jr.)	July 23	12 40	24 18	.....	.....	.....	.....	m	24	5	5	5	268	2
	Aug. 9	10 40	9 21	s.c.	1	22	− 7	m	9	6	5	3	299	3
	Aug. 11	00 44	11 20	s.c.	1	91	−21	ms	11	6	6	6	240	4
	Aug. 21	05 07	21 21	s.c.	0	11	− 2	ms	21	5, 6	6	9	208	4
	Aug. 23	12 00	24 21	.....	.....	.....	.....	s	24	6	8	9	396	5
	Aug. 31	10 16	31 21	s.c.	0	20	−10	m	31	5, 6, 7	5	5	265	5
	Sep. 2	02 30	3 17	s.c.	0	46	−12	ms	2	2	7	11	281	4
	Sep. 8	10 06	8 23	s.c.	1	15	− 5	s	8	6	9	20	864	7
	Sep. 20	04 37	21 06	s.c.	0	23	− 2	ms	20	6	7	9	435	3
Elisabethville (N. v.d. Elst)	Apr. 21	11 02	22 12	s.c.	− 1	+33	....	ms	....	7, 8	.....	10	293	3
	Apr. 26	21 12	28 08	s.c.	− 1	+63	− 5	ms	....	3, 4	.....	16	265	3
	Apr. 30	01 39	30 19	s.c.	....	+37	....	m	....	1, 2	.....	6	126	5
	May 16	04 16	17 06	s.c.	+ 1	+11	− 2	ms	....	3, 4	.....	18	254	2
	May 20	06 36	21 ..	s.c.	− 3	+30	+ 3	ms	....	3, 4	.....	13	146	4
	May 24	05 47	25 02	s.c.	− 2	+18	+ 2	ms	....	3, 4	.....	8	168	2
	June	Néant												
Apia (A.A. Thomson)	June 26	05 48	27 15	.....	.....	.....	.....	m	27	2	5	4	67	2
	July 18	22 12	20 01	.....	.....	.....	.....	m	19	8	5	6	57	2
	July 22	19 40	30 12	.....	.....	.....	.....	ms	24	3	6	7	197	3
	Aug. 9	10 41	10 03	s.c.	0	+16	− 4	m	9	4	5	6	71	3
	Aug. 10	22 00	13 23	.....	.....	.....	.....	m	11	1, 2, 3	5	6	174	2
	Aug. 16	21 40	17 17	.....	.....	.....	.....	ms	17	2	6	6	129	2
	Aug. 21	05 08	28 06	s.c.?	0	(†)	− 1	m	23	8	5	7	136	3
				†No trace					24	2	5			
									26	1	5			
	Aug. 31	10 16	3 19	s.c.	0	+13	− 4	ms	2	2	7	7	287	5
	Sep. 8	10 06	11 10	s.c.	0	+20	− 8	ms	8	5	6	7	128	3
	Sep. 19	20 34	23 13	.....	.....	.....	.....	ms	21	1	6	6	187	3
Hermanus (A. M. van Wijk)	July 24	12 46	24 18	s.c.?	+ 1	+ 6	+ 6	m	24	3	5	6	39	2
	July 29	06 ..	29 09	(Large bay in *D*)				m	29	3	5	.....	.....	...
	Aug. 9	10 41	10 06	s.c.*	+ 2	+25	+23	m	9	4, 6, 8	4	Minor disturbances		
	Aug. 11	00 44	12 23	s.c.	+ 4	+38	+30	m	11	1, 6	5	10	138	9
				(*Note:* Initial impulse in *D* only)										
	Aug. 17	00 ..	17 18	.....	.....	.....	.....	m	17	2	5	Minor disturbances		
	Aug. 21	05 08	22 01	s.c.	+ 1	+ 5	+ 6	ms	21	5	6	15	97	7
	Aug. 23	08 ..	26 21	.....	.....	.....	.....	ms	24	5	6	24	148	9
	Aug. 31	10 16	31 22	s.c.	+ 1	+19	+13	m	31	4, 6	5	13	120	8
	Sep. 2	02 30	2 20	s.c.	+ 3	+37	+28	ms	2	2, 3	6	30	197	12
	Sep. 3	01 ..	3 15	.....	.....	.....	.....	m	3	1, 2, 3, 4	5	28	106	11
	Sep. 6	04 ..	6 15	.....	.....	.....	.....	m	6	5	5	Minor disturbances		
	Sep. 8	10 06	9 02	s.c.	+ 1	+12	+ 8	ms	8	5, 6	6	32	181	17
	Sep. 20	04 38	22 20	s.c.	− 1	+ 9	+ 6	m	20	5, 6	5	22	151	13
									22	4	5			
Watheroo (W. D. Parkinson)	July	None												
	Aug. 11	00 44	12 23	s.c.*	− 6	+22	−25	m	11	1, 3	5	16	112	12
	Aug. 23	22 02	26 09	s.c.*	+ 2	+ 3	+12	m	24	1, 5, 6	6	23	114	15
	Sep. 2	02 30	3 16	s.c.	− 2	+ 9	− 7	ms	2	2, 4	6	32	210	14
	Sep. 8	10 07	.. ..	s.c.*	− 2	+13	− 5	..	..	..	..	.....	.....	...

(*Note:* Followed by activity lasting 10 hours, with moderately severe movements from $14^h\ 30^m$ to $16^h\ 30^m$ GMT, and accompanied by auroral display. Aurora seen from $14^h\ 43^m$ to about $15^h\ 25^m$ GMT; brightest about $14^h\ 45^m$. It was predominantly a diffuse glow, with some rays between $14^h\ 43^m$ and $14^h\ 55^m$.)

PRINCIPAL MAGNETIC STORMS—Concluded

Observatory (Observer-in-Charge)	Greenwich date	Storm-time: GMT of begin.	Storm-time: GMT of ending[1]	Sudden commencement: Type[2]	Sudden commencement: Amplitudes[3] D	H	Z	C-figure, degree of activity[4]	Maximal activity on K-scale 0 to 9: Gr. day	Gr. 3-hr. period	K-index	Ranges D	H	Z
(1)	(2)	(3)	(4)	(5)	(6)	(7)	(8)	(9)	(10)	(11)	(12)	(13)	(14)	(15)
	1956	*h m*	*d h*		′	γ	γ					′	γ	γ
Binza	Apr. 21	11 04	23 21	s.c.	....	46	....	m	21	7	.....	11	283	37
(N. v.d. Elst)	Apr. 26	21 16	28 16	s.c.	− 2	69	....	m	27	1, 7	.....	13	250	41
	Apr. 28	19 05	30 24	s.c.	....	28	....	m	30	1, 3	.....	11	166	45
	May 16	4 18	18 17	s.c.	− 1	19	....	m	16	2	.....	12	236	28
	June 23	18 10	25 18	s.c.*	0	10	− 2	m	25	1	.....	9	164	27
Toolangi	July 23	21 50	27 13	.....	....	....	....	m	24	4	6	20	143	69
(I. B.	Aug. 11	00 44	12 23	s.c.	− 6	+40	+15	m	11	2	5	23	100	37
Everingham)									12	5	5			
	Aug. 23	22 02	26 11	s.c.*	− 2	−18	0	ms	24	6	6	29	159	59
	Sep. 2	01 11	3 17	.....	....	....	....	ms	2	2, 3, 4	6	31	225	169
	Sep. 8	10 06	10 04	s.c.*	− 3	+34	+ 5	ms	8	5	7	20	221	96
	Sep. 20	01 43	23 17	.....	....	....	....	m	22	4	5	24	145	65
Amberley	July 8	01 04	9 14	s.c.*	− 1	− 8	+ 6	..	..	..	..	.....	.....	.....
(A. L.	July 23	22 ..	29 12	.....	....	....	....	ms	24	4	6	22	174	87
Cullington)	Aug. 11	00 44	13 06	s.c.*	+ 3	+56	−11	m	11	1, 2	4	10	107	33
	Aug. 12	02 28	13 06	s.c.*	+ 1	+21	− 7	m	12	5	4	14	96	35
	Aug. 23	19 ..	27 12	.....	....	....	....	m	24	2, 6	5	25	129	107
	Sep. 2	02 30	3 16	s.c.*	+ 2	+27	−11	ms	2	3	7	37	263	162
	Sep. 8	10 07	10 06	s.c.*	+ 1	+41	− 2	m	8	5, 6	5	28	167	143
	Sep. 20	04 38	23 12	s.c.	+ 2	+36	− 8	m	22	4	5	21	122	69
				Reports added in galley-proof:										
College	July 25	02 00	27 14	.....	....	....	....	ms	25	4	7	210	1480	930
(C. J. Beers)	Aug. 11	00 43	12 23	s.c.*	−15	−114	−14	ms	12	5	6	120	910	510
	Aug. 23	08 00	25 18	.....	....	....	....	ms	24	4	7	200	1480	900
	Sep. 2	01 15	3 19	.....	....	....	....	ms	2	3	7	260	1420	1530
									3	4	7			
	Sep. 20	02 ..	23 00	.....	....	....	....	ms	22	4	7	190	1530	890
San Juan	July	None												
(P. G. Ledig)	Aug. 11	00 29	11 20	s.c.	+ 1	+50	−13	m	11	1, 2	5	13	103	20
	Aug. 23	22 02	24 24	s.c.	0	+ 8	− 3	m	23	8	5	12	81	57
									24	1	5			
	Sep. 2	02 30	2 12	s.c.	+ 1	+15	− 5	ms	2	2	7	9	200	22
	Sep. 8	10 06	8 21	s.c.	+ 1	+12	− 3	ms	8	5, 6	6	19	127	65
Alibag	July 22	23 46	24 19	.....	....	....	....	m	24	3	5	7	122	60
(A. S. Chaubal)	Aug. 11	00 43	12 00	s.c.	− 1	+60	− 7	m	11	1, 3, 4	5	8	192	48
	Aug. 21	05 06	22 21	s.c.	0	+15	− 5	m	21	5	5	5	116	57
	Aug. 23	22 02	26 11	s.c.	0	+ 9	− 3	m	23	8	5	8	158	97
									24	1,4,5,6,7	5			
	Aug. 31	10 17	31 22	s.c.	− 1	+17	− 9	m	31	4	5	4	107	32
	Sep. 2	01 14	4 00	.....	....	....	....	ms	2	2	7	9	292	88
	Sep. 8	10 06	9 02	s.c.	− 1	+17	− 9	ms	8	5, 6	6	8	246	40
	Sep. 19	23 ..	22 23	.....	....	....	....	ms	20	2, 5, 6	5	10	189	119
Tassouras	Apr. 21	11 02	22 18	s.c.	+ 2	+39	+15	m	21	7	5	13	365	70
(Lilio I. Gama)	Apr. 26	21 12	28 †	s.c.	+ 2	+57	+16	m	27	1	5	21	288	61
	Apr. 28	18 57	29 18	s.c.	+ 1	+31	+11	m	29	1	4	14	238	41
	Apr. 30	01 38	30 22	s.c.	+ 2	+38	+10	m	30	2	5	10	330	32
	May 16	04 18	17 04	s.c.	+ 2	+28	+ 9	m	16	5	5	11	180	18
	May 23	10 ..	25 10	.....	....	....	....	m	24	8	5	15	182	56
	Sep. 2	02 30	2 15	s.c.	+ 1	+42	+11	ms	2	2	7	13	188	62
	Sep. 8	10 06	9 02	s.c.	+ 1	+12	+ 3	ms	8	6	6	26	258	65

†Power failure

LETTERS TO EDITOR

THE LUNAR-DIURNAL MAGNETIC VARIATION AND ITS RELATION TO THE SOLAR-DIURNAL VARIATION

Abstract

Reexamining the question of a relation between the lunar-diurnal and the solar-diurnal variations, it was discovered that an abnormally large lunar-diurnal variation of Z existed at Amberley (New Zealand) during the night hours.

The possibility of a relation between the lunar-diurnal and solar-diurnal magnetic variations has been treated earlier by the author,[1] the examination being based on the idea that the lunar-diurnal variation originates from changes in the solar-diurnal variation caused by tide-generating forces of the moon. The procedure consisted in a comparison of the amplitude for the lunar-diurnal variation of the second harmonic term (c_2) and the range of the solar-diurnal variation (R), taking into account the dependency of the tidal forces on latitude (φ). The following formula, where C is a constant, seemed to be valid:

$$\frac{c_2}{R \cos^2 \varphi} = C \qquad (1)$$

However, J. Bartels[2] obtained the following result for H at Huancayo, Peru:

Season	s_2	c_2	s_2/c_2
	γ	γ	
S. summer (Nov.-Feb.)	23.6	8.0	3.0
Equinoxes	28.5	5.9	4.8
S. winter (May-Aug.)	20.2	2.4	8.4

where s_2 is the amplitude of the second harmonic term of the solar-diurnal variation. From this result, it appears that c_2 does not vary through the year in the same way as s_2 ; nor does c_2 vary as R.

Further, Bullen and Cummack[3] have shown that for Z in the case of Amberley the ratio $s_2 : c_2$ is "extremely low in comparison with evaluations obtained by

[1]J. Egedal, The lunar-diurnal magnetic variation and its relation to the solar-diurnal variation, Terr. Mag., **31**, 193–199 (1926), and **32**, 139–141 (1927).

[2]S. Chapman and J. Bartels, Geomagnetism, Clarendon Press, Oxford, p. 264 (1940).

[3]J. M. Bullen and C. H. Cummack, The lunar diurnal-variation of the earth's magnetic field for all elements at Amberley, New Zealand, J. Geophys. Res., **58**, 554-556 (1953).

other observatories." This result also disagrees with the above formula (1), so that the idea on which the formula is based is not tenable.

In order to examine the question more closely, the data for Z from Amberley were treated, and the solar-diurnal variation of Z for January 1950 for Amberley and Hermanus were compared. Although the range of the solar-diurnal variation should be nearly equal, the range for Amberley was 17γ and for Hermanus 35γ. As to the lunar-diurnal variation of Z, Bullen and Cummack found an amplitude of the second harmonic term of 2γ while this variation at other places does not exceed 1γ. The author then determined the lunar-diurnal variation of Z for night hours during the months June and July 1953 and found

$$\Delta Z = (2.3 \pm 0.2\gamma) \sin (2t + 70°)$$

This amplitude of more than 2γ found for the night hours, where no solar-diurnal variation exists, shows that the lunar-diurnal variation found does not depend on the solar-diurnal variation. Neither does the lunar-diurnal variation found depend on the ionization of the upper atmosphere. The variation found may be due to sea electric currents produced by local oceanic currents, the speed of which contains a lunar-diurnal term.

The solar-diurnal magnetic variation may consist of other effects than those caused by electric currents in the upper atmosphere, and the lunar-diurnal variation is as shown composed of different effects. Therefore, an examination of the two variations must be preceded by an investigation of the elements of each of the variations.

J. Egedal

Birkerød, Denmark,
September 14, 1956
(Received September 17, 1956)

IONOSPHERE ELECTRON-DENSITY MEASUREMENTS WITH THE NAVY AEROBEE-HI ROCKET

Electron densities in the ionosphere above White Sands, New Mexico, were measured continuously from the E region up to the lower $F2$ region with the Aerobee-Hi NRL No. 50, a rocket instrumented by the U. S. Naval Research Laboratory. This rocket was fired at 12:09 p.m. MST on 29 June 1956 and reached an altitude of 263.7 km.

The method[1] used consists in refractive index measurements based on propagation phenomena. Two harmonically related c-w signals, at 7.75 Mc and 46.5 Mc, respectively, are transmitted from the moving rocket to two receiving stations on the ground. The rocket motion causes each signal to experience a Doppler shift, which is related to the refractive index of the medium near the rocket. The high frequency is used as a reference, since its index is essentially unity. Comparison techniques used on the ground plus a knowledge of the rocket trajectory

[1] J. C. Seddon, J. Geophys. Res., 58, 323 (1953).

yield, as a function of altitude, the 7.75-Mc refractive indices for both ordinary and extraordinary rays. Since the electron density can be computed from either index, a check of the internal consistency of the data is possible.

The preliminary analysis of the Aerobee NRL No. 50 flight indicates that the c-w propagation experiment has provided reliable electron-density measurements up to 260 km. The rocket was fired during a period of moderate ionospheric disturbances (light sporadic-E up to 8 Mc, and complete absorption below 2.8 Mc). The rocket-borne transmitting antennas consisted of two 15-foot whips. These were retracted along the rocket skin during the powered flight and deployed at an altitude of 55 km. The c-w transmission itself was initiated at 58 km. Ionosphere data were continuously received and recorded at the ionosphere ground stations until 500 seconds after take-off, at which time the rocket whip antennas were probably torn off due to re-entry into the lower atmosphere. The data reduction is the most straightforward when the propagation is nearly vertical, since ray bending effects can be ignored. This was the case during ascent when the straight-line paths between the rocket and the ground stations remained within $\pm 4°$ of the vertical. However, during descent, due to the 90-km horizontal range of the rocket, the propagation was quite oblique, with an inclination reaching 35° in the E region. It is expected, therefore, that the exact analysis of the descent data will be much more difficult, unless it can be shown that the straight-line approximations made in the preliminary data reduction provide adequate accuracy. The electron density expressed in electrons per cubic centimeter was about 10^4 at 85 km; it increased linearly to 16×10^4 at 100 km and then more gradually to 28×10^4 at 150 km. It remained approximately at this value until 240 km. It then began to increase again up to 36×10^4 at 260 km. The equivalent vertical-incidence wave-frequency corresponding to the density at 260 km is 5.3 Mc. The ionization measured is consistent with the 5.3-Mc virtual height indicated by the P'-f record taken during the flight. Extrapolation of the profile with the aid of the P'-f record[2] revealed the peak density of the $F2$ region to be in the vicinity of 310 km.

The electron-density profile obtained appears to be very similar to the profile obtained from the Viking 10 flight[3] of 7 May 1954, but with densities approximately 50 per cent greater above 100 km. The denser ionosphere is in accordance with the increased solar activity since 1954. The initial linear ionization increase in the E region occurred about 6 km lower, which may explain the high absorption reported by the Virtual Height Ionosphere Sounding Station. The latest results confirm the general structure of the daytime ionosphere above White Sands as deduced from previous NRL flights, namely, that the ionosphere remains dense between the E and $F2$ regions, with only minor valleys in the electron-density profiles.[4] This latest flight lends additional substantiation to the method recently developed by one of the authors[2] for the analysis of the P'-f records, since the method is based on the existence of a nearly-linear electron-density gradient in the lower E region and on the absence of deep valleys in the electron-density profile. The height of the $F2$ region was also in agreement with previous NRL findings, indicating the approximate altitude constancy of this region.

[2]J. E. Jackson, J. Geophys. Res., **61**, 107 (1956).
[3]J. C. Seddon, A. D. Pickar, and J. E. Jackson, J. Geophys. Res., **59**, 513 (1954).
[4]J. C. Seddon and J. E. Jackson, Phys. Rev., **97**, 1182 (1955).

In addition to the electron-density measurements, an attempt was made to obtain attenuation data at 7.75 Mc by using crossed linearly-polarized antennas at one ground station. This provides the sum and difference of the ordinary (E_o) and extraordinary (E_x) amplitudes. The amplitude ratio is a measure of the differential absorption

$$\frac{\mathrm{d}}{\mathrm{d}z}\left[-ln\,\frac{E_x}{E_o}\right]$$

where z represents altitude. It was found that the differential absorption was negligible up to 80 km, but became very apparent beginning at 87 km. At 94 km, the differential absorption increased abruptly, with the ratio E_x/E_o changing from a value of 0.85 at 94 km to 0.33 at 97 km. The usual additional rays previously reported[1] then made an appearance, which introduced major complications in the analysis of the higher altitude attenuation data.

The success of these experiments is particularly encouraging, since the equipment used was the prototype of the instrumentation to be used at Fort Churchill, Canada, during the International Geophysical Year. Extensive preparations now under way for the IGY program prevent the publication of a more detailed report at this time.

J. E. Jackson
J. A. Kane
J. C. Seddon

U. S. Naval Research Laboratory,
Washington, 25, D. C., September 28, 1956
(Received October 5, 1956)

METEORITE IMPACTS TO ALTITUDE OF 103 KILOMETERS

For many years, experiments have been conducted in an attempt to determine the space density of meteorites and their contribution to mechanisms in our upper atmosphere. The usual methods of obtaining such meteorite data have included visual and radio observations of meteorite trails and the collecting and analysis of fallen meteorites and meteoritic dust. Recently, rocket-borne microphones have recorded numerous mechanical pulses which are believed to have been due to meteor impacts on the rocket skin.[1]

A new-type meteorite-impact detector has been flown by the Naval Research Laboratory in an Aerobee rocket. This rocket was launched from the White Sands Proving Ground in New Mexico on November 17, 1955, at 0200 hours MST, and it attained an altitude of 103 kilometers. A cutaway view of the detector used and its position relative to the rocket skin is shown in Figure 1. With the exception of the exit window at the apex, the polished lucite cone was completely coated with an opaque layer of aluminum, 8×10^{-6} cm thick. As shown, the window was adjacent to a 1P21 photomultiplier.

[1]J. L. Bohn and F. H. Nadig, Researches in the Physical Properties of the Upper Atmosphere with Special Emphasis on Accoustical Studies with V-2 Rockets, Research Institute of Temple University, Rep. No. 8, 1–26 (1950).

A meteoritic impact upon this detector caused penetration of the opaque aluminum coating.[2] Also, upon impact, a portion of the kinetic energy of the meteorite was transformed into visible light. This light was captured within the cone and reflected into the photomultiplier. The resulting pulse, suitably amplified and stretched, was thence telemetered to ground.

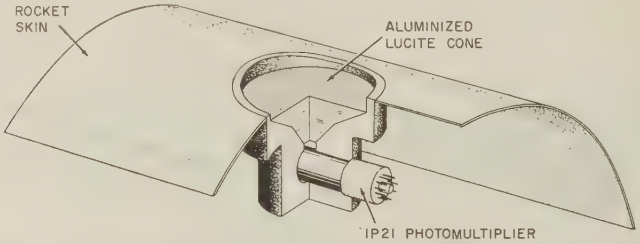

Fig. 1—Showing the aluminized lucite cone inserted in its plastic housing in the rocket, with its clear (non-aluminized) exit window adjacent to the photomultiplier. The detector was located 2 inches below the ogive of the rocket.

The extremely high velocity of meteorites (11 to 72 km/sec) precluded the feasibility of precision pre-flight calibration techniques normally used in upper-air investigations wherein the measurement is simulated as nearly as is possible in the laboratory. As an alternative, the sensitivity of the detector in terms of the amount of visual light required to produce a detectable pulse was determined. This calibration showed that light pulses of 0.0001 lumen sec/m^2 or greater could be readily detected.

In order to determine the system's sensitivity in terms of meteorite energy, it is necessary to consider the fact that when a meteorite is stopped upon impact with a solid its kinetic energy is transformed into heat, visible light, and ionization in some ratio. If the assumption is made that there is a similar distribution of released energies for meteorite impact as for meteors traversing the rarified atmosphere, then the ratio is (theoretically) 10^4 heat : 10^2 light : 10^0 ionization.[3] Using this ratio, it was found that the detector could detect impacts of meteorites having as low an energy as 0.005 erg. Such an energy, for example, corresponds to an iron meteorite with a one-micron diameter and a velocity of only 0.5 km/sec.

Figure 2 shows the measured impacts superimposed on the rocket trajectory. The zenith angle of the missile was less than 38° from take-off until re-entry, at about 225 seconds, at which time it tipped over very rapidly into its descent zenith angle of about 170°.

From the Figure, the symmetry of the counting rate about the peak altitude is evident. Also evident from the curve is the absence of a cyclic impact frequency corresponding to the six-second roll period of the rocket. This indicates that the particles are not coming in from a single radiant.

The data show a total of 114 impacts upon the 75 cm^2 detector. Of these

[2]F. L. Whipple, Physics and Medicine of the Upper Atmosphere, University of New Mexico Press, Albuquerque, 137 pp. (1952).

[3]E. Opik, Acta and Comm., Univ. Tartuensis, A, 26, No. 2 (1933).

impacts, 101 occurred during the 84 seconds when the rocket was above 85 km (the altitude above which there is no apparent increase in impact frequency). This is one impact per cm^2 per 57 seconds.

It should be mentioned that two similar detectors were used in this flight.

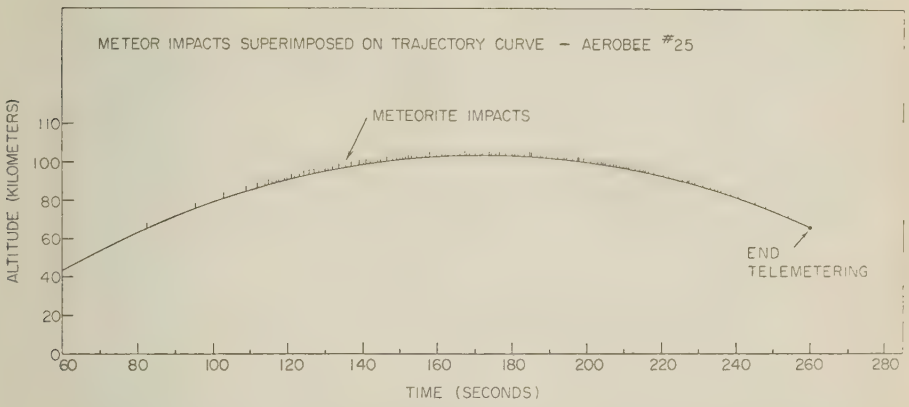

FIG. 2—The end of powered flight (burnout) occurred at 43 seconds.

The above data were obtained from one detector only, the other detector having become inoperative early in flight. On examination of the recovered missile, it was found that a considerable portion of the aluminum coating had been burned off the surface of the detector that failed. It is believed that this photomultiplier was saturated by exposure to the night sky light, rendering it non-sensitive to low-amplitude, short-duration pulses.

Although the statistics are not good in this measurement, the data are believed to be valid for the following reasons:

(1) The pulses appeared only above a given altitude, both on ascent and descent, with a marked symmetry of occurrence about peak altitude.

(2) There was no increase in impact frequency above a certain altitude. This is to be expected if one accepts Grimminger's[4] method of calculations of the atmospheric penetration distances of micrometeorites and adapts it to the Rocket Panel atmospheres.[5]

(3) On the basis of Grimminger's calculations and the assumption that the results of Öpik[3] apply, the output pulse lengths and altitude dependence of the impact rate are both consistent with the detected meteorites being only a few microns in diameter.

(4) During the short time while the rolling rocket was tipped over upon re-entry with its axis parallel to the earth's surface, pulses occurred only while the detector looked upward, but none occurred while the detector looked downward (that is, while the detector was shieleded by the earth).

[4]G. Grimminger, Probability that a meteorite will hit or penetrate a body situated in the vicinity of the earth, J. Appl. Phys., **19**, 947–956 (1948).

[5]The Rocket Panel, Pressures, densities, and temperatures in the upper atmosphere, Phys. Rev., **88**, 1027–1032 (1952).

The reader may note that the time of this measurement coincides with the time of the Leonid meteor shower, and may therefore think that the data are not representative of the daily accretion of meteorites. However, most investigations agree that there is no increase in space density of micrometeorites within our atmosphere during this meteor shower.

The authors are grateful to H. M. Caulk and J. E. Kupperian, who determined the orientation of the rocket during its flight from their magnetic and optical data.

Otto E. Berg
L. H. Meredith

U. S. Naval Research Laboratory,
Washington 25, D. C., September 27, 1956
(Received October 5, 1956)

NOTES

(29) *Symposium on Very-Low-Frequency Propagation*—A symposium on very-low-frequency propagation, sponsored by the National Bureau of Standards and the Professional Group on Antennas and Propagation of the Institute of Radio Engineers, will be held at Boulder, Colorado, January 23-25, 1957. Persons wishing to attend this meeting should notify Mrs. M. Halter, National Bureau of Standards, Boulder, Colorado. It is expected that the three mornings will be devoted to regular technical papers, with the afternoon being reserved for round-table discussions.

(30) *New officers, Society of Exploration Geophysicists*—The Society of Exploration Geophysicists have elected the following 1956-1957 officers to serve beginning Octobe 29, 1956: president, Roy F. Bennett, Oklahoma City, chief geophysicist of the Sohio Petroleum Company; vice-president, Dr. J. P. Woods, Dallas, director of the geophysical research laboratory for the Atlantic Refining Company; secretary-treasurer, Prof. John C. Hollister, Golden, of the Colorado School of Mines. Dr. Norman Ricker, of the Carter Oil Company, continues his two-year term as editor. The 26th annual convention, held at New Orleans, October 29 to November 1, 1956, included discussion of offshore exploration, instrumentation and research, foreign exploration, model studies, International Geophysical Year, economics, and case histories. Formation of a Venezuelan Geophysical Association and two local sections in Canada was recently announced.

(31) *Publication of proceedings of symposium on the U.S. Earth Satellite Program*—The papers presented before the national convention of the Institute of Radio Engineers in New York City, March 19-22, 1956, session on the U.S. Earth Satellite Program, are given in "IRE Convention Record," Part 1, Telemetry, Antennas, and Propagation, pages 96-128, published recently by the Institute of Radio Engineers, Inc.

(32) *Graduate program in astro-geophysics at the University of Colorado*—The University of Colorado has made plans for a graduate program in astro-geophysics (leading to the Ph.D. degree). It will emphasize solar-terrestrial phenomena and the upper atmosphere.

(33) *Experiments in space laboratory*—Two U.S. Navy observers have completed a high-altitude meteorological experiment while on a "Skyhook" balloon flight. It is one phase under Project Stratolab to conduct research from a manned "space" laboratory attached to a balloon. The initial manned flight in the office of Naval Research Stratolab program reached an altitude of 40,000 feet. The observers rode in an open fibreglass gondola, suspended below a plastic balloon, built and launched by General Mills, Inc., Minneapolis, Minnesota. Future flights are planned for significantly higher altitudes in the stratosphere, when observers will use a special pressurized spherical aluminum gondola. [Nov. 8, 1956: A giant Skyhook balloon today carried two naval officers to a record height of 76,000 feet.]

(34) *Automatic aurora recorder*—A device so sensitive that it will "see" auroras,

or northern lights, too faint to be spotted by human beings, has been developed by Dr. D. M. Hunten, of the University of Saskatchewan, Saskatoon, Canada, for use during the International Geophysical Year at isolated stations. The automatic aurora recorder produces tabulated results directly. The sky's light is caught on a small mirror that automatically tilts to different positions across the sky from horizon to horizon every five minutes. A second mirror reflects the light beam through a light chopper, a lens, and an aperture to a photo-multiplier. The photo-multiplier's readings are recorded directly on a strip chart for immediate viewing and as numbers on punched tape for later study or for possible automatic analysis.

(35) *Swedish ship "Lommaren" to chart map of cosmic rays*—The Swedish merchant ship *Lommaren* sailed from Göteborg, Sweden, in September 1956 to gather data for a cosmic-ray "map" of the world. The shipboard study is being sponsored by the National Geographic Society and the Bartol Research Foundation of the Franklin Institute, in collaboration with the National Research Council of Canada, the Physics Institute of Uppsala University, and the Transatlantic Company of Sweden. The sea-going laboratory will operate throughout the International Geophysical Year of 1957-58. It is hoped that the cosmic-ray map will give some clue to the source of the rays. Data on these rays are expected also to provide a chart of the magnetic field surrounding the earth.

(36) *New York University's research ship "Action"*—Realizing the importance of linking academic knowledge with first-hand observation, Dr. Gerhard Neumann, professor of oceanography at New York University and oceanographic scientist of international repute, arranged for the University's purchase of its first research ship, the 65-foot schooner *Action*. In addition to early practical experience, Dr. Neumann served as an oceanographer in the German Hydrographic Service, and taught and did research at the University of Hamburg. In 1950 and 1951, on a small freighter, he made a total of 27,000 individual ocean wave observations in the Atlantic. From this basic data, he and Dr. Willard J. Pierson, another New York University oceanographer, formulated a fairly complete theory of ocean wave behavior. Dr. Neumann is now engaged also in research on ocean-atmosphere interaction and long-range weather forecasting.

(37) *Japanese Antarctic Expedition*—An antarctic expedition composed of 53 men left for the South Pole on November 8, 1956, aboard the icebreaker *Muroya* to prepare for geophysical observations during the International Geophysical Year 1957-58. Dr. Takesi Nagata, of the Geophysical Institute, Tokyo University, will head the party.

(38) *Global air-flight to determine earth's magnetic field*—By circling the world at the equator in a Boeing KC-97, flying a 1500-pound cosmic-ray meter, the Air Research and Development Command hopes to determine the shape of the magnetic field, far out from the earth's surface. It is expected that the information gained will be of general assistance to agencies engaged in projects for the International Geophysical Year 1957-58. Heretofore, assumptions regarding the pattern of the magnetic field above the ionosphere have been based on measurements made at the earth's surface and projected outward into space. Studies of cosmic rays, however, which are influenced by the earth's magnetic field as far out in space as 4,000 miles, have given indication that the magnetic field is "twisted" and may

vary from the previous assumption. The measurements obtained on this special flight are expected to permit fairly accurate mapping of the outer magnetic equator. The expedition is a joint undertaking of the Air Research and Development Command, the Strategic Air Command, and the University of Chicago, having been proposed by Drs. John A. Simpson and Peter Meyer of the Enrico Fermi Institute for Nuclear Studies.

(39) *Geomagnetic activities of the United States Coast and Geodetic Survey*—Because of shortage of operating funds, the U.S. Coast and Geodetic Survey has found it necessary to modify the magnetic observatory program. The Cheltenham Observatory was permanently shut down on October 1, 1956, some three months earlier than originally planned, and all of its functions will be carried on by the Fredericksburg Magnetic Observatory. A series of comparison observations has been made with a view to transferring the instruments, on which the magnetic standards of D, H, and I have been based, from one location to the other without danger of a change of instrumental constants.

The San Juan Magnetic Observatory (Puerto Rico) will continue operation with a reduced staff after October 1, 1956. On that date, the magnetograph recorder was reduced to half-speed (10 mm per hour), so that each magnetogram will contain 48 hours of record. It is hoped that a standard recording speed can be resumed at a later date.

Mr. Joel B. Campbell, IGY Operations Officer, made an inspection trip to Alaska and reported excellent progress on preparation of the IGY magnetic observatories.

Captain Elliott B. Roberts, Chief of the Geophysics Division, attended the joint CSAGI-CPAGI conference on the International Geophysical Year at Rio de Janeiro in July 1956.

Colonel Alexandro Forch of Chile, Sr. Augusto Llano of Chile, and Mr. Radomir Turajlic of Yugoslavia have been studying the methods and procedures of the U.S. Coast and Geodetic Survey in office and field work in geomagnetism. During August 1956, Mr. Turajlic visited the observatories at Tucson and College.

(40) *Personalia*—Mr. *J. Egedal*, state meteorologist of the Det Danske Meteorologiske Institut, Copenhagen, Denmark, as also chief of the Geophysical Section and magnetic observatory of Rude Skov, retired on October 31, 1956. He contributed numerous articles in *Terr. Mag.* dealing with the lunar-diurnal magnetic variation and its relation to the solar-diurnal variation, as well as on other subjects. His private address following retirement will be Kongevejen 126, Birkerød, Denmark.

Dr. *Edward H. Smith* retired in August 1956 from his post as director of the Woods Hole Oceanographic Institution in Massachusetts. He will be succeeded by Dr. Columbus O. Iselin, senior oceanographer in the Institution and professor of oceanography at Harvard University.

Prof. *Walter H. Bucher*, Newberry professor emeritus of geology at Columbia University, New York, has retired.

Dr. *Paul H. Dike*, retired Leeds and Northrup Company physicist, died on June 25, 1956, at Jenkintown, Pennsylvania, at the age of 78. In 1903 he was observer-in-charge of the U.S. Coast and Geodetic Survey's magnetic observatory

in Puerto Rico. Later he carried out research for the Department of Terrestrial Magnetism, of the Carnegie Institution of Washington. In 1907 he was magnetic observer and in charge of atmospheric-electric work on the magnetic survey ship *Galilee*.

(41) *Corrigenda* In the September 1956 number of this Journal in Pemmaraju S. Pant's article on "Circulation in the upper atmosphere," the legends of Figures 2 and 3 on pages 464 and 465 were interchanged. Figure 3 represents the summer distribution of the zonal wind and Figure 2 the winter distribution.

Dr. Runcorn has advised us that in the September 1956 number of this Journal in the article by C. D. Campbell and S. K. Runcorn entitled "Magnetization of the Columbia River basalts in Washington and northern Oregon," the stereograms of Figures 2 to 5 (pp. 452-455) should have "*N*" marked at the top of the page as in Figures 6 and 7. In Figure 2, showing the directions of magnetization of the Imnaha River basalt series, the following points have been plotted incorrectly. The correct declinations and inclinations are listed here:

122a	given as	N69E	+75°	should be		S36E	−74°
122c	"	" N24W	+73°	"	"	S24E	−73°
125c	"	" S 1E	+73°	"	"	N 1W	−73°
125b	"	" N78E	+16°	"	"	S78W	−16°
126c	"	" S13E	−73°	"	"	N13W	+73°
126d	"	" S85E	−68°	"	"	N85W	+68°

Thus, specimen 126b has magnetization seriously different from other specimens from the same flow: this might be due to a mistake in orientation. Consequently, in Figure 1, the Imnaha River flows 22 and 25 should be marked R and 26 should be marked N. Flow 9 should have been marked N.

LIST OF RECENT PUBLICATIONS

By W. E. Scott

Department of Terrestrial Magnetism,
Carnegie Institution of Washington,
Washington 15, D.C.

(Received September 29, 1956)

A—*Terrestrial Magnetism*

Amberley Observatory. Magnetic results for 1953. Wellington, R. E. Owen, Govt. Printer, 58 pp. (1955). [Issued under the authority of the Hon. R. M. Algie, Minister of Scientific and Industrial Research.]

Backus, G. The external electric field of a rotating magnet. Astroph. J., **123**, No. 3, 508-512 (1956).

Bartels, J., A. Romañá, and J. Veldkamp. International data on magnetic disturbances, first quarter, 1956. J. Geophys. Res., **61**, No. 3, 559-562 (1956).

Bates, L. F., and A. Hart. Magnetization curves and domain structure. Proc. Phys. Soc., B, **69**, No. 437, 497-505 (1956).

Bodle, R. R. Cheltenham three-hour-range indices *K* for April to June, 1956. J. Geophys. Res., **61**, No. 3, 563 (1956).

Cahill, L. J., Jr., and J. A. Van Allen. High altitude measurements of the earth's magnetic field with a proton precession magnetometer. J. Geophys. Res., **61**, No. 3, 547-558 (1956).

Campbell, C. D., and S. K. Runcorn. Magnetization of the Columbia River basalts in Washington and northern Oregon. J. Geophys. Res., **61**, No. 3, 449-458 (1956).

Chapman, S., and M. Sugiura. Arc-lengths along the lines of force of a magnetic dipole. J. Geophys. Res., **61**, No. 3, 485-488 (1956).

Chatterjee, J. S. The crust as the possible seat of earth's magnetism. J. Atmos. Terr. Phys., **8**, Nos. 4/5, 233-239 (1956).

Chatterjee, J. S. Induction in the core by magnetic storms and earth's magnetism. Science and Culture, **21**, No. 10, 623-624 (1956). [Letter to Editor.]

Coimbra. Observacões méteorológicas, magnéticas e sismológicas feitas no Instituto Geofisico (Observatório Meteorológico Magnético e Sismológico) no ano de 1951. 2ª Parte—Magnetismo terrestre. Vol. XCI Coimbra, Tipografia da Atlântida, 37 pp. (1952). [Received Sept. 10, 1956.]

Elsasser, W. M. Hydromagnetic dynamo theory. Rev. Modern Phys., **28**, No. 2, 135-163 (1956).

Frøshaug, J. Mean results of geomagnetic observations in Tromsø, Norway, for the years 1930-50. J. Geophys. Res., **61**, No. 3, 435-444 (1956).

Griffiths, D. H. The remanent magnetism of varved clays from Sweden. Mon. Not. R. Astr. Soc., Geophys. Sup., **7**, No. 3, 103-114 (1956).

Hulburt, E. O. Geomagnetic program of the International Geophysical Year. Sci. Mon., **83**, No. 2, 87-91 (1956).

Ingall, L. N. Magnetic results from Heard Island, 1952. Commonwealth of Australia, Bureau of Mineral Resources, Geology and Geophysics, Rep. No. 21, 8 pp. + 46 tables + 7 pls. (1955). [Rec'd Sept. 10, 1956.]

Jacobs, J. A. Effect of altitude on the position of the magnetic pole. Nature, **178**, 35-36 (July 7, 1956). [Letter to Editor.]

Karmohapatro, S. B., and S. K. Majunder. Measurement of gradients of inhomogeneous magnetic fields. Science and Culture, **21**, No. 10 621-622 (1956). [Letter to Editor.]

Kato, Y., and S. Akasofu. Outer atmosphere oscillation and geomagnetic micropulsation. Sci. Rep. Tôhoku Univ., **7**, No. 3, 103-124 (1956).

Kato, Y., and M. Okuda. The effect of the solar eclipse on the rapid pulsation of the earth's magnetic field. Sci. Rep. Tôhoku Univ., **7**, supp. to No. 3, 37-41 (1956).

Kato, Y., and J. Ossaka. The effect of the solar eclipse on the *Sq* current of the diurnal variation. Sci. Rep. Tôhoku Univ., **7**, supp. to No. 3, 21-29 (1956).

Kato, Y., J. Ossaka, T. Watanabe, M. Okuda, and T. Tamao. Investigation on the magnetic disturbance by the induction magnetograph, Part V—On the rapid pulsation, p.s.c. Sci. Rep. Tôhoku Univ., **7**, No. 3, 136-146 (1956).

King, R. F. The remanent magnetism of artificially deposited sediments. Mon. Not. R. Astr. Soc., Geophys. Sup., **7**, No. 3, 115-134 (1956).

Mayaud, P. N. Rapports Scientifiques des Expéditions Polaires Françaises S IV 2, Activité magnétique dans les régions polaires. Ann. Géophys., **12**, No. 1, 84-101 (1956).

McGregor, P. M. Magnetic results from Macquarie Island, 1952. Commonwealth of Australia, Bureau of Mineral Resources, Geology and Geophysics, Rep. No. 27, 9 pp. + 41 tables + 3 pls. (1956).

Munuera, J. M. Avance de resultados del mapa magnetico de Guinea. Rev. Geofísica, **15**, No. 57, 45-51 (1956).

Naschke, E. Dispersion et absorption magnétiques du 1er entre 0 et 7000 mégahertz. J. Phys. Radium, **17**, No. 4, 330-337 (1956).

Opdyke, N. D., and S. K. Runcorn. New evidence for reversal of the geomagnetic field near the Pliocene-Pleistocene boundary. Science, **123**, 1126-1127 (June 22, 1956).

Powell, D. W. Gravity and magnetic anomalies in North Wales, with an appendix on the magnetic anomalies over the Lleyn Peninsula by D. H. Griffiths and R. F. King. Q. J. Geol. Soc. London, **111**, Pt. 4, 375-397 (1955).

Rikitake, T. Magneto-hydrodynamic oscillations of a conducting fluid sphere under the influence of the Coriolis force. Bull. Earthquake Res. Inst., Tokyo, **34**, Pt. 2, 139-156 (1956).

Rimbert, F. Sur l'action de champs alternatifs sur des roches portant une aimantation rémanente isotherme de viscosité. Paris, C.-R. Acad. sci., **242**, No. 21, 2536-2538 (1956).

Roquet, J. Sur les propriétés magnetiques des roches volcaniques riches en pyrite. Ann. Géophys., **12**, No. 2, 147-150 (1956).

Sivaramakrishnan, M. V. A comparative study of geomagnetic and ionospheric changes at Kodaikanal and Huancayo. Indian J. Met. Geophys., **7** No. 2, 137-146 (1956).

Sucksdorff, E. Die erdmagnetismus Aktivitätszahlen AZ von Sodankyla in den Jahren 1935-1944. Helsinki, Veröff Finn. Geod. Inst., No. 30, 7 pp. (1955).

Takeuchi, H. The dynamo theory of the earth's main magnetic field. J. Phys. Earth, **4**, No. 1, 11-20 (1956).

United States Coast and Geodetic Survey. Magnetograms and hourly values, College, Alaska, 1951. Washington, D.C., U.S. Coast Geod. Surv., No. MHV-Co51, 197 pp. (1955).

Zmuda, A. J. Note on the components of magnetic intensity at inverse points relative to a spherical boundary. Trans. Amer. Geophys. Union, **37**, No. 3, 273-274 (1956).

B—*Terrestrial Electricity*

Whitlock, W. S., and J. A. Chalmers. Short-period variations in the atmospheric electric potential gradient. Q. J. R. Met. Soc., **82**, No. 353, 325-336 (1956).

Wilson, C. T. R. A theory of thundercloud electricity. Proc. R. Soc., A, **236**, No. 1206, 297-317 (1956).

C—*Cosmic Rays*

Bachelet, F., and A. M. Conforto. Increase of cosmic ray intensity associated with the solar flare of February 23, 1956. Nuovo Cimento, **3**, No. 5, 1153-1155 (1956).

Bozóki, G., E. Fenyves, and L. Jánossy. On the penetrating non-ionizing component of cosmic rays. Nuclear Physics, **1**, No. 7, 501-515 (1956).

Brode, R. B., and A. Goodwin, Jr. Extraordinary increase of the cosmic radiation on February 23, 1956. Phys. Rev., **103**, No. 2, 377 (1956).

Cocconi, G. Intergalactic space and cosmic rays. Nuovo Cimento, **3**, No. 6, 1433-1442 (1956).

Cranshaw, T. E., W. Galbraith, and N. A. Porter. Cosmic-ray observations during the flare of 23 February 1956. J. Atmos. Terr. Phys., **8**, No. 4/5, 274-276 (1956). [Research note.]

Dorman, L. I., N. S. Kaminer, V. K. Koiava, Yu. G. Shafer, and B. F. Shwarzman. Observations of the large cosmic-ray increase of February 23, 1956 in the U.S.S.R. Nuclear Physics, **1**, No. 8, 585-592 (1956).

Ellison, M. A., and J. H. Reid. A long-wave anomaly associated with the arrival of cosmic-ray particles of solar origin on 23 February 1956. J. Atmos. Terr. Phys., 8, Nos. 4/5, 291-293 (1956). [Research note.]

Fan, C. Y. Nonthermal radio emission of the galaxy and the origin of cosmic radiations. Astroph. J., **123**, No. 3, 491-497 (1956).

Fenton, A. G., K. G. McCracken, N. R. Parsons, and P. A. Trost. Cosmic-ray increase observed at high southern latitudes on February 23, 1956. Nature, **177**, 1173-1174 (June 23, 1956). [Letter to Editor.]

Filosofo, I., I. Modena, E. Pohl, and J. Pohl-Rüling. The increase in the total cosmic ray intensity and in the positive excess due to the solar flare of 23rd February 1956. Nuovo Cimento, **3**, No. 5, 1112-1118 (1956).

Ginzburg, V. L. The nature of cosmic radio emission and the origin of cosmic rays. Nuovo Cimento, **3**, No. 1, 38-48 (1956).

Gold, T., and D. R. Palmer. The solar outburst, 23 February 1956. Observations by the Royal Greenwich Observatory. J. Atmos. Terr. Phys., 8, Nos. 4/5, 287-291 (1956). [Research note.]

Jory, F. S. Influence of geomagnetic quadrupole fields upon cosmic-ray intensity. Phys. Rev., **102**, No. 4, 1167-1173 (1956).

Lambie, M., and H. Elliot. Cosmic rays and the solar flare of 23 February 1956. J. Atmos. Terr. Phys., 8, Nos. 4/5, 277-278 (1956). [Research note.]

Lockwood, J. A., H. E. Yingst, A. R. Calawa, and G. Sarmaniote. Cosmic-ray neutron intensity increase associated with solar flare of February 23, 1956. Phys. Rev., **103**, No. 1, 247-248 (1956).

Marsden, P. L., J. W. Berry, P. Fieldhouse, and J. G. Wilson. Variation of cosmic-ray nucleon intensity during the disturbance of 23 February 1956. J. Atmos. Terr. Phys., 8, Nos. 4/5, 278-281 (1956). [Research note.]

Miyazaki, Y. Cosmic-ray records of the Scientific Research Institute (II). J. Sci. Res. Inst., **49**, Nos. 1407-1414, 267-284 (1955).

Morrison, P. Solar origin of cosmic-ray time variations. Phys. Rev., **101**, No. 4, 1397-1404 (1956).

Neher, H. V. Low-energy primary cosmic-ray particles in 1954. Phys. Rev., **103**, No. 1, 228-236 (1956).

Norman, R. J. Influence of the earth's magnetic field on air showers. Phys. Rev., **101**, No. 4, 1405-1406 (1956).

Peters, B. The primary cosmic radiation. Science and Culture, **21**, No. 10, 576-586 (1956). [Presidential address before Physics Section, Indian Science Congress, at Agra, January 1956.]

Possener, M., and I. J. van Heerden. The daily variation of the cosmic ray intensity measured near the 1954 sunspot minimum. Phil. Mag., Ser. 8, **1**, No. 3, 253-260 (1956).

Sarabhai, V., S. P. Duggal, H. Razdan, and T. S. G. Sastry. A solar flare type increasing in cosmic rays at low latitudes. Proc. Indian Acad. Sci., A, **43**, No. 5, 309-318 (1956).

Singer, S. F. Cosmic ray effects on matter at high altitudes. J. Aviation Medicine, 27, 111-116 (April 1956).

Soberman, R. K. High-altitude cosmic-ray neutron intensity variations. Phys. Rev., **102**, No. 5, 1399-1409 (1956).

Steinmaurer, R. Ein ungewöhnlicher, plötzlicher Intensitätsanstieg der kosmischen Strahlung. Naturwiss., **43**, Heft 8, 174 (1956).

Trefall, H., and B. Trumpy. Observations of cosmic radiation following the solar flare of February 23rd, 1956. Physica, **22**, No. 7, 579-583 (1956).

Van Allen, J. A., and C. E. McIlwain. Cosmic-ray intensity at high altitudes on February 23, 1956. J. Geophys. Res., **61**, No. 3, 569-571 (1956). [Letter to Editor.]

Wada, M. The statistical analysis of the atmospheric effect on cosmic-ray mesons. Ionosphere Res. Japan, **10**, No. 2, 95-100 (1956).

Wada, M., and S. Kudō. A statistical investigation for the atmospheric temperature effect on cosmic-ray intensity. J. Sci. Res. Inst., Tokyo, **50**, No. 1415, 1-9 (1956).

D—*Upper Air Research*

Andrillat, Y. Exposé et mise au point bibliographique, Les bandes de vibration-rotation de la molécule OH dans le spectre infrarouge du ciel nocturne. J. Phys. Radium, **17**, No. 5, 442-448 (1956).

Bartman, F. L., L. W. Chaney, L. M. Jones, and V. C. Liu. Upper-air density and temperature by the falling-sphere method. J. Appl. Phys., **27**, No. 7, 706-712 (1956).

Baum, W. A. A fundamental cosmological experiment for the artificial satellite. Pub. Astr. Soc. Pacific, **68**, No. 401, 118-120 (1956).

Becker, W. Über ein Verfahren zur routinemässigen Bestimmung der wahren Verteilung der Elektronendichte in einer Ionosphärenschicht aus den Durchdrehaufnahmen dieser Schicht. Arch. Elektr. Übertrag., **10**, Heft 5, 207-214 (1956).

Belrose, J. S., M. H. Devenport, and K. Weekes. Some unusual radio observations made on 23 February 1956. J. Atmos. Terr. Phys., **8**, Nos. 4/5, 281-286 (1956). [Research note.]

Booker, H. G. A theory of scattering by nonisotropic irregularities with application to radar reflections from the aurora. J. Atmos. Terr. Phys., **8**, Nos. 4/5, 204-221 (1956).

Busch, R., E. Harnischmacher, et K. Rawer. Observations ionosphériques effectuées durant l'éclipse solaire du 30 juin 1954 à Fribourg. Ann. Géophys., **12**, No. 1, 1-15 (1956).

Butler, S. R., J. S. Gibbons, G. S. Levy, and T. J. May. Solution of the coupled wave equations for vertical ionospheric propagation at 75 and 150 kc/s. Pennsylvania State University, Ionosphere Res. Lab., Sci. Rep. No. 84, 131 pp., mim. (rec'd June 21, 1956).

Chapman, F. W., and R. C. Macario. Propagation of audio-frequency radio waves to great distances. Nature, **177**, 930-933 (May 19, 1956).

Chapman, S. The aurora in middle and low latitudes. Washington, D.C., Nation. Bur. Stan., NBS Rep. No. 5004, 14 pp. + 5 figs., mim. (Aug. 15, 1956). [Draft chapter for the Manual for Aurora and Airglow to be compiled under the auspices of the Comité Spécial de l'Année Géophysique International (CSAGI).]

Dave, J. V. On the intensity and polarization of the night light from the sky during twilight—Part II. Proc. Indian Acad. Sci., A, **43**, No. 6, 336-358 (1956).

Duncan, R. A. Lunar variations in the ionosphere. Aust. J. Phys., **9**, No. 1, 112-132 (1956).

Elsässer, H., und H. Siedentopf. Die Emissionshöhe der 5577 AE-Linie des Nachthimmelsleuchtens nach Messungen am Jungfraujoch. J. Atmos. Terr. Phys., **8**, Nos. 4/5, 222-232 (1956).

Friedland, S. S., J. Katzenstein, and M. R. Zatzick. Pulsed searchlighting the atmosphere. J. Geophys. Res., **61**, No. 3, 415-434 (1956).

Goldberg, P. A. Electromagnetic phenomena of natural origin in the 1.0-150 c./s. band. Nature **177**, 1219-1220 (June 30, 1956).

Goldman, D. T., and S. F. Singer. Studies of a minimum orbital unmanned satellite of the earth (Mouse). Pt. IV—Radiation equilibrium and temperature. College Park, University of Maryland, Physics Dept. Tech. Rep. No. 46, 31 pp. + 15 figs., mim. (June 1956).

Hunten, D. M. Automatic auroral recorder. J. Optical Soc. Amer., **46**, No. 8, 578-583 (1956).

IRE Convention Record. 1956 National Convention, Part 1—Telemetry, Antennas, and Propagation. Inst. Radio Engs., Pt. 1, 247 pp. (1956).

Jacobs, J. A., and D. W. Allan. Thermal aspects of the origin of meteorites. J. R. Astr. Soc. Can., **50**, No. 3, 122-123 (1956).

Johnson, C. Y., and J. P. Heppner. Daytime measurement of positive and negative ion composition to 131 km by rocket-borne spectrometer. J. Geophys. Res., **61**, No. 3, 575 (1956). [Letter to Editor.]

Kallmann, H. K., W. B. White, and H. E. Newell, Jr. Physical properties of the atmosphere from 90 to 300 kilometers. J. Geophys. Res., **61**, No. 3, 513-524 (1956).

Kamiyama, H. Ionospheric changes associated with geomagnetic bays. Sci. Rep. Tôhoku Univ., **7**, No. 3, 125-135 (1956).

Kaplan, J., G. F. Schilling, and H. K. Kallmann. Methods and results of upper atmosphere research. Air Force Cambridge Res. Center, Geophys. Res. Papers No. 43, 162 pp., mim. (Nov. 1955).

Kasuya, I., and K. Sawada. Comparison of *foF*2 at four observatories in Japan. J. Radio Res. Lab. Japan, **3**, No. 11, 45-53 (1956).

Kato, Y., and T. Tamao. Hydromagnetic oscillations in a conducting medium with Hall conductivity under the uniform magnetic field. Sci. Rep. Tôhoku Univ., **7**, No. 3, 147-164 (1956).

Kato, Y., and K. Yôkoto. The decrease of the electrical conductivity in the ionosphere associated with the solar eclipse. Sci. Rep. Tôhoku Univ., **7**, supp. to No. 3, 30-36 (1956).

King, G. A. M., and C. H. Cummack. Electron distribution in the ionosphere. J. Atmos. Terr. Phys., **8**, Nos. 4/5, 270-273 (1956).

Landmark, B. A study of the limiting polarization of high frequency radio waves reflected vertically from the ionosphere. Geofys. Pub., **19**, No. 7, 46 pp. (1955).

Lange-Hesse, G. Systematische Untersuchungen über den Einfluss der erdmagnetischen Unruhe auf die Nachtgrenzfrequenzen der F_2-Schicht. Archiv Elektr. Uebertrag., **10**, Heft 4, 139-144 (1956).

Martyn, D. F. Processes controlling ionization distribution in the F_2 region of the ionosphere. Aust. J. Phys., **9**, No. 1, 161-165 (1956). [Short communication.]

McKinley, D. W. R. Some factors affecting the radio determination of meteoric velocities. Naturwiss., **43**, Heft 10, 221-222 (1956).

McKinley, D. W. R., and A. G. McNamara. Meteoric echoes observed simultaneously by back scatter and forward scatter. Can. J. Phys., **34**, 625-637 (1956).

Meadows, E. B., and J. W. Townsend, Jr., Neutral gas composition of the upper atmosphere by a rocket-borne mass spectrometer. J. Geophys. Res., **61**, No. 3, 576-577 (1956). [Letter to Editor.]

Minnis, C. M. Interpretation of ionospheric measurements made during solar eclipses. Nature, **178**, 33-34 (July 7, 1956). [Letter to Editor.]

Nicolet, M. The aeronomic problem of helium. Pennsylvania State University, Ionosphere Res. Lab., Sci. Rep. No. 86, 35 pp., mim. (May 15, 1956).

Nicolet, M. The origin of atmospheric argon. Pennsylvania State University, Ionosphere Res. Lab., Res. Rep. No. 87, 27 pp., mim. (June 1, 1956).

Pant, P. S. Circulation in the upper atmosphere. J. Geophys. Res., **61**, No. 3, 459-474 (1956).

Pierce, J. A. VLF phase shift associated with the disturbance of February 23, 1956. J. Geophys. Res., **61**, No. 3, 475-483 (1956).

Ramachandra Rao, B., and D. Satyanarayana Murty. A simple method of studying winds in the ionosphere by using continuous-wave radio. Nature, **177**, 1222-1223 (June 30, 1956). [Letter to Editor.]

Ratcliffe, J. A. The formation of the ionospheric layers *F*-1 and *F*-2. J. Atmos. Terr. Phys., **8**, Nos. 4/5, 260-269 (1956).

Rawer, K. Focusing on a "rippled" ionosphere. J. Atmos. Terr. Phys., 8, Nos. 4/5, 296 (1956). [Research note.]

Riehl, H. On the atmospheric circulation at 500 mb in the auroral belt. J. Geophys. Res., **61**, No. 3, 525-534 (1956).

Roach, F. E. Manual for photometric observations of the airglow during the International Geophysical Year. Washington, D.C., Nation. Bur. Stan., NBS Rep. No. 5006, 33 pp., mim. (Aug. 20, 1956). [Draft report of the Manual for Photometric Observations of the Airglow during the International Geophysical Year; prepared for distribution to the September 1956 meeting of CSAGI at Barcelona.]

Sato, T. Disturbances in the *F*2 region of the ionosphere associated with geomagnetic storms. Rep. Ionosphere Res. Japan, **10**, No. 2, 35-48 (1956).

Sekihara, K. Studies of the distribution of ultraviolet sky radiation (VII). Pap. Met. Geophys., No. 2, 150-163 (1955).

Shimazaki, T. The structure of the *F*2 layer as deduced from its daily variations. J. Radio Res. Lab. Japan, **3**, No. 11, 17-43 (1956).

Silverman, R. A. Turbulent mixing theory applied to radio scattering. J. Appl. Phys., **27**, No. 7, 699-705 (1956).

Singer, S. F. A crucial experiment concerning the origin of meteorites. College Park, University of Maryland, Physics Dept. Tech. Rep. No. 47, 4 pp. (July 1956).

Thomas, J. A., A. C. Svenson, and H. E. Brown. Ionospheric recorders and sporadic *E*. Aust. J. Phys., **9**, No. 1, 159-161 (1956). [Short communication.]

Wait, J. R. A basis of a proposed method to measure the characteristics of an arbitrary down-coming radio wave. Boulder Laboratories, Nation. Bur. Stan., NBS Rep. No. 3587, 9 pp., mim. (May 9, 1956).

Wait, J. R., and L. B. Perry. Calculations of ionospheric reflection coefficients at very low radio frequencies. Boulder Laboratories, Nation. Bur. Stan., NBS Rep. No. 3588, 20 pp., mim. (May 15, 1956).

Whale, H. A. Effective tilts of the ionosphere at places about 1000 km apart. Proc. Phys. Soc., B, **69**, No. 435, 301-310 (1956).

Whale, H. A., and W. J. Ross. An automatic direction finder for recording rapid fluctuations of the bearing of short radio waves. Proc. Phys. Soc., B, **69**, No. 435, 311-320 (1956).

White, M. L. Gravitational and thermal oscillations in the earth's upper atmosphere. J. Geophys. Res., **61**, No. 3, 489-499 (1956).

Wild, J. P., and J. A. Roberts. Regions of the ionosphere responsible for radio star scintillations. Nature, **178**, 377-378 (Aug. 18, 1956). [Letter to Editor.]

Wright, R. W., J. R. Koster, and N. J. Skinner. Spread *F*-layer echoes and radio-star scintillation. J. Atmos. Terr. Phys., **8**, Nos. 4/5, 240-246 (1956).

Yerg, D. G. Observations and analysis of ionospheric drift. J. Atmos. Terr. Phys., **8**, Nos. 4/5, 247-259 (1956).

Yonezawa, T. A new theory of formation of the *F*2 layer. J. Radio Res. Lab. Japan, **3**, No. 11, 1-16 (1956).

E—*Radio Astronomy*

André, P., I. Kazes, et J.-L. Steinberg. Mesure de l'absorption atmosphérique sur 9350 Mhz utilisant le rayonnement radioélectrique solaire. Paris, C.-R. Acad. sci., **242**, No. 17, 2099-2101 (1956).

Ashburn, E. V., J. G. Moore, and P. St. Amand. Auroral radiation in the 2 to 3 micron range. J. Geophys. Res., **61**, No. 3, 568 (1956). [Letter to Editor.]

Baade, W. Polarization in the jet of Messier 87. Astroph. J., **123**, No. 3, 550-551 (1956). [Note.]

Berkner, L. V. Plan for a National Radio Astronomy Facility. Astr. J., 61, No. 4, 165-166 (1956). [Symposium: Radio telescopes, present and future; held at the 94th meeting of the American Astronomical Society, Columbus, Ohio, March 21-24, 1956.]

Blum, É.-J., A. Boischot, et M. Ginat. L'interféromètre à antennes multiples de la Station de Nançay. Paris, C.-R. Acad. sci., **243**, No. 1, 19-22 (1956).

Bolton, J. G. Radio telescopes for position finding. Astr. J., **61**, No. 4, 168-169 (1956). [Symposium: Radio telescopes, present and future; held at the 94th meeting of the American Astronomical Society, Columbus, Ohio, March 21-24, 1956.]

Burbidge, G. R. Galactic radio emission and the energy released in nuclear collisions of primary cosmic-ray protons. Phys. Rev., **103**, No. 1, 264-265 (1956). [Letter to Editor.]

Burke, B. F. Mills cross telescopes. Astr. J., **61**, No. 4, 167-168 (1956). [Symposium: Radio telescopes, present and future; held at the 94th meeting of the American Astronomical Society, Columbus, Ohio, March 21-24, 1956.]

Cohen, M. H. Interpretation of radio polarization data in terms of Faraday rotation. Cornell University, School of Elec. Eng., Res. Rep. No. EE 295, 20 pp., mim. (May 30, 1956). [Radio Astronomy and Solar Radio Noise Joint Report No. 3.]

Dueño, B. Low-angle fluctuations of the radio-star Cassiopeia as observed at Ithaca, N.Y., and its relation to the incidence of sporadic-*E*. J. Geophys. Res., **61**, No. 3, 535-540 (1956).

Forbush, S. E., and B. F. Burke. Absorption of cosmic radio noise at 22.2 Mc/sec following solar flare of February 23, 1956. J. Geophys. Res., **61**, No. 3, 573-575 (1956). [Letter to Editor.]

Heeschen, D. S. Harvard's new radio telescope. Sky and Telescope, **15**, No. 9, 388-390 (1956).

Kerr, F. J., and G. de Vaucouleurs. The masses of the Magellanic clouds from radio observations. Aust. J. Phys., **9**, No. 1, 90-111 (1956).

Kraus, J. D. Radio telescope designs of large aperture and low cost. Astr. J., **61**, No. 4, 169-170 (1956). [Symposium: Radio telescopes, present and future; held at the 94th meeting of the American Astronomical Society, Columbus, Ohio, March 21-24, 1956.]

Kraus, J. D. Impulsive radio signals from the planet Venus. Nature, **178**, 33 (July 7, 1956). [Letter to Editor.]

Kraus, J. D. The radio sky. Sci. Amer., **195**, No. 1, 32-37 (1956).

Kraus, J. D. Radio observations of the planet Venus at a wavelength of 11 m. Nature, **178**, 103-104 (July 14, 1956). [Letter to Editor.]

Kraus, J. D. Class II radio signals from Venus at a wave-length of 11 meters. Nature, **178**, 159-160 (July 21, 1956). [Letter to Editor.]

McKerrow, C. A. Sudden decrease in low-frequency atmospheric noise during the cosmic-radiation storm of February 23. Nature, **177**, 1223-1224 (June 30, 1956). [Letter to Editor.]

Mills, B. Y., A. G. Little, and K. V. Sheridan. Radio emission from novae and supernovae. Aust. J. Phys., **9**, No. 1, 84-89 (1956).

Muller, C. A. A receiver for the radio waves from interstellar hydrogen. I. The investigation of the hydrogen radiation. II. Design of the receiver. Philips Tech. Rev., **17**, No. 11, 305-315, and No. 12, 351-361 (1956).

Oort, J. H., and Th. Walraven. Polarization and composition of the Crab nebula. Bull. Astron. Inst. Netherlands, **12**, No. 462, 285-308 (1956).

Piddington, J. H., and G. H. Trent. Cosmic radio sources observed at 600 Mc/s. Aust. J. Phys., **9**, No. 1, 74-83 (1956).

Ramanathan, K. R., R. V. Bhonsle, K. M. Kotadia, and R. G. Rastogi. The great solar flare of February 23, 1956 and associated ionospheric effects at Ahmedabad. Proc. Indian Acad. Sci., A, **43**, No. 5, 306-308 (1956).

Shain, C. A. 18.3 Mc/s radiation from Jupiter. Aust. J. Phys., **9**, No. 1, 61-73 (1956).

Stanley, G. J., and R. Price. An investigation of monochromatic radio emission of deuterium from the galaxy. Nature, **177**, 1221-1222 (June 30, 1956). [Letter to Editor.]

Tanaka, H. Some notes on the solar radio emission at centimetre region around the period of sunspot (minimum). Proc. Res. Inst. Atmos., Nagoya Univ., **3**, 117-119 (Nov. 1955).

Tanaka, H., and T. Kakinuma. Multiple element interferometer for locating sources of solar noise at 4,000 megacycles. Proc. Res. Inst. Atmos., Nagoya Univ., **3**, 102-109 (Nov. 1955).

Tanaka, H., T. Kakinuma, T. Hatanaka, K. Akabane, and F. Moriyama. A model for the solar enhanced region at centimeter region derived from partial eclipse observations. Proc. Res. Inst. Atmos., Nagoya Univ., **3**, 84-95 (Nov. 1955).

Wells, H. W. Flux measurements of discrete radio sources at frequencies below 30 megacycles. J. Geophys. Res., **61**, No. 3, 541-545 (1956).

Westerhout, G. Search for polarization of the Crab nebula and Cassiopeia A at 22 cm wavelength. Bull. Astron. Inst. Netherlands, **12**, No. 462, 309-311 (1956).

F—*Earth's Crust and Interior*

Aldrich, L. T. Measurement of radioactive ages of rocks. Science, **123**, No. 3203, 871-875 (1956).

Bass, L. Radiation with a finite rest-mass and the heat balance of the earth. Nuovo Cimento, **3**, No. 6, 1204-1212 (1956).

Burkhart, K. Der Erdstrom, seine entstehung und wahrscheinlicher Rückwirkung auf das erdmagnetische Feld. Geofisica pura e appl., **33**, 49-77 (1956).

Burkhart, K. Konstruktionsunterlagen der Induktiven Pulsations—und Erdstrom-Anlage am Erdmagnetischen Observatorium in Fürstenfeldbruck. Geofisica pura e appl., **33**, 78-85 (1956).

Chadwick, P. Heat-flow from the earth at Cambridge. Nature, **178**, 105-106 (July 14, 1956). [Letter to Editor.]

Davies, J. T. Age of the universe. Research, **9**, No. 4, 119-123 (1956).

Deutsch, S., E. Picciotto, and F. G. Houtermans. Radioactivity of iron meteorites by the photographic method. Nature, **177**, 885-886 (May 12, 1956). [Letter to Editor.]

Evernden, J. F., and J. Verhoogen. Electrical resistivity of meteorites. Nature, **178**, 106-107 (July 14, 1956). [Letter to Editor.]

Gutenberg, B. Damping of the earth's free nutation. Nature, **177**, 887-888 (May 12, 1956). [Letter to Editor.]

Gutenberg, B., and C. F. Richter. Earthquake magnitude, intensity, energy, and acceleration (second paper). Bull. Seis. Soc. Amer., **46**, No. 2, 105-143 (1956).

Hill, J. E., and J. J. Gilvarry. Application of the Baldwin crater relation to the scaling of explosion craters. J. Geophys. Res., **61**, No. 3, 501-511 (1956).

Honda, H., H. Sima, and K. Nakamura. The ScS wave, the mechanism of deep earthquake and the rigidity of the earth's core. Sci. Rep. Tôhoku Univ., **7**, No. 3, 169-179 (1956).

Hooker, M. Data of rock analyses—II. Bibiligraphy and index of rock analyses in the African periodical and serial literature. Geochim. et Cosmochim. Acta, **9**, No. 4, 190-213 (1956).

Runcorn, S. K. Experiments on the displacement of the ultraviolet absorption edge of olivine at high pressures. J. Appl. Phys., **27**, No. 6, 598-602 (1956).

Shima, M. On the variation in bulk modulus/density in the mantle. J. Phys. Earth, **4**, No. 1, 7-10 (1956).

Shimazu, Y. Chemical phase equilibrium and physical structure within the earth's mantle. J. Phys. Earth, **4**, No. 1, 1-6 (1956).

Sitter, L. U. de. Structural geology. New York, McGraw-Hill Book Co., Inc., 552 pp. + 311 figs. (1956). 23 cm.

Toledo, Observatorio Central Geofísico. Corrientes telúricas, año 1953. Madrid, Instituto Geográfico y Catastral, 52 pp. + 10 figs. (1955). [Prepared by Luis de Miguel y Gonzalez-Miranda.]

Venkatasubramanian, V. S. Some aspects of helium leakage from rocks and minerals. J. Indian Inst. Sci., **38**, No. 2, 96-99 (1956).

Wetherill, G. W. An interpretation of the Rhodesia and Witwatersrand age patterns. Geochim. et Cosmochim., **9**, Nos. 5/6, 290-292 (1956). [Geochemical notes.]

Wetherill, G. W., G. R. Tilton, G. L. Davis, and L. T. Aldrich. New determinations of the age of the Bob Ingersoll pegmatite, Keystone, S. Dakota. Geochim. et Cosmochim., **9**, Nos. 5/6, 292-297 (1956). [Geochemical notes.]

G—*Miscellaneous*

Allan, D. W., and J. A. Jacobs. The melting of asteroids and the origin of meteorites. Geochim. et Cosmochim. Acta, **9**, Nos. 5/6, 256-272 (1956).

Berkner, L. V. The international Geophysical Year. QST, **40**, No. 7, 11-14 and 126 (1956).

Commission mixte pour l'Étude des relations entre les phénomènes solaires et terrestres, Conseil International des Unions Scientifiques. Réunion du 6 Septembre 1955 à Dublin. Paris, J. and R. Sennac, 37 pp. (April 25, 1956).

Ferraro, V. C. A. Italian Society for Geophysics and Meteorology (fourth General Assembly). Nature, **178**, 24-25 (July 7, 1956).

Gold, T. The symmetry of the corona of 1954 June 30. Mon. Not. R. Astr. Soc., **115**, No. 4, 340-342 (1955).

Kuiper, G. P. The formation of the planets, Part III. J. R. Astr. Soc. Can., **50**, No. 4, 158-176 (1956).

Meek, J. H. A method for drawing the great-circle path between any two points on earth. J. Geophys. Res., **61**, No. 3, 445-448 (1956).

Mercure, R., S. C. Miller, Jr., W. A. Rense, and F. Stuart. The sun's disk in Lyman-alpha radiation. J. Geophys. Res., **61**, No. 3, 571-573 (1956). [Letter to Editor.]

Meteorological Office. The observatories' year book 1938. London, Met. Office, M.O. 578, Air Ministry, x + 223 pp. (1955). [Comprising the meteorological and geophysical results obtained from autographic records and eye observations at the Lerwick, Aberdeen, Eskdalemuir, Valencia, and Kew observatories, and the records of soundings of the upper atmosphere by means of registering balloons.]

Newton, H. W., and A. S. Milsom. Note on the observed differences in spottedness of the sun's northern and southern hemispheres. Mon. Not. R. Astr. Soc., **115**, No. 4, 398-404 (1955).

Pfotzer, G. Die Impulsverteilung der solaren Ultrastrahlung in der Abklingphase der strahlungseinbruches am 23 Februar 1956. Mitt. Max Planck-Institut für Physik der Stratosphäre, No. 7, 20 pp., mim. (1956).

Singer, S. F. Geophysical researches with artificial earth satellites. College Park, University of Maryland, Physics Dept. Tech. Rep. No. 53, 22 pp. + 6 tables + ref., mim. (1956). [From a chapter in "Advances in Geophysics," Vol. 3, H. E. Landsberg (Ed.), Academic Press, Inc., New York (1956).]

Struve, O. On the origin of the solar system. Sky and Telescope, **15**, No. 8, 349-352 (1956).

Tandberg-Hanssen, E. A study of the penumbra-umbra ratio of sunspot pairs. Astroph. Norvegica, **5**, No. 7, 207-227 (Jan. 1956).

Waldmeier, M. Provisonal sunspot-numbers for April to June, 1956. J. Geophys. Res., **61**, No. 3, 563 (1956).

INDEX OF AUTHORS

Volume 61, 1956

NOTICE

When available, single unbound volumes can be supplied at $6 each and single numbers at $2 each, postpaid.

Charges for reprints and covers

Reprints can be supplied, but prices have increased considerably and costs depend on the number of articles per issue for which reprints are requested. It is no longer possible to publish a schedule of reprint charges, but if reprints are requested approximate estimates will be given when galley proofs are sent to authors. Reprints without covers are least expensive; standard covers (with title and author) can be supplied at an additional charge. Special printing on covers can also be supplied at further additional charge.

Fifty reprints, without covers, will be given to institutions paying the publication charge of $8 per page.

Alterations

Major alterations made by authors in proof will be charged at cost. Authors are requested, therefore, to make final revisions on their typewritten manuscripts.

Orders for back issues and reprints should be sent to Editorial Office, 5241 Broad Branch Road, N.W., Washington 15, D. C., U.S.A.

Subscriptions are handled by The Editorial Office, 5241 Broad Branch Road, N.W., Washington 15, D. C., U.S.A.

CONTENTS—Concluded